# REPORT TO BEIS

# LONG-TERM ATMOSPHERIC MEASUREMENT AND INTERPRETATION

# (OF RADIATIVELY ACTIVE TRACE GASES)

**BEIS contract number: GA0201**

**Annual Report (Sept 2017 - Sept 2018)**

**Date: 10th September 2018**


**University of Bristol: Simon O'Doherty, Kieran Stanley, Matt Rigby, Ann Stavert**

**Met Office: Alistair Manning, Alison Redington**

**INSCON: Peter Simmonds**

**Terra Modus Consultants Ltd: Dickon Young**

**University of East Anglia: Bill Sturges, Adam Wisher**

**University of Edinburgh: Paul Palmer**

**NPL: Chris Rennick, Tim Arnold**

1 Executive Summary ..... 4
1.1 Headline Summary ..... 4
1.2 Project Summary ..... 4
1.3 Summary of the main findings on inventory verification ..... 5
1.4 Summary of Progress ..... 6
1.5 Future Plans ..... 7
1.6 Recent Publications ..... 7
1.7 Meetings ..... 9
1.8 Related information ..... 10
2 Instrumentation ..... 10
2.1 Sites ..... 10
2.1.1 Mace Head (MHD) ..... 10
2.1.2 Tacolneston (TAC) ..... 11
2.1.3 Ridge Hill (RGL) ..... 11
2.1.4 Bilsdale (BSD) ..... 12
2.1.5 Heathfield (HFD) (Affiliated to UK DECC Network) ..... 12
3 Annual Northern Hemispheric trends ..... 14
3.1 Baseline Mole Fractions ..... 14
4 Regional emission estimation ..... 17
4.1 Introduction ..... 17
4.2 Summary of InTEM inverse modelling ..... 17
4.3 Summary of the greenhouse gases reported to the UNFCCC ..... 19
4.4 Methane ($CH_4$) ..... 20
4.5 Nitrous oxide ($N_2O$) ..... 24
4.6 Carbon dioxide ($CO_2$) ..... 28
4.7 HFC-125 ..... 29
4.8 HFC-134a ..... 32
4.9 HFC-143a ..... 35
4.10 HFC-152a ..... 38
4.11 HFC-23 ..... 41
4.12 HFC-32 ..... 44
4.13 HFC-227ea ..... 47
4.14 HFC-245fa ..... 50
4.15 HFC-43-10mee ..... 53
4.16 HFC-365mfc ..... 56
4.17 PFC-14 ($CF_4$) ..... 59
4.18 PFC-116 ..... 63
4.19 PFC-218 ..... 67
4.20 PFC-318 ..... 70
4.21 $SF_6$ ..... 73
4.22 $NF_3$ ..... 77
5 Global emission estimates ..... 78
5.1 Introduction ..... 78
5.2 Recent trends in non-$CO_2$ Kyoto gases ..... 78
5.2.1 $CH_4$ ..... 78
5.2.2 $N_2O$ ..... 78
5.2.3 HFCs ..... 78
5.2.4 PFCs, $SF_6$ and $NF_3$ ..... 79
6 Estimating biogenic and anthropogenic $CO_2$ ..... 87
7 Use of satellite data in inversion modelling ..... 88
7.1 Introduction ..... 88
7.2 Preparation of existing satellite data ..... 88
7.3 Future mission concepts ..... 89
7.4 Emission estimates using satellite observations of $CO_2$ and $CH_4$ ..... 90

8 Results and analysis of additional gases ..... 91
8.1 Introduction ..... 91
8.2 CFC-11 ..... 92
8.3 CFC-12 ..... 95
8.4 CFC-113 ..... 96
8.5 HCFC-124 ..... 97
8.6 HCFC-141b ..... 98
8.7 HCFC-142b ..... 99
8.8 HCFC-22 ..... 100
8.9 HFC-236fa ..... 101
8.10 $SO_2F_2$ ..... 102
8.11 $CH_3Cl$ ..... 103
8.12 $CH_2Cl_2$ ..... 104
8.13 $CHCl_3$ (chloroform) ..... 105
8.14 $CCl_4$ (carbon tetrachloride) ..... 106
8.15 $CH_3CCl_3$ (methyl chloroform) ..... 107
8.16 $CCl_2CCl_2$ ..... 107
8.17 Methyl bromide ($CH_3Br$) ..... 109
8.18 Halon-1211 ..... 110
8.19 Halon-1301 ..... 111
8.20 Halon-2402 ..... 112
8.21 Carbon monoxide (CO) ..... 113
8.22 Ozone ($O_3$) ..... 114
8.23 Hydrogen ..... 115
9 References ..... 116

# 1 Executive Summary

## *1.1 Headline Summary*

- The overriding aim of the project is to estimate UK emissions of the principle greenhouse gases using the UK Deriving Emissions related to Climate Change (DECC) network of observations and compare these to the compiled inventory. The Inversion Technique for Emission Modelling (InTEM) has been developed to deliver these estimates. These comparisons enable BEIS to be more informed in their inventory improvement programme.
- The northern hemisphere atmospheric concentrations of ALL of the 'Kyoto basket' of gases except HFC-152a are increasing.
- InTEM estimates for UK methane are lower than the reported inventory although in recent years the agreement is good.
- The trend in UK emissions of nitrous oxide is in good agreement with the inventory but the InTEM estimates are consistently higher.
- The UK emissions of all the HFCs are estimated to be lower using InTEM compared to the inventory, the only exception being HFC-23.
- Estimates of UK PFCs and $SF_6$ are consistently higher using InTEM compared to the inventory.
- The rate of decline of atmospheric CFC-11 has slowed considerably since 2012 although the emissions from the UK are estimated to be small.

## *1.2 Project Summary*

Monitoring the atmospheric concentrations of gases is important in assessing the impact of international policies related to the atmospheric environment. The effects of control measures on greenhouse gases in the so called 'Kyoto basket': carbon dioxide ($CO_2$), methane ($CH_4$), nitrous oxide ($N_2O$), hydrofluorocarbons (HFC), perfluorocarbons (PFC), nitrogen trifluoride ($NF_3$) and sulphur hexafluoride ($SF_6$), are now being observed. Likewise, measures introduced under the Montreal Protocol to protect the stratospheric ozone layer are also being observed in the atmosphere. Understanding the effectiveness and impacts of policies on the atmospheric abundance of these key gases is vitally important to policy makers.

This project has two principle aims:

- **Estimate the background atmospheric concentrations of the principle greenhouse and ozone-depleting gases from the DECC network of observations.**

- **Estimate the UK emissions of the principle greenhouse gases using the DECC network of observations and compare these to the compiled inventory.**

Since 1987, high frequency, real time measurements of the principal halocarbons and radiatively active trace gases have been made as part of the Global Atmospheric Gases Experiment (GAGE) and Advanced Global Atmospheric Gases Experiment (AGAGE) at Mace Head, County Galway, Ireland. For much of the time, the Mace Head measurement station (MHD), which is situated on the Atlantic coast, monitors clean westerly air that has travelled across the North Atlantic Ocean. However, when the winds are easterly, MHD receives substantial regional scale pollution in air that has travelled from the populated and industrial regions of Europe. The site is therefore uniquely situated to record trace gas concentrations associated with both the northern hemisphere background levels and with the more polluted air arising from European emissions.

To this aim, the UK has developed a network of observation stations called the UK Deriving Emissions related to Climate Change (DECC) network. Along with MHD, it consists of three tall tower stations: Ridge Hill (RGL) near Hereford; Tacolneston (TAC) near Norwich; Bilsdale

(BSD) in North Yorkshire (originally Angus (TTA) near Dundee). RGL became operational in February 2012, TAC in July 2012 and TTA began operating for the network in April 2012, but was decommissioned and replaced with BSD in September 2015. The expanded network makes it possible to resolve emissions on a higher resolution, both spatially and temporally, across the UK.

The UK DECC network measures, to very high precision, all of the principle greenhouse gases in the inventory 'Kyoto basket' of gases as well as many ozone-depleting gases. The Inversion Technique for Emission Modelling (InTEM) (please refer to Methodology report for more details) has been developed to use these observations to estimate both Northern Hemisphere concentration trends and UK emissions of each gas. The InTEM emission estimates, as well as those reported through the inventory process, have uncertainties. The comparisons between the inventory and InTEM estimates enable BEIS to be more informed in their inventory improvement programme.

The atmospheric measurements and emission estimates of greenhouse gases provide an important independent cross-check for the national Green House Gas Inventories (GHGI) of emissions submitted annually to the United Nations Framework Convention on Climate Change (UNFCCC). The GHGI are estimated through in-country submissions of Activity Data and Emission Factors that are, in some cases, very uncertain. Independent emissions verification is considered good practice by the Intergovernmental Panel on Climate Change (IPCC).

The UK is one of only two countries worldwide (Switzerland is the other) that currently routinely verify their reported inventory emissions as part of their annual UNFCCC submission of emissions. The UK is the only country to do so for all of the principle Kyoto gases.

## *1.3 Summary of the main findings on inventory verification*

- The northern hemisphere atmospheric concentrations of all 'Kyoto basket' gases except HFC-152a are increasing.

- Methane ($CH_4$): The UK InTEM estimates are lower than the UK inventory (GHGI) estimates (as reported to the UNFCCC in 2016) in the 1990s and 2000s. By 2004 the uncertainties of the two methods overlap and from 2012 onwards there is good agreement. The inclusion of the extended DECC network observations and the data from the NERC Greenhouse gAs Uk and Global Emissions (GAUGE) project has allowed the InTEM time frame to be reduced from 3-years to 1-year, or 3-months if the NAEI prior is used. A noticeable difference is seen between using global resolution (12-17 km) meteorology compared to high resolution (1.5 km) meteorology, this is to be further investigated.

- Nitrous oxide ($N_2O$): The UK GHGI and InTEM trend in UK estimates are similar but the InTEM estimates are ~20 Gg $yr^{-1}$ higher. The DECC 1-year inversions agree with the 3-year MHD-only inversion estimates from 2012 onwards. DECC 3-month InTEM results using the 2015 NAEI prior emissions to inform the inversions show a strong seasonal cycle in UK $N_2O$ emissions with peaks in spring.

- HFC-134a: The UK GHGI is higher than that estimated by InTEM and the uncertainties of the two methods do not overlap.

- HFC-32: The UK GHGI estimates (used in refrigerant blends) are increasing. UK InTEM estimates are approximately one third lower than the GHGI but with a similar trend.

- HFC-125: The UK GHGI estimates are increasing. UK InTEM estimates are approximately one third lower than the GHGI. From 2012 the InTEM emission estimates have been relatively flat.

- HFC-143a and HFC-365mfc: UK InTEM estimates broadly agree with the GHGI.

- HFC-227ea, HFC-43-10-mee, HFC-245fa: UK InTEM estimates are significantly lower than reported in the inventory.

- Sulphur hexafluoride ($SF_6$): The UK InTEM estimates are consistently elevated compared to the GHGI.

- PFCs: The InTEM estimates for all four gases (PFC-14, PFC-116, PFC-218, PFC-318) are elevated compared to the inventory. For the first 3 gases in the list, InTEM estimates the main source in the UK is a point source in the NW of England, north-east of Liverpool.

- CFC-11: InTEM estimates of UK emissions fell rapidly in the early 1990s and has since slowly declined.

## *1.4 Summary of Progress*

Significant progress has been made during the final 12 months of the contract period. There have been significant improvements to how uncertainty in the inversion process is represented and how the baseline and boundary conditions are estimated. The section on satellite observations and how they are currently used in inversion modelling has been updated. Global emissions of the key greenhouse gases have also been updated in this report.

- **Mace Head** continues to be a baseline station at the forefront of global atmospheric research. This is evident through the high volume of peer-reviewed publications related to work using the MHD observational record. The recent publications related to this contract are detailed in the publication section of this report. In addition, the inclusion of MHD in many EU funded atmospheric research programmes, such as ICOS, InGOS, ACTRIS, and continued support from other global programmes such as AGAGE and NOAA-ESRL indicates its international significance.

- **CO and $N_2O$ nonlinearity have been reassessed at Mace Head and Tacolneston.** A suite of cylinders spanning above and below ambient concentrations of CO and $N_2O$ were used to reassess instrumental nonlinearity.

- **Radon detectors have been built and are awaiting shipment from ANSTO, Australia.** As part of the NERC Advanced UK Observing Network for Air Quality, Public Health and Greenhouse Gas award (NE/R011532/1) award, two radon detectors are being built by ANSTO, Australia, and will be installed at Tacolneston and Bilsdale (or Ridge Hill) to measure atmospheric radon and help better constrain inversion models.

- **Meteorological equipment will be installed on the tall towers at Bilsdale, Tacolneston and Ridge Hill.** As part of the NE/R011532/1 award, wind speed and direction, temperature, humidity, and barometric pressure will be measured at each of the UK DECC sites. Instrumentation has been selected and is awaiting installation on the tall towers.

- **Optical $N_2O$ and CO analyser for Bilsdale being tested at UoB.** A Picarro G5310 was bought as part of the NE/R011532/1 award. The instrument was received at UoB in June 2018 and has been undergoing laboratory tests before the instrument is deployed at Bilsdale.

- **New GCMS measurements at Tacolneston**. An Agilent 5977 GCMS was purchased as part of the NE/R011532/1 award. The GCMS has been installed and tested in Bristol, and will replace the current older 5973 GCMS at Tacolneston. Ultimately, the Medusa GCMS system will also be updated to allow $NF_3$ measurements.

- **Mid-latitude Northern Hemisphere baseline trends have been updated.** The trends have been extended up to and including June 2018 observations.

- **UK emission estimates**. Inversion emission estimates for the UK are reported up to and including 2016 and have been compared to the UK GHGI inventory submitted in 2018 (the 2018 GHGI submission covers UK emissions up to and including 2016).

- **UNFCCC verification appendix chapter** for the UK National Inventory Report (NIR) submission was delivered (March 2018).

- **Improved data selection and uncertainty calculation in InTEM.** The observations from multiple inlet heights allowed a better understanding of how well the UM-NAME model represents turbulent mixing, this has been used to better inform InTEM.

- **Emissions of CFC-11 from UK and North West Europe are small**. Globally there is a slowdown in the decrease of CFC-11 in the atmosphere. In the mid-latitude Northern Hemisphere, the growth rate reported last year from the MHD observations was -1.49 ppt $yr^{-1}$, this year it is -0.85 ppt $yr^{-1}$. This has led researchers to estimate that there are renewed emissions of this gas. The first indications are for increased emissions from East Asia (Montzka et al, 2018).

## *1.5 Future Plans*

- High resolution modelling of the areas directly surrounding each station may improve the overall modelling of the observations. This will be investigated.
- Use of measured meteorology and radon at the stations to further improve the InTEM uncertainty estimates.
- Use of the new ECMWF meteorological re-analysis data (ERA-5) to compare to the UM data and improve the 1989-2002 meteorology currently used.

## *1.6 Recent Publications*


Adcock, K. E., … O'Doherty, S., et al.: **Continued increase of CFC-113a ($CCl_3CF_3$) mixing ratios in the global atmosphere: emissions, occurrence and potential sources**, *Atmos. Chem. Phys., 18(7), 4737–4751*, doi:10.5194/acp-18-4737-2018, 2018.

Arnold, T., Manning, A., … O'Doherty, S., **Inverse modelling of $CF_4$ and $NF_3$ emissions in East Asia**, *Atmospheric Chemistry and Physics Discussions (accepted)*, 1–29, doi:10.5194/acp-2017-1171, 2018.

Bergamaschi, P., … Manning, A. J., et al**.: Inverse modelling of European $CH_4$ emissions during using different inverse models and reassessed atmospheric observations**, *Atmos. Chem. Phys, 18, 901–920*, doi:10.5194/acp-18-901-2018, 2018.

Derwent, R. G., Manning, A. J., Simmonds, P. G., Spain, T. G. and O'Doherty, S.: **Long-term trends in ozone in baseline and European regionally-polluted air at Mace Head, Ireland over a 30-year period**, *Atmos. Environ., 179, 279–287*, doi:10.1016/j.atmosenv.2018.02.024, 2018.

Hernández-Paniagua, I. Y., … O'Doherty, S., et al.: **Diurnal, seasonal, and annual trends in tropospheric CO in Southwest London during 2000–2015: Wind sector analysis and comparisons with urban and remote sites**, *Atmos. Environ., 177, 262–274*, doi:10.1016/j.atmosenv.2018.01.027, 2018.

Li, S., … O'Doherty, S., et al.: **Chemical evidence of inter-hemispheric air mass intrusion into the Northern Hemisphere mid-latitudes**, *Sci. Rep., 8(1)*, doi:10.1038/s41598-018-22266-0, 2018.

Montzka, S. A., …Rigby, M., Manning, et al.: **An unexpected and persistent increase in global emissions of ozone-depleting CFC-11**, Nature, 557, 413-417, doi 10.1038/s41586-018-0106-2, 2018.

Pison, I., … Ganesan, A., O 'Doherty, S., Spain, T. G., et al.: **How a European network may help with estimating methane emissions on the French national scale**, *Atmos. Chem. Phys, 185194, 3779–3798*, doi:10.5194/acp-18-3779-2018, 2018.

Prinn, R. G., … Arnold, T., Ganesan, A. L., Manning, A. J., O'Doherty, S., Rigby, M., Simmonds, P. G., Young, D. et al.: **History of chemically and radiatively important atmospheric gases from the Advanced Global Atmospheric Gases Experiment (AGAGE)**, *Earth Syst. Sci. Data, 10, 985–1018*, doi:10.3334/CDIAC, 2018.

Schoenenberger, F., … O'Doherty, S., et al.: **Abundance and sources of atmospheric halocarbons in the Eastern Mediterranean**, *Atmos. Chem. Phys., 18(6), 4069–4092*, doi:10.5194/acp-18-4069-2018, 2018.

Simmonds, P. G., Rigby, … O'Doherty, S., Manning, A. J., Young, D., et al.: **Recent increases in the atmospheric growth rate and emissions of HFC-23 ($CHF_3$) and the link to HCFC-22 ($CHClF_2$) production**, *Atmos. Chem. Phys., 18(6), 4153–4169*, doi:10.5194/acp-18-4153-2018, 2018.

Stanley, K. M., …, O'Doherty, S., Young, D., Manning, A.J., Spain, T. G., Simmonds, P. G., et al.: **Greenhouse gas measurements from a UK network of tall towers: technical description and first results**, *Atmos. Meas. Tech., 11(3), 1437–1458*, doi:10.5194/amt-11-1437-2018, 2018.

Vollmer, M. K., Young, D., … Rigby, M., O'Doherty, S., Simmonds, P. G., et al.: **Atmospheric histories and emissions of chlorofluorocarbons CFC-13 ($CClF_3$), ΣCFC-114 ($C_2Cl_2F_4$) and CFC-115 ($C_2ClF_5$)**, *Atmos. Chem. Phys., 18(2), 979–1002*, doi:10.5194/acp-18-979-2018, 2018.

Wells, K. C., … O'Doherty, S., Young, D., et al.: **Top-down constraints on global $N_2O$ emissions at optimal resolution: application of a new dimension reduction technique**, *Atmos. Chem. Phys., 18(2), 735–756*, doi:10.5194/acp-18-735-2018, 2018.

Bader, W., … O'Doherty, S., et al.: **The recent increase of atmospheric methane from 10 years of ground-based NDACC FTIR observations since 2005**, *Atmos. Chem. Phys., 17(3), 2255–2277*, doi:10.5194/acp-17-2255-2017, 2017.

Brunner, D., Arnold, T., Manning, A.J., … O'Doherty, S., et al.: **Comparison of four inverse modelling systems applied to the estimation of HFC-125, HFC-134a, and $SF_6$ emissions over Europe**, *Atmos. Chem. Phys, 175194, 10651–10674*, doi:10.5194/acp-17-10651-2017, 2017.

Cain, M., … S., Manning, A. J., et al.: **A cautionary tale: Identifying the sources of a methane enhancement observed over the North Sea using a meteorological model and measurements of carbon isotopes**, *J. Geophys. Res. Atmos.*, 122, 7630-7645, doi: 10.1002/2017JD026626, 2017.

France, J., … Manning, A. J., et al.: **Using D13C in $CH_4$ and particle dispersion modelling to characterize sources of Arctic methane within an air mass**, *J. Geophys. Res*, 121, 14,257-14,270, doi: 10.1002/2016JD026006, 2017.

Graziosi, F., … O'Doherty, S., Young, D. and Maione, M.: **European emissions of the powerful greenhouse gases hydrofluorocarbons inferred from atmospheric measurements and their comparison with annual national reports to UNFCCC**, *Atmos. Environ., 158, 85–97*, doi:10.1016/j.atmosenv.2017.03.029, 2017.

Harris, N.R., … Manning, A. J., et al.: Coordinated Airborne Studies in the Tropics (CAST). *Bull. Amer. Meteor. Soc.,* 98, 145–162, https://doi.org/10.1175/BAMS-D-14-00290.1, 2017.

Mahieu, E., … O'Doherty, S.: **Retrieval of HCFC-142b ($CH_3CClF_2$) from ground-based high-resolution infrared solar spectra: Atmospheric increase since 1989 and comparison with surface and satellite measurements**, *J. Quant. Spectrosc. Radiat. Transf., 186, 96–105*, doi:10.1016/j.jqsrt.2016.03.017, 2017.

Meinshausen, M., … O'Doherty, S., et al.: **Historical greenhouse gas concentrations for climate modelling (CMIP6),** *Geosci. Model Dev., 10(5), 2057–2116*, doi:10.5194/gmd-10-2057-2017, 2017.

Riddick, S., … Manning, A. J., et al.: **Estimating the size of a methane emission point-source at different scales: from local to landscape**, *Atmos. Chem. Phys*., 17, 7839-7851, doi: 10.5194/acp-17-7839-2017, 2017.

Rigby, M., … Young, D., O'Doherty, Ganesan, A. L., Manning, A. J., Simmonds, P. G., et al.: **Role of atmospheric oxidation in recent methane growth**, *Proc. Natl. Acad. Sci., 114(21), 5373–5377*, doi:10.1073/pnas.1616426114, 2017.

Saunois, M., … O'Doherty, S., et al.: **Variability and quasi-decadal changes in the methane budget over the period 2000–2012**, *Atmos. Chem. Phys., 17(18), 11135–11161*, doi:10.5194/acp-17-11135-2017, 2017.

Simmonds, P. G., Rigby, M., … O'Doherty, S., Young, et al.: **Changing trends and emissions of hydrochlorofluorocarbons (HCFCs) and their hydrofluorocarbon (HFCs) replacements**, *Atmos. Chem. Phys., 17(7), 4641–4655*, doi:10.5194/acp-17-4641-2017, 2017.

Zhang, G., … O'Doherty, S., et al.: **Ambient mixing ratios of atmospheric halogenated compounds at five background stations in China**, *Atmos. Environ., 160, 55–69*, doi:10.1016/j.atmosenv.2017.04.017, 2017.

Chipperfield, … O 'Doherty, S., Young, D., Simmonds, P. G., et al.: **Model sensitivity studies of the decrease in atmospheric carbon tetrachloride**, *Atmos. Chem. Phys, 16, 15741–15754*, doi:10.5194/acp-16-15741-2016, 2016.

Chirkov, M., … O'Doherty, S., Young, D., et al.: **Global HCFC-22 measurements with MIPAS: retrieval, validation, global distribution and its evolution over 2005–2012**, *Atmos. Chem. Phys., 16(5), 3345–3368*, doi:10.5194/acp-16-3345-2016, 2016.

Ganesan, A. L., Manning, A. J., … Young, O 'Doherty, S., et al.: **Quantifying methane and nitrous oxide emissions from the UK and Ireland using a national-scale monitoring network**, *Atmos. Chem. Phys, 15, 6393–6406*, doi:10.5194/acp-15-6393-2015, 2015.

Graziosi, F., … Manning, A. J., O'Doherty, S., Simmonds, P.G., et al.: **Emissions of carbon tetrachloride from Europe**, *Atmos. Chem. Phys., 16(20), 12849–12859*, doi:10.5194/acp-16-12849-2016, 2016.

Lunt, E. M., Rigby, M., Ganesan, A., Manning, A. J.: **Estimation of trace gas fluxes with objectively determined basis functions using reversible-jump Markov chain Monte Carlo**, *Geosci. Model Dev*., 9, 3213-3229, doi: 10.5194/gmd-9-3213-2016, 2016.

McNorton, J., … Rigby, M., O'Doherty, S., Young, D., et al.: **Role of OH variability in the stalling of the global atmospheric $CH_4$ growth rate from 1999 to 2006**, *Atmos. Chem. Phys., 16, 7943–7956*, doi:10.5194/acp-16-7943-2016

Obersteiner, F., … O'Doherty, S., et al.: **A versatile, refrigerant- and cryogen-free cryofocusing–thermodesorption unit for preconcentration of traces gases in air**, *Atmos. Meas. Tech., 9(11), 5265–5279*, doi:10.5194/amt-9-5265-2016, 2016.

Różański, K., O'Doherty, S., et al.: **Monitoring of greenhouse gases in the atmosphere – a Polish perspective**, *Pap. Glob. Chang. IGBP, 23(1), 111–126*, doi:10.1515/igbp-2016-0009, 2016.

Saunois, M., … O'Doherty, S., et al.: **The global methane budget 2000–2012**, *Earth Syst. Sci. Data, 8(2), 697–751*, doi:10.5194/essd-8-697-2016, 2016.

Say, D., Manning, A. J., O'Doherty, S., Rigby, M., Young, D. and Grant, A.: **Re-evaluation of the UK's HFC-134a emissions inventory based on atmospheric observations**, *Environ. Sci. Technol., 50(20), 11129–11136*, doi:10.1021/acs.est.6b03630, 2016.

Simmonds, P. G., Rigby, M., Manning, A. J., …O'Doherty, S., Young, D., Arnold, T., et al.: **Global and regional emissions estimates of 1,1-difluoroethane (HFC-152a, $CH_3CHF_2$) from in situ and air archive observations**, *Atmos. Chem. Phys., 16(1), 365–382*, doi:10.5194/acp-16-365-2016, 2016.

Trudinger, C. M., … Rigby, M., O'Doherty, S., et al.: **Atmospheric abundance and global emissions of perfluorocarbons $CF_4$, $C_2F_6$ and $C_3F_8$ since 1900 inferred from ice core, firn, air archive and in situ measurements**, Atmos. Chem. Phys., 16, 11733–11754, doi:10.5194/acp-16-11733-2016, 2016.

Vollmer, M. K., … M., Rigby, M., D., Young, D., O'Doherty, S., Simmonds, P. G., et al.: **Atmospheric histories and global emissions of halons H-1211 ($CBrClF_2$), H-1301 ($CBrF_3$), and H-2402 ($CBrF_2CBrF_2$)**, *J. Geophys. Res. Atmos., 121(7), 3663–3686*, doi:10.1002/2015JD024488, 2016.

## *1.7 Meetings*

- **AGAGE meeting (Bologna, Italy, October 2017)**
- **DECC contract meeting (London, November 2017)**
- **NISC meeting (London, November 2017)**
- **DECC contract meeting (London, February 2018)**
- **DECC contract meeting (London, April 2018)**

- **NISC meeting (London, April 2018)**
- **AGAGE meeting (Beijing, China, May 2018)**
- **DECC network meeting (Royal Tunbridge Wells, July 2018)**

## *1.8 Related information*

Project websites:
www.metoffice.gov.uk/atmospheric-trends
and
www.gov.uk/government/publications/uk-greenhouse-gas-emissions-monitoring-and-verification

Methodology Report (Dec 2015)

Technical Document (May 2016)

# 2 Instrumentation

## *2.1 Sites*

A brief summary of site operations over the last year is presented here. A more detailed account of the instruments and their operations is presented in the methodology report and at http://www.metoffice.gov.uk/research/monitoring/atmospheric-trends/instrumentation. All UK DECC data are available from EBAS (http://ebas.nilu.no/), the MHD data are also available from ESS-DIVE (https://ess-dive.lbl.gov/).

### 2.1.1 Mace Head (MHD)

- Medusa GC-MS: The Medusa has encountered a number of problems over the past 12-months. The GO back-pressure regulator (BPR) in the air sample module was dismantled on 4th July 2017 as the delivery pressure continually fluctuated, and the BPR was found to be dirty. The BPR was cleaned and reassembled; however, it became obvious that contamination from R-410A refrigerant (HFC-32 and HFC-125 escaping from a leak in the air-conditioner) was getting into the air sample module and effecting the ambient air analysis. On 19th July 2017 a pump was setup to blow outside air over the air sample module (a method that had worked previously). The air-conditioner contamination resulted in data loss for HFC-32 and HFC-125 between 30th June and 19th July 2017. On 13th Sept 2017, the Mass Spectrometer (MS) was shutdown to replace filaments 1 & 2. Upon restart, the MS acquired two samples before filament 1 and 2 appeared to fail. The filaments were inspected and shown to be intact, and a number of tests were then run on the instrument without resolving the problem. An Agilent engineer was called to site. After extensive component replacements (side board and main board) it was determined that the MS failure was an issue with the ion-source. A further complication was caused when the Agilent engineer used Chemstation software to control the 5975 MSD. This resulted in a change to the firmware and GCWerks was unable to communicate with the MS. This issue was fixed by uploading and flashing a necessary module to the MS. In total there were 41 days data loss. In mid-December, 2-weeks of data was lost due to a failing filament. A period of data from 24th April to 30th April 2018 was lost when the new quaternary (H-340) inlet pressure was not matched correctly with the ambient air inlet pressure.
- GC-MD: The MD has generally continued to run well. In August 2017 the new tertiary standard J-206 showed signs of CFC-11 drift. In addition, on 9th May 2018, H-344 also showed signs of drift/contamination. After extensive investigation it was determined that the sample regulators were contaminated and needed replacing at the next tert/quat change. Noticeable retention time drift occurred for $CH_4$ (channel0). It appeared to be caused by an increasing imbalance between inline and backflush flows and was

temporarily corrected by adjusting the backflush needle valves. All needle valves were replaced; however, the issue remained. Removal and cleaning the valve 4 channel0 backflush valve rotor on 25th May, appears to have resolved the issue. Non-linearity tests using a range of calibration tanks (including three NOAA standards) were conducted on 18th April 2018. A new 10-port Valco valve was connected to the MD to facilitate the analysis of such a large number of tanks as well as automate periodic future calibrations.

### 2.1.2 Tacolneston (TAC)

- General: A critical lab air-conditioner failure resulted in the temperature inside the mobile laboratory reaching > 60 ˚C on 4th September 2017. All instruments were shutdown to reduce the heat load into the lab. A new air-conditioner unit was installed on 13th October 2017. The CRDS, OA-ICOS and GC-MD were restarted one at a time once the temperature in the laboratory had stabilised, with the Medusa being the last to be restarted on 7th November 2017. A computer crash on 26th April 2018 resulted in 4 days data loss for all instruments until a site visit was made to hard-reset the instrument. Reduced flow on the 185m sample inlet line caused by a potential blockage was cleared by back-pressuring and flushing the line with zero air in November and December 2017, as well as at a higher pressure (40 psig) in January 2018. A leak developed on a water trap at the base of the tower associated with the 185m sample line on 19th December 2017. As a temporary solution, the 54m line water trap was swapped with the 185m line to maintain measurements on the highest inlet as it is used by all instruments. The 54m line was removed from sampling until the trap was replaced on 2nd January 2018, resulting in 17 days data loss from the 54m line for the CRDS and OA-ICOS.
- Medusa GC-MS: The air-conditioner failure in Autumn 2017 resulted in 64 days of data loss. A faulty baseplate Omega temperature controller was replaced on 6th November 2017. The EPC5 (helium pressure controller) developed a leak and the instrument was stopped on 10th November 2017. An Agilent engineer was able to visit site to replace the EPC unit and site boards to the GC-MS on 23rd January 2018, resulting in 74 days data loss. The downstream All-Sensor pressure sensor malfunctioned on 24th January 2018 but was replaced on 20th February 2018. The ion source was replaced on 13th March 2018. A new PoraBOND Q column was fitted in the GC on 26th June 2018 and new ion acquisition and integration parameters set on the same day.
- GC-MD: Operated well over the reporting period. The main cause of data loss was caused by the air-conditioner failure in Autumn 2017, resulting in 42 days of data loss. The sample module Omega temperature controller failed on 3rd November 2017, resulting in the heated valve box being at ambient temperature – the data was not negatively affected. The instrument nonlinearity was reassessed using a suite of 7 cylinders spanning ambient to polluted concentrations between 5th and 8th February 2018. The instrument was decommissioned on 13th March 2018.
- CRDS: The CRDS has been running well, apart from the air-conditioner failure in Autumn 2017, resulting in 42 days of data loss. Picarro engineers logged on remotely to adjust the laser temperatures to improve the cycle time of the instrument on 21st November 2017 and 8th May 2018.
- OA-ICOS: The OA-ICOS has been running well over the reporting period, apart from the air-conditioner failure in Autumn 2017, resulting in 42 days of data loss. A hard reset of the instrument resulted in GCWerks sampling not being properly restarted on 5th Dec 2017 resulting in 3 days data loss.

### 2.1.3 Ridge Hill (RGL)

- General: The water traps at the base of the tower were changed on 23rd March 2018 for both 45 and 90 m inlets.
- GC-MD: The GC-MD has been running well over the past 12 months. Four cylinders spanning below and above ambient $N_2O$ mole fractions were installed in May 2017 and were analysed on the instrument until 12th August 2017 to characterise instrument

nonlinearity. A number of aborted drivers on the instrument were caused by the USB-serial board crashing (used to control/communicate with the Valco valves, All-Sensor and mass flow controller). The USB-serial board was replaced with a Moxa Nport 5450 serial hub on 2nd November 2017. A gas leak developed on the P5 carrier gas line and was detected on 23rd March 2018. The carrier gas tubing was replaced the same day.

- CRDS: The CRDS has been working well over the last 12 months. Sampling was changed from 30 minutes on each air inlet to 50 minutes on the highest inlet (90 m) and 10 minutes on the lowest inlet (45 m) on the 18th October 2017 to harmonise sampling with the rest of the network. The 45 m inlet pump failed on 12th February 2018 and was replaced 7 days later, resulting in 7 days data loss from the 45 m inlet. A temperature error resulted in the CRDS shutting down on 19th April 2018 until the instrument was restarted on 25th April 2018, resulting in 6 days data loss. A mis-calibration resulted in the CRDS not registering the $H_2O$ peak from 7th May 2018 until a Picarro engineer logged on remotely and changed the laser temperature settings and recalibrated the instrument the next day, resulting in 1 day of data loss.

### 2.1.4 Bilsdale (BSD)

- General: The 248 m line pump failed on 8th March 2018 and was replaced on 22nd March 2018, resulting in 13 days data loss.
- GC-MD: The MD at Bilsdale has been running well during the past 12 months. Four cylinders spanning below and above ambient $N_2O$ mole fractions were installed on 22nd August 2017 and were analysed on the instrument overnight to investigate instrument nonlinearity. An alarm shutdown caused by the USB-serial board crashing resulted in 2 days data loss from 5th September 2017. As per Ridge Hill, it is planned to replace this USB-serial unit with a Moxa NPort 5450 in the near future.
- CRDS: The CRDS has also been working well over the last 12 months. On 7th September 2017 a labair sampling line was added to V1-6 on the frontend system to check potential contamination contributions from leakage of labair for $CO_2$ and $CH_4$.

### 2.1.5 Heathfield (HFD) (Affiliated to UK DECC Network)

- General: The 50 m inlet filter blocked on 26th September 2017 resulting in data loss until both inlet filters were replaced on 19th December 2017. Only the CRDS samples from the 50 m inlet, so no GC-MD data was lost. The 50 m inlet pump failed on 21st March 2018 and was replaced on 26th April 2018. In July 2017 daily lab air sampling was added to the sampling system on the second multi-position valve. These measurements showed a higher amount of methane than the ambient samples, which is likely from the GC-MD carrier gas. The GC-MD detector vent was re-routed to minimise contamination.
- GC-MD: As described in the 2017 report, there was a period of poor precision until July 2017 when a small air leak was found in the column. During this time, a drift in the mole fraction of $N_2O$ and $SF_6$, compared to MHD, became apparent. This was traced to an insufficient time delay between sampling and injection: the pressure in the sampling loop decays to ambient for the air sample but not the standard. The consequence is that a slightly larger amount of standard is injected, causing the air sample to be calibrated too low. This resulted in 33 days data loss from February 2017 and another 91 days from July 2017. The pressure of the standard was also high in December 2017 due to the tank running low resulting in 75 days data loss. The standard tank H-234 was replaced by H-245 in February 2018; H-234 has returned to MHD for calibration and re-filling. Alarm shutdown events occurred in May 2018 due to USB-serial board failure resulting in 1-day data loss. The system was restarted remotely. As with Ridge Hill and Bilsdale this will be replaced with a Moxa NPort 5450 soon.
- CRDS: The CRDS has been running well over the year. On 6th March 2018 the standard H-285 was replaced by a tank filled at Weybourne, designated UEA-001. This is a temporary replacement until a MHD-filled tank calibrated at EMPA has been received; the mole fraction of methane, carbon dioxide and carbon monoxide in tank UEA-001 have been estimated by comparison with H-285.

# 3 Annual Northern Hemispheric trends

## *3.1 Baseline Mole Fractions*

For each gas observed at Mace Head a baseline analysis has been performed. ECMWF meteorology is used from 1989 – 2002 inclusive and Met Office meteorology from 2003 – 2018 inclusive. For each gas, monthly and annual northern hemisphere (NH) baselines, annual growth rates and the average seasonal cycle seen within the observations are calculated. Table 1 – Table 4 summarises the annual baseline mole fractions for each of the gases observed.

| Year | $CH_4$ | $N_2O$ | $CO_2$ | HFC-125 | HFC-134a | HFC-143a | HFC-152a | HFC-23 | HFC-32 |
|---|---|---|---|---|---|---|---|---|---|
| | ppb | ppb | ppm | ppt | ppt | ppt | ppt | ppt | ppt |
| 1990 | 1787 | 309 | | | | | | | |
| 1991 | 1810 | 310 | | | | | | | |
| 1992 | 1798 | 310 | | | | | | | |
| 1993 | 1811 | 310 | 357 | | | | | | |
| 1994 | 1810 | 311 | 359 | | | | | | |
| 1995 | 1815 | 312 | 360 | | 2 | | 1.2 | | |
| 1996 | 1818 | 313 | 361 | | 4 | | 1.2 | | |
| 1997 | 1818 | 314 | 364 | | 6 | | 1.3 | | |
| 1998 | 1828 | 314 | 366 | | 9 | | 1.7 | | |
| 1999 | 1831 | 315 | 368 | 1.4 | 13 | | 2.1 | | |
| 2000 | 1832 | 316 | 369 | 1.7 | 17 | | 2.4 | | |
| 2001 | 1834 | 317 | 371 | 2.2 | 21 | | 2.8 | | |
| 2002 | 1835 | 318 | 373 | 2.6 | 25 | | 3.4 | | |
| 2003 | 1843 | 319 | 375 | 3.2 | 29 | | 4.0 | | |
| 2004 | 1842 | 319 | 377 | 3.8 | 34 | 5.4 | 4.7 | | 1.0 |
| 2005 | 1841 | 320 | 379 | 4.6 | 39 | 6.3 | 5.5 | | 1.5 |
| 2006 | 1835 | 320 | 381 | 5.3 | 43 | 7.4 | 6.6 | | 2.0 |
| 2007 | 1845 | 321 | 384 | 6.2 | 48 | 8.3 | 7.8 | | 2.7 |
| 2008 | 1858 | 322 | 385 | 7.4 | 53 | 9.5 | 8.6 | 22.4 | 3.3 |
| 2009 | 1862 | 323 | 387 | 8.5 | 57 | 10.6 | 8.8 | 22.9 | 4.0 |
| 2010 | 1867 | 324 | 389 | 9.9 | 63 | 11.8 | 9.4 | 23.6 | 5.1 |
| 2011 | 1870 | 325 | 391 | 11.6 | 68 | 13.0 | 9.8 | 24.6 | 6.4 |
| 2012 | 1876 | 326 | 393 | 13.4 | 73 | 14.4 | 10.0 | 25.4 | 7.6 |
| 2013 | 1881 | 327 | 396 | 15.4 | 78 | 15.8 | 9.8 | 26.6 | 9.1 |
| 2014 | 1897 | 328 | 398 | 17.8 | 84 | 17.3 | 9.9 | 27.8 | 10.9 |
| 2015 | 1907 | 329 | 401 | 20.1 | 89 | 18.7 | 9.8 | 28.7 | 12.9 |
| 2016 | 1916 | 329 | 404 | 22.5 | 96 | 20.3 | 9.8 | 29.5 | 14.9 |
| 2017 | 1920 | 330 | 406 | 25.7 | 102 | 22.1 | 9.8 | 30.5 | 18.3 |
| | | | | | | | | | |
| AvGrow | 4.91 | 0.80 | 2.03 | 1.33 | 4.6 | 1.29 | 0.40 | 0.9 | 1.32 |
| AvGr12 | 4.91 | 1.08 | 2.58 | 2.96 | 6.6 | 1.71 | -0.04 | 1.0 | 3.06 |

**Table 1: Annual northern hemisphere baseline mass mixing ratios for Kyoto gases measured at Mace Head (ppt unless stated) and growth rates (ppt $yr^{-1}$ unless stated). AvGrow = Average growth since records began and AvGr12 = Average growth over most recent year.**

| Year | HFC-227ea | HFC-4310mee | HFC-365mfc | PFC-14 | PFC-116 | PFC-218 | PFC-318 | $SF_6$ | $NF_3$ |
|---|---|---|---|---|---|---|---|---|---|
| | ppt | ppt | ppt | ppt | ppt | ppt | ppt | ppt | ppt |
| 2004 | | | | 74.8 | 3.6 | 0.4 | | 5.5 | |
| 2005 | | | 0.3 | 75.4 | 3.7 | 0.4 | | 5.8 | |
| 2006 | | | 0.4 | 76.1 | 3.8 | 0.5 | | 6.0 | |
| 2007 | 0.5 | | 0.5 | 76.8 | 3.9 | 0.5 | | 6.3 | |
| 2008 | 0.5 | | 0.6 | 77.6 | 4.0 | 0.5 | | 6.6 | |
| 2009 | 0.6 | | 0.6 | 78.1 | 4.0 | 0.5 | | 6.9 | |
| 2010 | 0.7 | | 0.7 | 78.7 | 4.1 | 0.5 | | 7.1 | |
| 2011 | 0.8 | 0.2 | 0.8 | 79.4 | 4.2 | 0.6 | 1.3 | 7.5 | |
| 2012 | 0.9 | 0.2 | 0.8 | 80.2 | 4.3 | 0.6 | 1.4 | 7.8 | |
| 2013 | 1.0 | 0.2 | 0.9 | 81.0 | 4.4 | 0.6 | 1.4 | 8.1 | |
| 2014 | 1.1 | 0.3 | 1 | 81.7 | 4.4 | 0.6 | 1.5 | 8.4 | 1.2 |
| 2015 | 1.2 | 0.3 | 1.1 | 82.5 | 4.5 | 0.6 | 1.5 | 8.7 | 1.4 |
| 2016 | 1.3 | 0.3 | 1.2 | 83.3 | 4.6 | 0.6 | 1.6 | 9.1 | 1.5 |
| 2017 | 1.4 | 0.3 | 1.2 | 84.2 | 4.7 | 0.6 | 1.6 | 9.4 | 1.7 |
| | | | | | | | | | |
| AvGrow | 0.10 | 0.01 | 0.07 | 0.73 | 0.08 | 0.02 | 0.05 | 0.30 | 0.16 |
| AvGr12 | 0.13 | 0.00 | 0.05 | 0.83 | 0.09 | 0.01 | 0.06 | 0.34 | 0.18 |

**Table 2: Annual northern hemisphere baseline mass mixing ratios for Kyoto gases measured at Mace Head (ppt) and growth rates (ppt $yr^{-1}$). AvGrow = Average growth since records began and AvGr12 = Average growth over most recent year.**

| Year | CFC-11 | CFC-12 | CFC-113 | HCFC-124 | HCFC-141b | HCFC-142b | HCFC-22 | HFC-236fa | HFC-245fa | $SO_2F_2$ | $CH_3Cl$ | $CH_2Cl_2$ |
|---|---|---|---|---|---|---|---|---|---|---|---|---|
| | ppt | ppt | ppt | ppt | ppt | ppt | ppt | ppt | ppt | ppt | ppt | ppt |
| 1990 | 263 | 495 | 74.9 | | | | | | | | | |
| 1991 | 267 | 505 | 81.6 | | | | | | | | | |
| 1992 | 267 | 515 | 83.9 | | | | | | | | | |
| 1993 | 269 | 520 | 84.9 | | | | | | | | | |
| 1994 | 268 | 528 | 83.9 | | | | | | | | | |
| 1995 | 267 | 532 | 84.1 | | 5.2 | 7.9 | | | | | | |
| 1996 | 266 | 537 | 84.0 | | 7.3 | 9.2 | | | | | | 35.6 |
| 1997 | 264 | 540 | 83.5 | | 9.5 | 10.5 | | | | | | 35.4 |
| 1998 | 263 | 542 | 82.8 | | 11.4 | 11.3 | | | | | | 31.0 |
| 1999 | 261 | 543 | 82.3 | 1.3 | 13.1 | 12.3 | 144 | | | | 528 | 30.6 |
| 2000 | 260 | 545 | 82.0 | 1.4 | 15.0 | 13.5 | 150 | | | | 515 | 29.6 |
| 2001 | 258 | 546 | 81.2 | 1.5 | 16.2 | 14.5 | 157 | | | | 511 | 28.6 |
| 2002 | 256 | 546 | 80.4 | 1.6 | 17.5 | 15.0 | 163 | | | | 512 | 28.9 |
| 2003 | 254 | 546 | 79.7 | 1.6 | 18.5 | 15.5 | 168 | | | | 515 | 30.2 |
| 2004 | 252 | 545 | 79.0 | 1.6 | 19.1 | 16.2 | 173 | | | | 519 | 30.1 |
| 2005 | 250 | 544 | 78.4 | 1.6 | 19.0 | 16.9 | 179 | | | 1.4 | 520 | 29.8 |
| 2006 | 248 | 542 | 77.6 | 1.6 | 19.5 | 18.0 | 186 | | | 1.5 | 514 | 31.5 |
| 2007 | 246 | 540 | 76.8 | 1.6 | 20.2 | 19.2 | 194 | 0.1 | 1.0 | 1.5 | 530 | 33.8 |
| 2008 | 244 | 538 | 76.3 | 1.6 | 20.8 | 20.5 | 203 | 0.1 | 1.3 | 1.6 | 531 | 35.6 |
| 2009 | 242 | 535 | 75.7 | 1.5 | 21.2 | 21.3 | 211 | 0.1 | 1.4 | 1.6 | 533 | 36.1 |
| 2010 | 240 | 533 | 74.9 | 1.5 | 21.9 | 21.8 | 219 | 0.1 | 1.5 | 1.7 | 524 | 39.3 |
| 2011 | 238 | 530 | 74.4 | 1.4 | 23.0 | 22.6 | 225 | 0.1 | 1.8 | 1.8 | 514 | 38.6 |
| 2012 | 236 | 527 | 73.8 | 1.4 | 24.1 | 23.0 | 230 | 0.1 | 2.0 | 1.9 | 524 | |
| 2013 | 234 | 525 | 73.2 | 1.3 | 24.8 | 23.2 | 236 | 0.1 | 2.2 | 2.0 | 528 | |
| 2014 | 233 | 523 | 72.7 | 1.3 | 25.3 | 23.3 | 241 | 0.1 | 2.4 | 2.1 | 531 | |
| 2015 | 232 | 520 | 72.0 | 1.2 | 25.6 | 23.3 | 245 | 0.1 | 2.5 | 2.2 | 538 | |
| 2016 | 231 | 516 | 71.3 | 1.1 | 25.9 | 23.3 | 249 | 0.2 | 2.8 | 2.3 | 537 | |
| 2017 | 230 | 513 | 70.6 | 1.1 | 25.9 | 23.4 | 252 | 0.2 | 3.0 | 2.4 | 519 | |
| | | | | | | | | | | | | |
| AvGrw | -1.20 | 0.80 | -0.11 | -0.01 | 0.93 | 0.70 | 6.00 | 0.01 | 0.19 | 0.08 | -0.3 | 0.49 |
| AvG12 | -0.85 | -3.22 | -0.67 | -0.06 | 0.07 | 0.03 | 3.24 | 0.01 | 0.21 | 0.10 | -17.4 | |

**Table 3: Annual northern hemisphere baseline mass mixing ratios for other gases measured at Mace Head and growth rates (ppt $yr^{-1}$). AvGrow = Average growth since records began and AvGr12 = Average growth over most recent year.**

| Year | $CHCl_3$ | $CCl_4$ | $CH_3$-$CCl_3$ | $CCl_2$=$CCl_2$ | $CH_3Br$ | Halon-1211 | Halon-1301 | Halon-2402 | CO | $H_2$ | $O_3$ |
|---|---|---|---|---|---|---|---|---|---|---|---|
| | ppt | ppt | ppt | ppt | ppt | ppt | ppt | ppt | ppb | ppb | ppb |
| 1990 | | 108 | 150 | | | | | | | | 35.3 |
| 1991 | | | 150 | | | | | | | | 35.8 |
| 1992 | | 104 | 148 | | | | | | | | 34.7 |
| 1993 | | 103 | 138 | | | | | | | | 35.7 |
| 1994 | 10.8 | 103 | 124 | | | | | | | 501 | 36.5 |
| 1995 | 11.4 | 102 | 110 | | | | | | | 506 | 35.6 |
| 1996 | 11.5 | 101 | 95 | | | | | | | 509 | 37.5 |
| 1997 | 11.2 | 100 | 79 | | | | | | 116 | 505 | 36.5 |
| 1998 | 11.0 | 99 | 66 | | | | | | 143 | 520 | 40.5 |
| 1999 | 10.6 | 97 | 55 | | 10.8 | 4.1 | 2.7 | | 121 | 520 | 42.6 |
| 2000 | 10.4 | 97 | 46 | | 10.4 | 4.3 | 2.9 | | 117 | 510 | 41.1 |
| 2001 | 10.6 | 96 | 38 | 5 | 9.8 | 4.4 | 3.0 | | 112 | 505 | 41.1 |
| 2002 | 10.4 | 95 | 32 | 4.6 | 9.1 | 4.4 | 3.0 | | 118 | 508 | 40.7 |
| 2003 | 10.7 | 94 | 27 | 4.6 | 8.7 | 4.4 | 3.0 | | 134 | 511 | 41.6 |
| 2004 | 10.7 | 93 | 22 | 4.3 | 9.1 | 4.5 | 3.0 | 0.5 | 121 | 508 | 41.0 |
| 2005 | 10.6 | 92 | 18 | 3.7 | 10.1 | 4.5 | 3.1 | 0.5 | 121 | 510 | 39.9 |
| 2006 | 10.6 | 91 | 15 | 3.7 | 9.3 | 4.4 | 3.2 | 0.5 | 121 | 512 | 41.2 |
| 2007 | 10.7 | 90 | 13 | 3.6 | 9.1 | 4.4 | 3.2 | 0.5 | 122 | 511 | 41.0 |
| 2008 | 10.9 | 89 | 11 | 3.3 | 9.1 | 4.4 | 3.2 | 0.5 | 119 | 512 | 41.4 |
| 2009 | 10.6 | 88 | 9 | 2.9 | 8.6 | 4.3 | 3.2 | 0.5 | 113 | 510 | 40.6 |
| 2010 | 11.2 | 87 | 8 | 3.0 | 8.2 | 4.2 | 3.3 | 0.5 | 121 | 507 | 40.3 |
| 2011 | 10.9 | 86 | 6 | 2.7 | 8.3 | 4.1 | 3.3 | 0.4 | 115 | 515 | 40.4 |
| 2012 | 11.1 | 85 | 5 | 2.4 | 8.2 | 4.1 | 3.3 | 0.4 | 123 | 517 | 39.7 |
| 2013 | 12.2 | 83 | 4 | 2.3 | 8.2 | 3.9 | 3.4 | 0.4 | 118 | 518 | 41.6 |
| 2014 | 14.5 | 83 | | 2.4 | 7.6 | 3.9 | 3.4 | 0.4 | 123 | 514 | 40.3 |
| 2015 | 13.8 | 81 | | 2.5 | 7.4 | 3.7 | 3.4 | 0.4 | 121 | 514 | 40.8 |
| 2016 | 14.4 | 80 | 2 | 2.3 | 7.3 | 3.6 | 3.4 | 0.4 | 115 | 515 | 39.7 |
| 2017 | 15.2 | 79 | 2 | 2.3 | 7.3 | 3.5 | 3.4 | 0.4 | 112 | 517 | 41.2 |
| | | | | | | | | | | | |
| AvGrow | 0.17 | -1.0 | -5.7 | -0.16 | -0.16 | -0.04 | 0.03 | -0.01 | -0.5 | 0.5 | 0.23 |
| AvGr12 | 0.56 | -0.8 | -0.5 | -0.04 | -0.04 | -0.11 | 0.00 | -0.01 | -5.3 | 2.5 | 0.61 |

**Table 4: Annual northern hemisphere baseline mass mixing ratios for other gases measured at Mace Head and growth rates (ppt $yr^{-1}$ unless stated). AvGrow = Average growth since records began and AvGr12 = Average growth over most recent year.**

# 4 Regional emission estimation

## *4.1 Introduction*

This chapter presents the InTEM inversion results, showing the atmospheric trends and regional emissions of the gases that are measured in the UK DECC network and that are reported to the UNFCCC (United Nations Framework Convention on Climate Change). For each gas, the mid-latitude Northern Hemisphere baselines are presented, followed by the UK estimated emissions, where a comparison is made to the reported inventory values (April 2018 submission).

InTEM is briefly presented but for more information the reader is referred to the Methodology report. The uses, atmospheric lifetimes, and global warming potentials for the different gases reported under the UNFCCC are presented in Table 5.

## *4.2 Summary of InTEM inverse modelling*

Each observation is comprised of two parts; a time-varying Northern Hemisphere baseline concentration and a perturbation above baseline. The perturbations above baseline, observed across the UK DECC network, are driven by emissions on regional scales that have yet to be fully mixed on the hemisphere scale and are the principle information used to estimate surface emissions across north-west Europe. A method for estimating emissions from observations, referred to as 'Inversion Technique for Emission Modelling' (InTEM), has been developed over many years and is used here to estimate UK emissions using the observations from the UK DECC network, and other networks where available.

InTEM links the observation time-series with the 2-hour NAME air history estimates of how surface emissions dilute as they travel to the observation stations. An estimated emission distribution, when combined with the NAME output, can be transformed into a modelled time-series at each of the measurement stations. The modelled and the observed time-series can be compared using a single or a range of statistics (referred to as cost functions) to produce a skill score for that particular emission distribution. InTEM uses a Bayesian statistical technique with a non-negative least squares solver to find the emission distributions that produces the modelled times-series at each observation station that has the best statistical match to the observations. The Bayesian method requires the use of a prior emission distribution with associated uncertainties as the starting point for the inversion. The prior information can influence and inform the inversion (posterior) solution. In this work the prior emission information has been obtained from the EDGAR v4.2 FT2010 database, using the 1990, 1995, 2000, 2005 and 2010 estimates, as appropriate. However, to preserve the independence of the inversion results presented here from the prior estimates, the priors chosen for the UK and Ireland were unconstrained by geographical distribution within each country (i.e. a uniform or flat prior over each country) and given very large uncertainties (±10,000%); this ensured the inversion was negligibly constrained by the prior over these regions, and thus dominated by the impact of the observations. For the rest of the domain, each defined geographical region (France, Spain/Portugal, Germany, Benelux, Denmark, Norway, SE Europe, NE Europe) also had no geographical distribution within each region but used a reduced uncertainty of +/- 50%. The outer domain regions, as discussed in the May 2017 6-month report, were likewise specified with +/- 50% uncertainty.

For InTEM to provide robust solutions for every area within the modelled domain, each region needs to significantly contribute to the air concentrations at the UK DECC network sites on a reasonable number of time periods. If the signal from an area is only rarely or poorly seen by the network, then its impact on the cost function is minimal and the inversion method will have little skill at determining its true emission. The contributions that different grid boxes make to the observed air concentration varies from grid to grid. Grid boxes that are distant from the observation site contribute little to the observation, whereas those that are close have a large

impact. To balance the contributions from different grid boxes, those that are more distant are grouped together into increasingly larger regions. The grouping cannot extend beyond country, region or Devolved Administration (DA) boundaries. The country boundaries extend into the surrounding seas to reflect both emissions from shipping, off-shore installations and river runoff but also because the inversion has geographical uncertainty.

For each greenhouse gas two types of inversion are performed. The first, using only Mace Head data, were performed with an inversion timeframe of 3 years. For $CH_4$ and $N_2O$, the inversions were started in 1989 to coincide with the availability of ECMWF ERA-Interim meteorology, for the other gases the inversions were started from when the observations were first available. For each gas 3-year inversions were performed covering entire calendar years. Each 3-year inversion was repeated 12 times, each time with the observations from 8, randomly chosen, blocks of 5-days per year removed from the dataset (approximately 10% of each year). Annual emission estimates were made by averaging the inversion results covering the appropriate year. The second type of inversion follows the same process but includes the observations from the UK DECC network (and HFD where available) and were performed over smaller inversion time-windows. For $CH_4$, $N_2O$ and $SF_6$, where observations are available from 5 or 6 sites, the inversion time-window was set to 1-year, for the remaining compounds, where only TAC and MHD data are available, the inversion time-window was 2-years. The repeating of each inversion multiple times and the random removal of ~10% of the observations from each inversion improves the estimates of uncertainty.

There are a range of uncertainties in the emissions that are estimated. Uncertainty arises from many factors: errors in the baseline estimate; emissions that vary over time-scales shorter than the inversion time-window e.g. diurnal, seasonal or intermittent; heterogeneous emissions i.e. emissions that vary within the regions solved for; errors in the transport model (NAME) or the underpinning 3-dimensional meteorology; errors in the observations themselves. The potential magnitudes of these uncertainties have been estimated and are incorporated within InTEM to inform the uncertainty of the modelled results.

At RGL, HFD, TAC and BSD $CH_4$ is observed at two or more heights. If, during a 2-hour period the observed $CH_4$ at different or the same height varies significantly, it is an indication that the meteorology is particularly complex and therefore the modelled meteorology will have significant uncertainty. In low boundary layer, low wind speed or stable conditions, it is also assumed that the meteorological model will have higher uncertainty. Such 2-hour periods are identified at each observation station and are excluded from the inverse modelling.

Estimating the model and observation uncertainty is an important part of InTEM. The observation uncertainty is estimated each day by repeatedly measuring the same tank of air. The standard deviation of these measurements is defined as the observation uncertainty for that day's observations of that gas. For the high frequency (1-minute) Picarro observations the variability over each 2-hour period is defined as the observation uncertainty. The model uncertainty is defined as having two components; a baseline uncertainty and a meteorological uncertainty. The baseline uncertainty is estimated during the fitting of the Northern Hemisphere baseline trend to the baseline observations. The meteorological uncertainty is proportional to the magnitude of the pollution event with a imposed minimum of the median pollution event for that gas for that year.

## *4.3 Summary of the greenhouse gases reported to the UNFCCC*

Table 5 describes the principle uses of each of the gases, their radiative efficiency, atmospheric lifetime and global warming potential in a 100-year framework ($GWP_{100}$).

| Gas | Chemical Formula | Main Use | Radiative Efficiency (W $m^{-2}ppb^{-1}$) | Atmos. lifetime (years) | $GWP_{100}$ |
|---|---|---|---|---|---|
| Methane | $CH_4$ | Landfill, farming, energy, wetlands | 0.00036 | 12.4 | 28 |
| Nitrous Oxide | $N_2O$ | Nylon manufacture, farming | 0.003 | 121 | 265 |
| Carbon Dioxide | $CO_2$ | Combustion | 0.0000138 | indefinite | 1 |
| HFC-125 | $CHF_2CF_3$ | Refrigeration blend, fire suppression | 0.23 | 28.2 | 3,170 |
| HFC-134a | $CH_2FCF_3$ | Mobile air conditioner | 0.16 | 13.4 | 1,300 |
| HFC-143a | $CH_3CF_3$ | Refrigeration blend | 0.16 | 47.1 | 4,800 |
| HFC-152a | $CH_3CHF_2$ | Aerosol propellant, foam-blowing agent | 0.10 | 1.5 | 138 |
| HFC-23 | $CHF_3$ | Bi-product of manufacture of HCFC-22 | 0.18 | 222 | 12,400 |
| HFC-32 | $CH_2F_2$ | Refrigeration blend | 0.11 | 5.2 | 677 |
| HFC-227ea | $CF_3CHFCF_3$ | Fire suppression, inhalers, foam blowing | 0.26 | 38.9 | 3,350 |
| HFC-245fa | $C_3H_3F_5$ | Blowing and insulation agent | 0.24 | 7.7 | 858 |
| HFC-43-10mee | $C_5H_2F_{10}$ | Electronics industry | 0.42 | 16.1 | 1,650 |
| HFC-365mfc | $C_4H_5F_5$ | Foam blowing | 0.22 | 8.7 | 804 |
| PFC-14 | $CF_4$ | Bi-product alum. production, electronics | 0.09 | 50,000 | 6,630 |
| PFC-116 | $C_2F_6$ | Electronics, bi-product alum. production | 0.25 | >10,000 | 11,100 |
| PFC-218 | $C_3F_8$ | Electronics, bi-product alum. production | 0.28 | 2,600 | 8,900 |
| PFC-318 | $C_4F_8$ | Semiconductor and electronics industries | 0.32 | 3,200 | 9,540 |
| Sulphur Hexafluoride | $SF_6$ | Circuit breaker in high voltage switchgear | 0.57 | 3,200 | 23,500 |
| Nitrogen Trifluoride | $NF_3$ | Electronics | 0.2 | 500 | 16,100 |

**Table 5: The principle use, radiative efficiency, atmospheric lifetime and 100-year global warming potential of the gases measured by the UK DECC network and that are reported to the UNFCCC. Data taken from the 5th IPCC Assessment Report Chapter 8 Appendix 8.A**

## 4.4 Methane ($CH_4$)

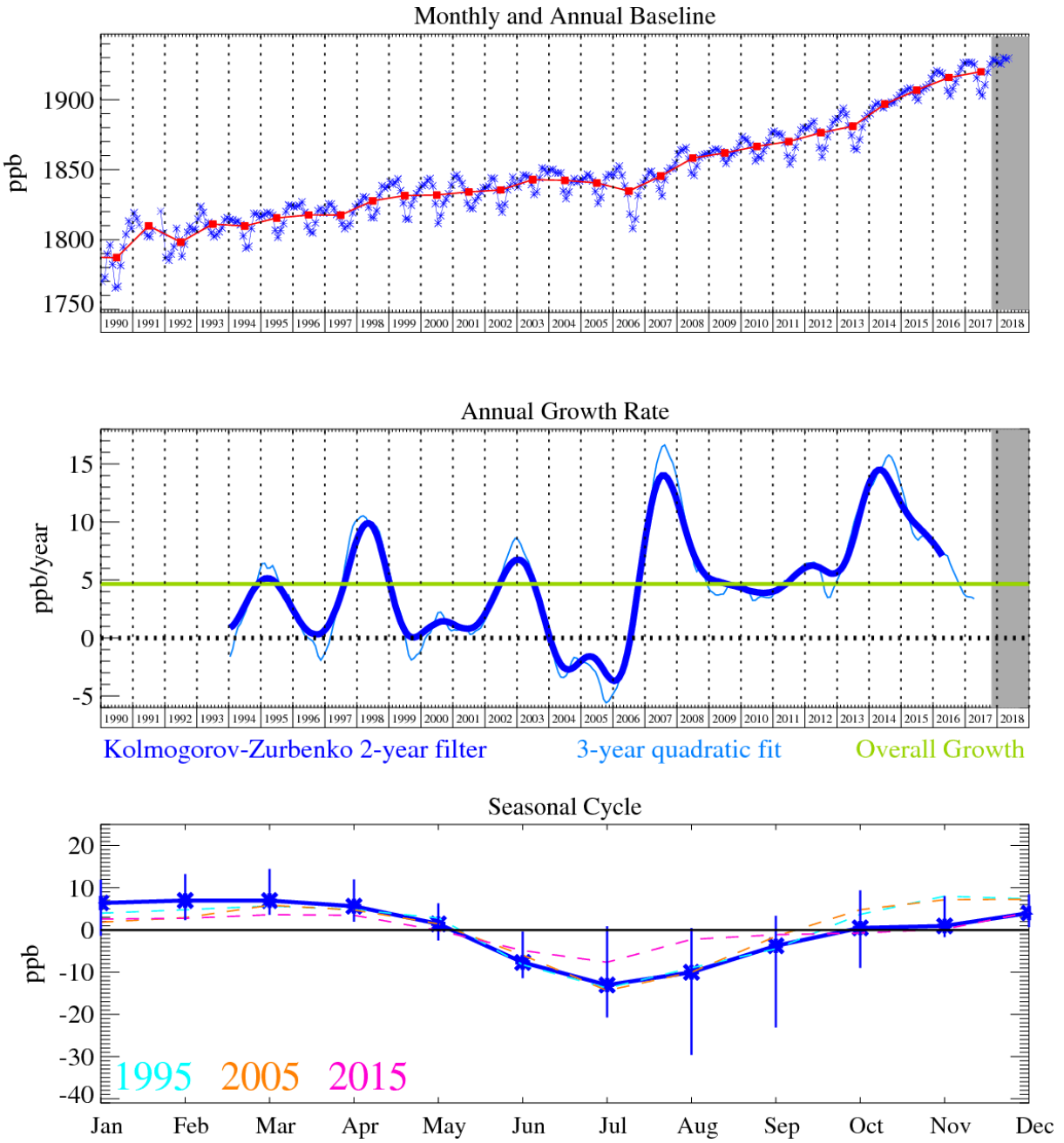


**Figure 1: Methane ($CH_4$): Monthly (blue) and annual (red) Northern Hemisphere baseline mole fractions (top plot). Annual (blue) and overall average growth rate (green) (middle plot). Seasonal cycle (de-trended) with year-to-year variability (lower plot). Grey area covers un-ratified and therefore provisional data.**

The amount of $CH_4$ in the atmosphere is continuing to grow at a strong rate although slowed to 5 ppb $yr^{-1}$ in 2017. It has a strong seasonal cycle, with the dip in the summer caused by its chemical removal by the OH radical.

The InTEM estimated emissions for the UK for $CH_4$ show a slower decline over the 28 years, from ~4000 Gg $yr^{-1}$ to ~2000 Gg $yr^{-1}$. The inventory has declined from 5400 Gg $yr^{-1}$ to 2100 Gg $yr^{-1}$ over the same period. Both methods have significant uncertainty, especially InTEM in the early 1990s when the observations were less precise. The uncertainties overlap from 2004 onwards. The use of the extended UK network from mid-2012, including the towers at Bilsdale (formerly GAUGE now in the UK DECC network) and Heathfield (formerly GAUGE now operated by NPL), has yielded results that are similar to the MHD-only inversions. The choice of meteorology to drive NAME, either global resolution (12-17 km) or UKV high resolution (1.5

km), makes a difference to the UK emission estimates, the InTEM estimates using UKV are higher by ~15%, although the uncertainties overlap strongly. This implies that NAME with UKV meteorology has greater mixing than with global meteorology. Planned observations of the true meteorology at the stations will help with the understanding of this difference.

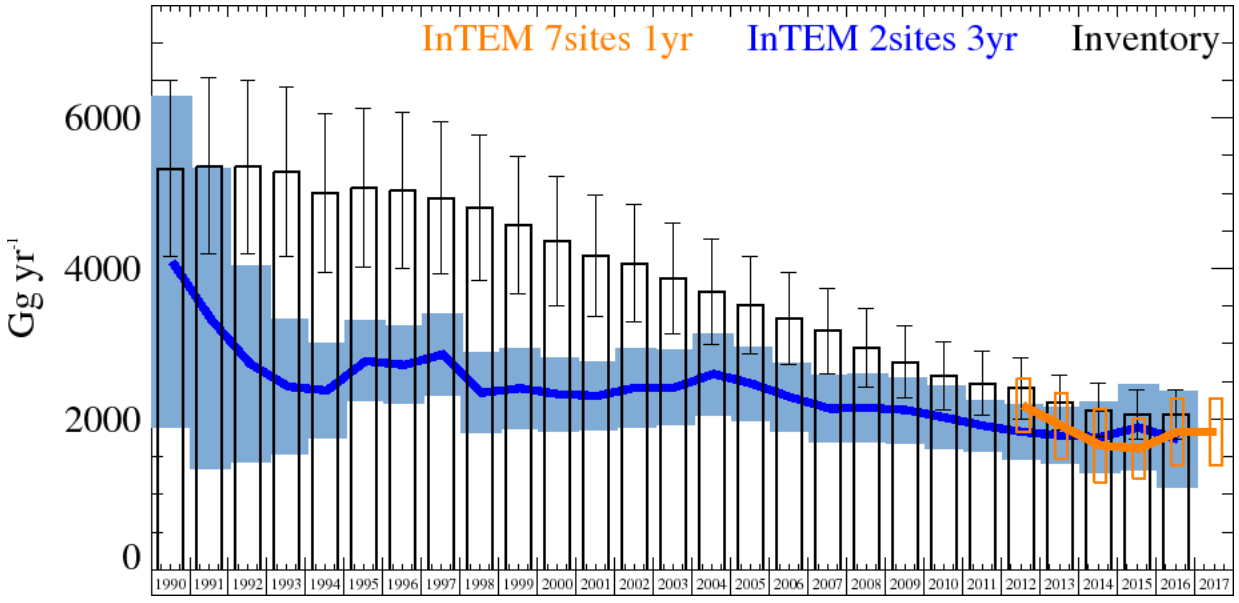


**Figure 2: $CH_4$ UK Emission estimates (Gg $yr^{-1}$) from the UNFCCC Inventory (black) and InTEM with global meteorology: 3-year MHD+CBW (blue) and 12-month DECC + GAUGE + CBW network (orange). The uncertainty bars represent 1 std.**

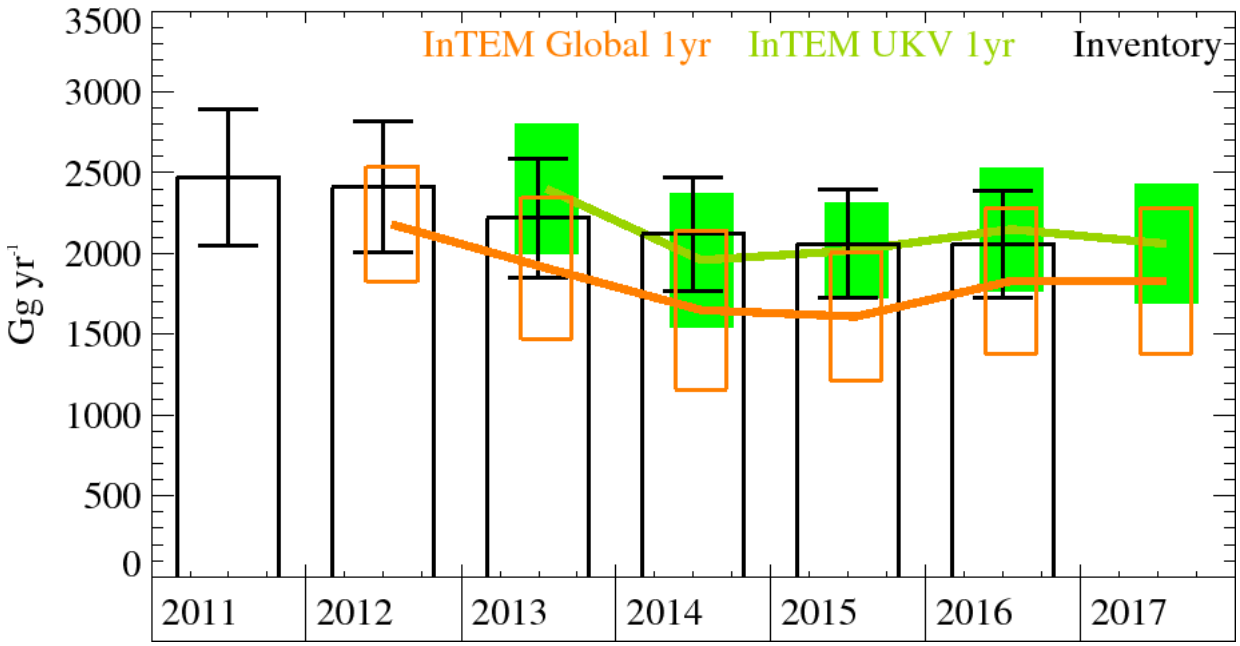


**Figure 3: $CH_4$ emission estimates for the UK (Gg $yr^{-1}$) from the UNFCCC Inventory (black) and InTEM using the DECC + GAUGE + CBW observations, 1-year inversions with different meteorology: (orange) global meteorology and (green) 1.5 km high resolution meteorology. The uncertainty bars represent 1 std.**

The average InTEM estimated spatial distribution of the emissions for $CH_4$ for 2004-2007 and 2014-2017 are shown in Figure 4 (a) and (b) respectively. The InTEM estimates use MHD+CBW observations, global meteorology and minimal prior information. The comparable average InTEM estimates for 2014-2017 using UKV meteorology and all available measurements (DECC+GAUGE+CBW) are shown in Figure 5, (a) uses minimal prior information and is solved in 1-year intervals, whilst (b) uses the NAEI and 3-month inversion intervals.

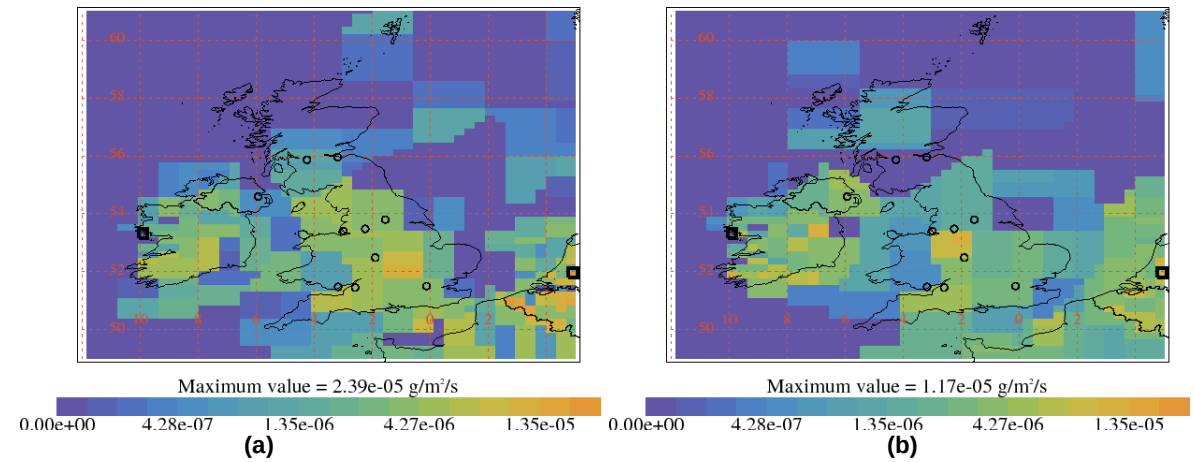


**Figure 4: InTEM estimates of spatial distribution of $CH_4$ emissions using global meteorology and MHD+CBW observations with minimal prior. Black squares are measurement stations and circles are major cities in UK. (a) Average 2004-2007 (b) Average 2014-2017.**

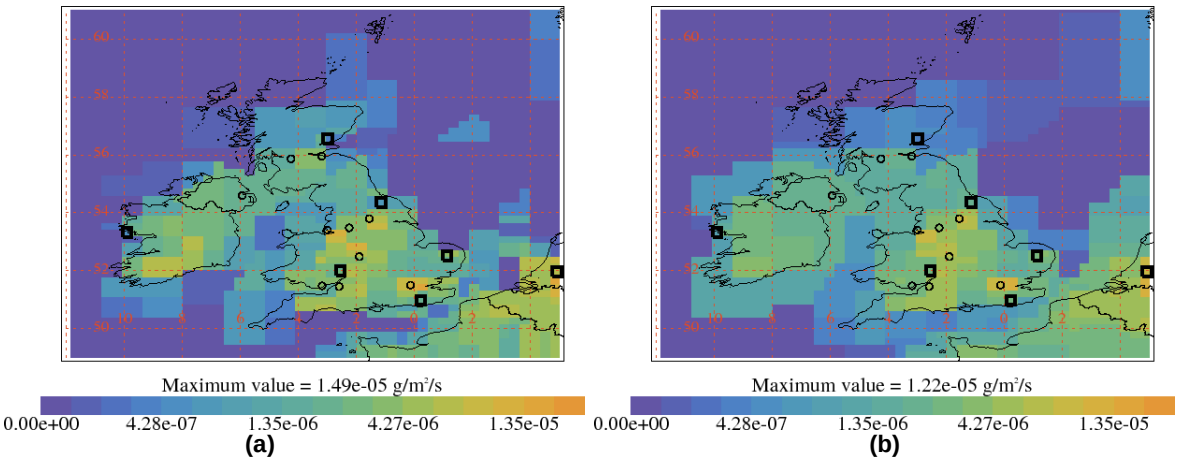


**Figure 5: Average InTEM estimates 2014-2017 of spatial distribution of $CH_4$ emissions using UKV meteorology and DECC+GAUGE+CBW observations. Black squares are measurement stations and circles are major cities in UK. (a) With minimal prior information (b) With NAEI prior.**

The standard InTEM setup uses a prior with minimal information meaning that the uncertainty of the prior emissions is set very high and the emissions are uniformly distributed. However, the UK inventory team produce a high resolution (1 km) emission map for $CH_4$ covering the UK, called the NAEI (National Atmospheric Emissions Inventory). The latest release is the 2015 map from the 2017 submission. A global inventory is produced by the EU Joint Research Centre (JRC) called the Emissions Database for Global Atmospheric Research (EDGAR) on a 0.5 degree resolution (~50 km), the latest release is for 2010. For each of the non-UK geographical regions the emissions have been uniformly distributed across the region and each region is defined to have a combined uncertainty of 50%. These two maps have been combined to produce a prior emission map covering the same domain as solved for in the InTEM inversions, the higher resolution NAEI (with a combined UK uncertainty of 40%) is used wherever available in preference to EDGAR. This prior has been used as extra information to allow 3-month InTEM inversions 2013-2017 using UKV meteorology. The results are compared to the inversions without the use of the UK NAEI prior information, Figure 6. The results are very comparable. The two inversion solutions are very close to the inventory from 2013 onwards.

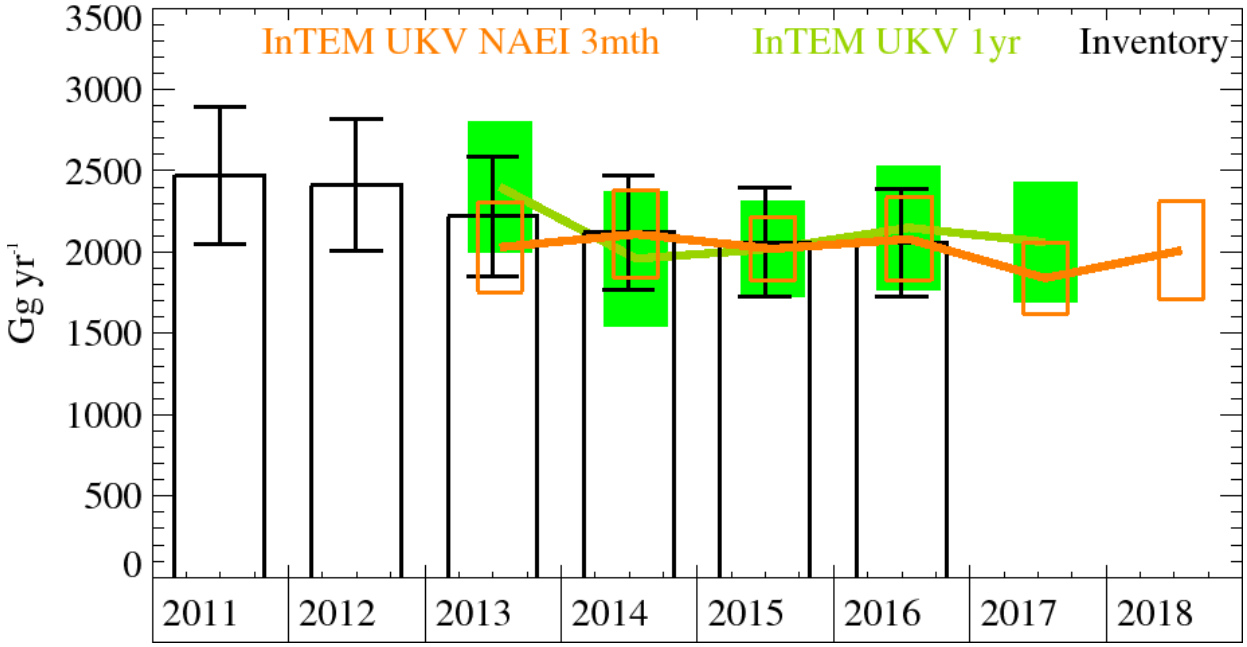


**Figure 6: $CH_4$ emission estimates for the UK (Gg $yr^{-1}$) from the UNFCCC Inventory (black) and InTEM using the DECC + GAUGE + CBW observations and 1.5 km high resolution meteorology with different priors: (green) 12-month inversions with minimal prior information and (orange) averaged 3-month inversions using NAEI 2015 prior.**

| Years | Inventory 1yr | MHD+CBW 3yr | DECC+CBW 1yr |
|---|---|---|---|
| 1990 | 5330. (4160.-6500.) | 4090. (1890.-6300.) | |
| 1991 | 5360. (4190.-6530.) | 3330. (1330.-5330.) | |
| 1992 | 5350. (4190.-6500.) | 2740. (1440.-4050.) | |
| 1993 | 5280. (4160.-6410.) | 2430. (1530.-3330.) | |
| 1994 | 5010. (3950.-6060.) | 2380. (1750.-3010.) | |
| 1995 | 5070. (4010.-6120.) | 2770. (2240.-3310.) | |
| 1996 | 5040. (4000.-6070.) | 2720. (2200.-3230.) | |
| 1997 | 4940. (3930.-5950.) | 2860. (2320.-3410.) | |
| 1998 | 4800. (3830.-5760.) | 2350. (1820.-2880.) | |
| 1999 | 4580. (3660.-5490.) | 2410. (1870.-2940.) | |
| 2000 | 4360. (3510.-5220.) | 2330. (1840.-2820.) | |
| 2001 | 4170. (3360.-4980.) | 2310. (1850.-2770.) | |
| 2002 | 4070. (3290.-4850.) | 2420. (1890.-2950.) | |
| 2003 | 3870. (3130.-4600.) | 2420. (1910.-2920.) | |
| 2004 | 3690. (3000.-4390.) | 2600. (2060.-3150.) | |
| 2005 | 3510. (2860.-4150.) | 2470. (1990.-2960.) | |
| 2006 | 3330. (2720.-3940.) | 2290. (1840.-2740.) | |
| 2007 | 3170. (2600.-3740.) | 2140. (1700.-2580.) | |
| 2008 | 2940. (2410.-3460.) | 2150. (1700.-2610.) | |
| 2009 | 2760. (2280.-3250.) | 2120. (1680.-2560.) | |
| 2010 | 2580. (2130.-3030.) | 2020. (1600.-2440.) | |
| 2011 | 2470. (2050.-2900.) | 1910. (1560.-2250.) | |
| 2012 | 2410. (2000.-2810.) | 1830. (1470.-2190.) | 2180. (1830.-2540.) |
| 2013 | 2220. (1850.-2590.) | 1780. (1400.-2150.) | 1910. (1470.-2350.) |
| 2014 | 2120. (1770.-2470.) | 1760. (1290.-2240.) | 1650. (1160.-2140.) |
| 2015 | 2060. (1730.-2400.) | 1890. (1320.-2460.) | 1610. (1210.-2000.) |
| 2016 | 2060. (1730.-2390.) | 1730. (1090.-2370.) | 1830. (1380.-2280.) |
| 2017 | | | 1830. (1380.-2280.) |

**Table 6: $CH_4$ emission (Gg $yr^{-1}$) estimates for the UK with uncertainty (1std).**

## 4.5 Nitrous oxide ($N_2O$)

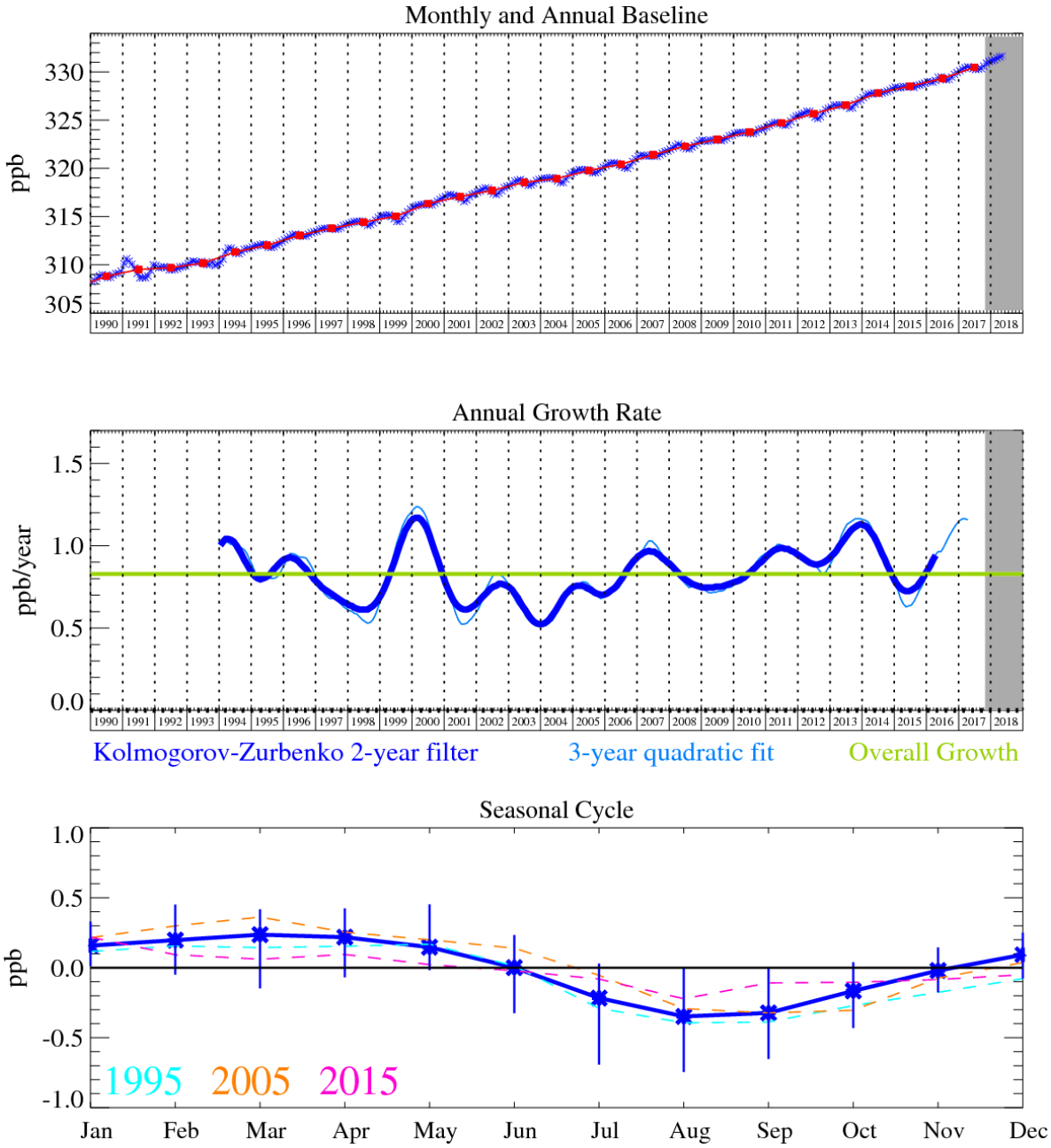


**Figure 7: Nitrous oxide ($N_2O$): Monthly (blue) and annual (red) Northern Hemisphere baseline mole fractions (top). Annual (blue) and overall growth rate (green) (middle). Seasonal cycle (de-trended) with year-to-year variability (lower plot). Grey area covers un-ratified and therefore provisional data.**

The atmospheric concentration of $N_2O$ continues to grow strongly in the atmosphere. The seasonal cycle in the baseline is driven by the seasonal cycle in the interaction of the stratosphere (relatively low concentration) with the troposphere (relatively high concentration). The stratosphere is the main atmospheric sink of $N_2O$.

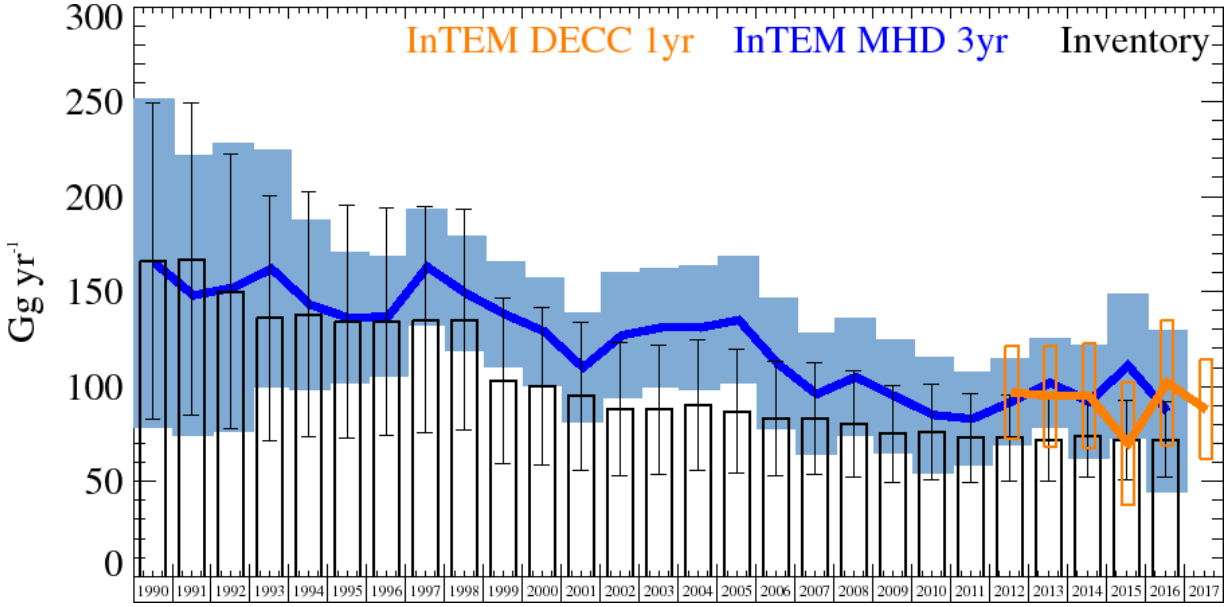


**Figure 8: $N_2O$ UK Emission estimates (Gg $yr^{-1}$) from the UNFCCC Inventory (black) and InTEM with global meteorology: 3-year MHD (blue) and 12-month DECC + GAUGE network (orange). The uncertainty bars represent 1 std.**

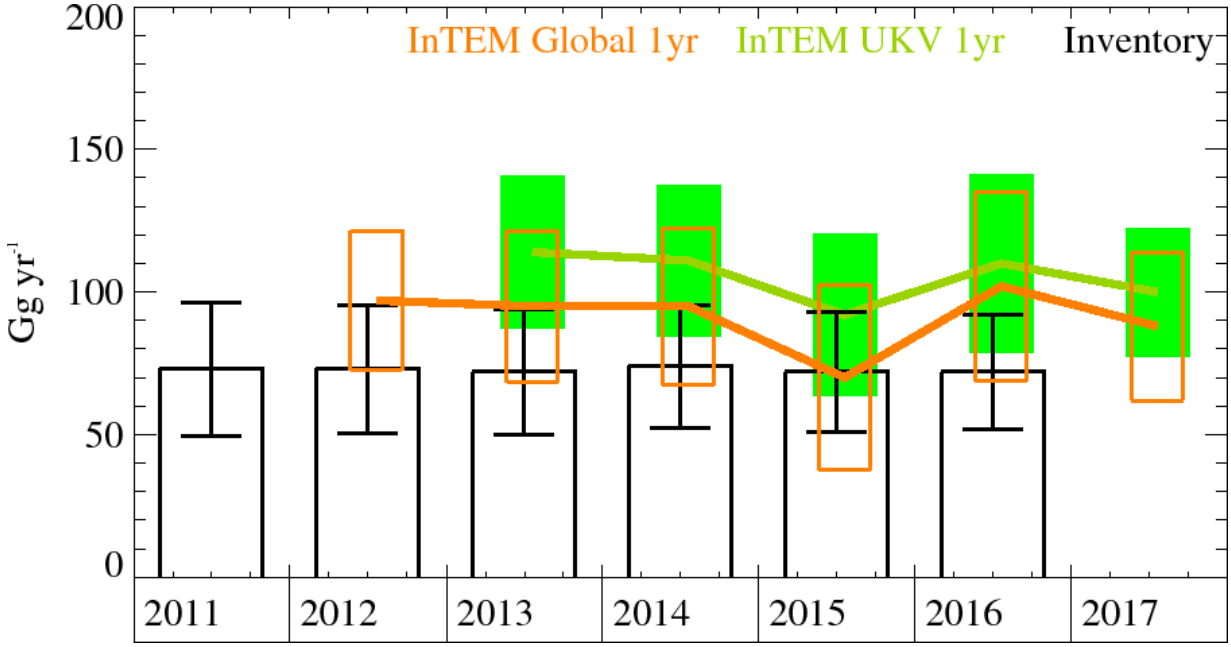


**Figure 9: $N_2O$ emission estimates for the UK (Gg $yr^{-1}$) from the UNFCCC Inventory (black) and InTEM using the DECC + GAUGE observations, 1-year inversions with different meteorology: (orange) global meteorology and (green) 1.5 km high resolution meteorology. The uncertainty bars represent 1 std.**

The UK inventory and InTEM estimates are in good agreement until 1996 after which time the InTEM estimates are larger by ~20 Gg $yr^{-1}$ although the uncertainties do overlap. A similar difference to that observed with $CH_4$ exists for $N_2O$ when different modelled meteorology is used, again the estimates using UKV are higher than when global meteorology is used (see Figure 9). There is a strong seasonal cycle in the InTEM UK estimates, as shown in Figure 10, when 3-month inversions are performed.

Over the last few years there have been significant changes to both the inventory and InTEM:

- The $N_2O$ calibration scale has been significantly revised. This has enhanced the modelled pollution events in the later years as a previous non-linearity has been corrected.
- The baseline algorithm has been improved. This has had the effect of lowering the baseline by a small degree, again this would enhance the magnitude of the modelled pollution events.
- The outer regions (South Atlantic, America, W. and E. Arctic, East Europe, Africa) have been included, giving the inversion more flexibility in discerning the mole fraction of the air entering the inversion domain.
- The model uncertainty algorithm has been improved by using the multi-height observations of $CH_4$ to select 'well-modelled' observations along with the local modelled boundary layer height, vertical temperature profile and wind speed to complement the previous 'localness' criteria.
- The inventory estimates have been changed significantly over different UNFCCC submissions, for example UK 2011 estimates were 110 in the 2013 submission, 117 in 2014, 93 in 2015, 72 in 2016, 77 in the 2017, and 73 Gg $yr^{-1}$ in the 2018 submission.

Discussions are ongoing with the inventory team to try and understand the differences between the inventory and the InTEM estimates. The spatial distribution as shown in Figure 11 and Figure 12 indicate that the emissions are wide-spread across the UK and that the 12-month network inversions with minimal prior information is very similar to the 3-month network inversion with NAEI prior information. The clear benefit of having the network of observations compared to just MHD can be seen by comparing Figure 11b with Figure 12a.

| Years | Inventory 1yr | MHD 3yr | DECC 1yr |
|---|---|---|---|
| 1990 | 166. (83.-250.) | 165. (79.-252.) | |
| 1991 | 167. (85.-249.) | 148. (74.-222.) | |
| 1992 | 150. (78.-223.) | 152. (76.-228.) | |
| 1993 | 136. (72.-201.) | 162. (100.-225.) | |
| 1994 | 138. (74.-203.) | 143. (98.-188.) | |
| 1995 | 134. (73.-196.) | 136. (101.-170.) | |
| 1996 | 134. (74.-194.) | 137. (105.-169.) | |
| 1997 | 135. (75.-194.) | 163. (132.-193.) | |
| 1998 | 135. (77.-193.) | 149. (118.-179.) | |
| 1999 | 103. (59.-146.) | 138. (111.-166.) | |
| 2000 | 100. (59.-142.) | 129. (100.-157.) | |
| 2001 | 95. (56.-134.) | 110. (81.-139.) | |
| 2002 | 88. (53.-123.) | 127. (94.-160.) | |
| 2003 | 88. (54.-122.) | 131. (100.-162.) | |
| 2004 | 90. (55.-124.) | 131. (98.-164.) | |
| 2005 | 87. (54.-119.) | 135. (102.-169.) | |
| 2006 | 83. (53.-113.) | 112. (78.-147.) | |
| 2007 | 83. (53.-112.) | 96. (64.-128.) | |
| 2008 | 80. (52.-108.) | 105. (74.-136.) | |
| 2009 | 75. (49.-100.) | 95. (65.-125.) | |
| 2010 | 76. (51.-101.) | 85. (54.-115.) | |
| 2011 | 73. (49.-96.) | 83. (58.-107.) | |
| 2012 | 73. (50.-95.) | 92. (69.-115.) | 97. (72.-121.) |
| 2013 | 72. (50.-94.) | 102. (79.-126.) | 95. (69.-122.) |
| 2014 | 74. (52.-95.) | 92. (62.-122.) | 95. (67.-122.) |
| 2015 | 72. (51.-93.) | 111. (73.-149.) | 70. (37.-102.) |
| 2016 | 72. (52.-92.) | 87. (45.-130.) | 102. (69.-135.) |
| 2017 | | | 88. (62.-114.) |

**Table 7: $N_2O$ emission (Gg $yr^{-1}$) estimates for the UK with uncertainty (1std).**

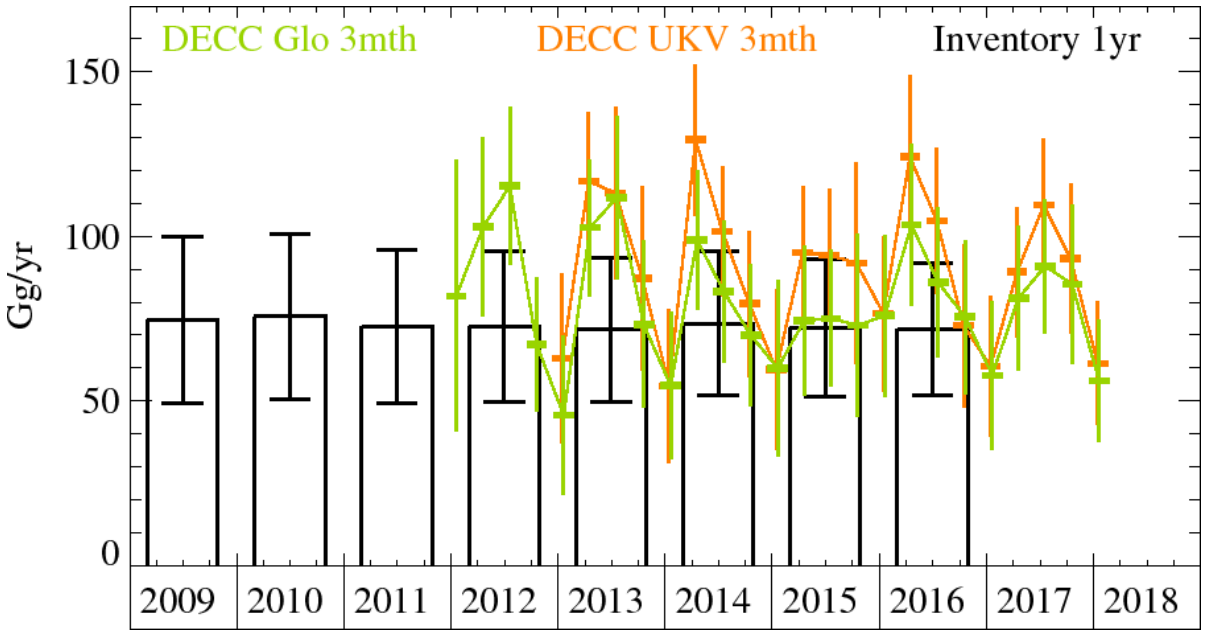


**Figure 10: $N_2O$ emission estimates (Gg $yr^{-1}$) from the UNFCCC Inventory (black) and InTEM using the DECC + GAUGE observations, 3-month inversions with the NAEI prior (80% uncertain NAEI 2015): (green) global meteorology and (orange) UKV meteorology.**

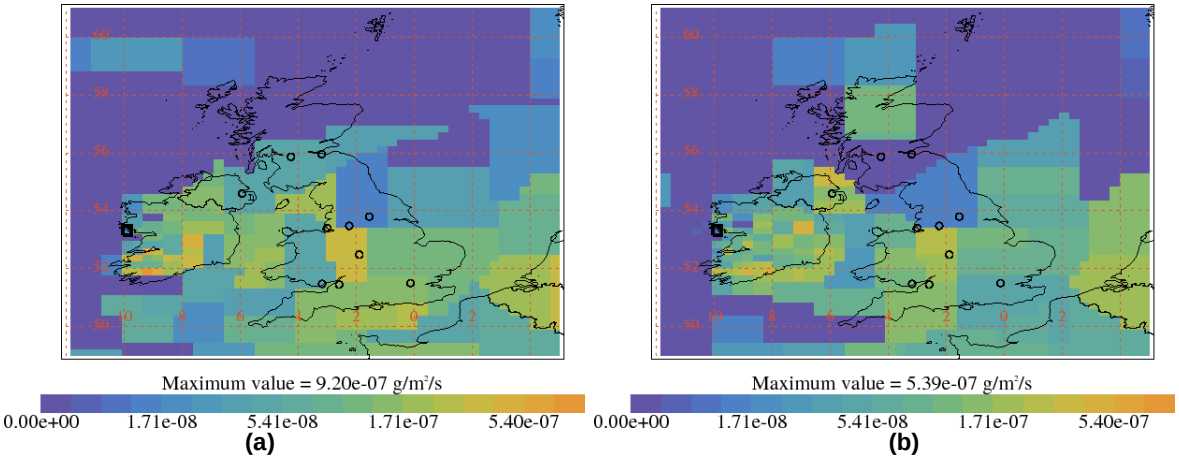


**Figure 11: InTEM estimates of spatial distribution of $N_2O$ emissions using global meteorology and MHD observations with minimal prior information. Black squares are measurement stations and circles are major cities in UK. (a) Average 2004-2007 (b) Average 2014-2017.**

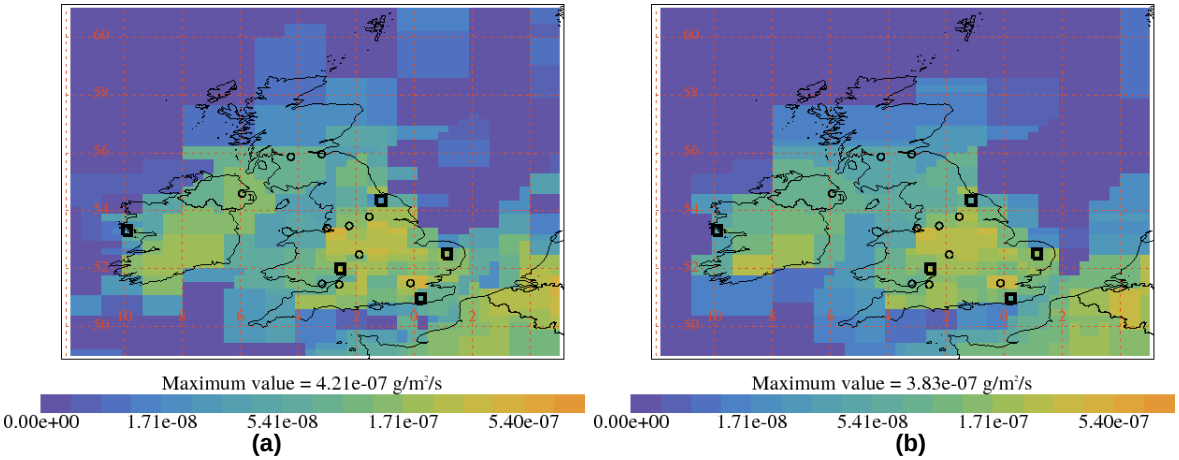


**Figure 12: Average InTEM estimates 2014-2017 of spatial distribution of $N_2O$ emissions using UKV meteorology and DECC+GAUGE observations. Black squares are measurement stations and circles are major cities in UK. (a) With minimal prior information (b) With NAEI prior.**

## 4.6 Carbon dioxide ($CO_2$)

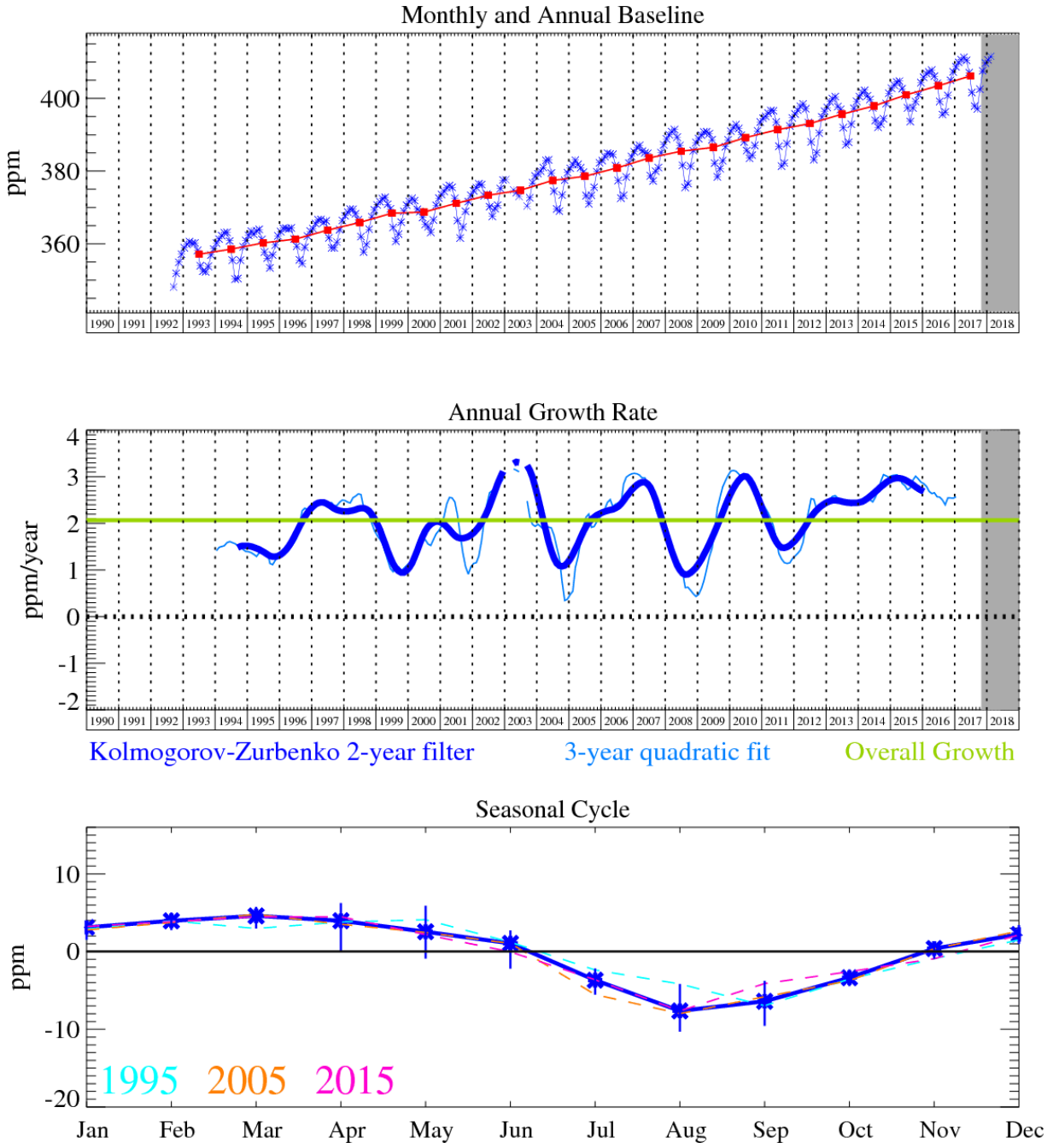


**Figure 13: Carbon dioxide ($CO_2$): Monthly (blue) and annual (red) Northern Hemisphere baseline mole fractions (top plot). Annual (blue) and overall average growth rate (green) (middle plot). Seasonal cycle (de-trended) with year-to-year variability (lower plot). Grey area covers un-ratified and therefore provisional data.**

$CO_2$ is the most important greenhouse gas, and has steadily grown at an annual average rate of 2 ppm $yr^{-1}$, calculated from the baseline-selected monthly means. Since 2012 the growth rate has averaged more than 2 ppm $yr^{-1}$. It has now reached an average annual mole fraction of 406 ppm (2017), the highest yet recorded at Mace Head, Ireland, and has shown significant growth rate anomalies in 1998/99 and 2002/03, which we suggest are a result of the global biomass burning events in those years. The average annual baseline mole fraction in the mid-latitude northern hemisphere surpassed 400 ppm in 2015.

## 4.7 HFC-125

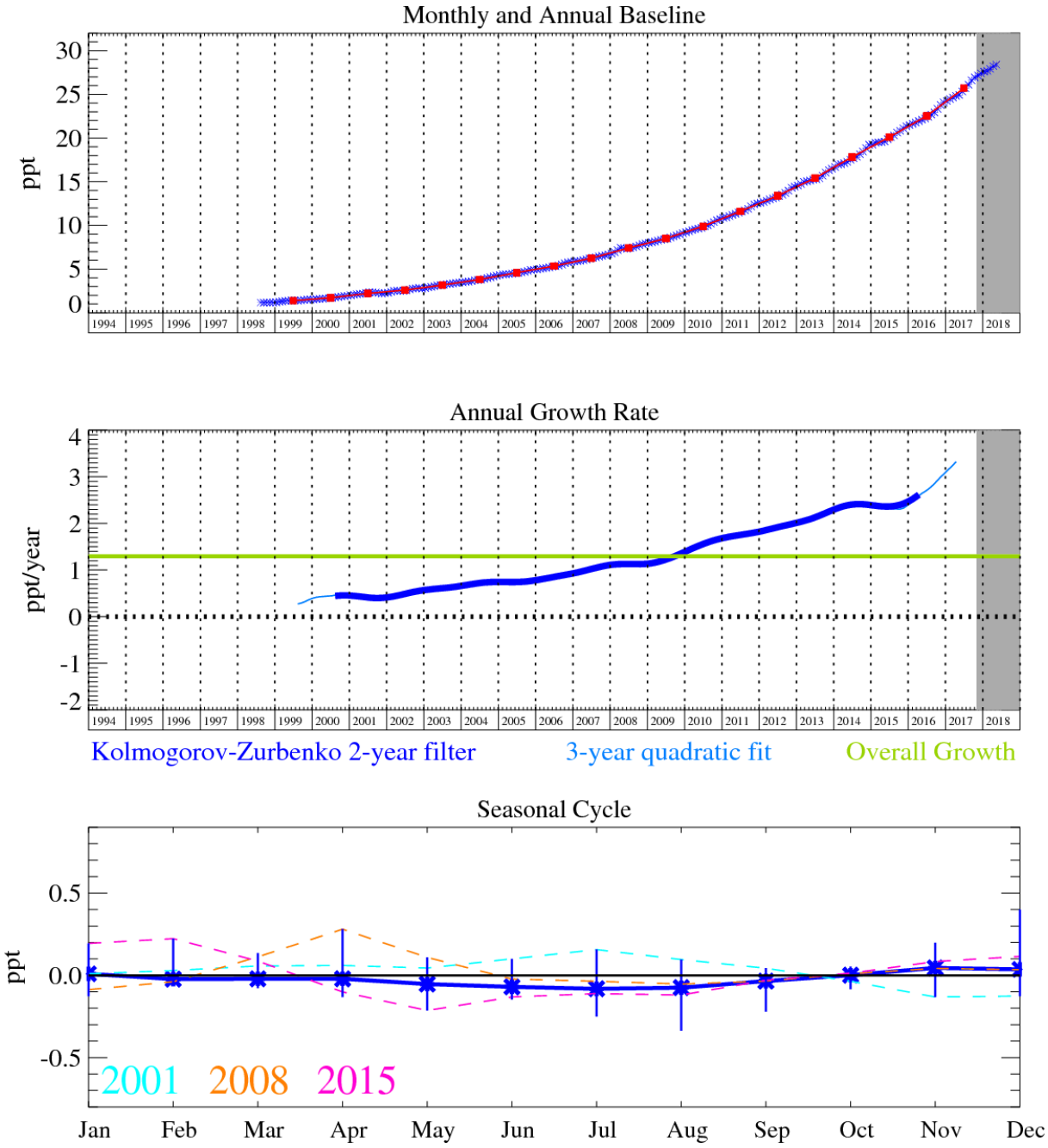


**Figure 14: HFC-125 ($CHF_2CF_3$): Monthly (blue) and annual (red) Northern Hemisphere baseline mole fractions (top plot). Annual (blue) and overall average growth rate (green) (middle plot). Seasonal cycle (de-trended) with year-to-year variability (lower plot). Grey area covers un-ratified provisional data.**

Unfortunately, the observations of HFC-125 (and HFC-32) at Mace Head were compromised by contamination from the air conditioning system (May 2014 – June 2015) and these data had to be removed. The current working solution is to flush the air sample module with clean ambient air to minimise contamination from laboratory air. A long-term solution will require modification of the air conditioner to use a chilled water heat exchanger with the refrigerant gases contained in a unit external to the laboratory. The northern hemisphere baseline during this period has been estimated using another AGAGE northern hemisphere station, Zeppelin (Ny-Ålesund).

Relative to the magnitude of the baseline the pollution events are very significant. Therefore, InTEM has plenty of clear information on which to base the emission estimates. The agreement in trend between the inventory and InTEM for the UK is good. However, the rate of increase in

the inventory is greater than that estimated by InTEM. The InTEM estimates using the DECC network (MHD+TAC) have shown overall no trend since 2012.

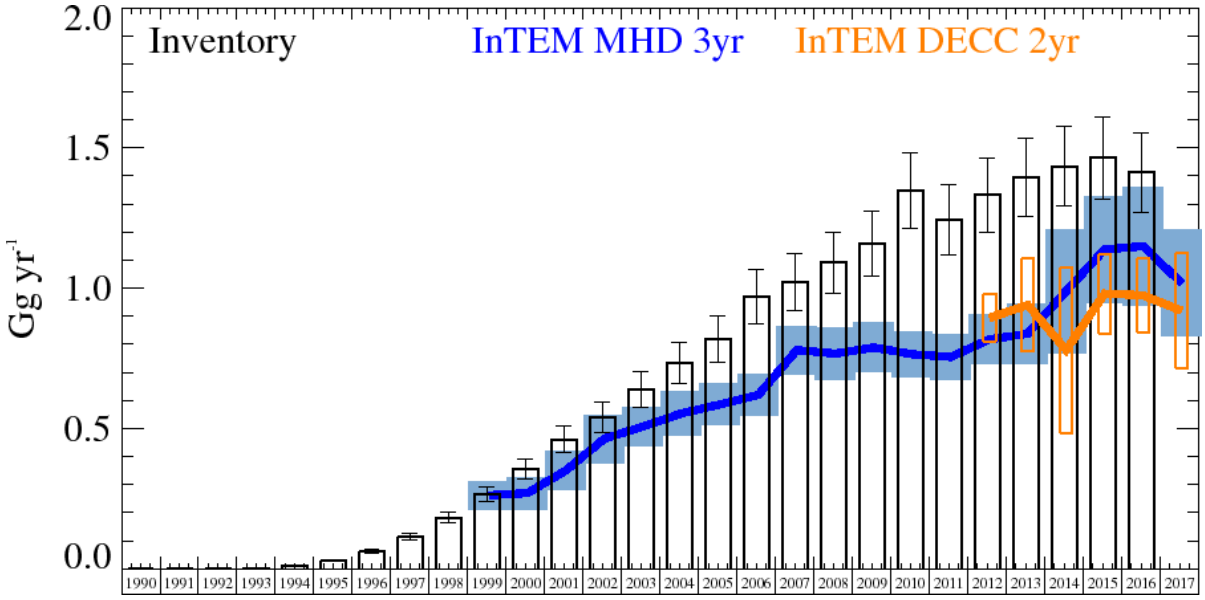


**Figure 15: HFC-125 UK Emission estimates (Gg yr$^{-1}$) from the UNFCCC Inventory (black) and InTEM with global meteorology: 3-year MHD (blue) and 2-year DECC network (orange). The uncertainty bars represent 1 std.**

| Years | Inventory 1yr | MHD 3yr | DECC 2yr |
|---|---|---|---|
| 1990 | 0.0000 (0.0000-0.0000) | | |
| 1991 | 0.0005 (0.0004-0.0005) | | |
| 1992 | 0.0013 (0.0012-0.0015) | | |
| 1993 | 0.0033 (0.0030-0.0037) | | |
| 1994 | 0.0120 (0.0110-0.0130) | | |
| 1995 | 0.0301 (0.0271-0.0331) | | |
| 1996 | 0.0634 (0.0571-0.0698) | | |
| 1997 | 0.1143 (0.1029-0.1257) | | |
| 1998 | 0.1831 (0.1648-0.2014) | | |
| 1999 | 0.265 (0.239-0.292) | 0.262 (0.211-0.314) | |
| 2000 | 0.356 (0.321-0.392) | 0.270 (0.212-0.328) | |
| 2001 | 0.462 (0.416-0.508) | 0.351 (0.282-0.420) | |
| 2002 | 0.541 (0.487-0.595) | 0.464 (0.378-0.550) | |
| 2003 | 0.638 (0.574-0.702) | 0.507 (0.436-0.578) | |
| 2004 | 0.735 (0.661-0.808) | 0.554 (0.474-0.634) | |
| 2005 | 0.819 (0.737-0.901) | 0.586 (0.513-0.660) | |
| 2006 | 0.968 (0.871-1.065) | 0.620 (0.545-0.695) | |
| 2007 | 1.023 (0.921-1.126) | 0.780 (0.694-0.865) | |
| 2008 | 1.091 (0.982-1.200) | 0.767 (0.676-0.859) | |
| 2009 | 1.158 (1.042-1.274) | 0.789 (0.701-0.877) | |
| 2010 | 1.349 (1.214-1.484) | 0.765 (0.685-0.845) | |
| 2011 | 1.243 (1.118-1.367) | 0.755 (0.672-0.839) | |
| 2012 | 1.332 (1.199-1.465) | 0.818 (0.728-0.907) | 0.894 (0.809-0.979) |
| 2013 | 1.397 (1.257-1.536) | 0.838 (0.731-0.946) | 0.940 (0.775-1.105) |
| 2014 | 1.435 (1.291-1.578) | 0.990 (0.770-1.210) | 0.780 (0.480-1.070) |
| 2015 | 1.466 (1.320-1.613) | 1.138 (0.947-1.330) | 0.981 (0.840-1.122) |
| 2016 | 1.412 (1.270-1.553) | 1.150 (0.940-1.360) | 0.975 (0.843-1.106) |
| 2017 | | 1.018 (0.828-1.207) | 0.920 (0.720-1.130) |

**Table 8: HFC-125 emission (Gg yr$^{-1}$) estimates for the UK with uncertainty (1std).**

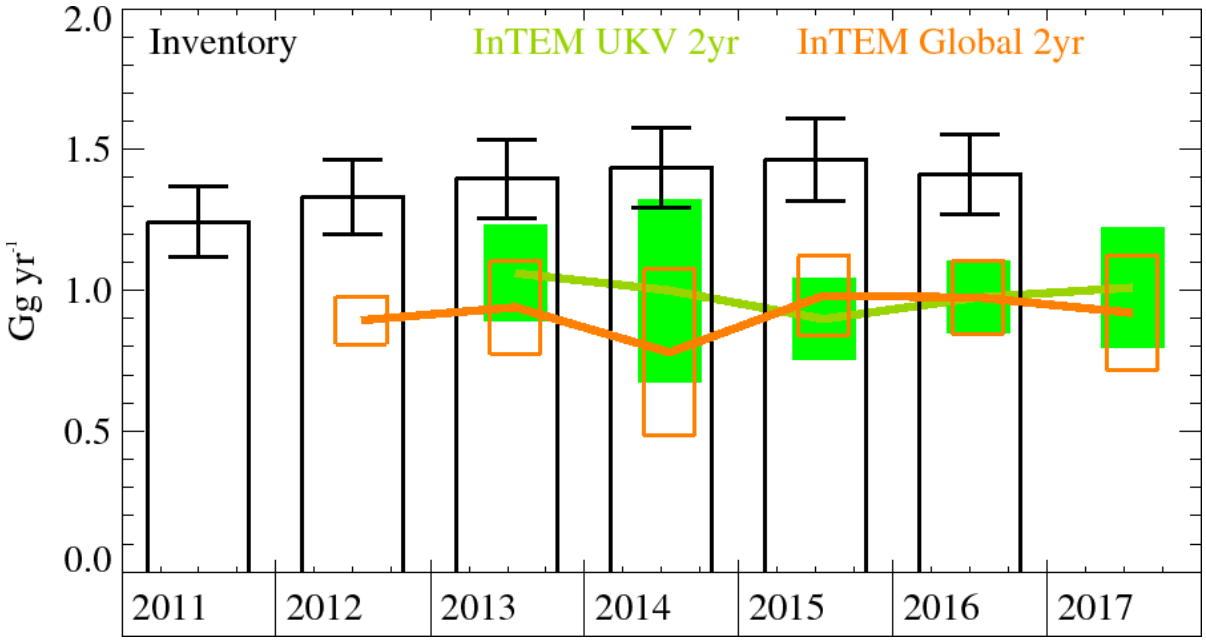


**Figure 16: HFC-125 emission estimates for the UK (Gg $yr^{-1}$) from the UNFCCC Inventory (black) and InTEM using the DECC observations, 2-year inversions with different meteorology: (orange) global meteorology and (green) 1.5 km high resolution meteorology. The uncertainty bars represent 1 std.**

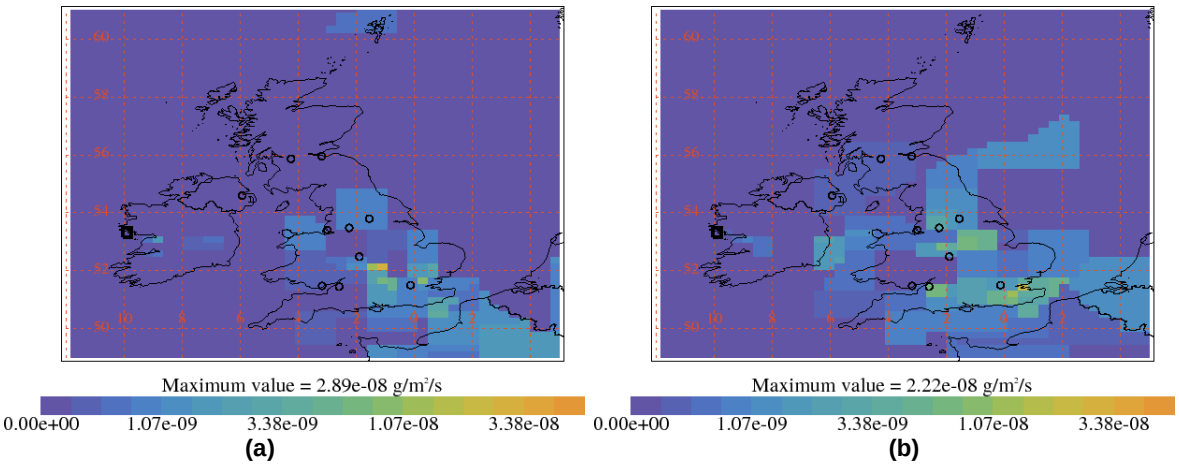


**Figure 17: InTEM estimates of spatial distribution of HFC-125 emissions using global meteorology and MHD observations with minimal prior information. Black squares are measurement stations and circles are major cities in UK. (a) Average 2004-2007 (b) Average 2014-2017.**

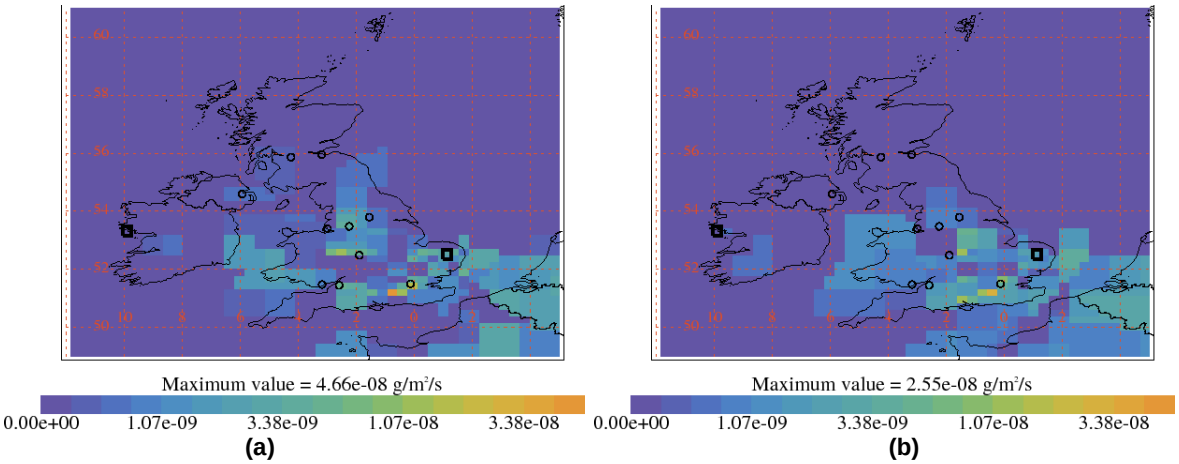


**Figure 18: Average InTEM estimates 2014-2017 of spatial distribution of HFC-125 emissions using DECC observations with minimal prior information. Black squares are measurement stations and circles are major cities in UK. (a) Global meteorology and (b) UKV meteorology.**

## 4.8 HFC-134a

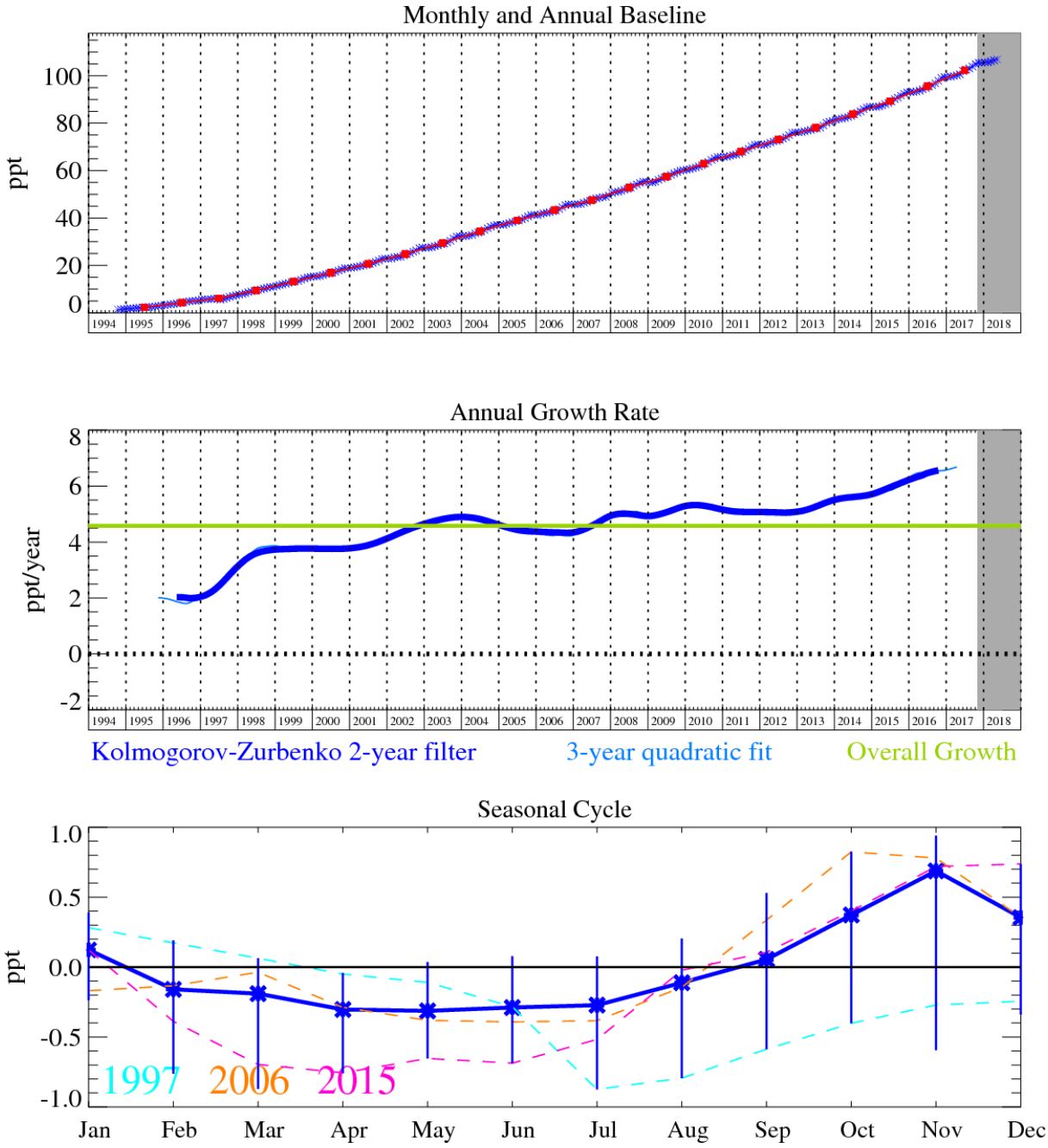


**Figure 19: HFC-134a ($CH_2FCF_3$): Monthly (blue) and annual (red) Northern Hemisphere baseline mole fractions (top plot). Annual (blue) and overall average growth rate (green) (middle plot). Seasonal cycle (de-trended) with year-to-year variability (lower plot). Grey area covers un-ratified and therefore provisional data.**

Globally HFC-134a ($CH_2FCF_3$) is the most abundant HFC present in the atmosphere and is used predominantly in refrigeration and mobile air conditioning (MAC). Due to its long lifetime, 13.5 years, and relatively high $GWP_{100}$ of 1370 (Forster *et al*., 2007), the use of HFC-134a (and any other HFCs with a $GWP_{100}$ >150) is being phased out in Europe between 2011 and 2017. It is proposed that a very gradual phase-out of the use of HFC-134a in cars will also take place outside Europe because of the global nature of the car industry. However, in developing countries the potential for growth of HFC-134a is still large (Velders *et al*., 2009).

The UK inventory and InTEM estimates increased from the mid-1990s until 2009. Since then both estimates have remained largely constant. However, the InTEM estimates for the UK are consistently around two thirds of the inventory estimates. A significant proportion of the HFC-

134a emitted is estimated to come from in-use vehicles (it is used in mobile air conditioning units). The UK inventory was modified downwards (5%) for the 2017 submission for data from 2009 onwards after further work on the activity data and emission factors used was undertaken. However, a key factor, the annual re-fill frequency, was kept at the conservative, albeit unrealistic, rate of 100% because of a limitation present in the inventory model.

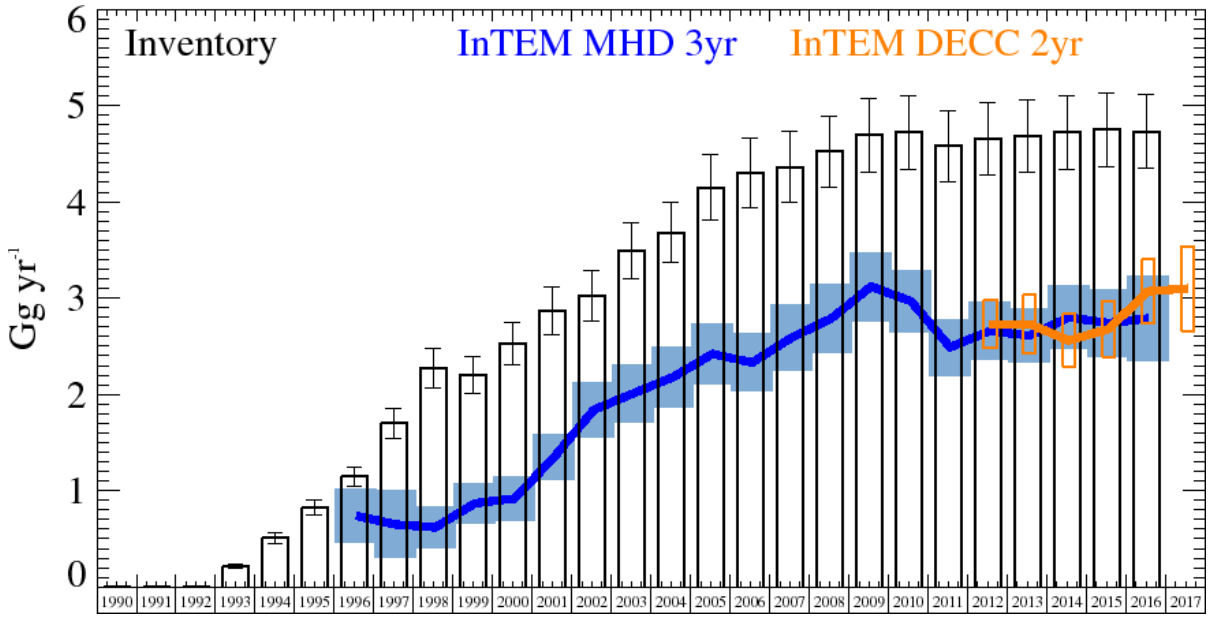


**Figure 20: HFC-134a UK Emission estimates (Gg $yr^{-1}$) from the UNFCCC Inventory (black) and InTEM with global meteorology: 3-year MHD (blue) and 2-year DECC network (orange). The uncertainty bars represent 1 std.**

| Years | Inventory 1yr | MHD 3yr | DECC 2yr |
|---|---|---|---|
| 1990 | 0.0008 (0.0007-0.0009) | | |
| 1991 | 0.0029 (0.0025-0.0034) | | |
| 1992 | 0.0073 (0.0063-0.0083) | | |
| 1993 | 0.214 (0.188-0.240) | | |
| 1994 | 0.508 (0.454-0.562) | | |
| 1995 | 0.828 (0.753-0.902) | | |
| 1996 | 1.146 (1.043-1.248) | 0.74 (0.45-1.02) | |
| 1997 | 1.700 (1.549-1.851) | 0.65 (0.30-1.00) | |
| 1998 | 2.27 (2.07-2.48) | 0.62 (0.40-0.83) | |
| 1999 | 2.202 (2.009-2.395) | 0.87 (0.66-1.08) | |
| 2000 | 2.53 (2.31-2.75) | 0.92 (0.69-1.15) | |
| 2001 | 2.87 (2.62-3.12) | 1.35 (1.11-1.58) | |
| 2002 | 3.02 (2.76-3.28) | 1.84 (1.55-2.12) | |
| 2003 | 3.49 (3.19-3.78) | 2.01 (1.71-2.30) | |
| 2004 | 3.68 (3.37-3.99) | 2.18 (1.87-2.49) | |
| 2005 | 4.15 (3.80-4.49) | 2.42 (2.11-2.73) | |
| 2006 | 4.30 (3.94-4.66) | 2.33 (2.03-2.63) | |
| 2007 | 4.36 (3.99-4.72) | 2.59 (2.24-2.93) | |
| 2008 | 4.52 (4.15-4.90) | 2.79 (2.43-3.15) | |
| 2009 | 4.69 (4.30-5.07) | 3.12 (2.77-3.48) | |
| 2010 | 4.72 (4.34-5.10) | 2.97 (2.64-3.29) | |
| 2011 | 4.58 (4.21-4.95) | 2.49 (2.19-2.78) | |
| 2012 | 4.66 (4.29-5.04) | 2.66 (2.36-2.96) | 2.73 (2.48-2.98) |
| 2013 | 4.68 (4.31-5.06) | 2.61 (2.33-2.89) | 2.73 (2.43-3.04) |
| 2014 | 4.72 (4.34-5.10) | 2.80 (2.47-3.13) | 2.56 (2.29-2.84) |
| 2015 | 4.75 (4.37-5.13) | 2.74 (2.39-3.09) | 2.68 (2.39-2.97) |
| 2016 | 4.73 (4.35-5.11) | 2.79 (2.35-3.23) | 3.07 (2.74-3.41) |
| 2017 | | | 3.10 (2.66-3.54) |

**Table 9: HFC-134a emission (Gg $yr^{-1}$) estimates for the UK with uncertainty (1std).**

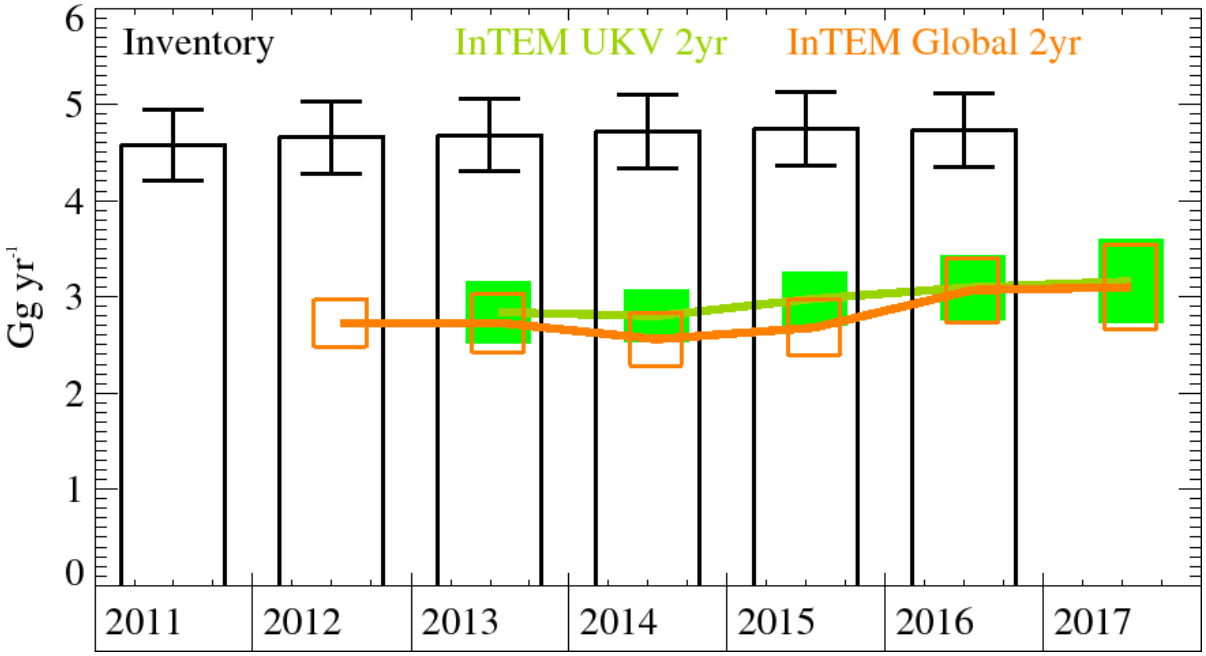


**Figure 21: HFC-134a emission estimates for the UK (Gg yr$^{-1}$) from the UNFCCC Inventory (black) and InTEM using the DECC observations, 2-year inversions with different meteorology: (orange) global meteorology and (green) 1.5 km high resolution meteorology. The uncertainty bars represent 1 std.**

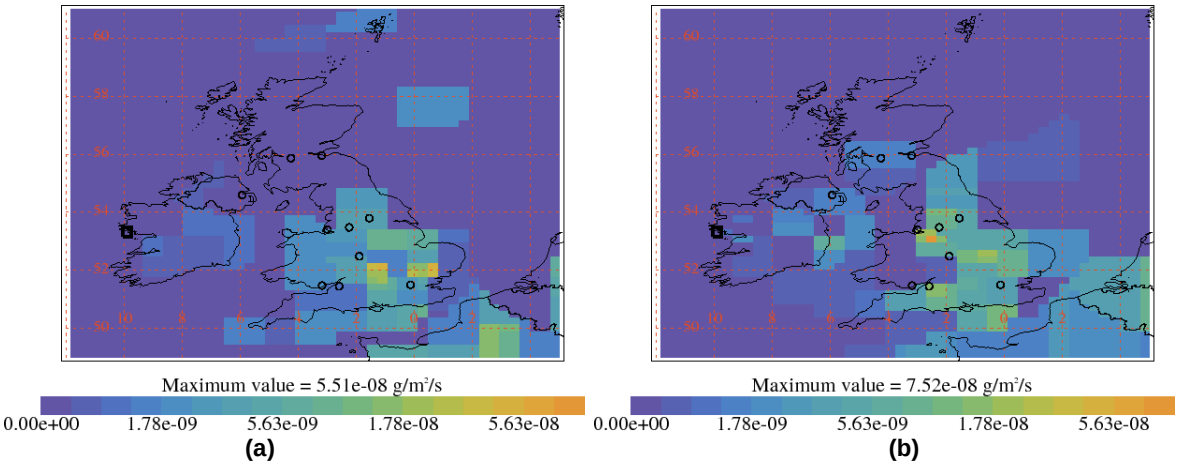


**Figure 22: InTEM estimates of spatial distribution of HFC-134a emissions using global meteorology and MHD observations with minimal prior information. Black squares are measurement stations and circles are major cities in UK. (a) Average 2004-2007 (b) Average 2014-2017.**

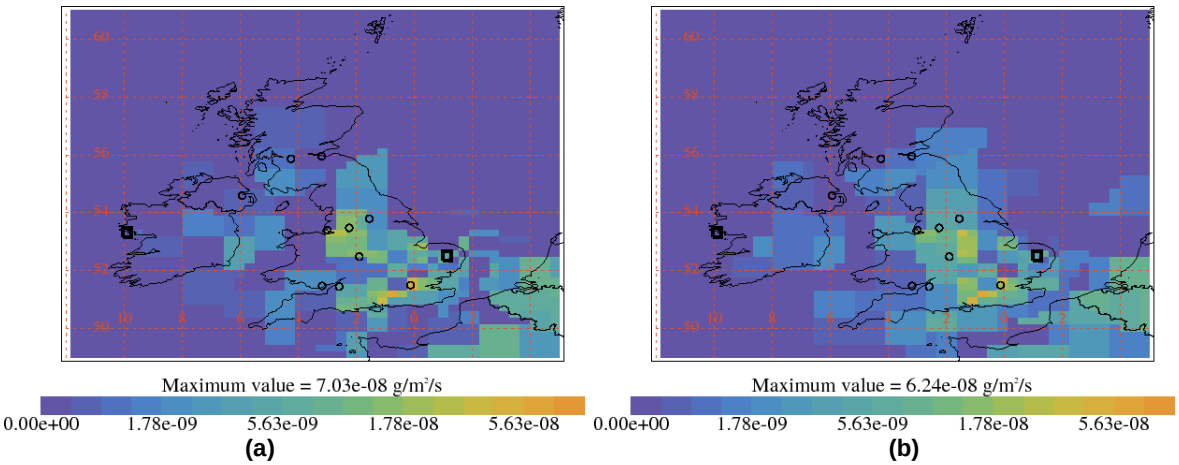


**Figure 23: Average InTEM estimates 2014-2017 of spatial distribution of HFC-134a emissions using DECC observations with minimal prior information. Black squares are measurement stations and circles are major cities in UK. (a) Global meteorology and (b) UKV meteorology.**

## 4.9 HFC-143a

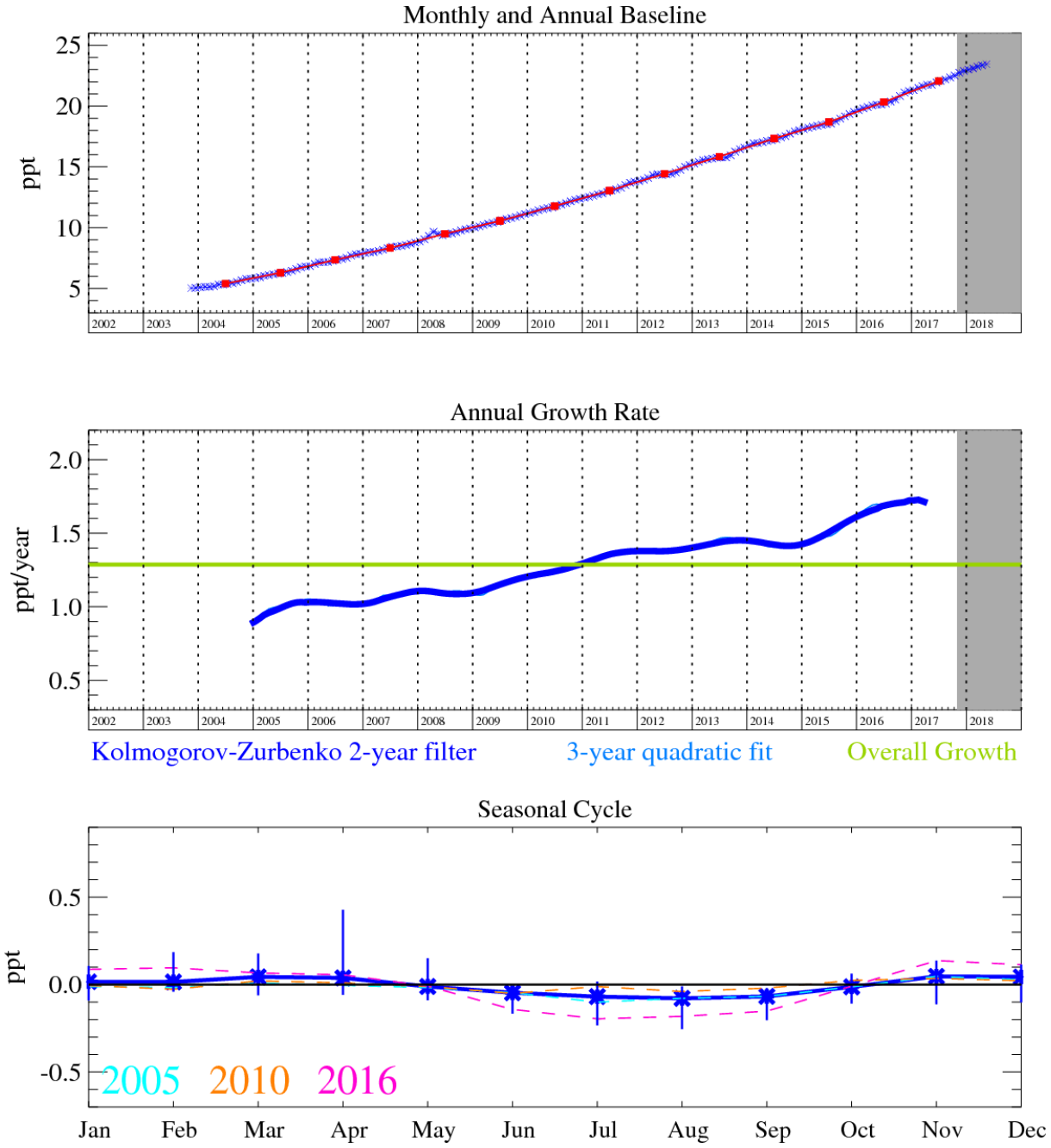


**Figure 24: HFC-143a ($CH_3CF_3$): Monthly (blue) and annual (red) Northern Hemisphere baseline mole fractions (top plot). Annual (blue) and overall average growth rate (green) (middle plot). Seasonal cycle (de-trended) with year-to-year variability (lower plot). Grey area covers un-ratified and therefore provisional data.**

HFC-143a ($CH_3CF_3$) is used mainly as a working fluid in refrigerant blends (R-404A and R-507A) for low and medium temperature commercial refrigeration systems. In 2016 the NH baseline mole exceeded 20 ppt for the first time. These levels have increased dramatically from the low levels observed in 2003 with an increasing growth rate. It has a relatively long atmospheric lifetime of 51.4 years and a significant radiative forcing value (third largest of all the HFCs) with a $GWP_{100}$ of 4400.

There is excellent agreement between the inventory and the InTEM estimates. The significant step down in the inventory in 2010-2011 is somewhat muted in the InTEM MHD-only inversions as they span 3-years. The inventory estimates are generally higher than the InTEM estimates by ~0.15 Gg $yr^{-1}$ except in 2016 when there is another significant step down in the inventory

estimates. The 2-year DECC network estimates however show a step down in 2017, the 2-year inversion period will again mute the immediate response of the InTEM estimates. As discussed for other gases, the InTEM UKV estimates (Figure 26) are higher than those using global meteorology and significantly close the gap between the inventory and the inversion estimates.

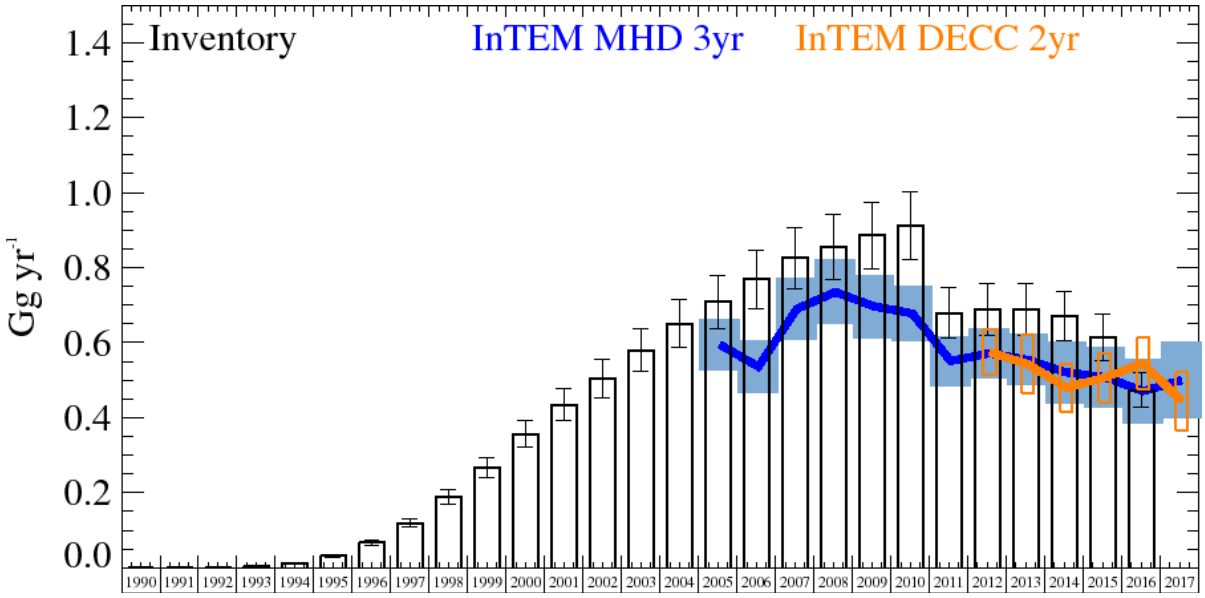


**Figure 25: HFC-143a UK Emission estimates (Gg $yr^{-1}$) from the UNFCCC Inventory (black) and InTEM with global meteorology: 3-year MHD (blue) and 2-year DECC network (orange). The uncertainty bars represent 1 std.**

| Years | Inventory 1yr | MHD 3yr | DECC 2yr |
|---|---|---|---|
| 1990 | 0.0001 (0.0000-0.0001) | | |
| 1991 | 0.0006 (0.0005-0.0006) | | |
| 1992 | 0.0016 (0.0014-0.0018) | | |
| 1993 | 0.0040 (0.0036-0.0044) | | |
| 1994 | 0.013 (0.012-0.014) | | |
| 1995 | 0.0321 (0.0289-0.0353) | | |
| 1996 | 0.0670 (0.0603-0.0737) | | |
| 1997 | 0.1194 (0.1075-0.1314) | | |
| 1998 | 0.1900 (0.1710-0.2091) | | |
| 1999 | 0.268 (0.241-0.295) | | |
| 2000 | 0.356 (0.320-0.391) | | |
| 2001 | 0.435 (0.391-0.478) | | |
| 2002 | 0.505 (0.454-0.555) | | |
| 2003 | 0.580 (0.522-0.638) | | |
| 2004 | 0.651 (0.586-0.716) | | |
| 2005 | 0.709 (0.638-0.780) | 0.595 (0.528-0.663) | |
| 2006 | 0.769 (0.692-0.846) | 0.536 (0.467-0.604) | |
| 2007 | 0.825 (0.743-0.908) | 0.690 (0.608-0.772) | |
| 2008 | 0.855 (0.769-0.940) | 0.735 (0.650-0.821) | |
| 2009 | 0.886 (0.797-0.974) | 0.697 (0.613-0.781) | |
| 2010 | 0.911 (0.820-1.002) | 0.678 (0.604-0.753) | |
| 2011 | 0.679 (0.611-0.746) | 0.551 (0.485-0.617) | |
| 2012 | 0.688 (0.619-0.757) | 0.572 (0.505-0.640) | 0.575 (0.516-0.634) |
| 2013 | 0.689 (0.620-0.758) | 0.554 (0.486-0.622) | 0.543 (0.465-0.621) |
| 2014 | 0.671 (0.604-0.738) | 0.521 (0.439-0.603) | 0.480 (0.417-0.544) |
| 2015 | 0.615 (0.554-0.677) | 0.508 (0.429-0.588) | 0.507 (0.441-0.572) |
| 2016 | 0.474 (0.426-0.521) | 0.471 (0.385-0.557) | 0.545 (0.477-0.612) |
| 2017 | | 0.500 (0.399-0.601) | 0.444 (0.366-0.521) |

**Table 10: HFC-143a emission (Gg $yr^{-1}$) estimates for the UK with uncertainty (1std).**

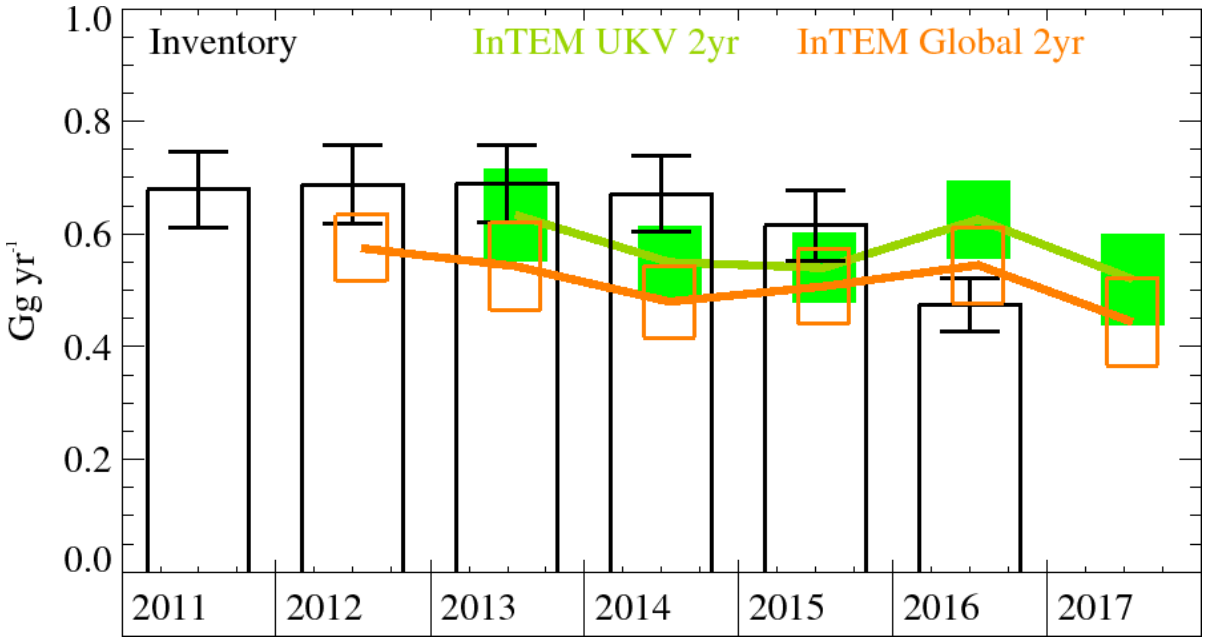


**Figure 26: HFC-143a emission estimates for the UK (Gg yr$^{-1}$) from the UNFCCC Inventory (black) and InTEM using the DECC observations, 2-year inversions with different meteorology: (orange) global meteorology and (green) 1.5 km high resolution meteorology. The uncertainty bars represent 1 std.**

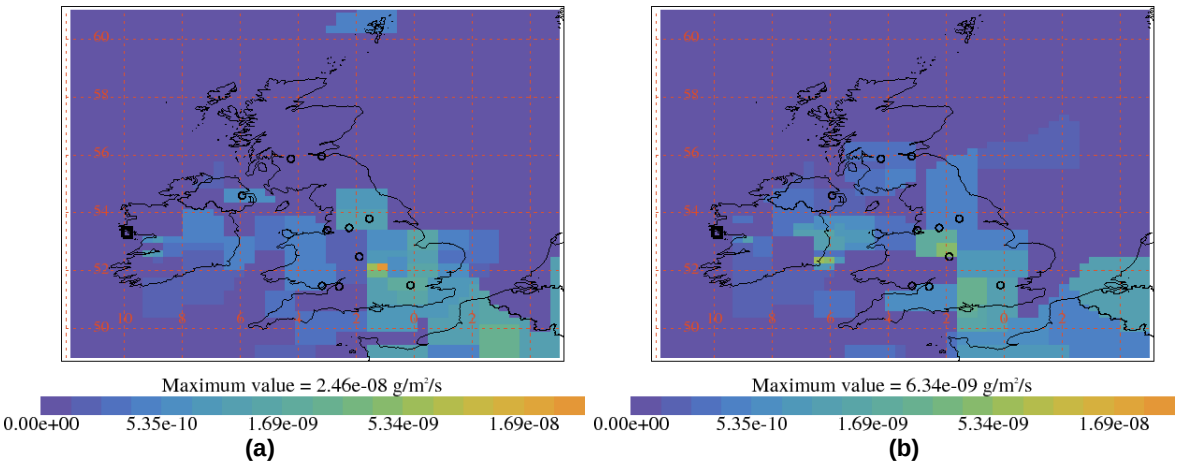


**Figure 27: InTEM estimates of spatial distribution of HFC-143a emissions using global meteorology and MHD observations with minimal prior information. Black squares are measurement stations and circles are major cities in UK. (a) Average 2004-2007 (b) Average 2014-2017.**

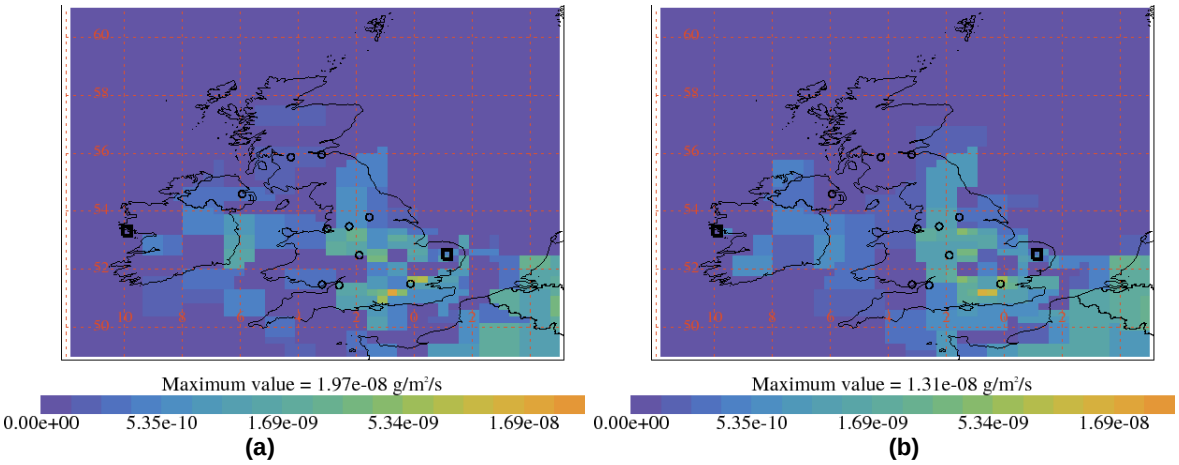


**Figure 28: Average InTEM estimates 2014-2017 of spatial distribution of HFC-143a emissions using DECC observations with minimal prior information. Black squares are measurement stations and circles are major cities in UK. (a) Global meteorology and (b) UKV meteorology.**

## 4.10 HFC-152a

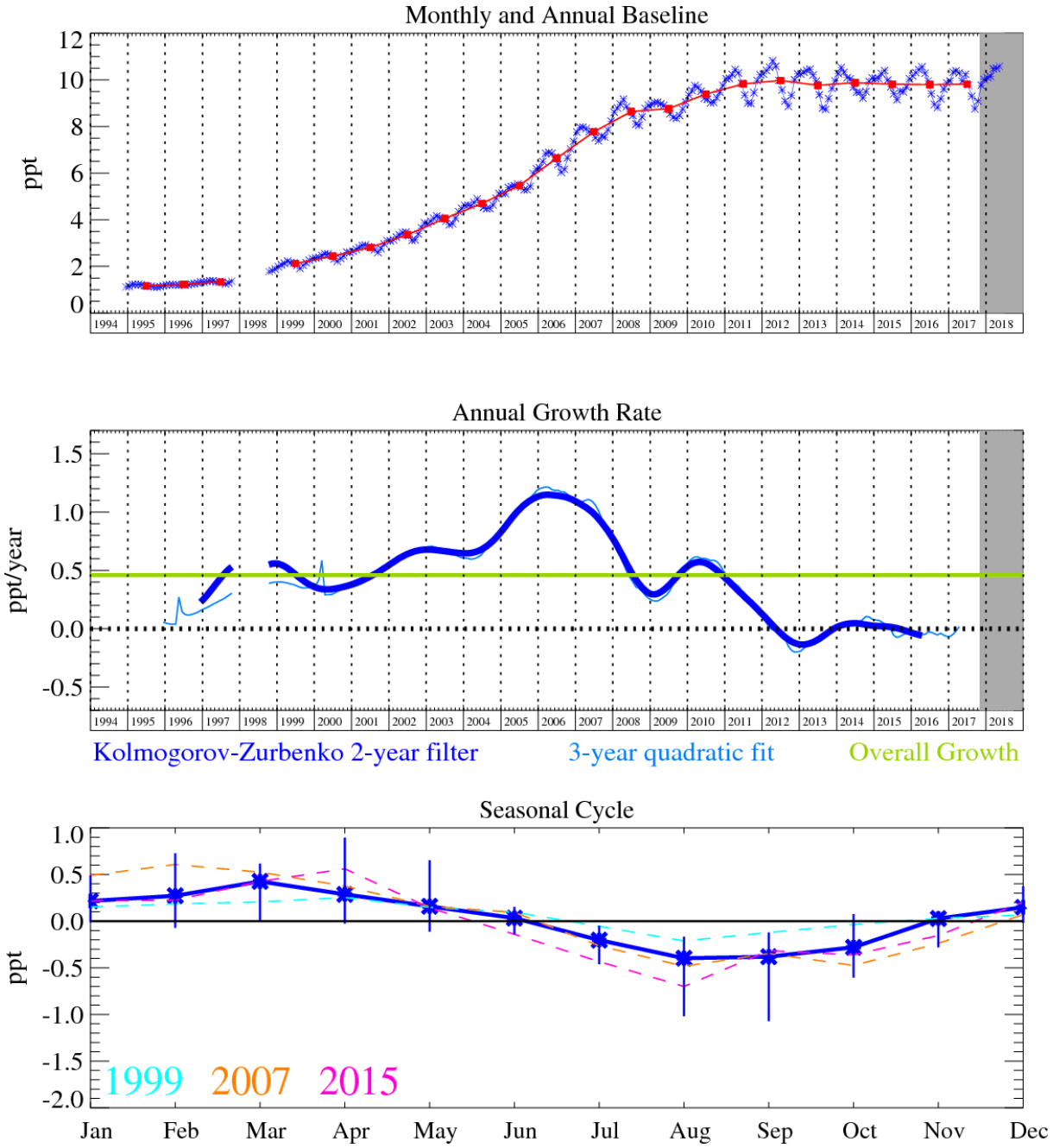


**Figure 29: HFC-152a ($CH_3CHF_2$): Monthly (blue) and annual (red) Northern Hemisphere baseline mole fractions (top plot). Annual (blue) and overall average growth rate (green) (middle plot). Seasonal cycle (de-trended) with year-to-year variability (lower plot). Grey area covers un-ratified and therefore provisional data.**

HFC-152a ($CH_3CHF_2$) has a relatively short lifetime of 1.6 years due to its efficient removal by OH oxidation in the troposphere, consequently it has the smallest $GWP_{100}$ at 133 of all of the major HFCs. It is used as a foam-blowing agent and aerosol propellant, and given its short lifetime has exhibited substantial growth in the atmosphere since measurements began in 1994, implying a substantial increase in emissions in these years. However, in the last few years the rate of growth slowed considerably and is now zero to negative. The maximum NH monthly mole fraction reached was 10.7 ppt (Apr 2012).

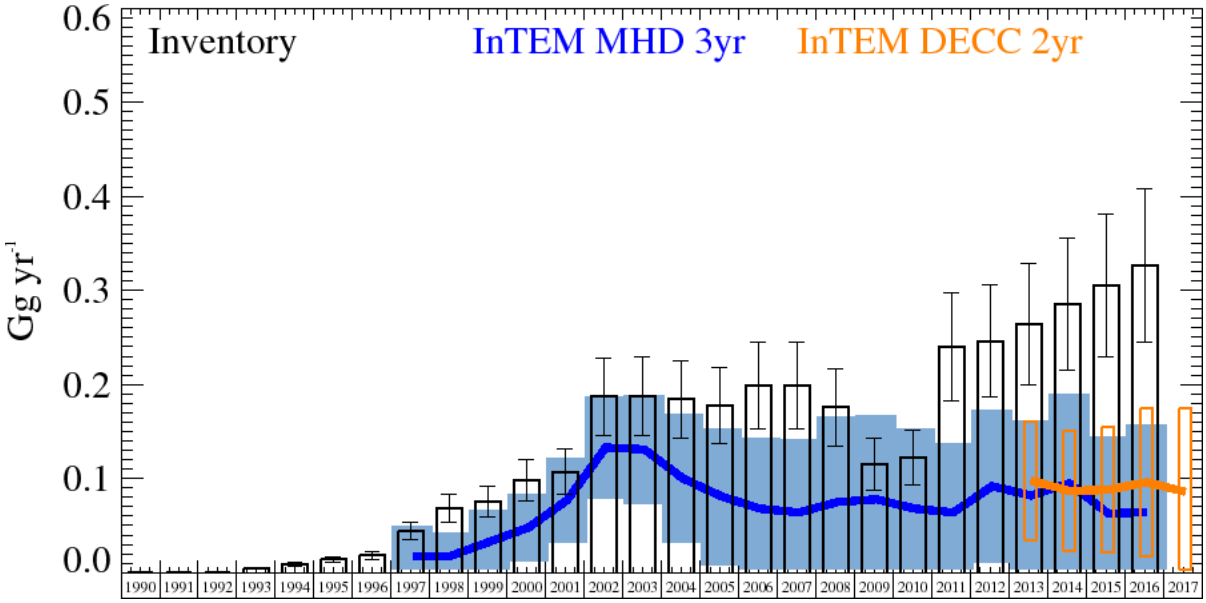


**Figure 30: HFC-152a UK Emission estimates (Gg $yr^{-1}$) from the UNFCCC Inventory (black) and InTEM with global meteorology: 3-year MHD (blue) and 2-year DECC network (orange). The uncertainty bars represent 1 std.**

The comparison for the UK shows that the InTEM estimates are substantially lower than the inventory although the uncertainties do overlap in the early years. The steadily rising UK emissions reported in the inventory are not reflected in the InTEM results. The improved InTEM resolution achieved with the addition of the TAC observations estimates the UK emissions primarily come from London – Surrey – Hampshire although the uncertainties are large. Belgium is also estimated to be a significant source of HFC-152a.

| Years | Inventory 1yr | MHD 3yr | DECC 2yr |
|---|---|---|---|
| 1990 | 0.0000 (0.0000-0.0000) | | |
| 1991 | 0.0000 (0.0000-0.0000) | | |
| 1992 | 0.0000 (0.0000-0.0000) | | |
| 1993 | 0.0047 (0.0037-0.0056) | | |
| 1994 | 0.0094 (0.0074-0.0113) | | |
| 1995 | 0.0141 (0.0111-0.0170) | | |
| 1996 | 0.0183 (0.0144-0.0222) | | |
| 1997 | 0.0443 (0.0348-0.0537) | 0.018 (0.000-0.062) | |
| 1998 | 0.0681 (0.0534-0.0828) | 0.018 (0.000-0.049) | |
| 1999 | 0.0757 (0.0592-0.0921) | 0.033 (0.000-0.068) | |
| 2000 | 0.098 (0.076-0.119) | 0.048 (0.012-0.084) | |
| 2001 | 0.107 (0.083-0.131) | 0.077 (0.032-0.123) | |
| 2002 | 0.187 (0.146-0.229) | 0.133 (0.079-0.187) | |
| 2003 | 0.187 (0.145-0.229) | 0.131 (0.073-0.189) | |
| 2004 | 0.184 (0.142-0.225) | 0.100 (0.032-0.168) | |
| 2005 | 0.177 (0.137-0.218) | 0.081 (0.008-0.153) | |
| 2006 | 0.199 (0.153-0.245) | 0.068 (0.000-0.151) | |
| 2007 | 0.199 (0.152-0.245) | 0.064 (0.000-0.155) | |
| 2008 | 0.176 (0.135-0.217) | 0.075 (0.000-0.181) | |
| 2009 | 0.115 (0.088-0.143) | 0.078 (0.000-0.178) | |
| 2010 | 0.122 (0.093-0.151) | 0.068 (0.000-0.169) | |
| 2011 | 0.240 (0.182-0.298) | 0.064 (0.000-0.146) | |
| 2012 | 0.246 (0.187-0.306) | 0.092 (0.011-0.173) | |
| 2013 | 0.264 (0.200-0.329) | 0.082 (0.002-0.162) | 0.098 (0.035-0.161) |
| 2014 | 0.285 (0.215-0.355) | 0.095 (0.000-0.190) | 0.087 (0.024-0.151) |
| 2015 | 0.305 (0.230-0.381) | 0.063 (0.000-0.164) | 0.088 (0.021-0.155) |
| 2016 | 0.326 (0.244-0.407) | 0.064 (0.000-0.187) | 0.096 (0.017-0.175) |
| 2017 | | | 0.086 (0.000-0.178) |

**Table 11: HFC-152a emission (Gg $yr^{-1}$) estimates for the UK with uncertainty (1std).**

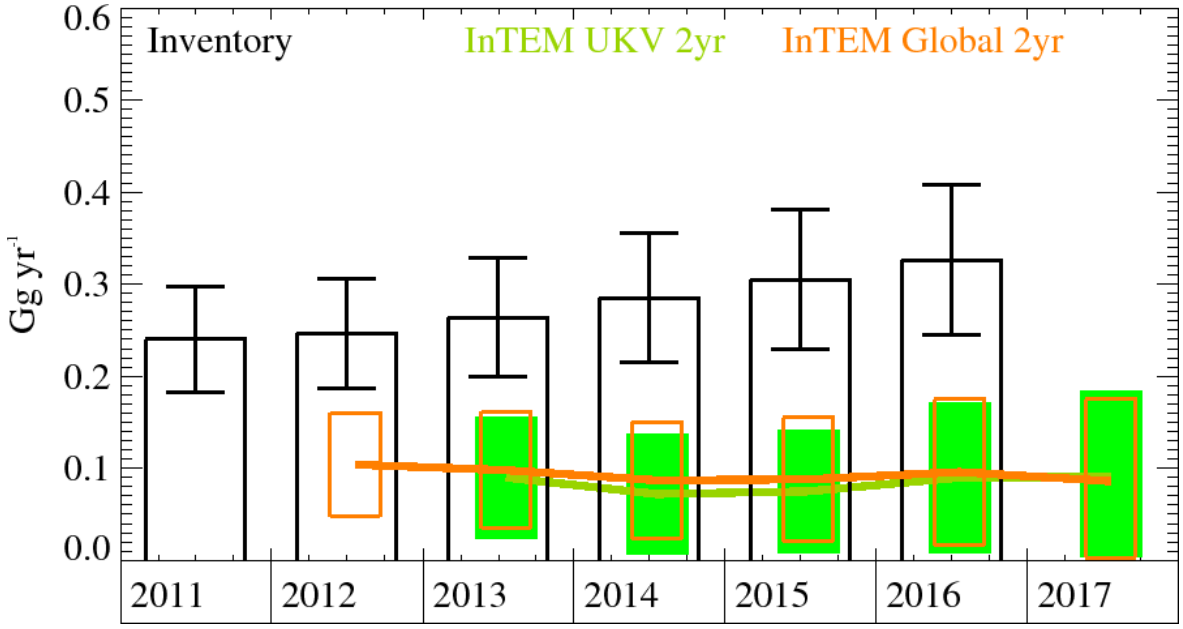


**Figure 31: HFC-152a emission estimates for the UK (Gg yr$^{-1}$) from the UNFCCC Inventory (black) and InTEM using the DECC observations, 2-year inversions with different meteorology: (orange) global meteorology and (green) 1.5 km high resolution meteorology. The uncertainty bars represent 1 std.**

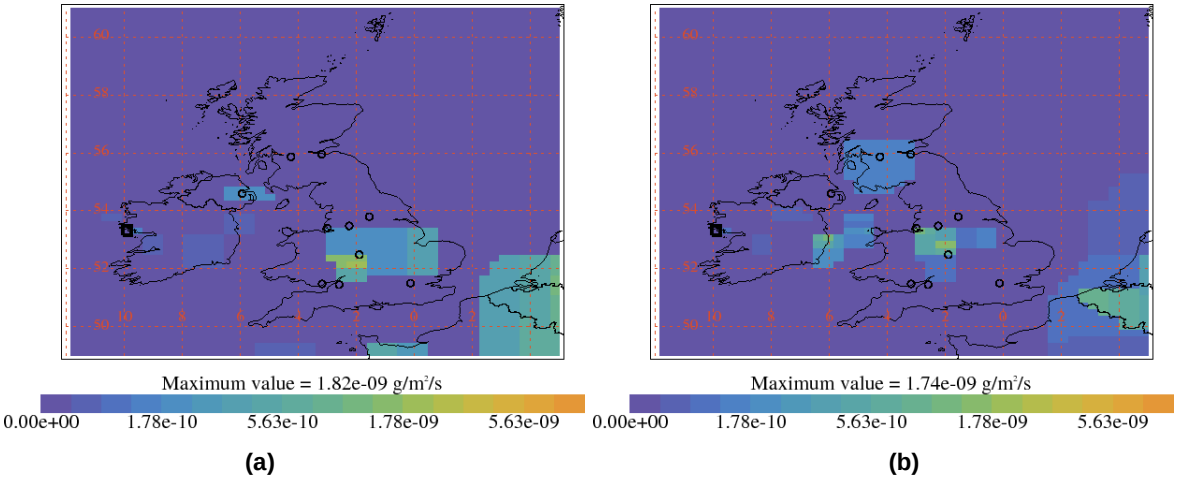


**(a)** **(b)**

**Figure 32: InTEM estimates of spatial distribution of HFC-152a emissions using global meteorology and MHD observations with minimal prior information. Black squares are measurement stations and circles are major cities in UK. (a) Average 2004-2007 (b) Average 2014-2017.**

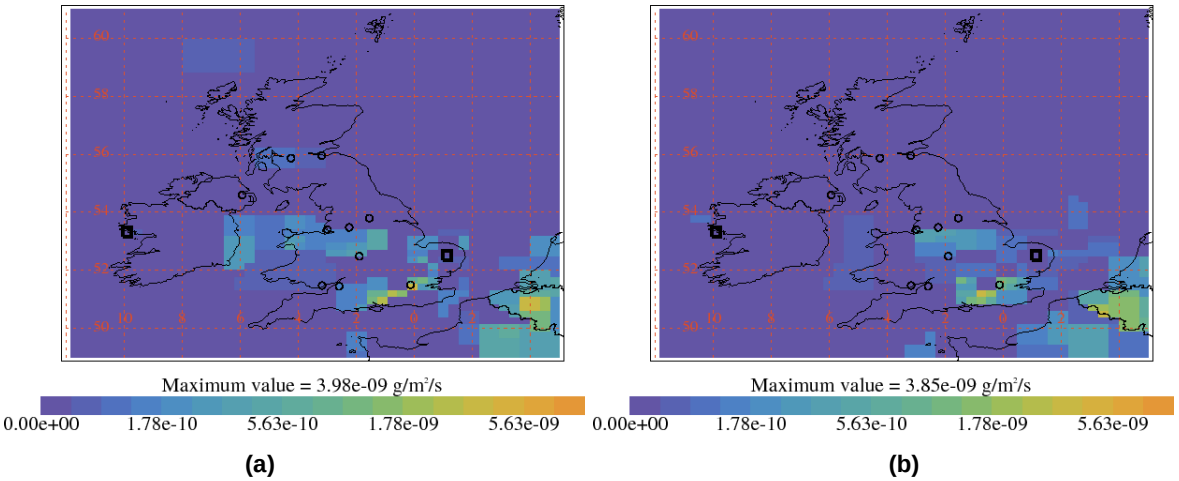


**(a)** **(b)**

**Figure 33: Average InTEM estimates 2014-2017 of spatial distribution of HFC-152a emissions using DECC observations with minimal prior information. Black squares are measurement stations and circles are major cities in UK. (a) Global meteorology and (b) UKV meteorology.**

## 4.11 HFC-23

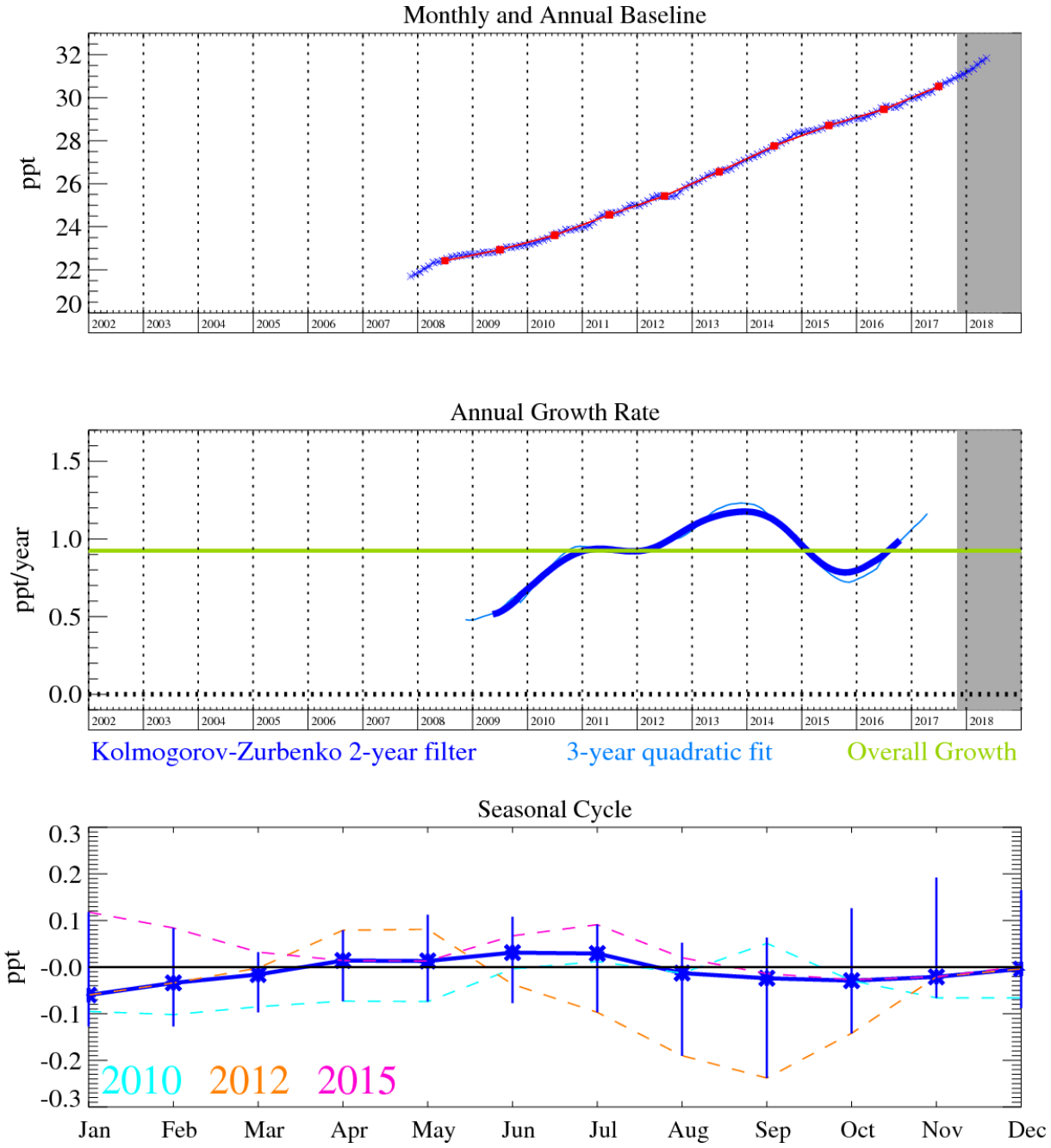


**Figure 34: HFC-23 ($CHF_3$): Monthly (blue) and annual (red) Northern Hemisphere baseline mole fractions. Annual (blue) and overall average growth rate (green) (lower plot). Grey area covers un-ratified provisional data.**

HFC-23 ($CHF_3$) is primarily a by-product formed by the over fluorination of chloroform during the production of HCFC-22. Other minor emissions arise from the electronic industry and fire extinguishers. It is the second most abundant HFC in the atmosphere after HFC-134a; this, combined with a long atmospheric lifetime of 228 years, makes this compound a potent GHG. Emissions of HFC-23 in developed countries have declined due to the Montreal Protocol phase-out schedule for HCFC-22; however, emissions from developing countries continues to drive global atmospheric concentrations up.

The InTEM estimates for the UK are higher than the inventory estimates and the uncertainty ranges do not overlap, however, the emissions are very small. There are no clear geographical areas where the emissions are particularly strong.

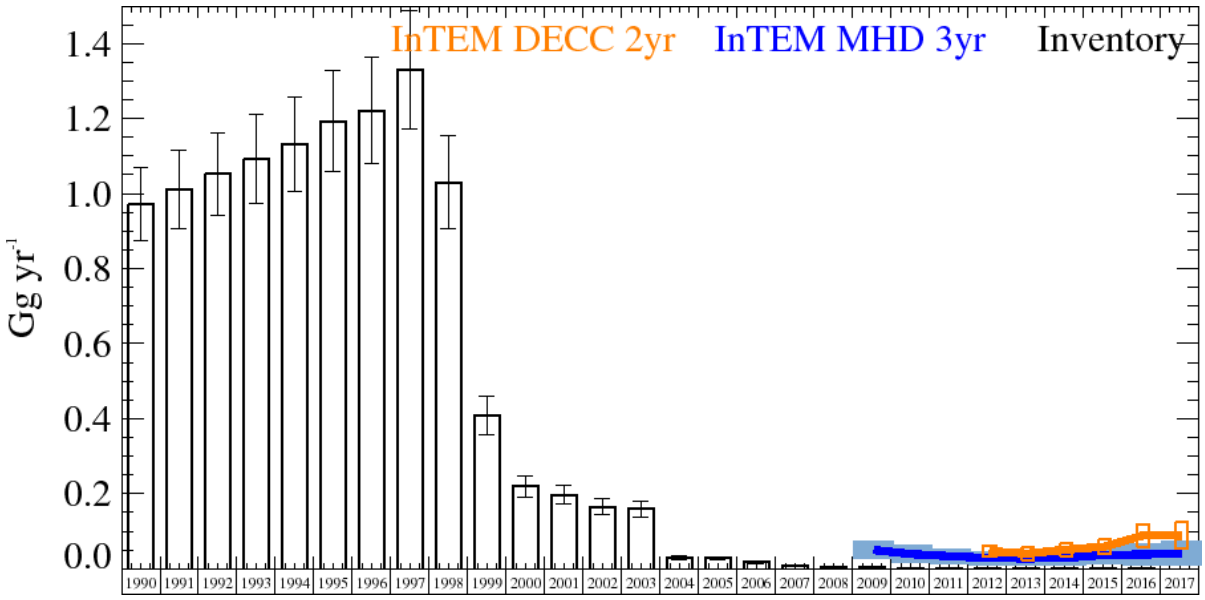


**Figure 35: HFC-23 UK Emission estimates (Gg $yr^{-1}$) from the UNFCCC Inventory (black) and InTEM with global meteorology: 3-year MHD (blue) and 2-year DECC network (orange). The uncertainty bars represent 1 std.**

| Years | Inventory 1yr | MHD 3yr | DECC 2yr |
|---|---|---|---|
| 1990 | 0.972 (0.875-1.070) | | |
| 1991 | 1.012 (0.908-1.116) | | |
| 1992 | 1.052 (0.941-1.163) | | |
| 1993 | 1.092 (0.974-1.211) | | |
| 1994 | 1.133 (1.007-1.258) | | |
| 1995 | 1.193 (1.057-1.328) | | |
| 1996 | 1.221 (1.079-1.362) | | |
| 1997 | 1.331 (1.173-1.489) | | |
| 1998 | 1.030 (0.905-1.155) | | |
| 1999 | 0.410 (0.359-0.461) | | |
| 2000 | 0.219 (0.191-0.247) | | |
| 2001 | 0.197 (0.171-0.222) | | |
| 2002 | 0.165 (0.144-0.187) | | |
| 2003 | 0.159 (0.137-0.180) | | |
| 2004 | 0.0294 (0.0253-0.0334) | | |
| 2005 | 0.0280 (0.0241-0.0319) | | |
| 2006 | 0.0172 (0.0148-0.0197) | | |
| 2007 | 0.0083 (0.0071-0.0095) | | |
| 2008 | 0.0047 (0.0040-0.0054) | | |
| 2009 | 0.0038 (0.0032-0.0044) | 0.050 (0.026-0.073) | |
| 2010 | 0.0011 (0.0010-0.0013) | 0.039 (0.015-0.063) | |
| 2011 | 0.0010 (0.0009-0.0012) | 0.0335 (0.0143-0.0527) | |
| 2012 | 0.0009 (0.0008-0.0011) | 0.0285 (0.0103-0.0467) | 0.0471 (0.0313-0.0629) |
| 2013 | 0.0010 (0.0009-0.0012) | 0.0278 (0.0096-0.0460) | 0.0406 (0.0236-0.0576) |
| 2014 | 0.0012 (0.0010-0.0015) | 0.029 (0.008-0.049) | 0.0512 (0.0341-0.0683) |
| 2015 | 0.0014 (0.0011-0.0016) | 0.037 (0.012-0.062) | 0.059 (0.038-0.079) |
| 2016 | 0.0015 (0.0012-0.0017) | 0.038 (0.010-0.067) | 0.089 (0.059-0.119) |
| 2017 | | 0.041 (0.006-0.076) | 0.088 (0.052-0.123) |

**Table 12: HFC-23 emission (Gg $yr^{-1}$) estimates for the UK with uncertainty (1std).**

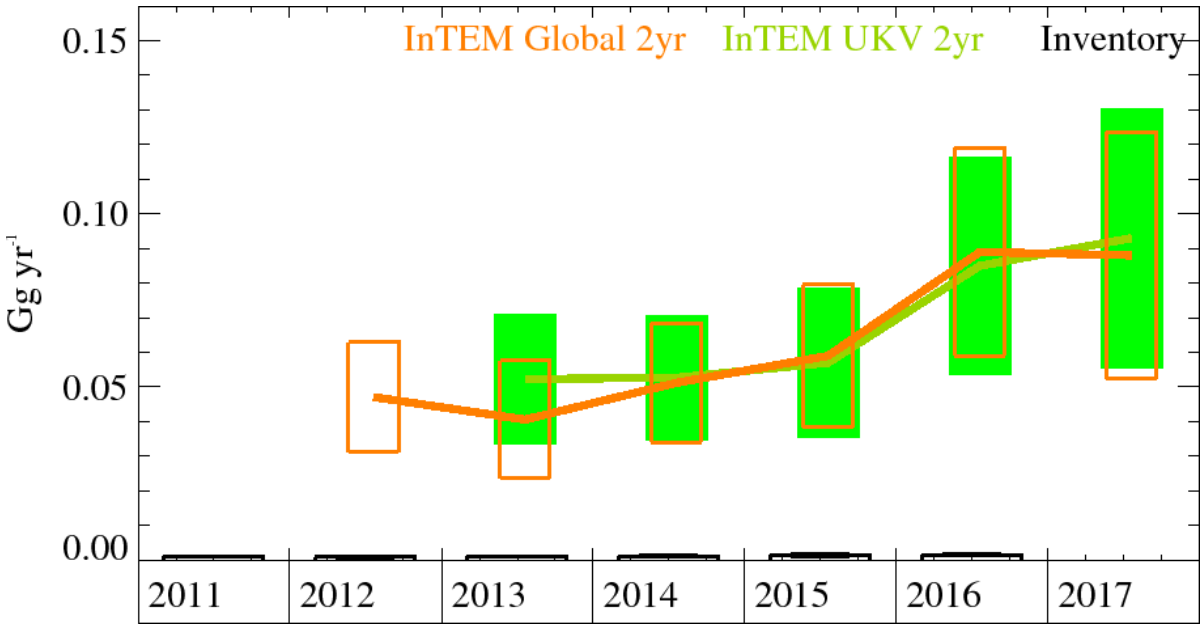


**Figure 36: HFC-23 emission estimates for the UK (Gg $yr^{-1}$) from the UNFCCC Inventory (black) and InTEM using the DECC observations, 2-year inversions with different meteorology: (orange) global meteorology and (green) 1.5 km high resolution meteorology. The uncertainty bars represent 1 std.**

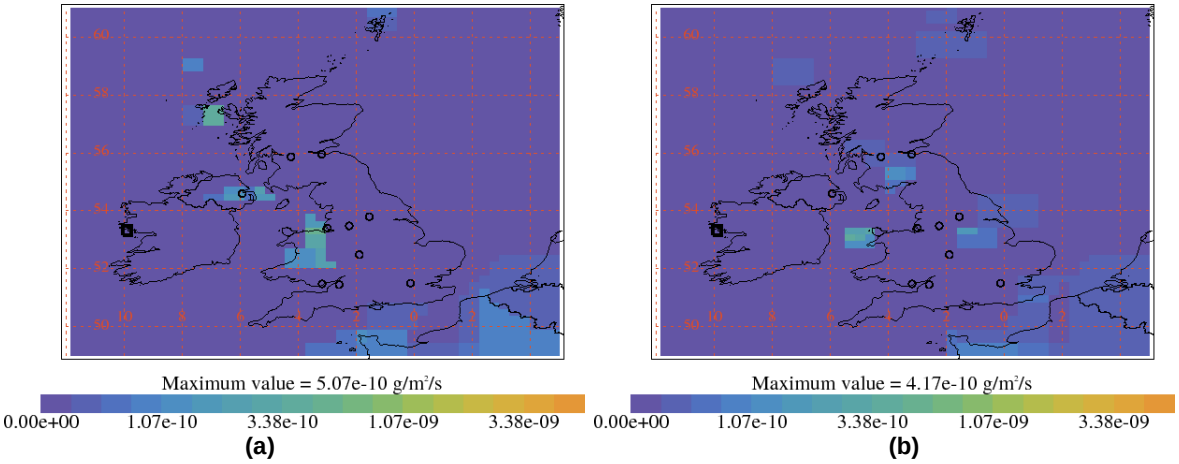


**Figure 37: InTEM estimates of spatial distribution of HFC-23 emissions using global meteorology and MHD observations with minimal prior information. Black squares are measurement stations and circles are major cities in UK. (a) Average 2008-2011 (b) Average 2014-2017.**

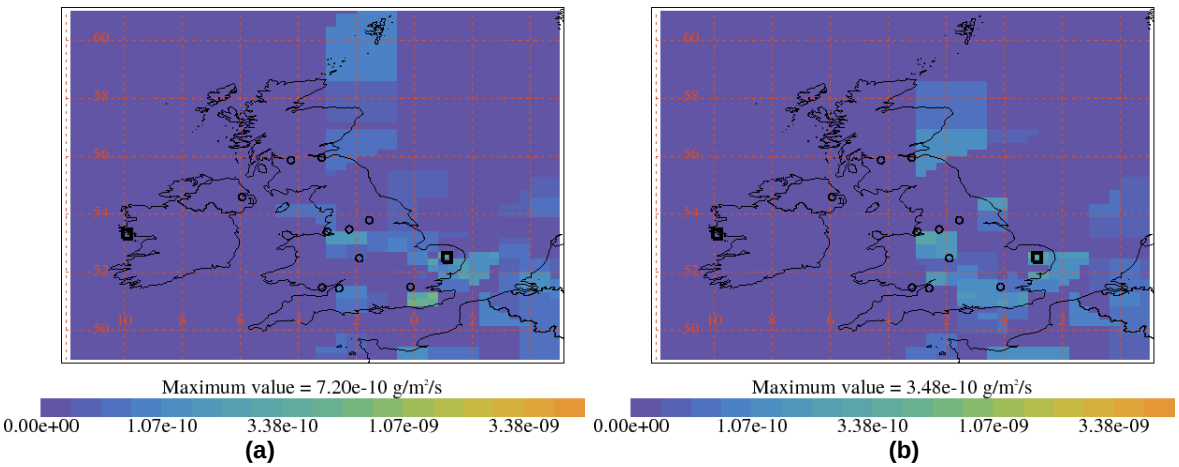


**Figure 38: Average InTEM estimates 2014-2017 of spatial distribution of HFC-23 emissions using DECC observations with minimal prior information. Black squares are measurement stations and circles are major cities in UK. (a) Global meteorology and (b) UKV meteorology.**

## 4.12 HFC-32

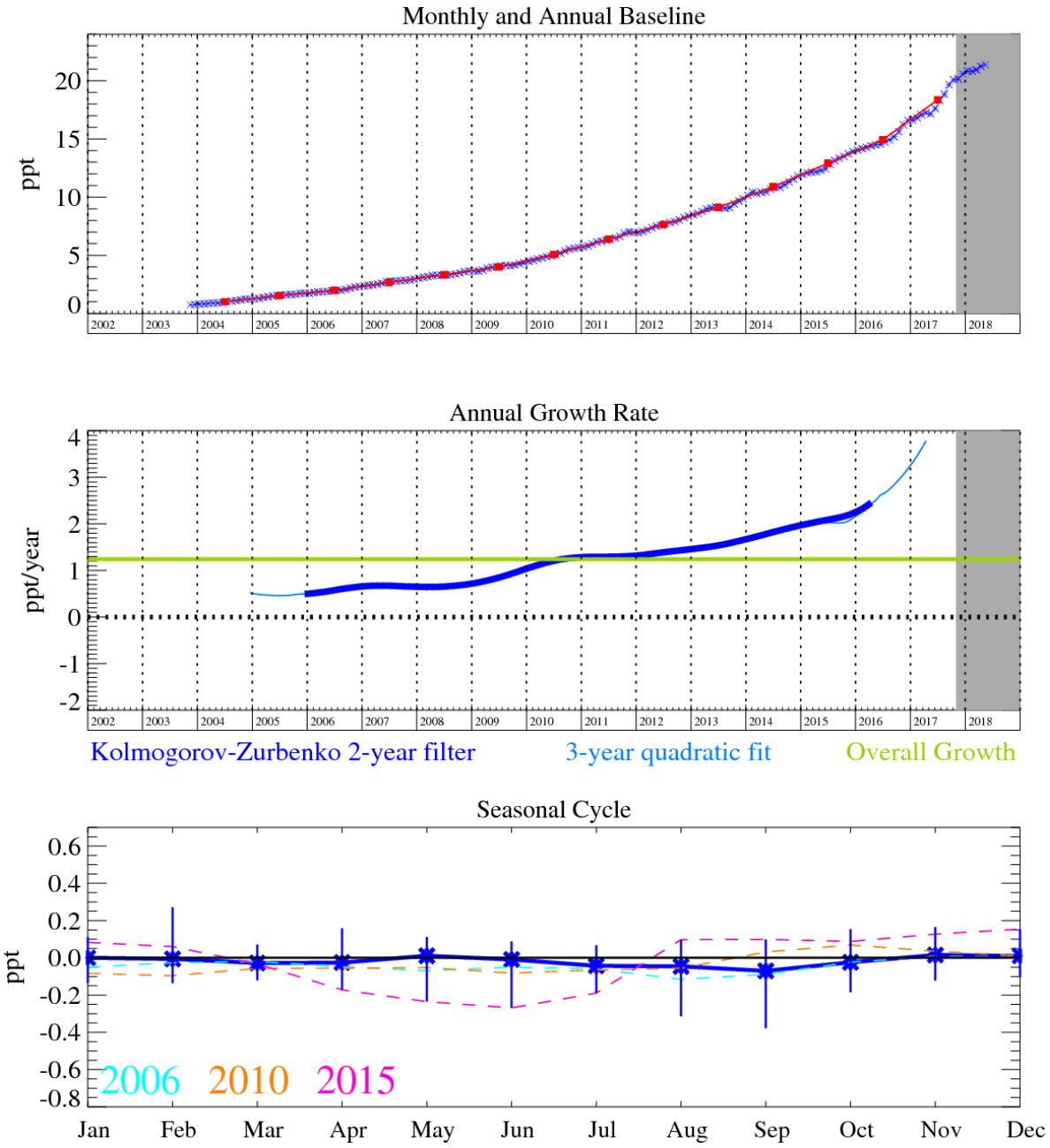


**Figure 39: HFC-32 ($CH_2F_2$): Monthly (blue) and annual (red) Northern Hemisphere baseline mole fractions (top plot). Annual (blue) and overall average growth rate (green) (middle plot). Seasonal cycle (de-trended) with year-to-year variability (lower plot). Grey area covers un-ratified and therefore provisional data.**

HFC-32 ($CH_2F_2$) has an atmospheric lifetime of 5.4 years and a $GWP_{100}$ of 716. It is used in air conditioning and refrigeration applications; R-410A (50% HFC-32, 50% HFC-125 by weight) and R-407C (23% HFC-32, 52% HFC-134a, 25% HFC-125 by weight) are used as replacements to HCFC-22. As the phase-out of HCFC-22 gains momentum it might be expected that demand for these refrigerant blends will increase. The pollution events measured at Mace Head are highly correlated with those of HFC-125.

Unfortunately, the observations of HFC-32 at Mace Head, like those of HFC-125, were compromised by contamination from the air conditioning system (May 2014 – June 2015) and these data had to be removed. Like HFC-125, during this period the NH baseline has been estimated using another AGAGE NH station, Zeppelin (Ny-Ålesund).

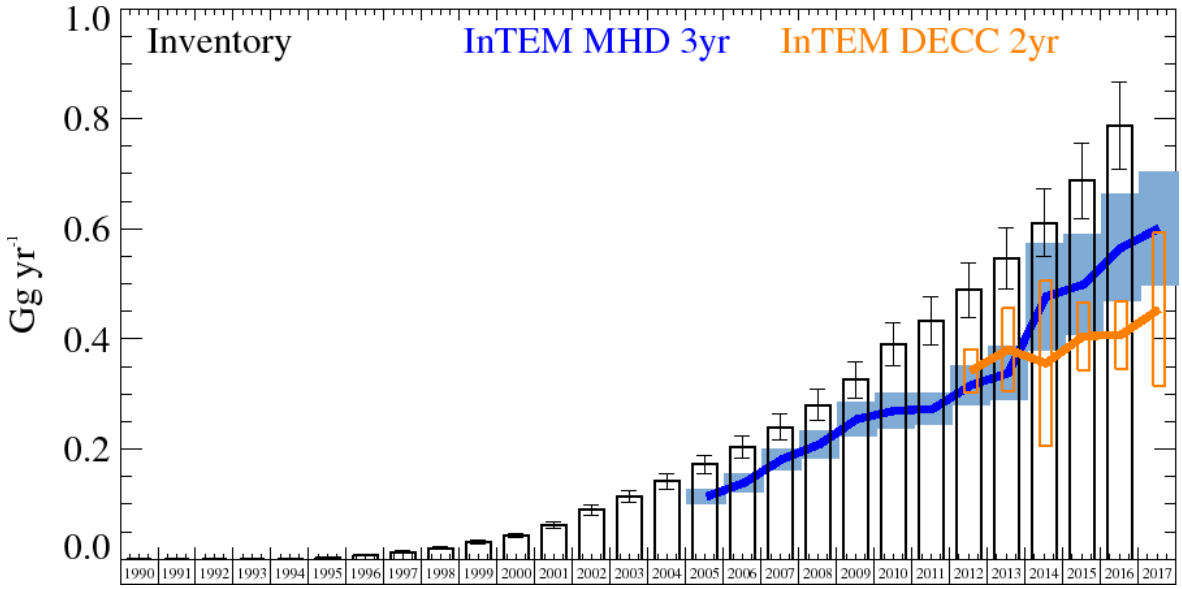


**Figure 40: HFC-32 UK Emission estimates (Gg $yr^{-1}$) from the UNFCCC Inventory (black) and InTEM with global meteorology: 3-year MHD (blue) and 2-year DECC network (orange). The uncertainty bars = 1 std.**

| Years | Inventory 1yr | MHD 3yr | DECC 2yr |
|---|---|---|---|
| 1990 | 0.0000 (0.0000-0.0000) | | |
| 1991 | 0.0000 (0.0000-0.0000) | | |
| 1992 | 0.0000 (0.0000-0.0000) | | |
| 1993 | 0.0000 (0.0000-0.0001) | | |
| 1994 | 0.0013 (0.0012-0.0014) | | |
| 1995 | 0.0033 (0.0030-0.0037) | | |
| 1996 | 0.0071 (0.0064-0.0079) | | |
| 1997 | 0.013 (0.011-0.014) | | |
| 1998 | 0.020 (0.018-0.021) | | |
| 1999 | 0.0308 (0.0277-0.0338) | | |
| 2000 | 0.0429 (0.0386-0.0471) | | |
| 2001 | 0.0626 (0.0563-0.0688) | | |
| 2002 | 0.0898 (0.0808-0.0988) | | |
| 2003 | 0.1141 (0.1027-0.1255) | | |
| 2004 | 0.1421 (0.1279-0.1563) | | |
| 2005 | 0.1723 (0.1551-0.1895) | 0.1138 (0.0995-0.1281) | |
| 2006 | 0.203 (0.183-0.223) | 0.1390 (0.1229-0.1551) | |
| 2007 | 0.240 (0.216-0.264) | 0.1815 (0.1627-0.2003) | |
| 2008 | 0.280 (0.252-0.308) | 0.209 (0.183-0.235) | |
| 2009 | 0.326 (0.293-0.358) | 0.255 (0.225-0.286) | |
| 2010 | 0.390 (0.351-0.429) | 0.270 (0.239-0.302) | |
| 2011 | 0.433 (0.390-0.477) | 0.273 (0.244-0.303) | |
| 2012 | 0.489 (0.440-0.538) | 0.316 (0.280-0.353) | 0.342 (0.302-0.381) |
| 2013 | 0.547 (0.492-0.602) | 0.338 (0.289-0.387) | 0.381 (0.306-0.456) |
| 2014 | 0.611 (0.550-0.672) | 0.477 (0.380-0.575) | 0.356 (0.205-0.506) |
| 2015 | 0.688 (0.620-0.757) | 0.499 (0.408-0.589) | 0.405 (0.343-0.467) |
| 2016 | 0.787 (0.709-0.866) | 0.566 (0.469-0.663) | 0.408 (0.347-0.470) |
| 2017 | | 0.601 (0.497-0.705) | 0.454 (0.314-0.593) |

**Table 13: HFC-32 emission (Gg $yr^{-1}$) estimates for the UK with uncertainty (1std).**

The UK inventory estimates grow strongly throughout the time-series. The InTEM estimates using only MHD data are increasing throughout. The InTEM estimates for the UK using the additional TAC observations do increase but at a slower rate than for the MHD-only inversions. The reason for this difference is unclear and is under investigation. The InTEM results using either data set are lower than the inventory estimates and the uncertainties do not overlap. The emissions are broadly population based. There is a noticeable difference observed in the InTEM results when TAC observations are included, this requires further investigation.

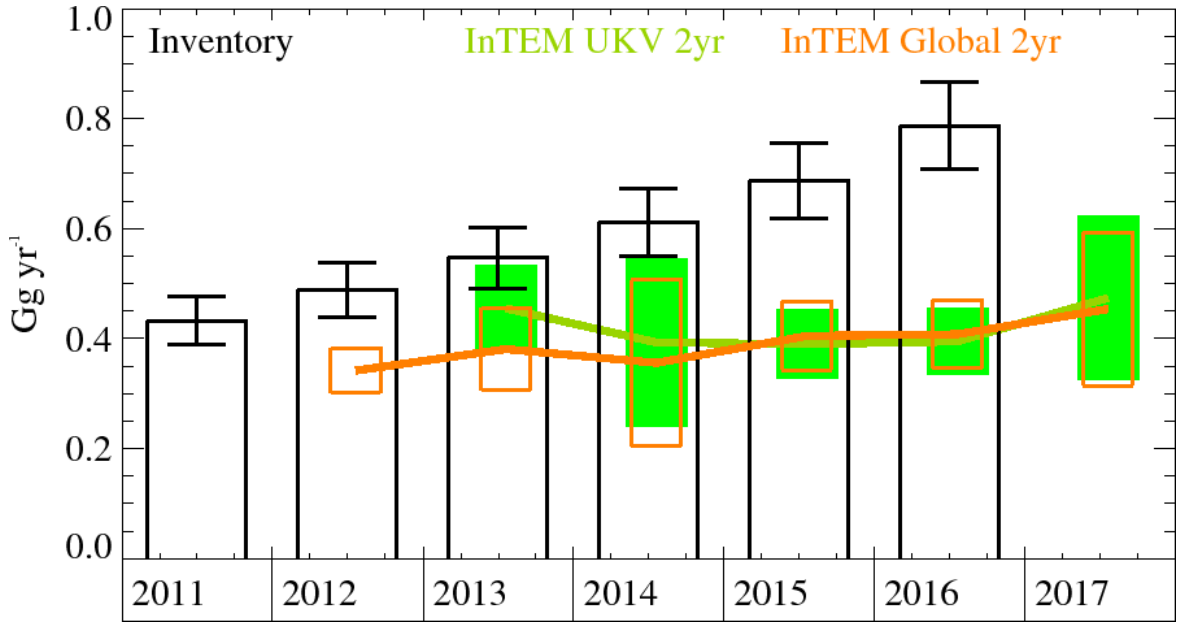


**Figure 41: HFC-32 emission estimates for the UK (Gg $yr^{-1}$) from the UNFCCC Inventory (black) and InTEM using the DECC observations, 2-year inversions with different meteorology: (orange) global meteorology and (green) 1.5 km high resolution meteorology. The uncertainty bars represent 1 std.**

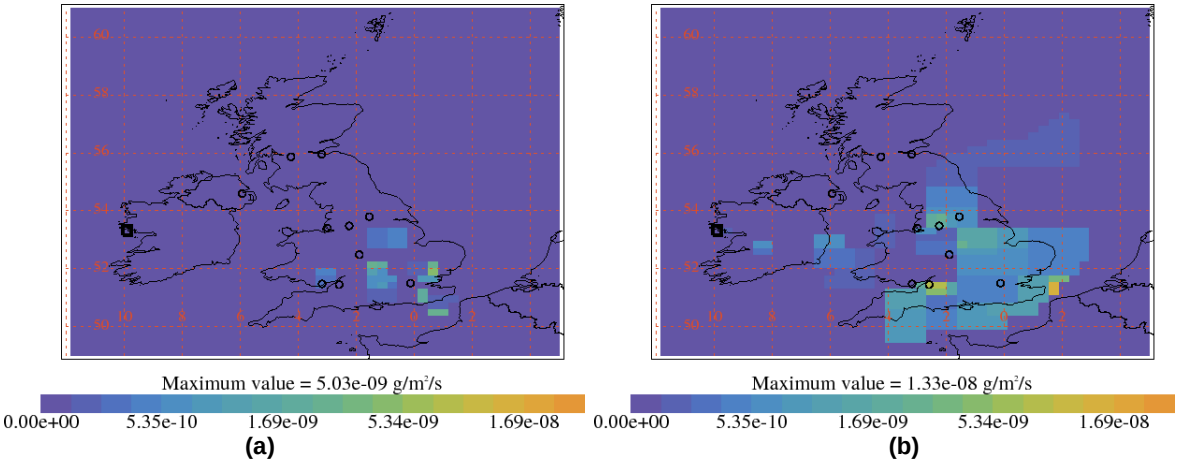


**Figure 42: InTEM estimates of spatial distribution of HFC-32 emissions using global meteorology and MHD observations with minimal prior information. Black squares are measurement stations and circles are major cities in UK. (a) Average 2004-2007 (b) Average 2014-2017.**

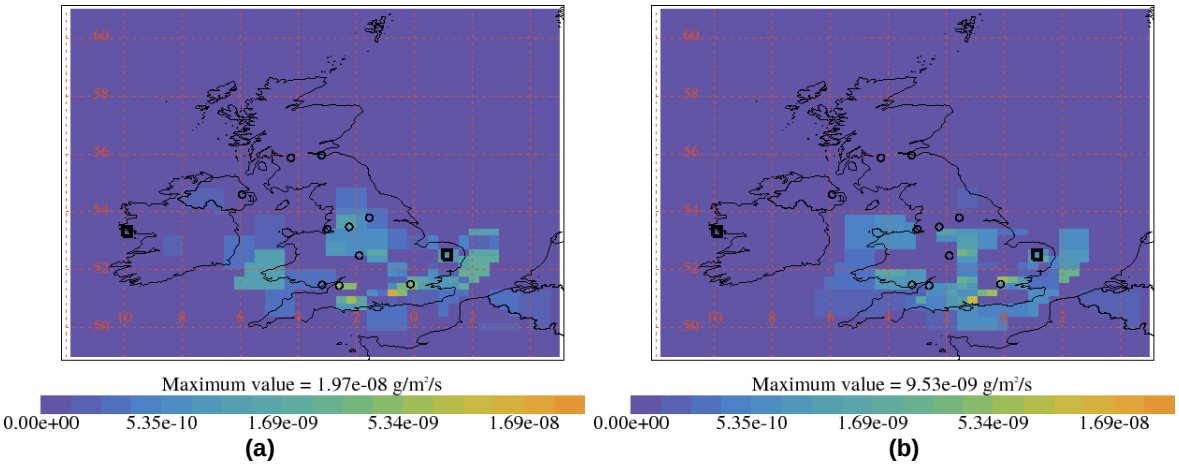


**Figure 43: Average InTEM estimates 2014-2017 of spatial distribution of HFC-32 emissions using DECC observations with minimal prior information. Black squares are measurement stations and circles are major cities in UK. (a) Global meteorology and (b) UKV meteorology.**

## 4.13 HFC-227ea

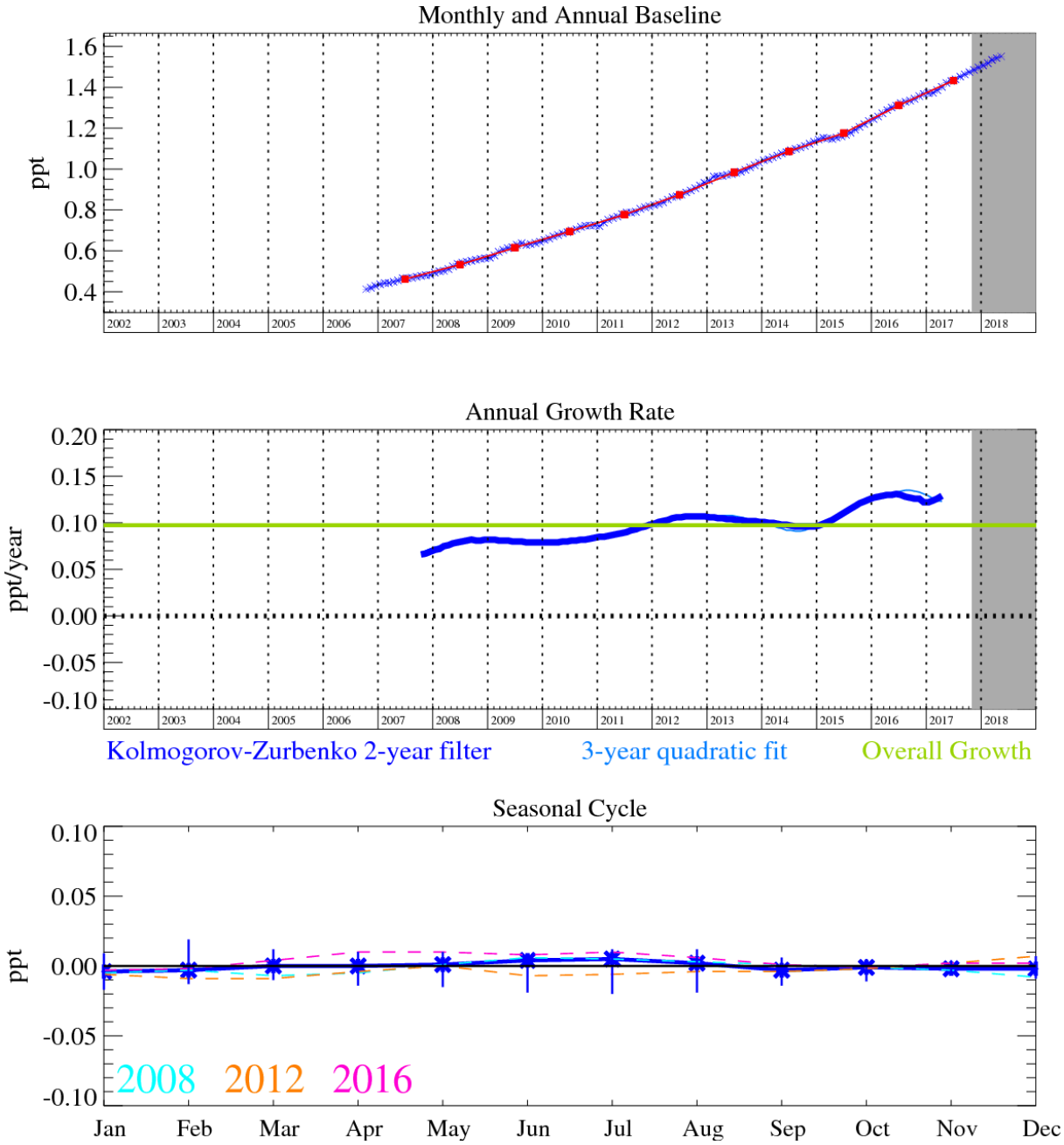


**Figure 44: HFC-227ea ($C_3HF_7$): Monthly (blue) and annual (red) Northern Hemisphere baseline mole fractions (top plot). Annual (blue) and overall average growth rate (green) (middle plot). Seasonal cycle (de-trended) with year-to-year variability (lower plot). Grey area covers un-ratified and therefore provisional data.**

HFC-227ea ($C_3HF_7$) was added to the Medusa analysis in October 2006. HFC-227ea is used as a propellant for medical aerosols and a fire-fighting agent and to a lesser extent in metered-dose inhalers, and foam blowing (atmospheric lifetime 35.8 years and $GWP_{100}$ of 3580).

The InTEM results are significantly lower (~50-60%) than the inventory estimates. The reason for this difference is unknown. The results, when the observations from TAC are incorporated, are similar to, but slightly lower than, the MHD-only InTEM results.

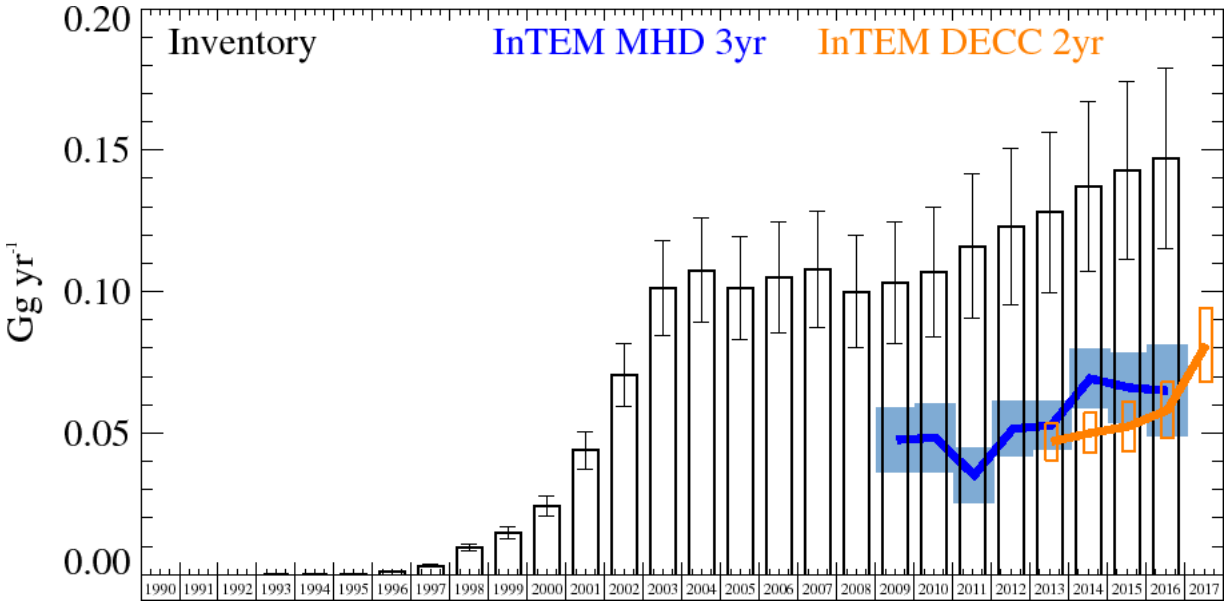


**Figure 45: HFC-227ea UK Emission estimates (Gg $yr^{-1}$) from the UNFCCC Inventory (black) and InTEM with global meteorology: 3-year MHD (blue) and 2-year DECC network (orange). The uncertainty bars = 1 std.**

| Years | Inventory 1yr | MHD 3yr | DECC 2yr |
|---|---|---|---|
| 1990 | 0.0 (0.0-0.0) | | |
| 1991 | 0.0 (0.0-0.0) | | |
| 1992 | 0.0 (0.0-0.0) | | |
| 1993 | 0.0000 (0.0000-0.0000) | | |
| 1994 | 0.0000 (0.0000-0.0000) | | |
| 1995 | 0.0003 (0.0003-0.0004) | | |
| 1996 | 0.0013 (0.0011-0.0015) | | |
| 1997 | 0.0032 (0.0028-0.0036) | | |
| 1998 | 0.0095 (0.0083-0.0108) | | |
| 1999 | 0.0149 (0.0128-0.0169) | | |
| 2000 | 0.0241 (0.0206-0.0276) | | |
| 2001 | 0.0439 (0.0373-0.0506) | | |
| 2002 | 0.0705 (0.0594-0.0817) | | |
| 2003 | 0.1014 (0.0847-0.1181) | | |
| 2004 | 0.1076 (0.0891-0.1260) | | |
| 2005 | 0.1013 (0.0832-0.1195) | | |
| 2006 | 0.1050 (0.0855-0.1245) | | |
| 2007 | 0.108 (0.087-0.128) | | |
| 2008 | 0.100 (0.080-0.120) | | |
| 2009 | 0.103 (0.081-0.124) | 0.0476 (0.0362-0.0590) | |
| 2010 | 0.107 (0.084-0.130) | 0.0484 (0.0362-0.0606) | |
| 2011 | 0.116 (0.090-0.141) | 0.0351 (0.0253-0.0449) | |
| 2012 | 0.123 (0.096-0.151) | 0.0515 (0.0418-0.0612) | |
| 2013 | 0.128 (0.100-0.157) | 0.0528 (0.0442-0.0614) | 0.0470 (0.0405-0.0535) |
| 2014 | 0.137 (0.107-0.167) | 0.0693 (0.0589-0.0797) | 0.0500 (0.0429-0.0571) |
| 2015 | 0.143 (0.112-0.175) | 0.0661 (0.0537-0.0785) | 0.0524 (0.0435-0.0613) |
| 2016 | 0.147 (0.115-0.179) | 0.0650 (0.0488-0.0812) | 0.0582 (0.0482-0.0682) |
| 2017 | | | 0.0812 (0.0680-0.0944) |

**Table 14: HFC-227ea emission (Gg $yr^{-1}$) estimates for the UK with uncertainty (1std).**

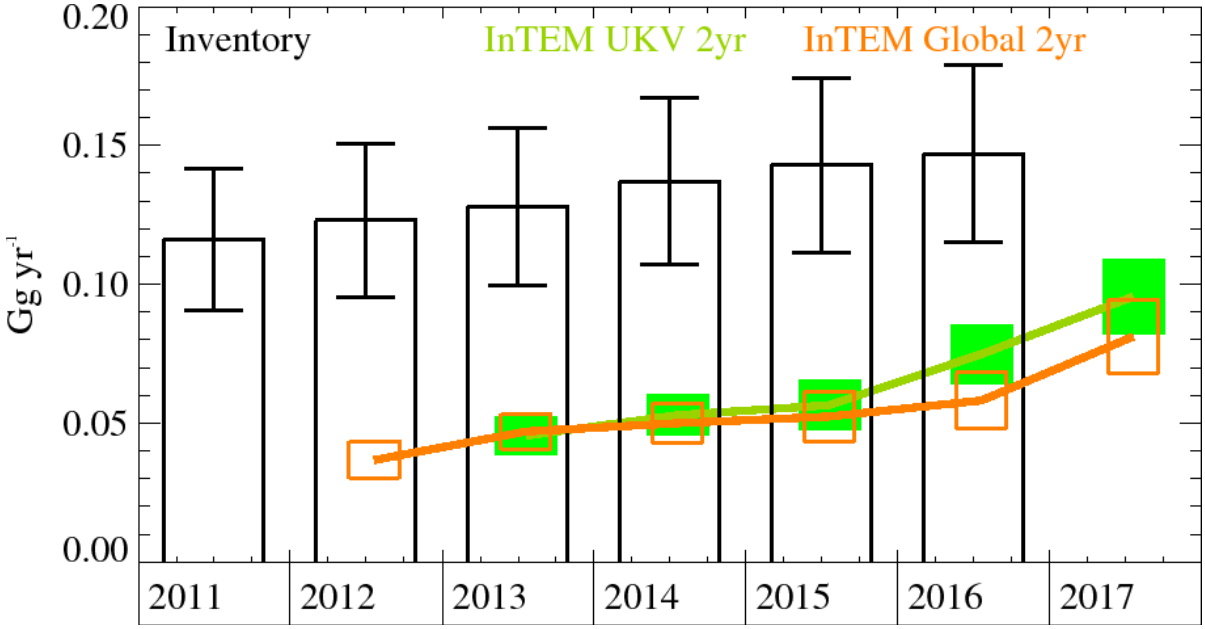


**Figure 46: HFC-227ea emission estimates for the UK (Gg $yr^{-1}$) from the UNFCCC Inventory (black) and InTEM using the DECC observations, 2-year inversions with different meteorology: (orange) global meteorology and (green) 1.5 km high resolution meteorology. The uncertainty bars represent 1 std.**

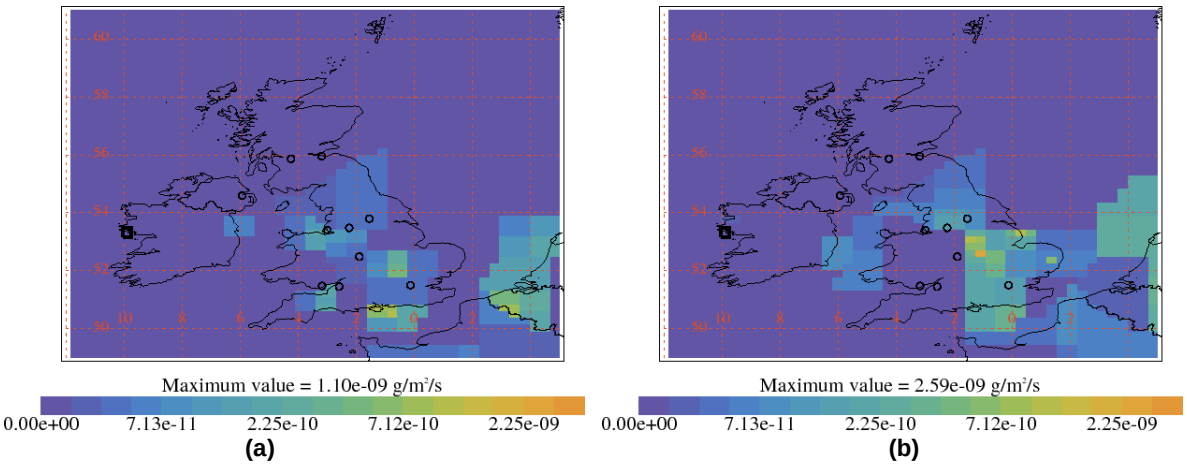


**Figure 47: InTEM estimates of spatial distribution of HFC-227ea emissions using global meteorology and MHD observations with minimal prior information. Black squares are measurement stations and circles are major cities in UK. (a) Average 2007-2010 (b) Average 2014-2017.**

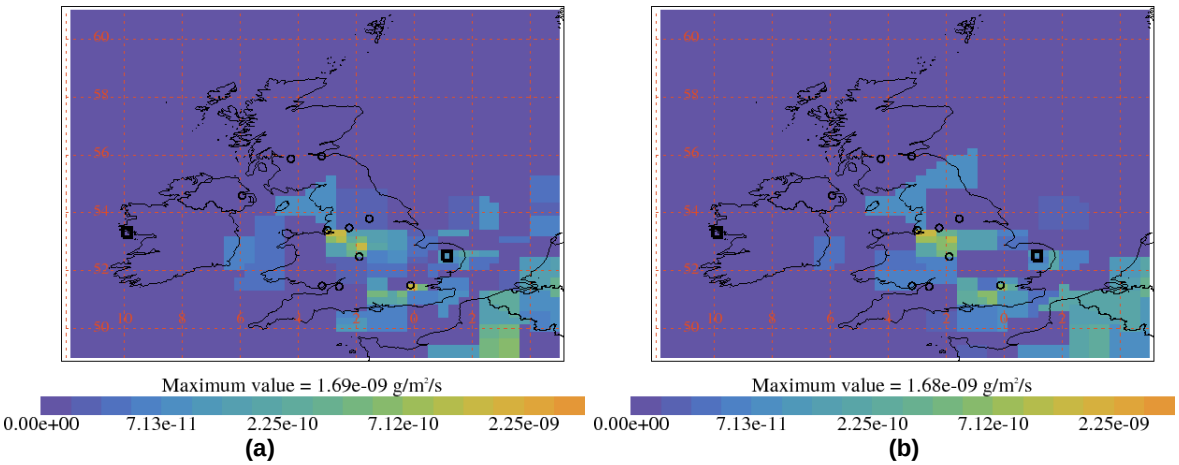


**Figure 48: Average InTEM estimates 2014-2017 of spatial distribution of HFC-227ea emissions using DECC observations with minimal prior information. Black squares are measurement stations and circles are major cities in UK. (a) Global meteorology and (b) UKV meteorology.**

## 4.14 HFC-245fa

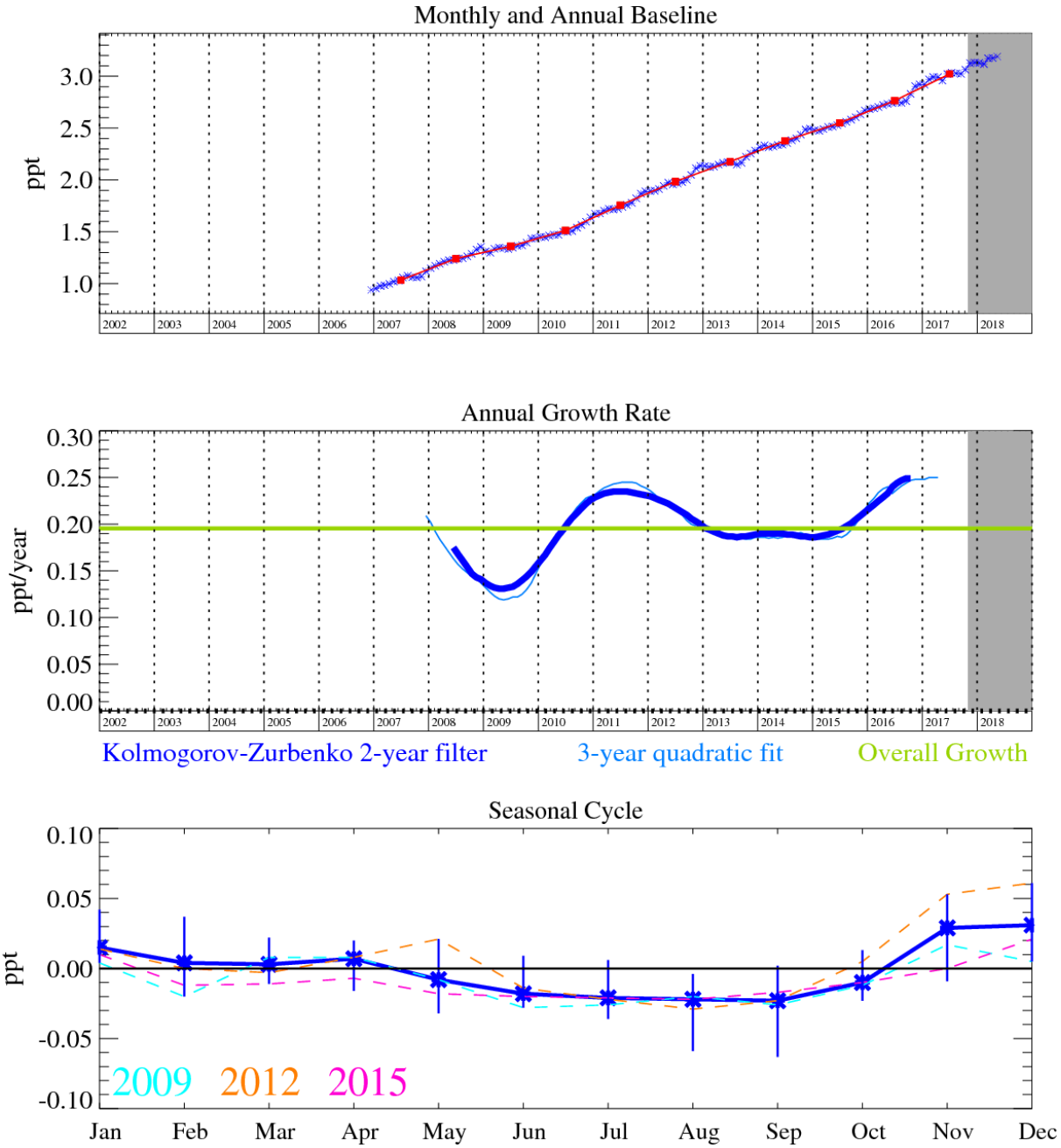


**Figure 49: HFC-245fa ($C_3H_3F_5$): Monthly (blue) and annual (red) baseline (top plot). Annual (blue) and overall average growth rate (green) (middle plot). Seasonal cycle (de-trended) with year-to-year variability (lower plot). Grey area covers un-ratified and therefore provisional data.**

The NH concentrations of HFC-245fa are steadily rising across the time-series of observations. The InTEM results for this gas are lower than those estimated in the inventory. The uncertainty bars for the InTEM results are large. The inclusion of TAC observations produces a broadly consistent picture to the MHD-only InTEM estimates. InTEM estimates for the UK are showing an upturn from 2015 onwards. Emissions are estimated to be population based.

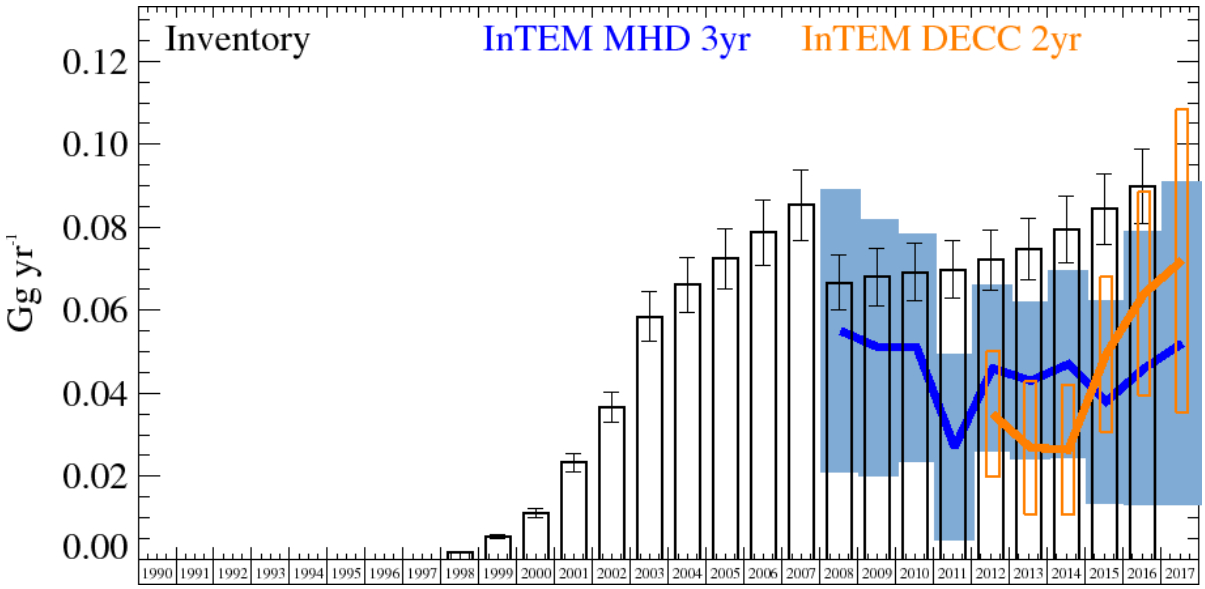


**Figure 50: HFC-245fa UK Emission estimates (Gg yr$^{-1}$) from the UNFCCC Inventory (black) and InTEM with global meteorology: 3-year MHD (blue) and 2-year DECC network (orange). The uncertainty bars represent 1 std.**

| Years | Inventory 1yr | MHD 3yr | DECC 2yr |
|---|---|---|---|
| 1990 | 0.0 (0.0-0.0) | | |
| 1991 | 0.0 (0.0-0.0) | | |
| 1992 | 0.0 (0.0-0.0) | | |
| 1993 | 0.0 (0.0-0.0) | | |
| 1994 | 0.0 (0.0-0.0) | | |
| 1995 | 0.0 (0.0-0.0) | | |
| 1996 | 0.0 (0.0-0.0) | | |
| 1997 | 0.0 (0.0-0.0) | | |
| 1998 | 0.0017 (0.0015-0.0019) | | |
| 1999 | 0.0054 (0.0049-0.0060) | | |
| 2000 | 0.0111 (0.0100-0.0122) | | |
| 2001 | 0.0233 (0.0210-0.0256) | | |
| 2002 | 0.0367 (0.0331-0.0404) | | |
| 2003 | 0.0585 (0.0527-0.0644) | | |
| 2004 | 0.0662 (0.0596-0.0728) | | |
| 2005 | 0.0725 (0.0653-0.0798) | | |
| 2006 | 0.0788 (0.0710-0.0867) | | |
| 2007 | 0.0854 (0.0769-0.0940) | | |
| 2008 | 0.0667 (0.0600-0.0734) | 0.055 (0.021-0.089) | |
| 2009 | 0.0680 (0.0612-0.0749) | 0.051 (0.020-0.082) | |
| 2010 | 0.0692 (0.0623-0.0761) | 0.051 (0.024-0.079) | |
| 2011 | 0.0698 (0.0628-0.0768) | 0.027 (0.005-0.050) | |
| 2012 | 0.0721 (0.0649-0.0793) | 0.046 (0.026-0.066) | 0.0350 (0.0198-0.0502) |
| 2013 | 0.0747 (0.0673-0.0822) | 0.043 (0.024-0.062) | 0.0269 (0.0109-0.0429) |
| 2014 | 0.0794 (0.0714-0.0873) | 0.047 (0.024-0.069) | 0.0264 (0.0107-0.0421) |
| 2015 | 0.0844 (0.0760-0.0928) | 0.038 (0.013-0.062) | 0.0494 (0.0308-0.0680) |
| 2016 | 0.0899 (0.0809-0.0989) | 0.046 (0.013-0.079) | 0.064 (0.040-0.089) |
| 2017 | | 0.052 (0.013-0.091) | 0.072 (0.035-0.108) |

**Table 15: HFC-245fa emission (Gg yr$^{-1}$) estimates for the UK with uncertainty (1std).**

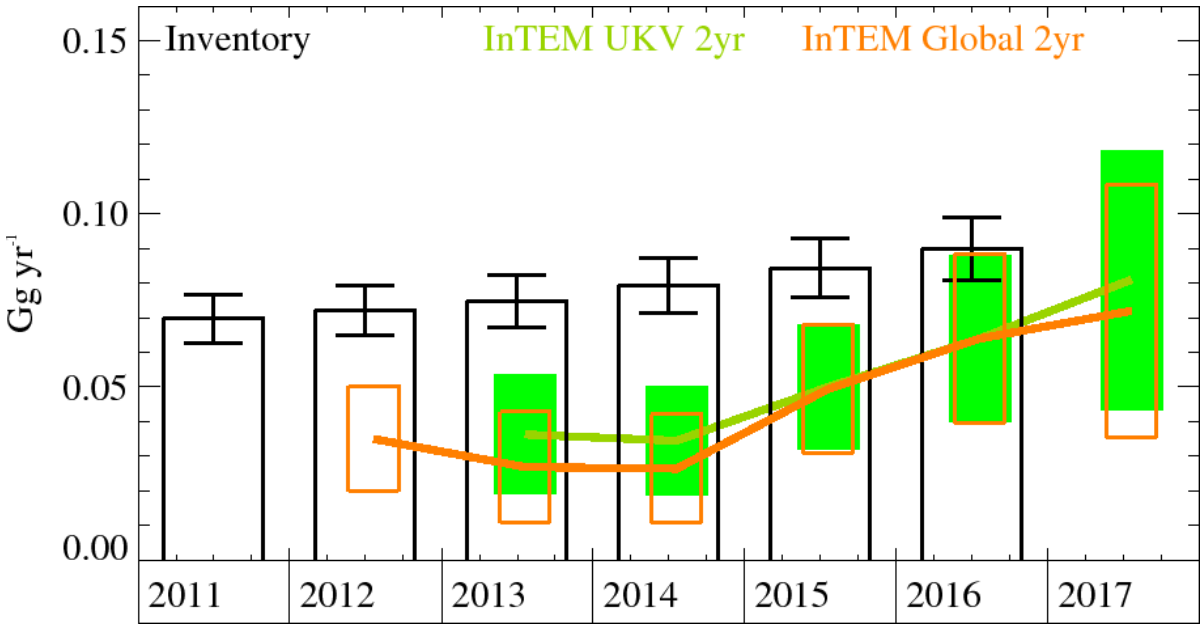


**Figure 51: HFC-245fa emission estimates for the UK (Gg yr$^{-1}$) from the UNFCCC Inventory (black) and InTEM using the DECC observations, 2-year inversions with different meteorology: (orange) global meteorology and (green) 1.5 km high resolution meteorology. The uncertainty bars represent 1 std.**

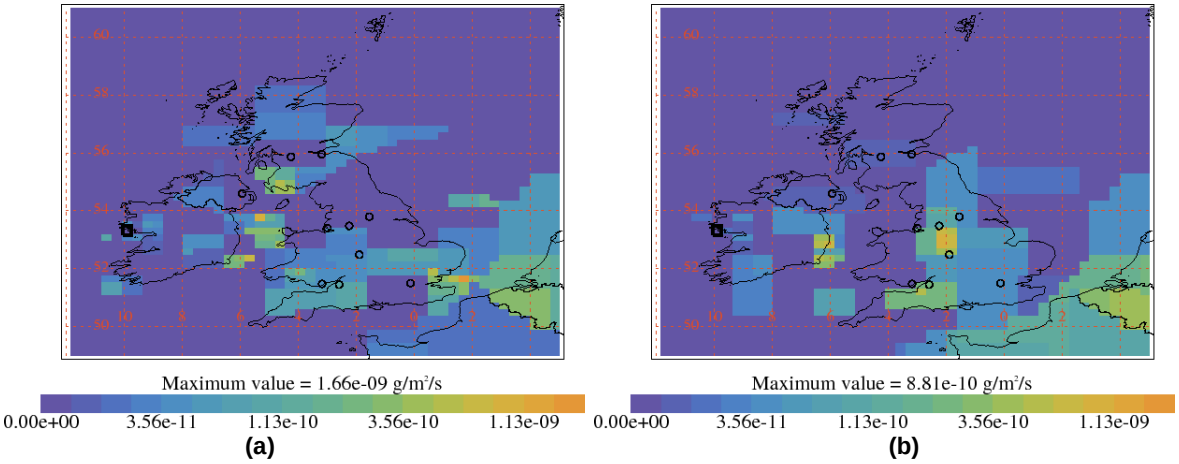


**Figure 52: InTEM estimates of spatial distribution of HFC-245fa emissions using global meteorology and MHD observations with minimal prior information. Black squares are measurement stations and circles are major cities in UK. (a) Average 2007-2010 (b) Average 2014-2017.**

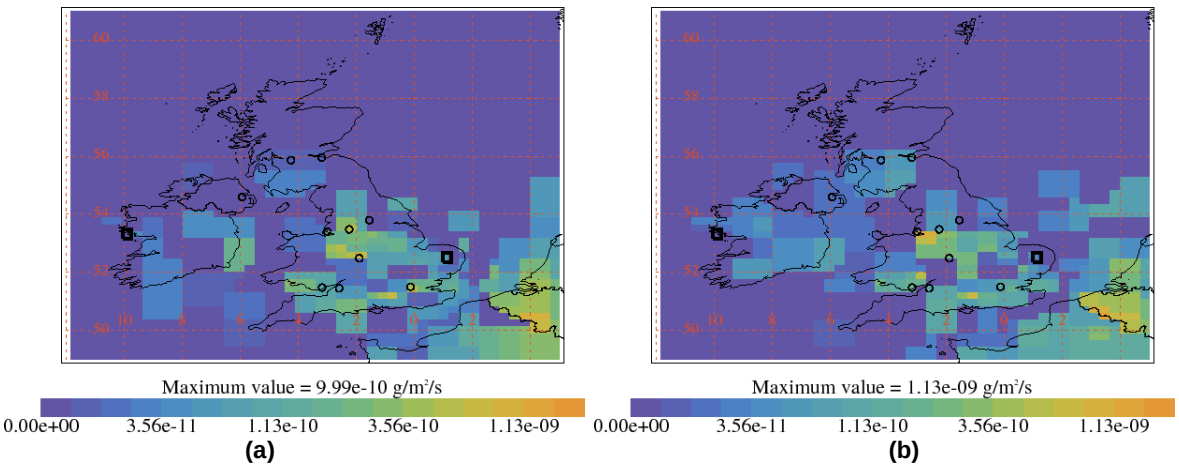


**Figure 53: Average InTEM estimates 2014-2017 of spatial distribution of HFC-245fa emissions using DECC observations with minimal prior information. Black squares are measurement stations and circles are major cities in UK. (a) Global meteorology and (b) UKV meteorology.**

## 4.15 HFC-43-10mee

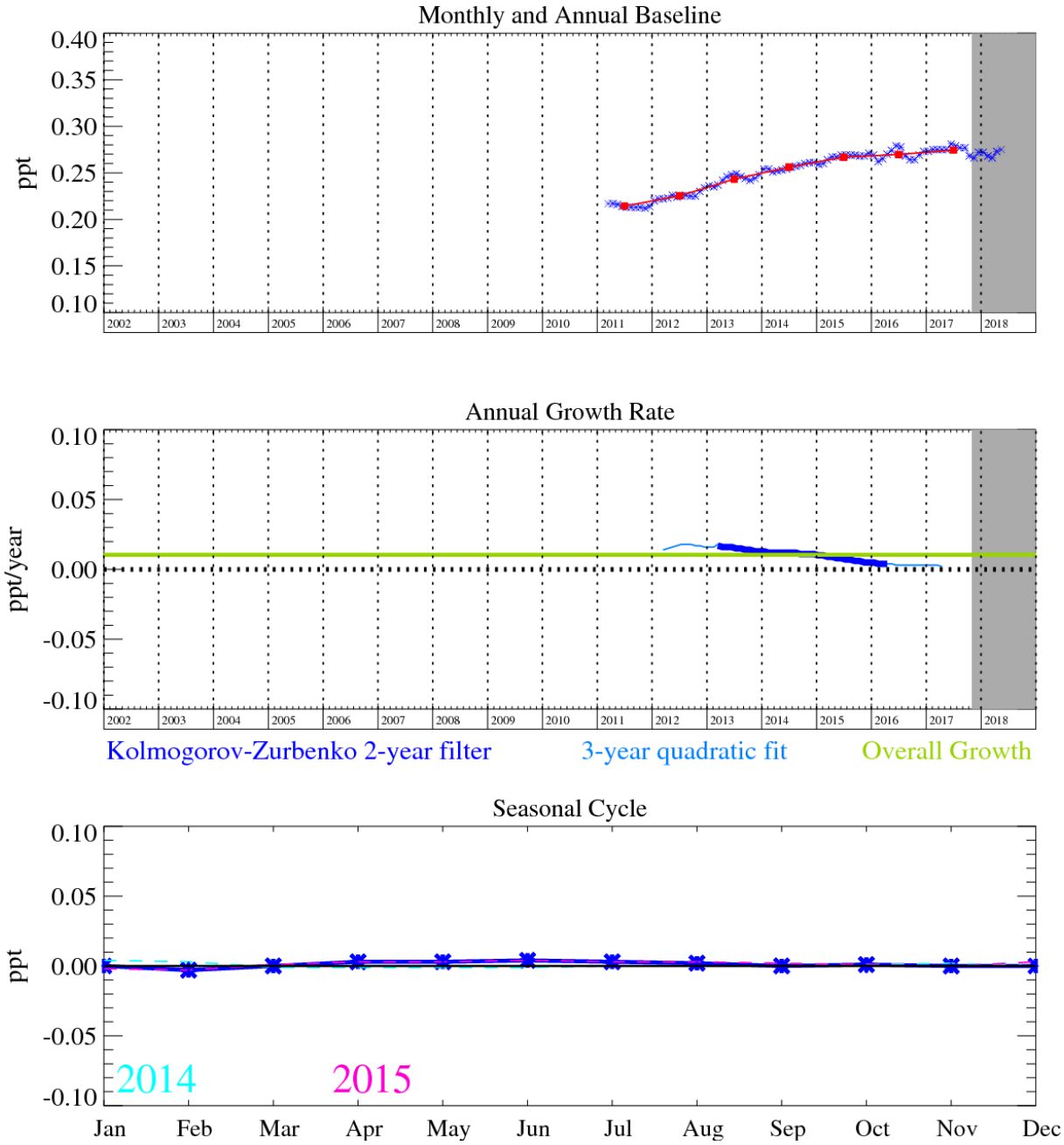


**Figure 54: HFC-43-10mee ($C_5H_2F_{10}$): Monthly (blue) and annual (red) Northern Hemisphere baseline mole fractions (top plot). Annual (blue) and overall average growth rate (green) (middle plot). Seasonal cycle (de-trended) with year-to-year variability (lower plot). Grey area covers un-ratified and therefore provisional data.**

HFC-43-10mee ($C_5H_2F_{10}$) was introduced in the mid 1990s as a replacement for CFC-113. It meets many requirements in the electronics industries and replaces PFCs in some uses such as a carrier fluid for lubricants applied to computer hard disks. It has an atmospheric lifetime of 16.1 years, a $GWP_{100}$ of 1,650 and a radiative efficiency of 0.42 W $m^{-2}$ $ppb^{-1}$. The NH concentration has grown very slowly since measurements began in 2011.

The inversion results for HFC-43-10mee show that there is disagreement between the inventory and the InTEM results, although the emissions are relatively small in both estimates. The InTEM estimates are about a quarter of the inventory estimates and the uncertainties do not overlap.

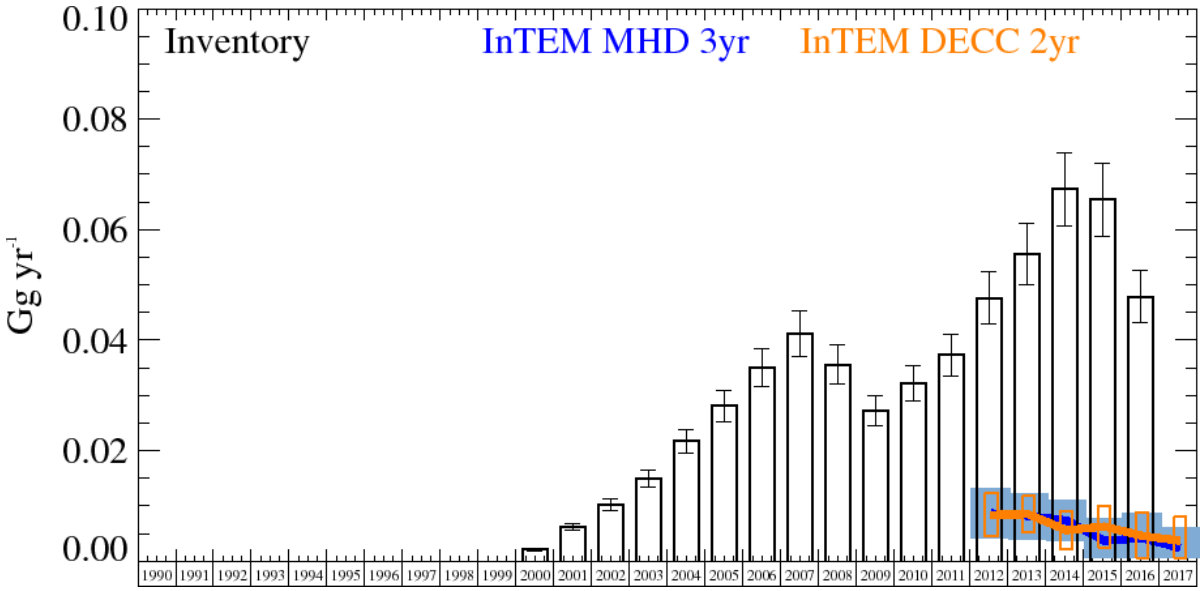


**Figure 55: HFC-43-10mee UK Emission estimates (Gg $yr^{-1}$) from the UNFCCC Inventory (black) and InTEM with global meteorology: 3-year MHD (blue) and 2-year DECC network (orange). The uncertainty bars represent 1 std.**

| Years | Inventory 1yr | MHD 3yr | DECC 2yr |
|---|---|---|---|
| 1990 | 0.0 (0.0-0.0) | | |
| 1991 | 0.0 (0.0-0.0) | | |
| 1992 | 0.0 (0.0-0.0) | | |
| 1993 | 0.0 (0.0-0.0) | | |
| 1994 | 0.0 (0.0-0.0) | | |
| 1995 | 0.0 (0.0-0.0) | | |
| 1996 | 0.0 (0.0-0.0) | | |
| 1997 | 0.0 (0.0-0.0) | | |
| 1998 | 0.0 (0.0-0.0) | | |
| 1999 | 0.0 (0.0-0.0) | | |
| 2000 | 0.0021 (0.0019-0.0023) | | |
| 2001 | 0.0062 (0.0056-0.0068) | | |
| 2002 | 0.0102 (0.0092-0.0113) | | |
| 2003 | 0.0150 (0.0140-0.0170) | | |
| 2004 | 0.0217 (0.0196-0.0239) | | |
| 2005 | 0.0281 (0.0253-0.0310) | | |
| 2006 | 0.0350 (0.0315-0.0384) | | |
| 2007 | 0.0412 (0.0370-0.0453) | | |
| 2008 | 0.0356 (0.0320-0.0392) | | |
| 2009 | 0.0273 (0.0246-0.0300) | | |
| 2010 | 0.0321 (0.0289-0.0353) | | |
| 2011 | 0.0373 (0.0335-0.0410) | | |
| 2012 | 0.0476 (0.0429-0.0524) | 0.0087 (0.0042-0.0132) | 0.0084 (0.0045-0.0123) |
| 2013 | 0.0557 (0.0501-0.0612) | 0.0082 (0.0040-0.0124) | 0.0085 (0.0052-0.0118) |
| 2014 | 0.0673 (0.0606-0.0740) | 0.0074 (0.0036-0.0112) | 0.0056 (0.0021-0.0091) |
| 2015 | 0.0654 (0.0588-0.0719) | 0.0037 (0.0000-0.0081) | 0.0063 (0.0025-0.0101) |
| 2016 | 0.0479 (0.0431-0.0527) | 0.0042 (0.0000-0.0090) | 0.0046 (0.0003-0.0089) |
| 2017 | | 0.0024 (0.0000-0.0077) | 0.0037 (0.0000-0.0086) |

**Table 16: HFC-43-10mee emission (Gg $yr^{-1}$) estimates for the UK with uncertainty (1std).**

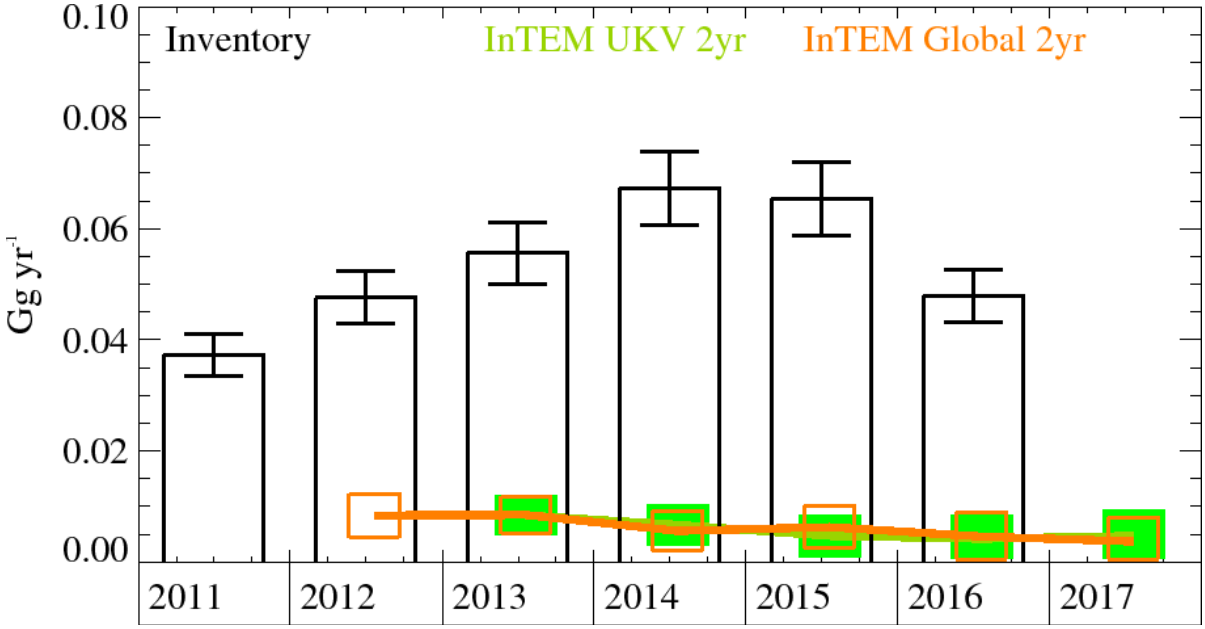


**Figure 56: HFC-43-10mee emission estimates for the UK (Gg $yr^{-1}$) from the UNFCCC Inventory (black) and InTEM using the DECC observations, 2-year inversions with different meteorology: (orange) global meteorology and (green) 1.5 km high resolution meteorology. The uncertainty bars represent 1 std.**

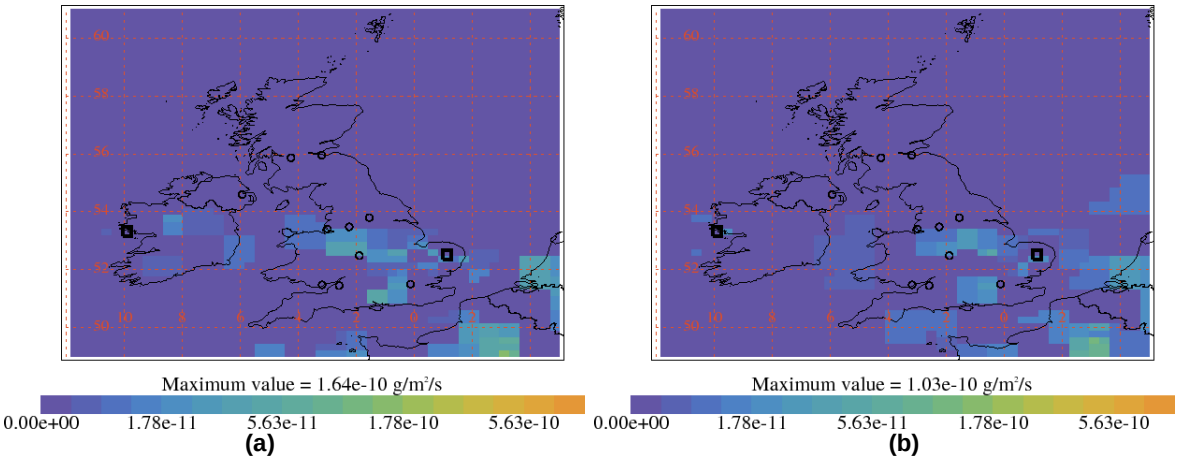


**Figure 57: Average InTEM estimates 2014-2017 of spatial distribution of HFC-43-10mee emissions using DECC observations with minimal prior information. Black squares are measurement stations and circles are major cities in UK. (a) Global meteorology and (b) UKV meteorology.**

## 4.16 HFC-365mfc

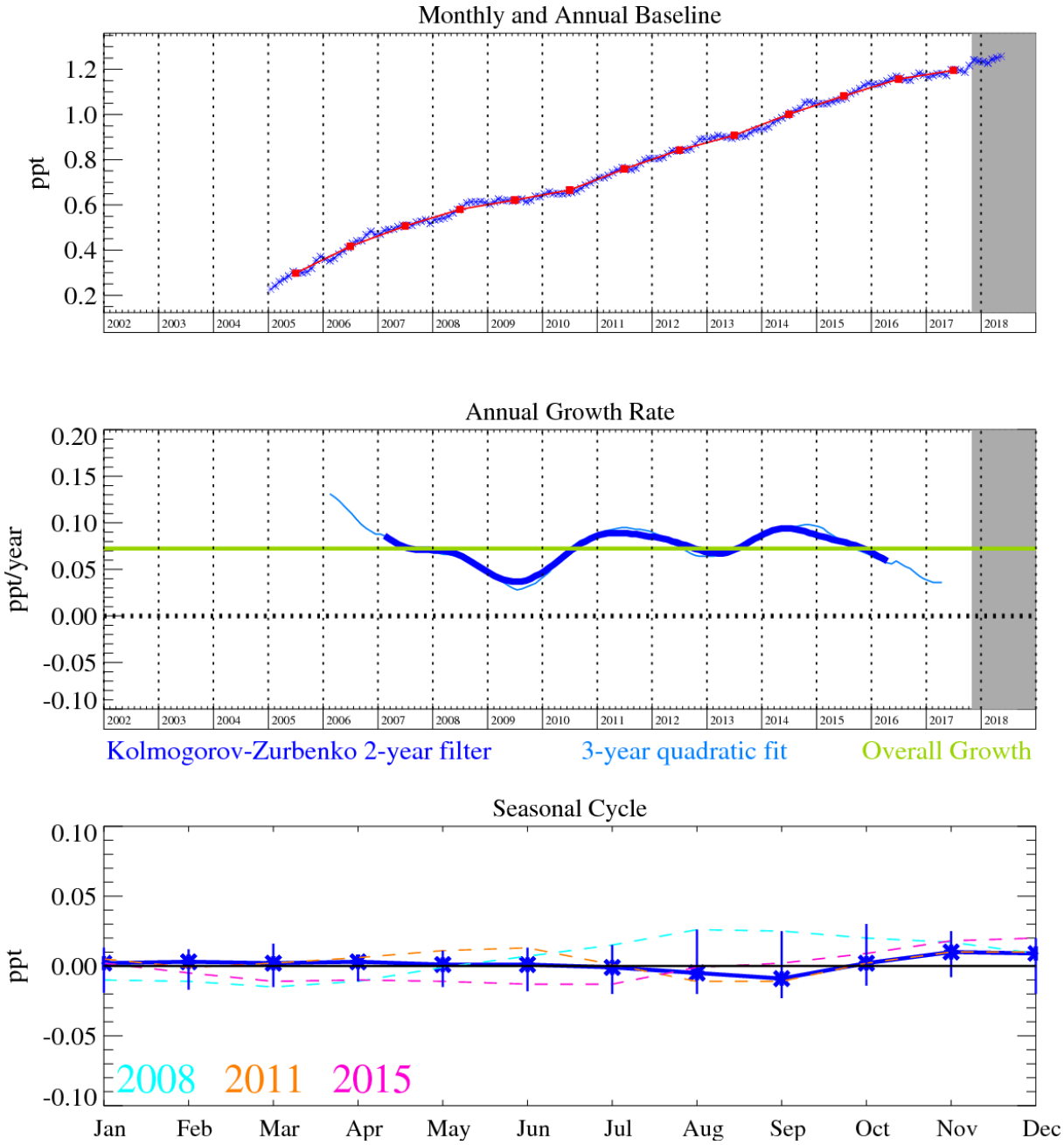


**Figure 58: HFC-365mfc ($C_4H_5F_5$): Monthly (blue) and annual (red) baseline (top plot). Annual (blue) and overall average growth rate (green) (middle plot). Seasonal cycle (de-trended) with year-to-year variability (lower plot). Grey area covers un-ratified and therefore provisional data.**

HFC-365mfc ($C_4H_5F_5$) is used predominantly for polyurethane structural foam blowing as a replacement for HCFC-141b, and to a minor extent as a blend component for solvents. It has an atmospheric lifetime of 8.6 years and an estimated GWP of 790-997 (100-year time horizon).

The InTEM emissions for the UK show a significant decrease between 2006-2011 and then a modest rise. The inventory shows a sharp decline between 2007 and 2008 and then a flat period followed by a modest rise. The agreement between the inventory and InTEM is overall good in both magnitude and trend. There is a divergence between the MHD-only and MHD+TAC (DECC) results in 2016. The InTEM results for 2017 using both sites shows a decline from the 2016 estimate, more data are required before this trend can be confirmed. The emissions are broadly population based.

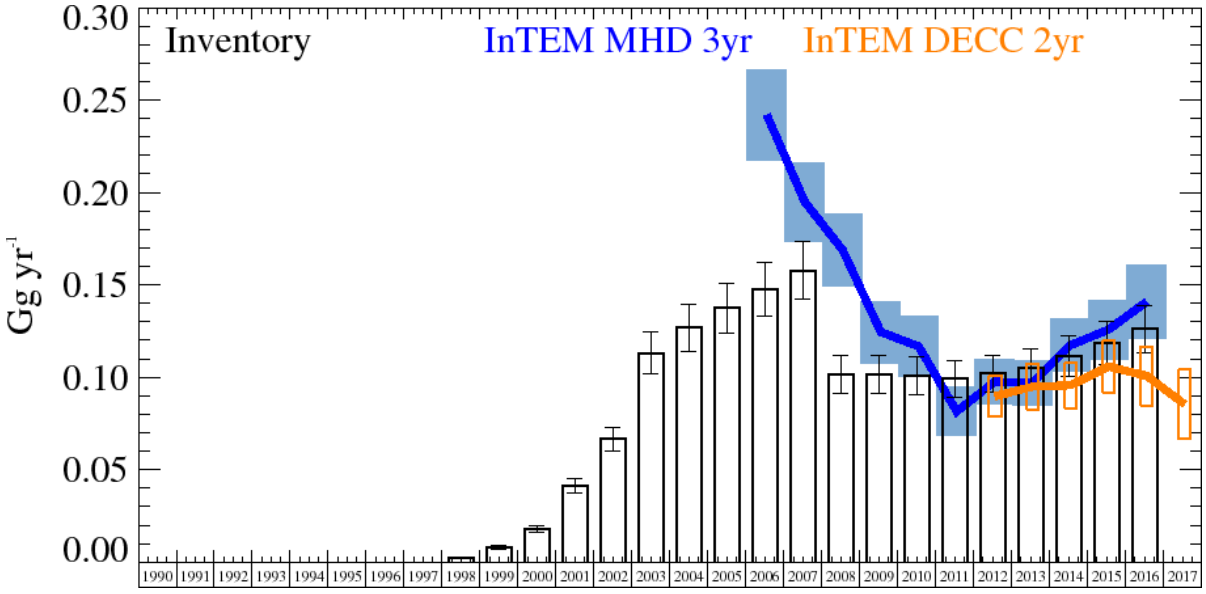


**Figure 59: HFC-365mfc UK Emission estimates (Gg yr$^{-1}$) from the UNFCCC Inventory (black) and InTEM with global meteorology: 3-year MHD (blue) and 2-year DECC network (orange). Uncertainty bars = 1 std.**

| Years | Inventory 1yr | MHD 3yr | DECC 2yr |
|---|---|---|---|
| 1990 | 0.0 (0.0-0.0) | | |
| 1991 | 0.0 (0.0-0.0) | | |
| 1992 | 0.0 (0.0-0.0) | | |
| 1993 | 0.0 (0.0-0.0) | | |
| 1994 | 0.0 (0.0-0.0) | | |
| 1995 | 0.0 (0.0-0.0) | | |
| 1996 | 0.0 (0.0-0.0) | | |
| 1997 | 0.0 (0.0-0.0) | | |
| 1998 | 0.0023 (0.0021-0.0026) | | |
| 1999 | 0.0080 (0.0072-0.0088) | | |
| 2000 | 0.0180 (0.0160-0.0200) | | |
| 2001 | 0.0412 (0.0371-0.0453) | | |
| 2002 | 0.0665 (0.0598-0.0731) | | |
| 2003 | 0.1132 (0.1018-0.1245) | | |
| 2004 | 0.1270 (0.1143-0.1397) | | |
| 2005 | 0.1374 (0.1236-0.1511) | | |
| 2006 | 0.1476 (0.1328-0.1623) | 0.2420 (0.2180-0.2670) | |
| 2007 | 0.1579 (0.1422-0.1737) | 0.1950 (0.1740-0.2170) | |
| 2008 | 0.1014 (0.0912-0.1115) | 0.1687 (0.1491-0.1883) | |
| 2009 | 0.1014 (0.0912-0.1115) | 0.1245 (0.1077-0.1413) | |
| 2010 | 0.1009 (0.0908-0.1110) | 0.1167 (0.1002-0.1332) | |
| 2011 | 0.0992 (0.0893-0.1092) | 0.0815 (0.0682-0.0948) | |
| 2012 | 0.1019 (0.0917-0.1120) | 0.0977 (0.0855-0.1099) | 0.0897 (0.0786-0.1008) |
| 2013 | 0.1052 (0.0947-0.1157) | 0.0969 (0.0847-0.1091) | 0.0950 (0.0825-0.1075) |
| 2014 | 0.1115 (0.1004-0.1227) | 0.1174 (0.1030-0.1318) | 0.0957 (0.0834-0.1080) |
| 2015 | 0.1184 (0.1066-0.1302) | 0.1258 (0.1097-0.1419) | 0.1058 (0.0918-0.1198) |
| 2016 | 0.1261 (0.1135-0.1387) | 0.1409 (0.1212-0.1606) | 0.1008 (0.0849-0.1167) |
| 2017 | | | 0.0855 (0.0666-0.1044) |

**Table 17: HFC-365mfc emission (Gg yr$^{-1}$) estimates for the UK with uncertainty (1std).**

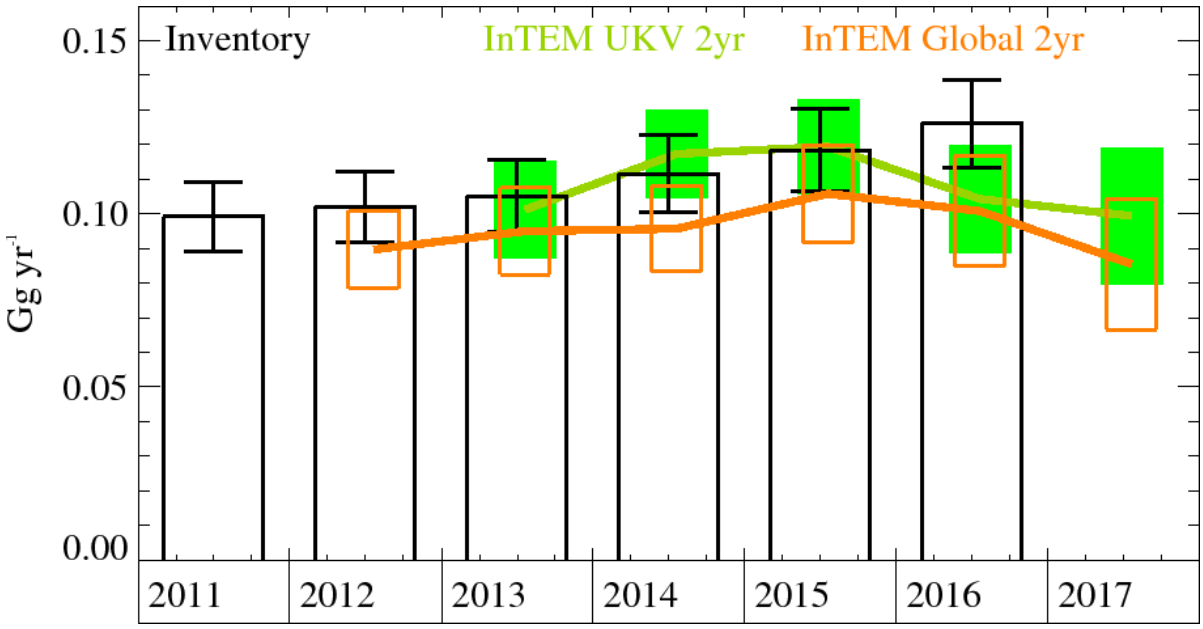


**Figure 60: HFC-365mfc emission estimates for the UK (Gg $yr^{-1}$) from the UNFCCC Inventory (black) and InTEM using the DECC observations, 2-year inversions with different meteorology: (orange) global meteorology and (green) 1.5 km high resolution meteorology. The uncertainty bars represent 1 std.**

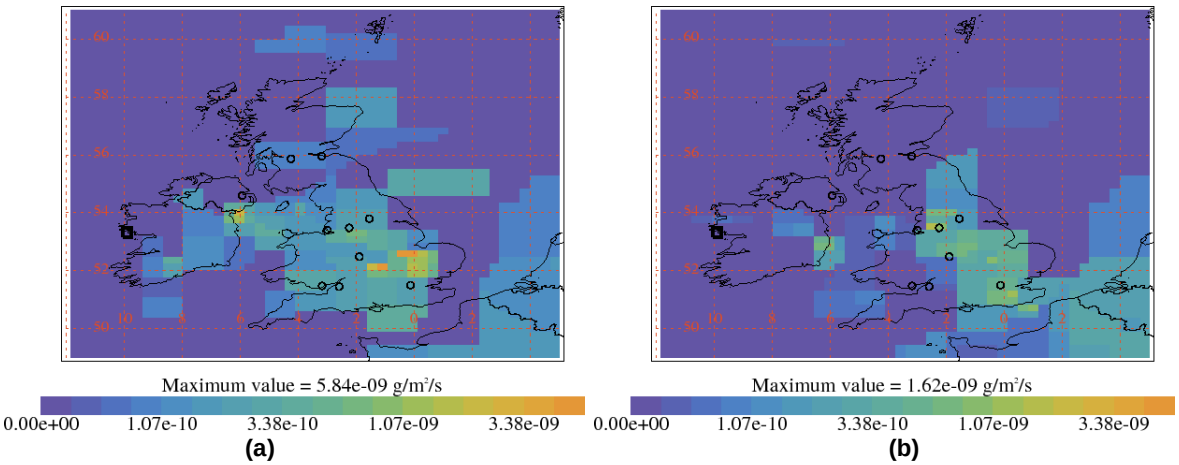


**Figure 61: InTEM estimates of spatial distribution of HFC-365mfc emissions using global meteorology and MHD observations with minimal prior information. Black squares are measurement stations and circles are major cities in UK. (a) Average 2004-2007 (b) Average 2014-2017.**

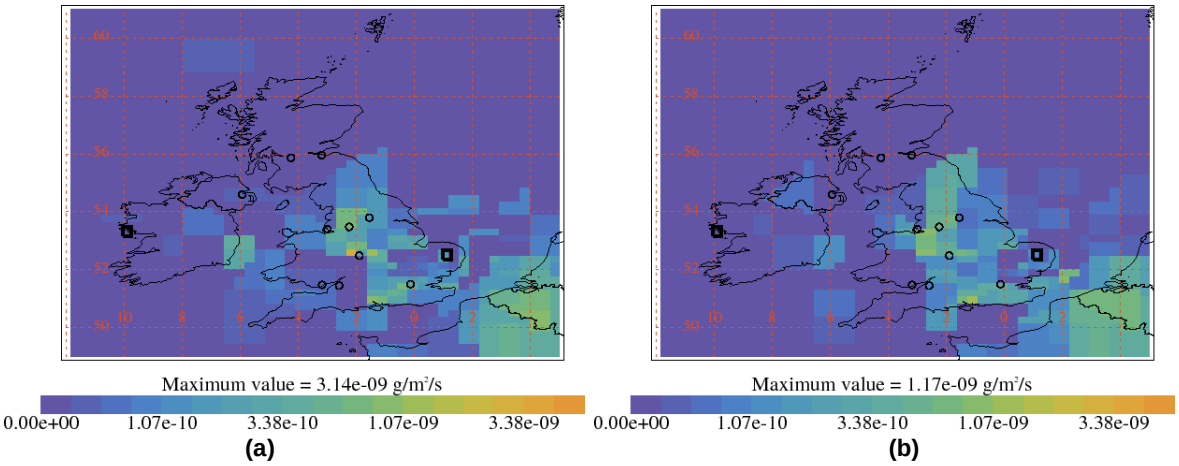


**Figure 62: Average InTEM estimates 2014-2017 of spatial distribution of HFC-365mfc emissions using DECC observations with minimal prior information. Black squares are measurement stations and circles are major cities in UK. (a) Global meteorology and (b) UKV meteorology.**

## 4.17 PFC-14 ($CF_4$)

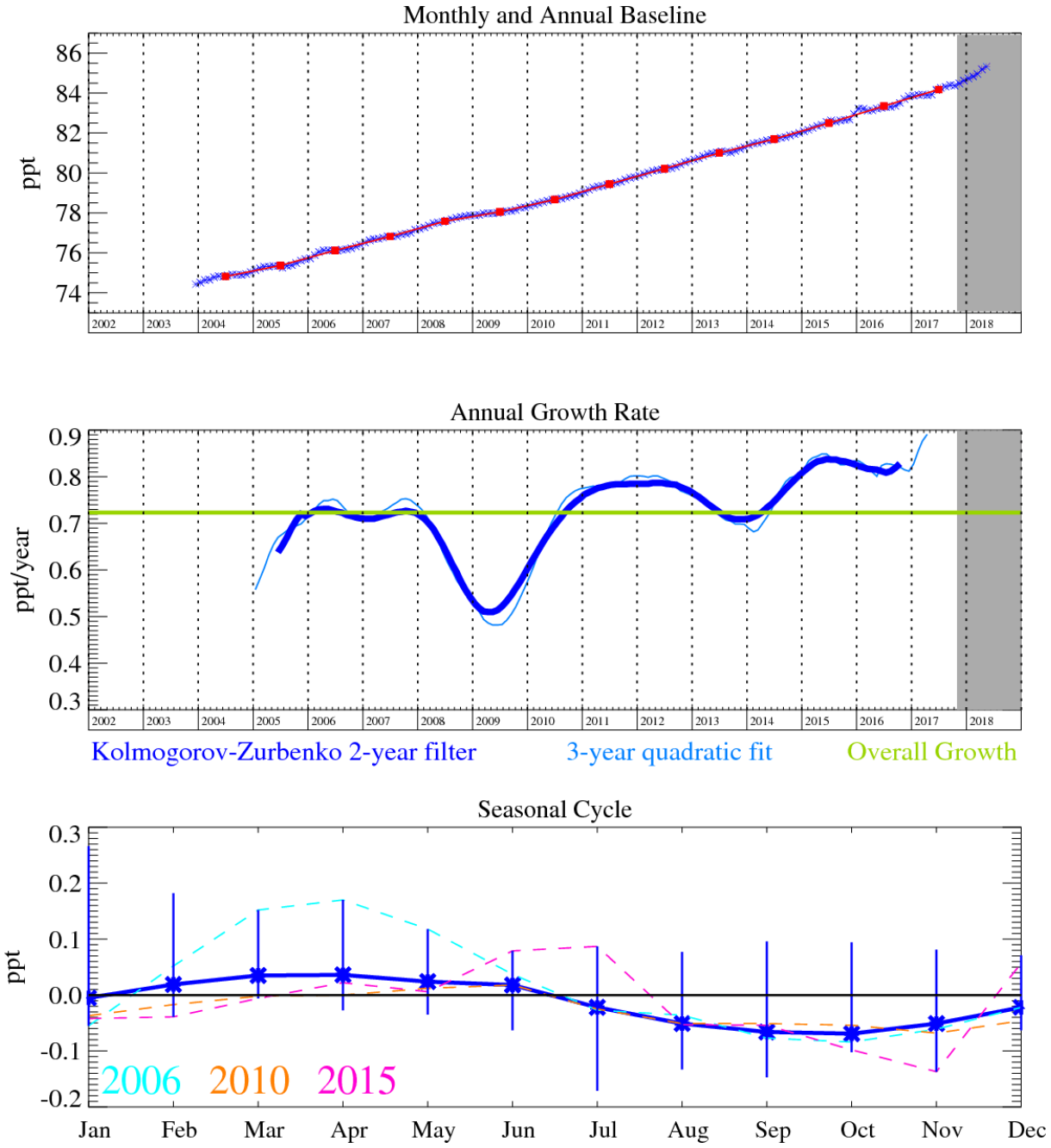


**Figure 63: PFC-14 ($CF_4$): Monthly (blue) and annual (red) Northern Hemisphere baseline mole fractions (top plot). Annual (blue) and overall average growth rate (green) (middle plot). Seasonal cycle (de-trended) with year-to-year variability (lower plot). Grey area covers un-ratified and therefore provisional data.**

PFC-14 ($CF_4$) possesses the longest known lifetime of anthropogenic molecules (>50,000 years), which, when coupled with its high absolute radiative forcing (0.08 W $m^{-2}$ $ppb^{-1}$) gives rise to a high $GWP_{100}$ of 5,820 and can equate to upwards of 1% of total radiative forcing. Its primary emission source is as an unwanted by-product of aluminium smelting during a fault condition known as an anode effect. Thus, the frequency of occurrence and duration of an anode effect event will determine the regional and global $CF_4$ emissions. $CF_4$ has some additional minor applications in the semiconductor industry (as a source of F radicals), but industry has shied away from using $CF_4$ knowing that its GWP is so high. The aluminium industry has recognised the $CF_4$ (and $C_2F_6$) emission problem and has been undergoing processes of replacement of older, less efficient aluminium production cells with more efficient designs, and automated and quicker intervention policies to prevent the occurrence of these anode effects. It is also thought that $CF_4$ has a natural source from crustal degassing. The

current growth rate of atmospheric $CF_4$ in the NH is close to 0.8 ppt $yr^{-1}$. This compound will accumulate in the atmosphere due to its very long atmospheric lifetime.

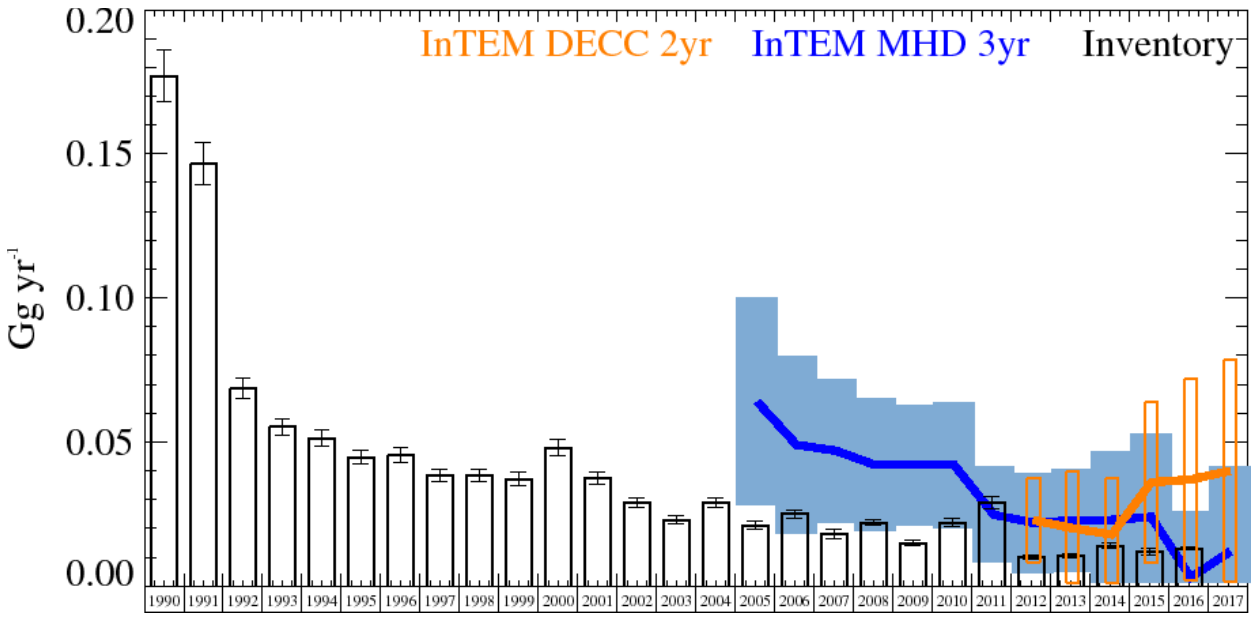


**Figure 64: PFC-14 UK Emission estimates (Gg $yr^{-1}$) from the UNFCCC Inventory (black) and InTEM with global meteorology: 3-year MHD (blue) and 2-year DECC network (orange). Uncertainty bars = 1 std.**

| Years | Inventory 1yr | MHD 3yr | DECC 2yr |
|---|---|---|---|
| 1990 | 0.1770 (0.1682-0.1859) | | |
| 1991 | 0.1467 (0.1392-0.1541) | | |
| 1992 | 0.0687 (0.0652-0.0723) | | |
| 1993 | 0.0552 (0.0523-0.0581) | | |
| 1994 | 0.0514 (0.0487-0.0541) | | |
| 1995 | 0.0447 (0.0423-0.0471) | | |
| 1996 | 0.0455 (0.0430-0.0480) | | |
| 1997 | 0.0385 (0.0364-0.0406) | | |
| 1998 | 0.0385 (0.0364-0.0407) | | |
| 1999 | 0.0372 (0.0351-0.0394) | | |
| 2000 | 0.0480 (0.0452-0.0508) | | |
| 2001 | 0.0375 (0.0353-0.0396) | | |
| 2002 | 0.029 (0.027-0.030) | | |
| 2003 | 0.023 (0.022-0.025) | | |
| 2004 | 0.029 (0.027-0.030) | | |
| 2005 | 0.021 (0.020-0.023) | 0.064 (0.028-0.100) | |
| 2006 | 0.025 (0.023-0.026) | 0.049 (0.018-0.080) | |
| 2007 | 0.018 (0.017-0.020) | 0.047 (0.022-0.072) | |
| 2008 | 0.022 (0.021-0.023) | 0.042 (0.019-0.065) | |
| 2009 | 0.015 (0.014-0.016) | 0.042 (0.021-0.063) | |
| 2010 | 0.022 (0.020-0.023) | 0.042 (0.020-0.064) | |
| 2011 | 0.029 (0.027-0.031) | 0.025 (0.008-0.042) | |
| 2012 | 0.010 (0.009-0.011) | 0.022 (0.005-0.039) | 0.023 (0.008-0.038) |
| 2013 | 0.010 (0.010-0.011) | 0.023 (0.005-0.041) | 0.020 (0.001-0.040) |
| 2014 | 0.014 (0.013-0.015) | 0.023 (0.000-0.048) | 0.018 (0.000-0.039) |
| 2015 | 0.012 (0.011-0.013) | 0.024 (0.000-0.058) | 0.036 (0.008-0.064) |
| 2016 | 0.013 (0.013-0.014) | 0.003 (0.000-0.046) | 0.037 (0.002-0.072) |
| 2017 | | 0.012 (0.000-0.059) | 0.040 (0.002-0.079) |

**Table 18: Emission (Gg $yr^{-1}$) estimates for the UK with uncertainty (1std).**

The large uncertainties in the InTEM results mainly overlap with the inventory estimates although the results are generally higher. In the InTEM inversions, the statistical match in time-series between the model time-series and the observations is weak. This is because the

emissions are principally from point sources (aluminium smelters). If the locations of the smelters are included and solved for as single grid cells (25 km) then the agreement between model and observation is much improved. The largest smelter in the UK, at Lynemouth on the north east coast of England ceased operations in March 2012. This is very clearly seen in the modelled emissions 2009-2012 (Figure 67). The MHD+TAC (DECC) InTEM results at the higher time resolution of 2 years show elevated emissions compared to the inventory, estimated to be principally emanating from a source near Liverpool, although the uncertainties are large. The MHD-only InTEM estimates show a significant source from near Dublin, Ireland in 2004-2007 (Figure 66a).

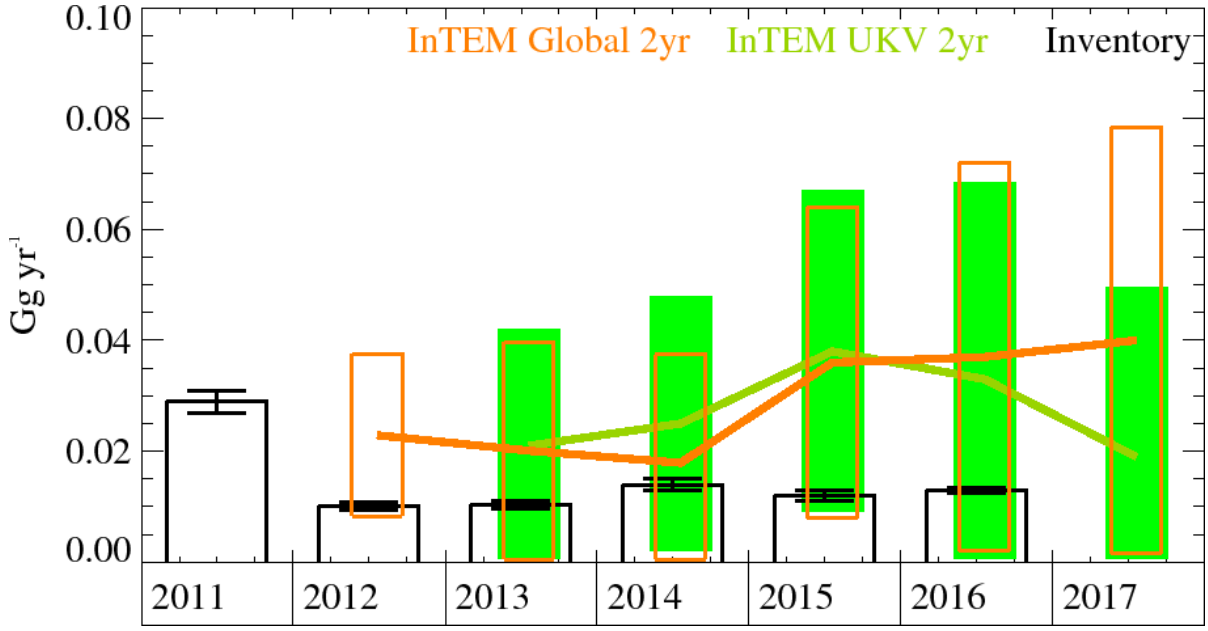


**Figure 65: PFC-14 emission estimates for the UK (Gg yr$^{-1}$) from the UNFCCC Inventory (black) and InTEM using the DECC observations, 2-year inversions with different meteorology: (orange) global meteorology and (green) 1.5 km high resolution meteorology. The uncertainty bars represent 1 std.**

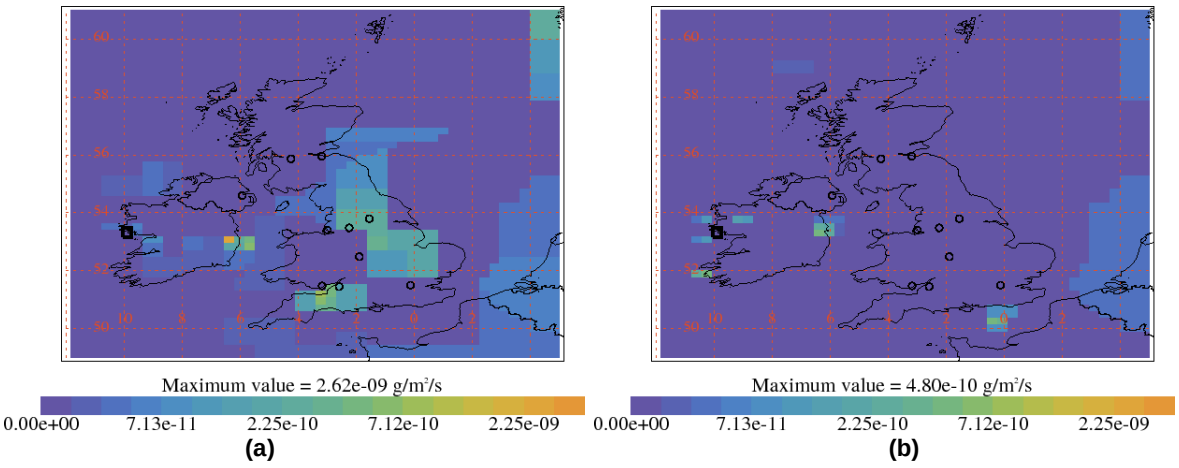


**Figure 66: InTEM estimates of spatial distribution of PFC-14 emissions using global meteorology and MHD observations with minimal prior information. Black squares are measurement stations and circles are major cities in UK. (a) Average 2004-2007 (b) Average 2014-2017.**

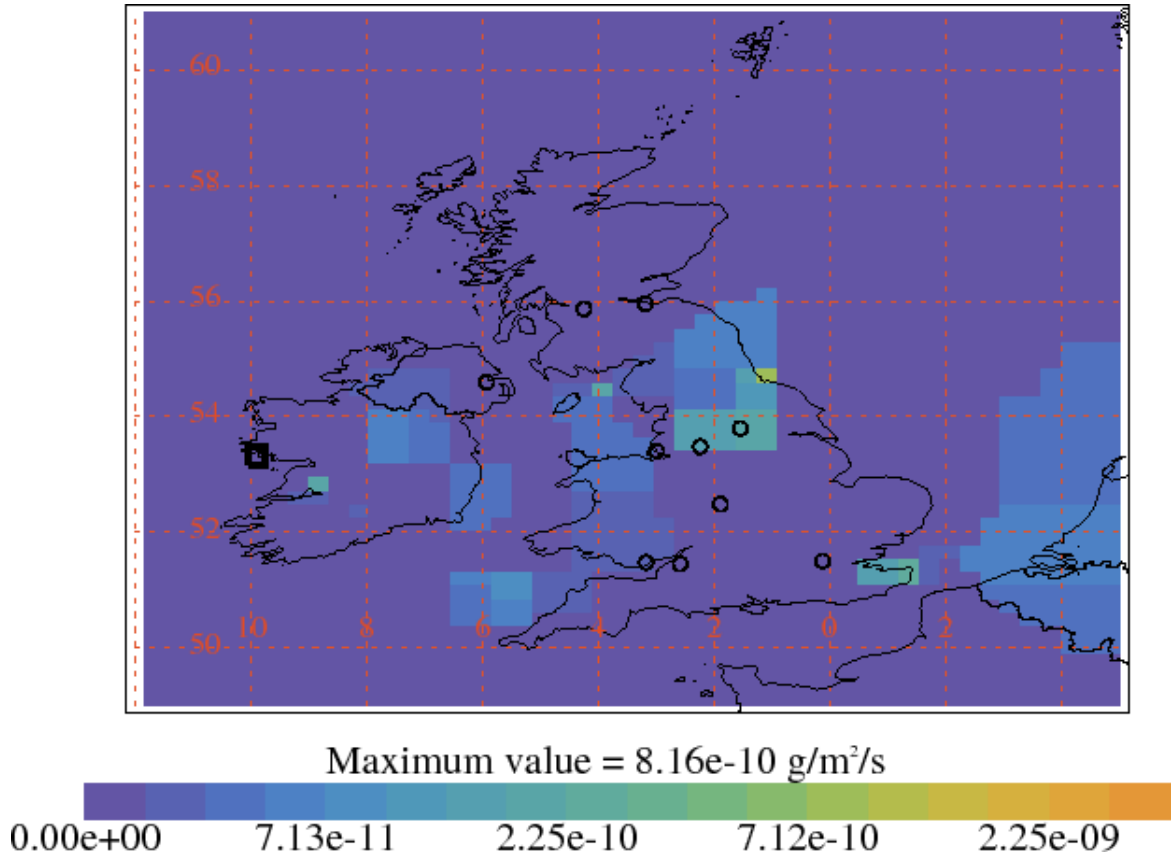


**Figure 67: InTEM estimate 2009-2012 of spatial distribution of PFC-14 emissions using global meteorology and MHD observations with minimal prior information. Black squares are measurement stations and circles are major cities in UK.**

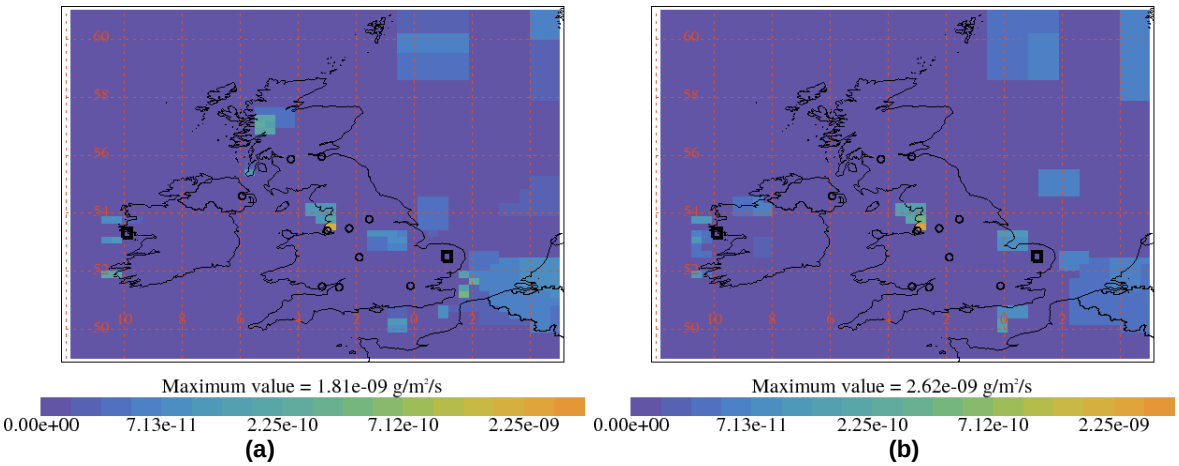


**Figure 68: Average InTEM estimates 2014-2017 of spatial distribution of PFC-14 emissions using DECC observations with minimal prior information. Black squares are measurement stations and circles are major cities in UK. (a) Global meteorology and (b) UKV meteorology.**

## 4.18 PFC-116

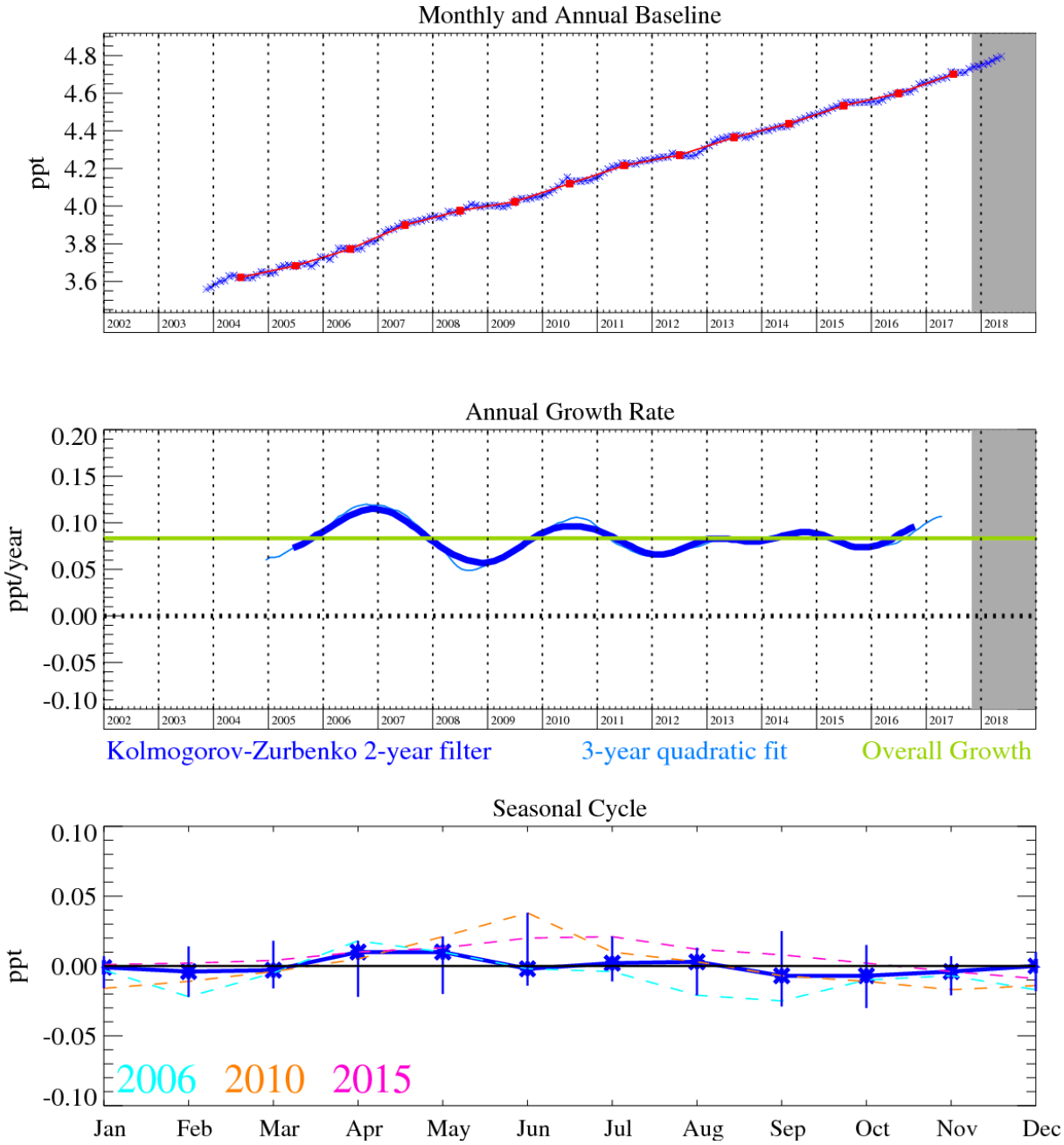


**Figure 69: PFC-116 ($C_2F_6$): Monthly (blue) and annual (red) Northern Hemisphere baseline mole fractions (top plot). Annual (blue) and overall average growth rate (green) (middle plot). Seasonal cycle (de-trended) with year-to-year variability (lower plot). Grey area covers un-ratified and therefore provisional data.**

PFC-116 ($C_2F_6$) is also a potent greenhouse gas with an atmospheric lifetime of >10,000 years. It has many common sources to $CF_4$, and serves to help explain why most of the $CF_4$ above-baseline (pollution) events are correlated with those of $C_2F_6$. However, we note that there are more frequent, and greater magnitude, $C_2F_6$ emissions relative to $CF_4$. This is due to the dominant source of $C_2F_6$ being from plasma etching in the semiconductor industry.

The InTEM uncertainty ranges for the UK emissions are large but consistently overlap the inventory estimates. The 2-site InTEM estimates are consistent with the MHD-only estimates.

The 2004-2007 InTEM estimates (Figure 72a) show a strong emission source south west of Dublin, Ireland that fades in more recent years. The InTEM comparison with Irish inventory shows very good agreement (Figure 74).

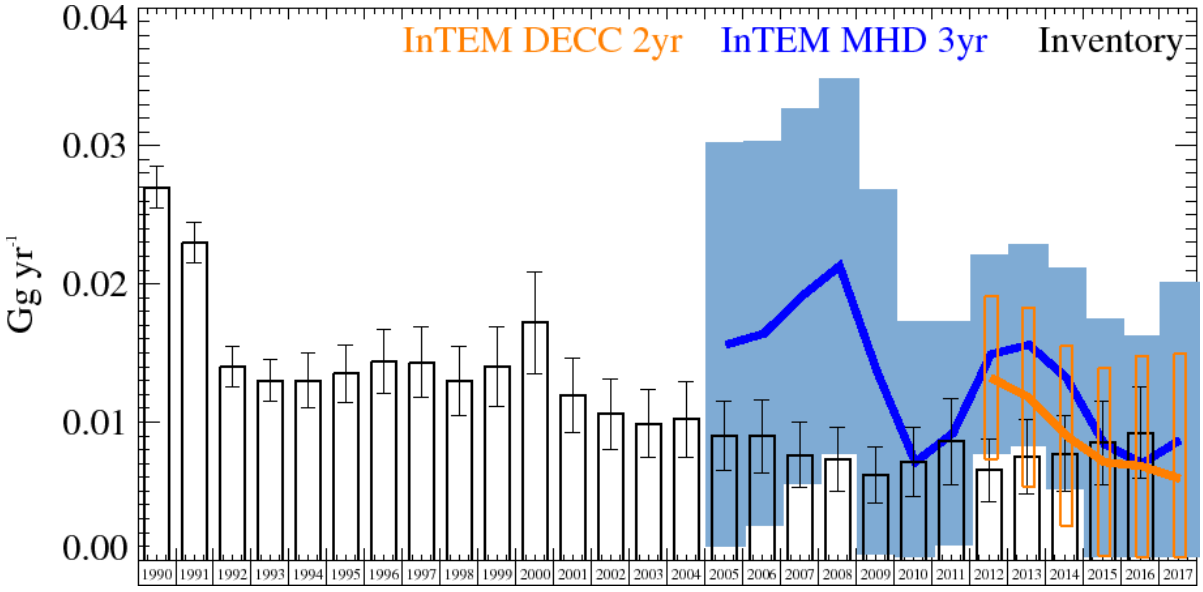


**Figure 70: PFC-116 UK Emission estimates (Gg $yr^{-1}$) from the UNFCCC Inventory (black) and InTEM with global meteorology: 3-year MHD (blue) and 2-year DECC network (orange). Uncertainty bars = 1 std.**

| Years | Inventory 1yr | MHD 3yr | DECC 2yr |
|---|---|---|---|
| 1990 | 0.027 (0.025-0.028) | | |
| 1991 | 0.023 (0.022-0.025) | | |
| 1992 | 0.014 (0.012-0.015) | | |
| 1993 | 0.013 (0.011-0.014) | | |
| 1994 | 0.013 (0.011-0.015) | | |
| 1995 | 0.0135 (0.0114-0.0155) | | |
| 1996 | 0.0144 (0.0121-0.0168) | | |
| 1997 | 0.0143 (0.0117-0.0168) | | |
| 1998 | 0.0130 (0.0105-0.0155) | | |
| 1999 | 0.0140 (0.0112-0.0169) | | |
| 2000 | 0.0172 (0.0135-0.0209) | | |
| 2001 | 0.0119 (0.0092-0.0146) | | |
| 2002 | 0.0106 (0.0081-0.0132) | | |
| 2003 | 0.0099 (0.0074-0.0124) | | |
| 2004 | 0.0102 (0.0075-0.0130) | | |
| 2005 | 0.0090 (0.0065-0.0115) | 0.0156 (0.0010-0.0302) | |
| 2006 | 0.0090 (0.0063-0.0116) | 0.0164 (0.0025-0.0303) | |
| 2007 | 0.0076 (0.0052-0.0099) | 0.0191 (0.0055-0.0327) | |
| 2008 | 0.0073 (0.0050-0.0097) | 0.0213 (0.0077-0.0349) | |
| 2009 | 0.0062 (0.0041-0.0082) | 0.0136 (0.0004-0.0268) | |
| 2010 | 0.0071 (0.0046-0.0096) | 0.0071 (0.0000-0.0204) | |
| 2011 | 0.0086 (0.0055-0.0117) | 0.0092 (0.0011-0.0173) | |
| 2012 | 0.0065 (0.0042-0.0088) | 0.0149 (0.0077-0.0221) | 0.0132 (0.0073-0.0191) |
| 2013 | 0.0075 (0.0048-0.0102) | 0.0156 (0.0083-0.0229) | 0.0118 (0.0053-0.0183) |
| 2014 | 0.0077 (0.0049-0.0104) | 0.0132 (0.0052-0.0212) | 0.0090 (0.0025-0.0155) |
| 2015 | 0.0085 (0.0054-0.0115) | 0.0084 (0.0000-0.0181) | 0.0071 (0.0003-0.0139) |
| 2016 | 0.0092 (0.0059-0.0125) | 0.0070 (0.0000-0.0185) | 0.0068 (0.0000-0.0160) |
| 2017 | | 0.0087 (0.0000-0.0229) | 0.0059 (0.0000-0.0181) |

**Table 19: PFC-116 emission (Gg $yr^{-1}$) estimates for the UK with uncertainty (1std).**

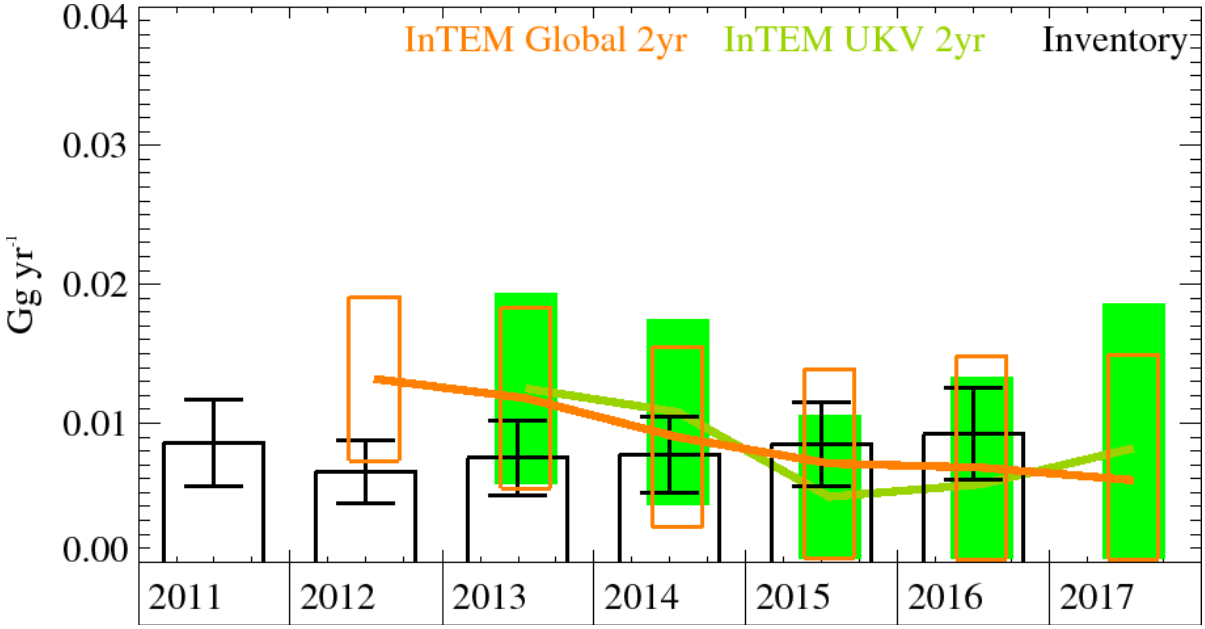


**Figure 71: PFC-116 emission estimates for the UK (Gg yr$^{-1}$) from the UNFCCC Inventory (black) and InTEM using the DECC observations, 2-year inversions with different meteorology: (orange) global meteorology and (green) 1.5 km high resolution meteorology. The uncertainty bars represent 1 std.**

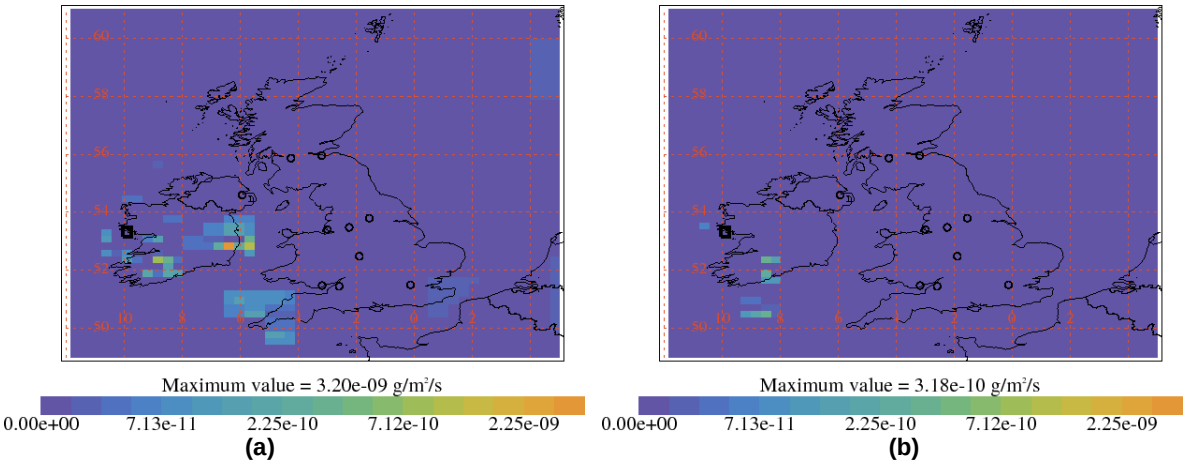


**Figure 72: InTEM estimates of spatial distribution of PFC-116 emissions using global meteorology and MHD observations with minimal prior information. Black squares are measurement stations and circles are major cities in UK. (a) Average 2004-2007 (b) Average 2014-2017.**

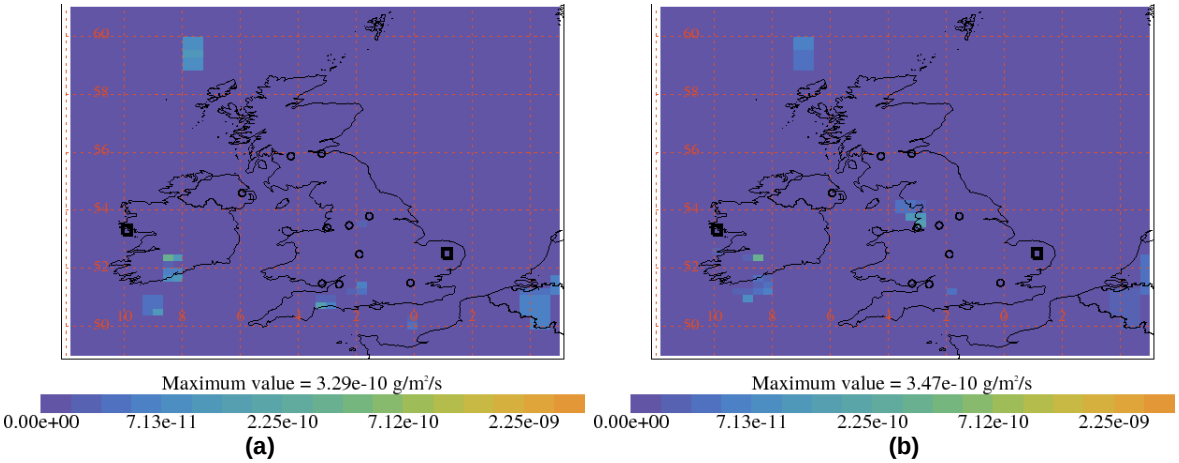


**Figure 73: Average InTEM estimates 2014-2017 of spatial distribution of PFC-116 emissions using DECC observations with minimal prior information. Black squares are measurement stations and circles are major cities in UK. (a) Global meteorology and (b) UKV meteorology.**

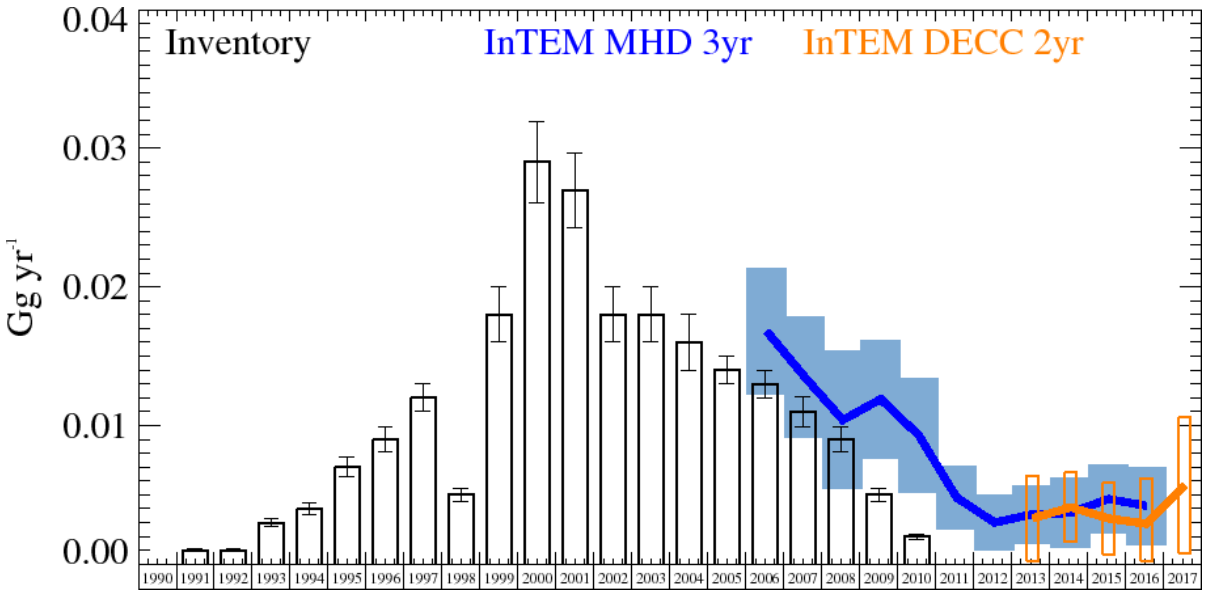


**Figure 74: PFC-116 Ireland emission estimates (Gg $yr^{-1}$) from the UNFCCC Inventory (black) and InTEM with global meteorology: 3-year MHD (blue) and 2-year DECC network (orange). The uncertainty bars represent 1 std.**

## 4.19 PFC-218

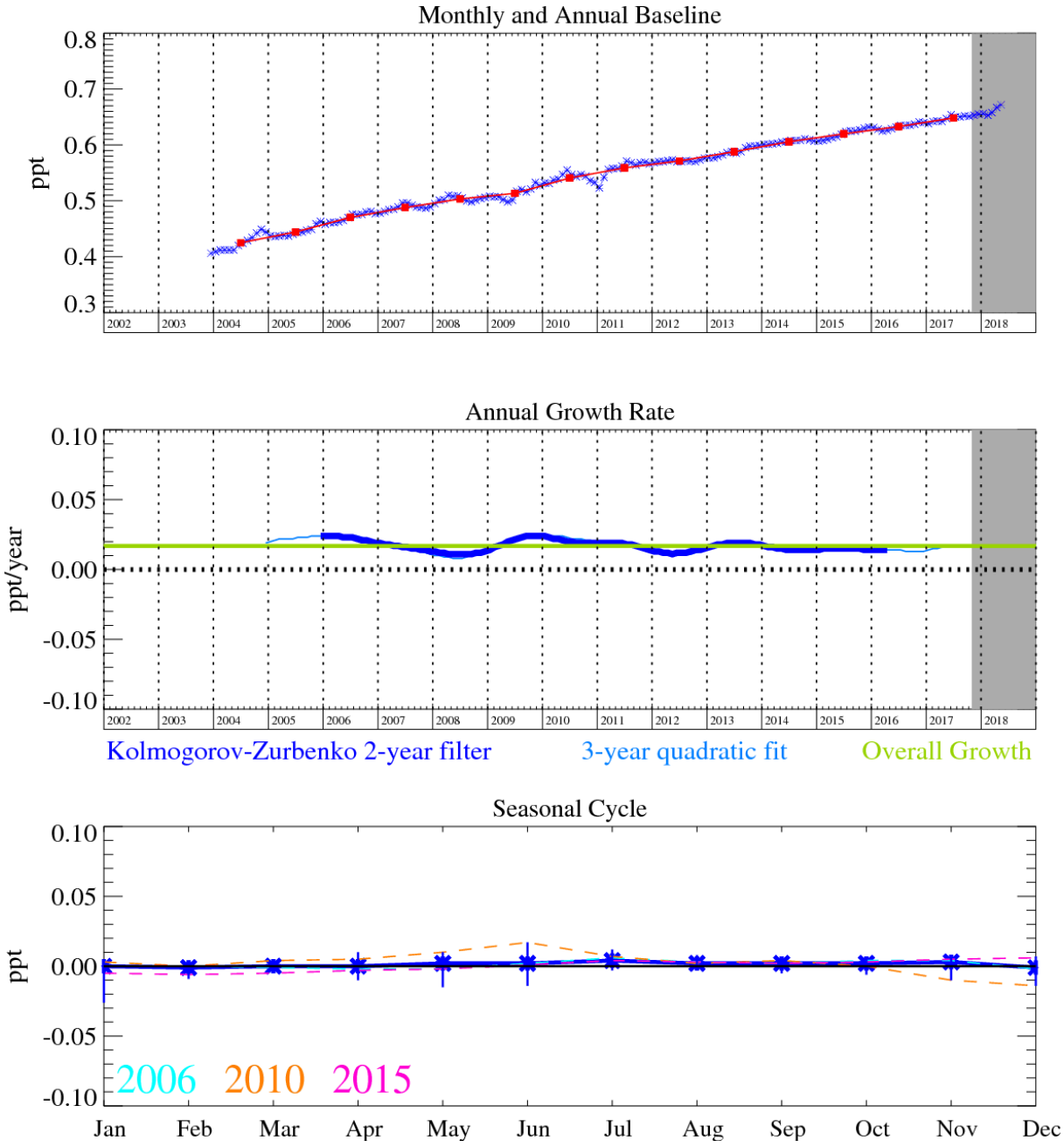


**Figure 75: PFC-218 ($C_3F_8$): Monthly (blue) and annual (red) Northern Hemisphere baseline mole fractions (top plot). Annual (blue) and overall average growth rate (green) (middle plot). Seasonal cycle (de-trended) with year-to-year variability (lower plot). Grey area covers un-ratified and therefore provisional data.**

PFC-218 ($C_3F_8$) has an atmospheric lifetime of 2600 years and a $GWP_{100}$ of 8690. It is also used in semiconductor manufacturing, but to a lesser extent than $C_2F_6$. It also has a very small contribution from aluminium smelting and has an increasing contribution from refrigeration use. Observations of above-baseline $C_3F_8$ emissions are less frequent than those of $C_2F_6$ but are of a higher relative magnitude.

The MHD-only InTEM and inventory results are remarkably consistent in trend, both showing dips in emissions in 2008 – 2010 and 2014. The MHD-only InTEM estimates are higher than those estimated in the inventory. The 2-site (DECC) InTEM estimates are closer in magnitude to the inventory but do not show the dip in 2014, they estimate a significant UK emission source in NW England close to Liverpool.

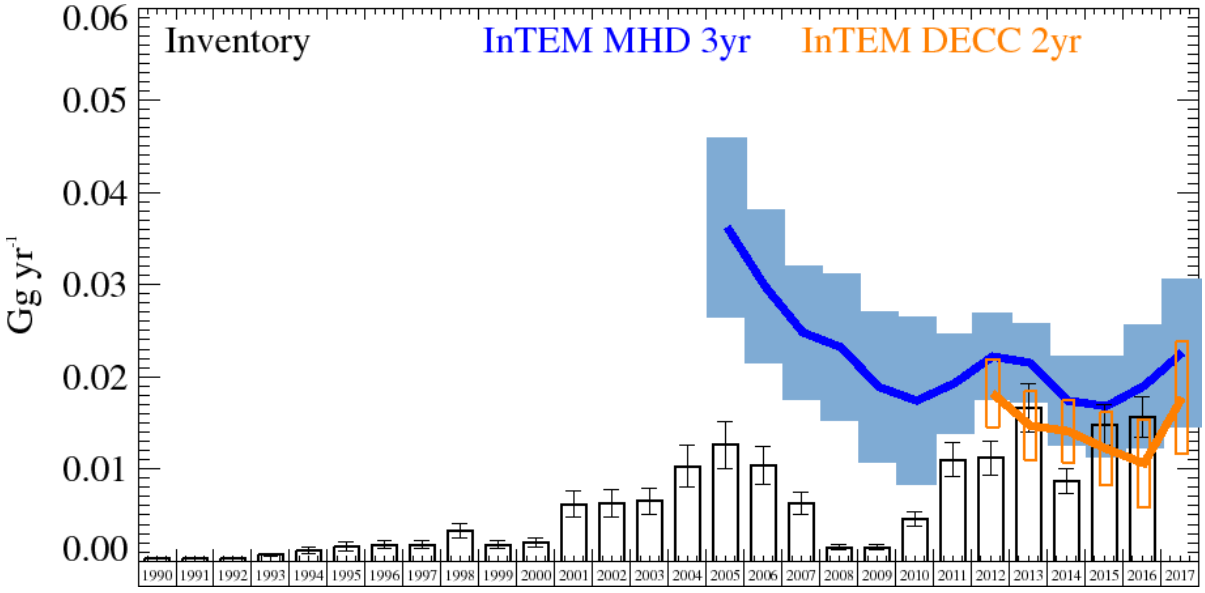


**Figure 76: PFC-218 UK Emission estimates (Gg yr$^{-1}$) from the UNFCCC Inventory (black) and InTEM with global meteorology: 3-year MHD (blue) and 2-year DECC network (orange). The uncertainty bars represent 1 std.**

| Years | Inventory 1yr | MHD 3yr | DECC 2yr |
|---|---|---|---|
| 1990 | 0.0003 (0.0002-0.0004) | | |
| 1991 | 0.0003 (0.0002-0.0004) | | |
| 1992 | 0.0003 (0.0002-0.0004) | | |
| 1993 | 0.0007 (0.0005-0.0009) | | |
| 1994 | 0.0012 (0.0008-0.0015) | | |
| 1995 | 0.0016 (0.0012-0.0021) | | |
| 1996 | 0.0018 (0.0013-0.0022) | | |
| 1997 | 0.0018 (0.0014-0.0023) | | |
| 1998 | 0.0033 (0.0025-0.0041) | | |
| 1999 | 0.0018 (0.0013-0.0022) | | |
| 2000 | 0.0020 (0.0015-0.0025) | | |
| 2001 | 0.0062 (0.0047-0.0076) | | |
| 2002 | 0.0063 (0.0049-0.0078) | | |
| 2003 | 0.0065 (0.0050-0.0079) | | |
| 2004 | 0.0103 (0.0081-0.0126) | | |
| 2005 | 0.0126 (0.0100-0.0152) | 0.0362 (0.0265-0.0459) | |
| 2006 | 0.0104 (0.0083-0.0124) | 0.0298 (0.0215-0.0381) | |
| 2007 | 0.0063 (0.0051-0.0076) | 0.0248 (0.0175-0.0321) | |
| 2008 | 0.0015 (0.0012-0.0018) | 0.0232 (0.0152-0.0312) | |
| 2009 | 0.0015 (0.0012-0.0018) | 0.0189 (0.0107-0.0271) | |
| 2010 | 0.0046 (0.0038-0.0054) | 0.0174 (0.0083-0.0265) | |
| 2011 | 0.0110 (0.0091-0.0128) | 0.0193 (0.0139-0.0247) | |
| 2012 | 0.0112 (0.0093-0.0130) | 0.0222 (0.0175-0.0269) | 0.0182 (0.0145-0.0219) |
| 2013 | 0.0166 (0.0140-0.0192) | 0.0215 (0.0172-0.0258) | 0.0147 (0.0110-0.0184) |
| 2014 | 0.0087 (0.0074-0.0100) | 0.0174 (0.0125-0.0223) | 0.0141 (0.0107-0.0175) |
| 2015 | 0.0148 (0.0126-0.0169) | 0.0168 (0.0113-0.0223) | 0.0122 (0.0082-0.0162) |
| 2016 | 0.0157 (0.0135-0.0179) | 0.0190 (0.0123-0.0257) | 0.0106 (0.0058-0.0154) |
| 2017 | | 0.0226 (0.0146-0.0306) | 0.0177 (0.0116-0.0238) |

**Table 20: PFC-218 emission (Gg yr$^{-1}$) estimates for the UK with uncertainty (1std).**

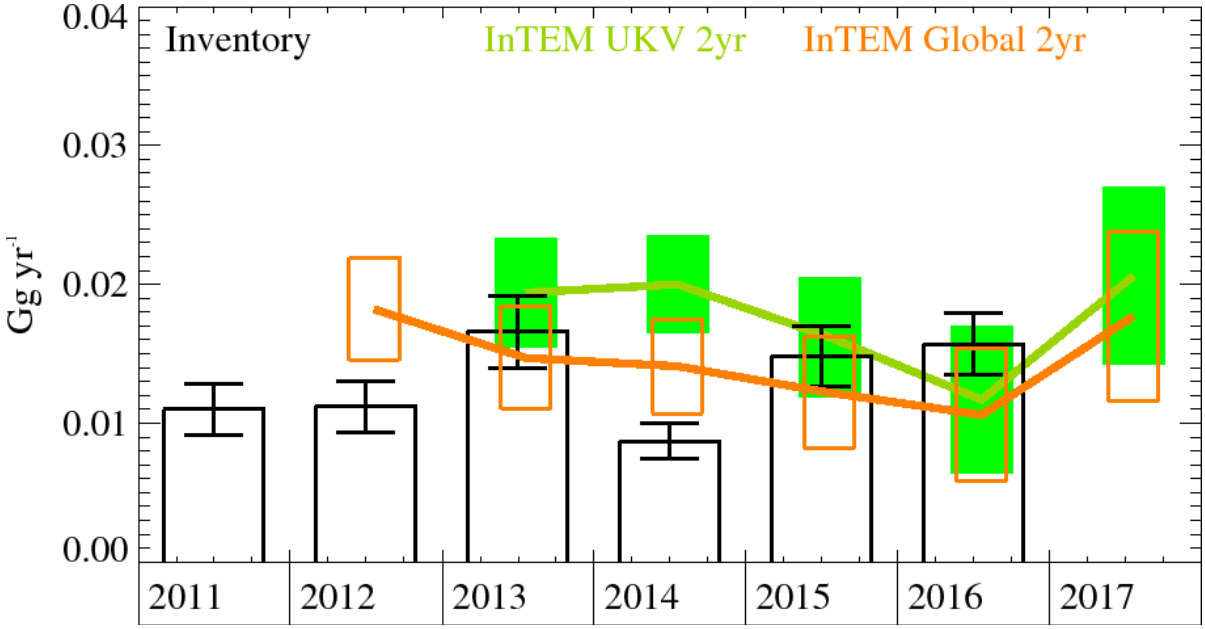


**Figure 77: PFC-218 emission estimates for the UK (Gg yr$^{-1}$) from the UNFCCC Inventory (black) and InTEM using the DECC observations, 2-year inversions with different meteorology: (orange) global meteorology and (green) 1.5 km high resolution meteorology. The uncertainty bars represent 1 std.**

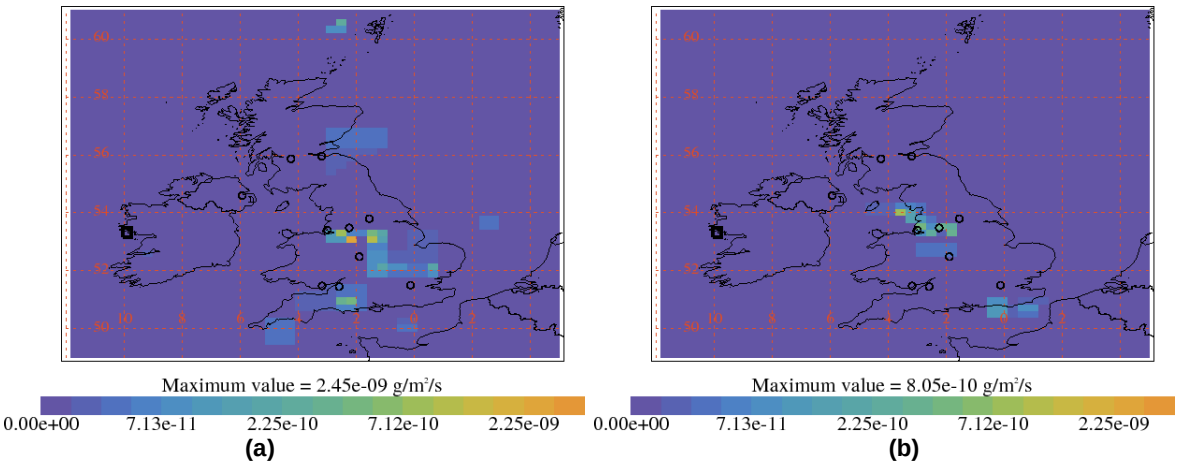


**Figure 78: InTEM estimates of spatial distribution of PFC-218 emissions using global meteorology and MHD observations with minimal prior information. Black squares are measurement stations and circles are major cities in UK. (a) Average 2004-2007 (b) Average 2014-2017.**

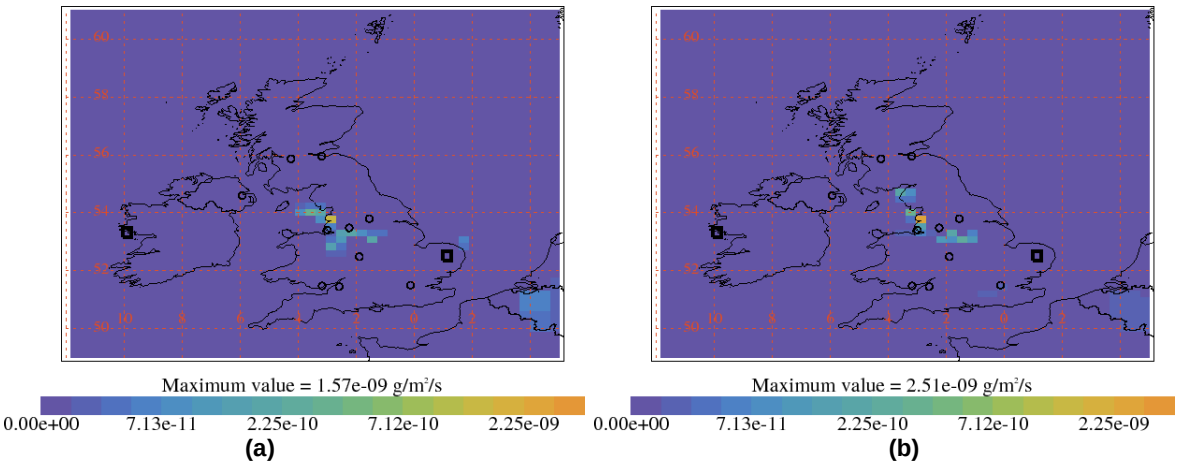


**Figure 79: Average InTEM estimates 2014-2017 of spatial distribution of PFC-218 emissions using DECC observations with minimal prior information. Black squares are measurement stations and circles are major cities in UK. (a) Global meteorology and (b) UKV meteorology.**

## 4.20 PFC-318

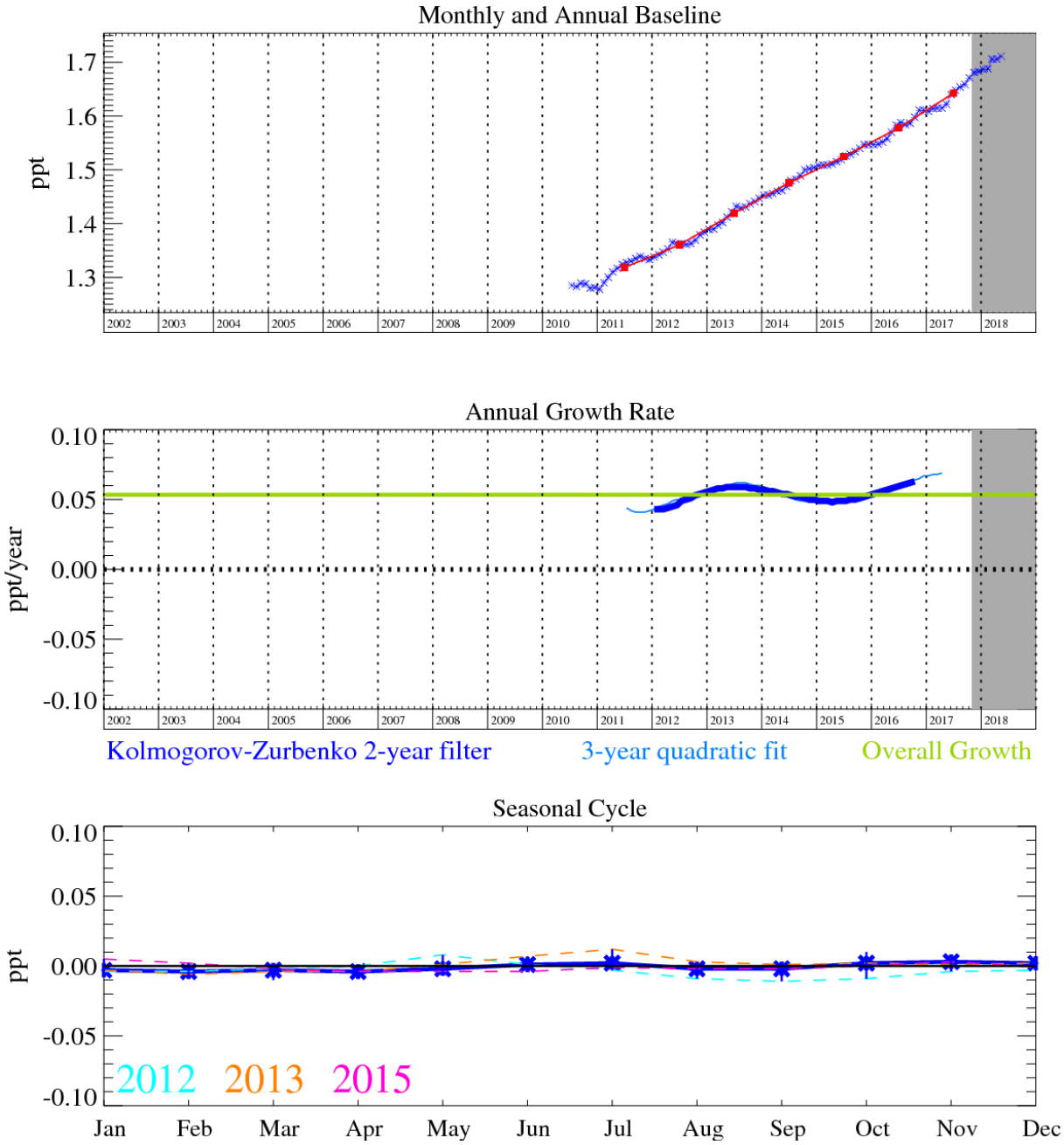


**Figure 80: PFC-318 (c-$C_4F_8$): Monthly (blue) and annual (red) Northern Hemisphere baseline mole fractions (top plot). Annual (blue) and overall average growth rate (green) (middle plot). Seasonal cycle (de-trended) with year-to-year variability (lower plot). Grey area covers un-ratified and therefore provisional data.**

PFC-319 (c-$C_4F_8$) is increasingly used in the semiconductor and electronics industries for cleaning, plasma etching and deposition gas, also it has more minor use in aerolysed foods, retinal detachment surgery, size estimation of natural gas and oil reservoirs, specialist military applications, tracer experiments and may also replace $SF_6$ as an electrically insulating gas. It has an atmospheric lifetime of 3,200 years, a $GWP_{100}$ of 10,300 and a radiative efficiency of 0.32 W $m^{-2}$ $ppb^{-1}$.

The reported UK inventory emissions of PFC-318 are very small (less than 0.00002 Gg $yr^{-1}$) compared to the InTEM emission estimates (~0.005 Gg $yr^{-1}$); however, the InTEM estimates have very significant uncertainty extending close to zero. The InTEM estimates with 2-sites, MHD+TAC (DECC) show a significant source of PFC-318 from The Netherlands in 2014-2017 (see Figure 84 for an extended geographical map of estimated emissions).

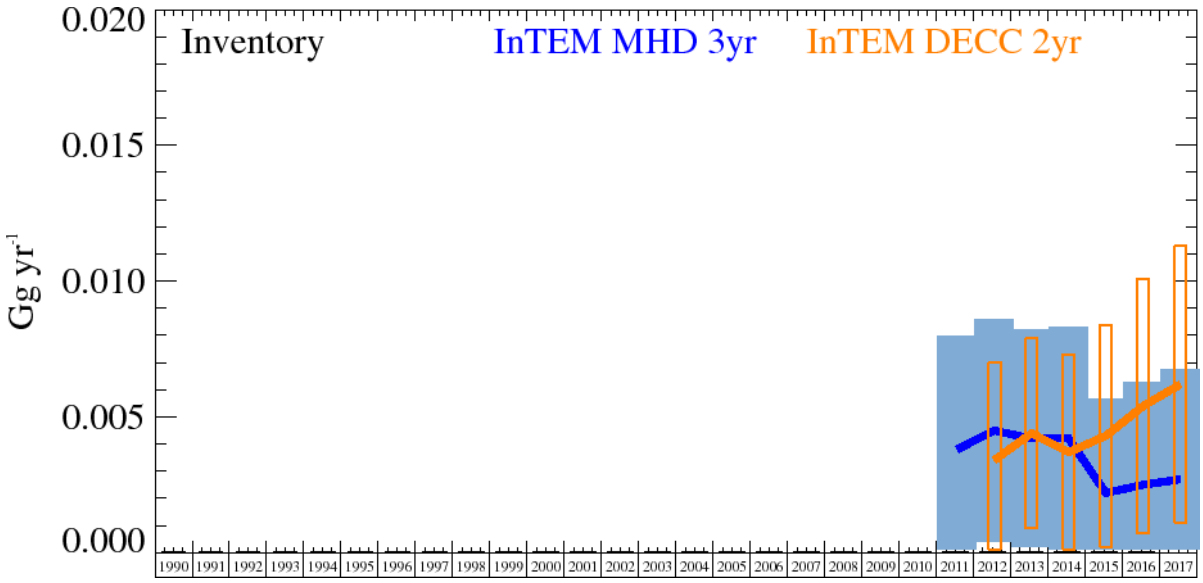


**Figure 81: PFC-318 UK Emission estimates (Gg yr$^{-1}$) from the UNFCCC Inventory (black) and InTEM with global meteorology: 3-year MHD (blue) and 2-year DECC network (orange). The uncertainty bars represent 1 std.**

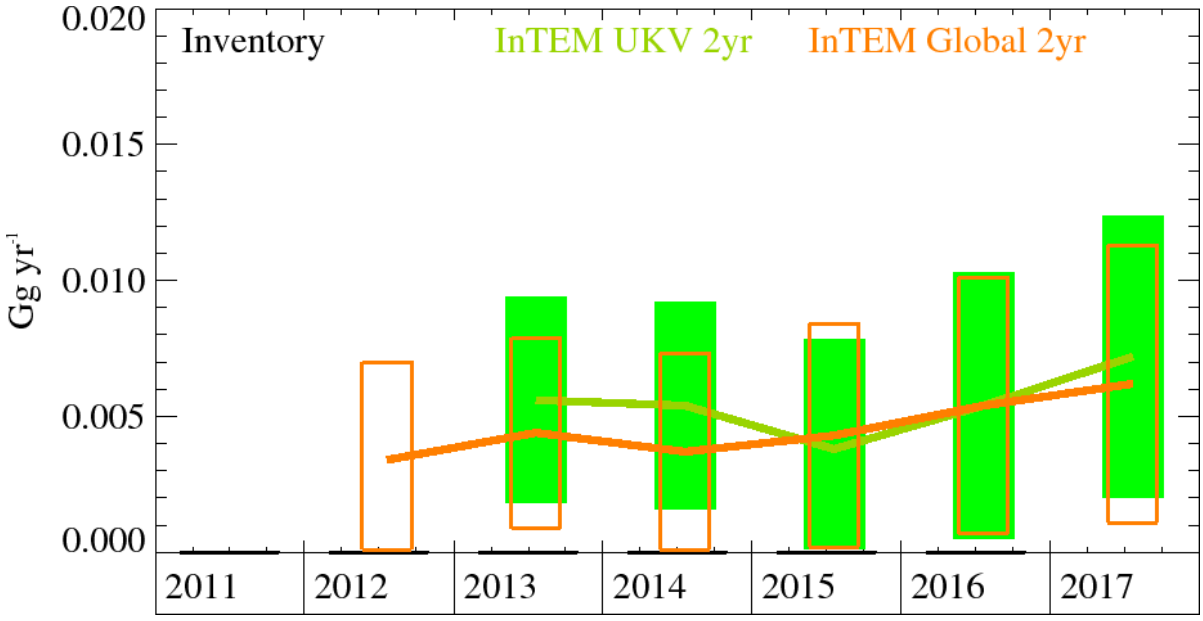


**Figure 82: PFC-318 emission estimates for the UK (Gg yr$^{-1}$) from the UNFCCC Inventory (black) and InTEM using the DECC observations, 2-year inversions with different meteorology: (orange) global meteorology and (green) 1.5 km high resolution meteorology. The uncertainty bars represent 1 std.**

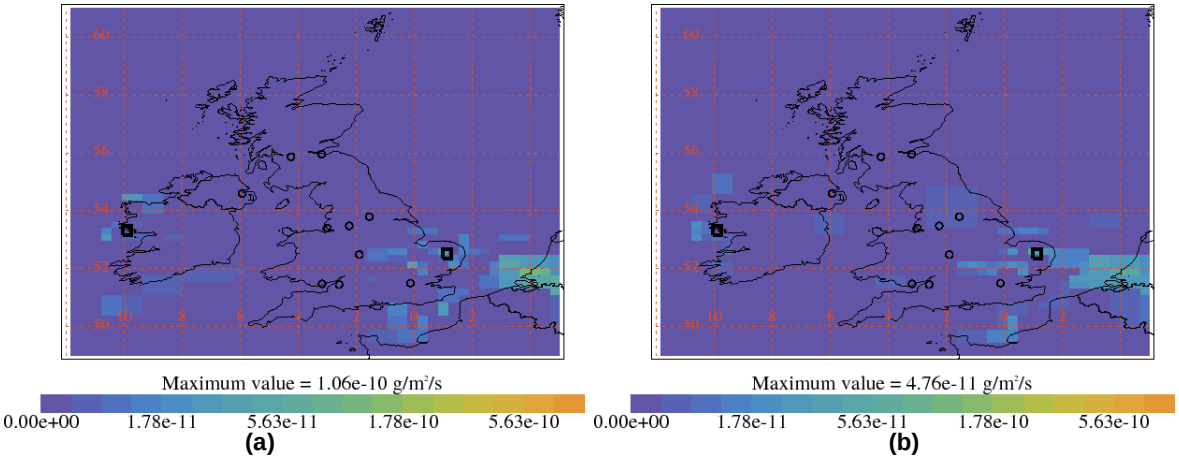


**Figure 83: Average InTEM estimates 2014-2017 of spatial distribution of PFC-318 emissions using DECC observations with minimal prior information. Black squares are measurement stations and circles are major cities in UK. (a) Global meteorology and (b) UKV meteorology.**

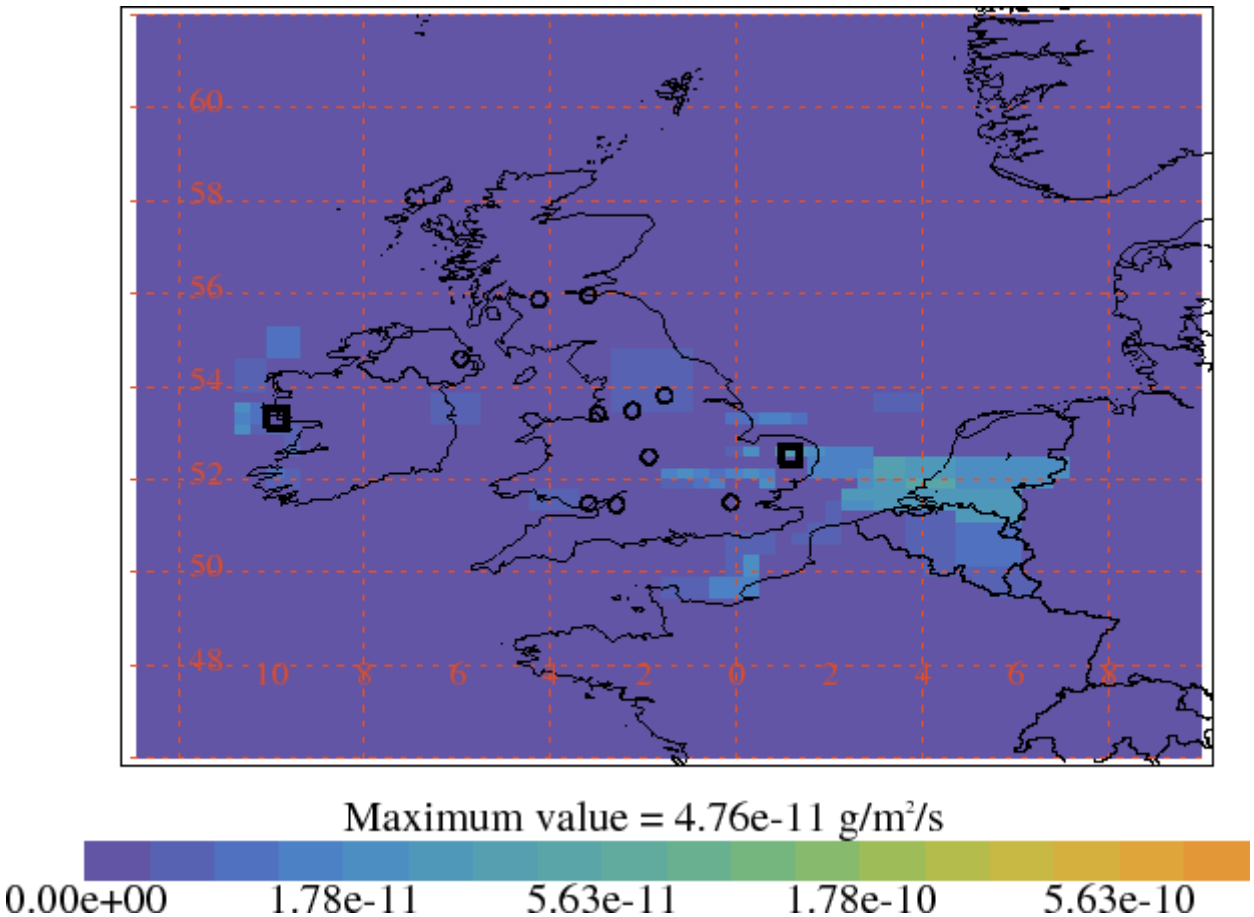


**Figure 84: Average InTEM estimates 2014-2017 of spatial distribution of PFC-318 emissions using DECC observations with minimal prior information using UKV meteorology. Black squares are measurement stations and circles are major cities in UK.**

## 4.21 $SF_6$

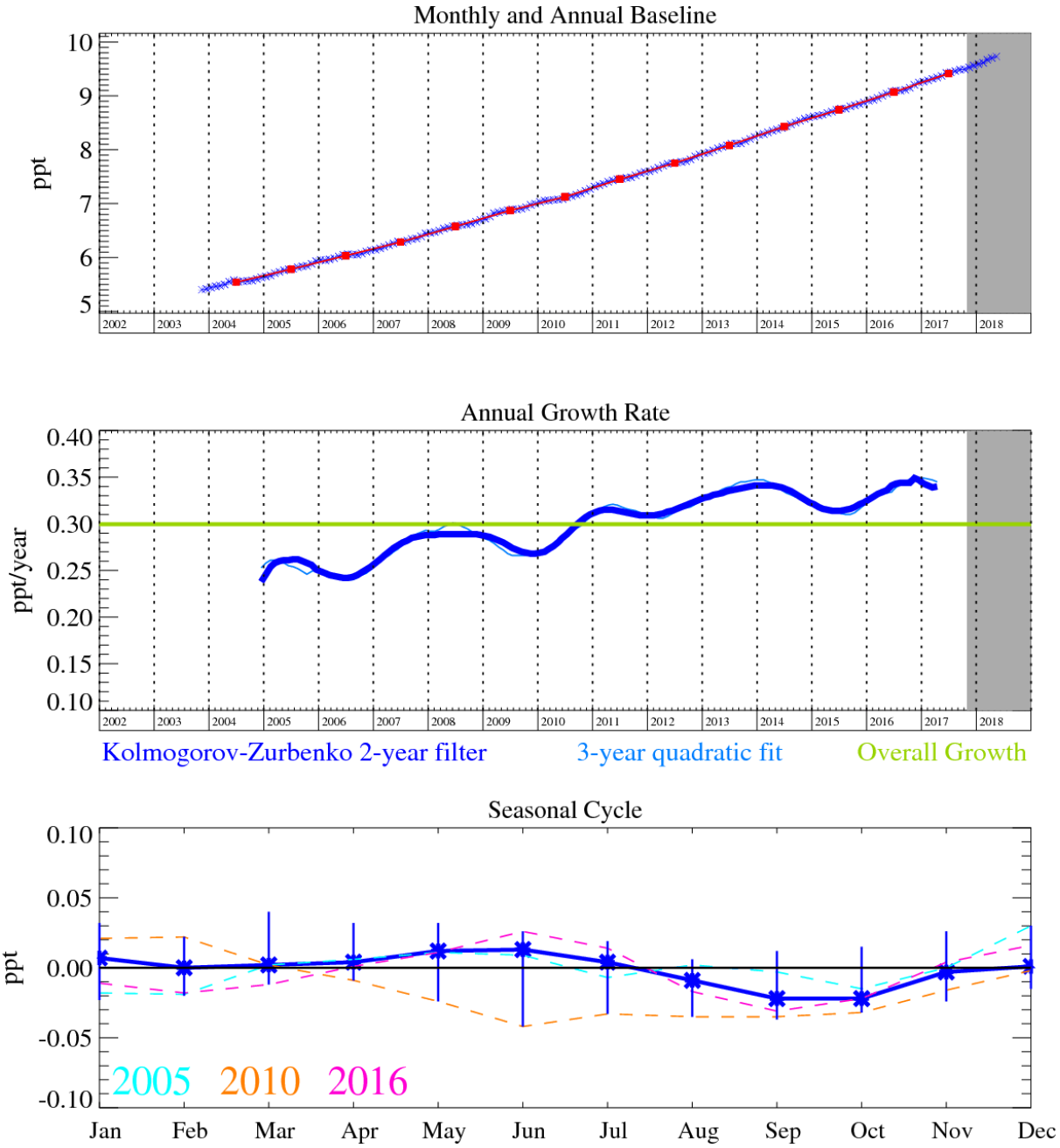


**Figure 85: $SF_6$: Monthly (blue) and annual (red) Northern Hemisphere baseline mole fractions (top plot). Annual (blue) and overall average growth rate (green) (middle plot). Seasonal cycle (de-trended) with year-to-year variability (lower plot). Grey area covers un-ratified and therefore provisional data.**

$SF_6$ is an important greenhouse gas since it has a long atmospheric lifetime of 3,200 years and a high radiative efficiency; giving rise to a $GWP_{100}$ of 22,800. Although having minor usage in the semiconductor industry, it is predominantly used in electrical circuit breakers, heavy-duty gas-insulated switchgear (GIS) for systems with voltages from 5,000-38,000 volts, and other switchgear used in the electrical transmission systems to manage high voltages (>38 kV). The electrical power industry uses roughly 80% of all $SF_6$ produced worldwide. Although the units themselves are hermetically sealed and pressurised, aging equipment, breakdown and disposal, alongside leakage from wear-and-tear will cause this sector to emit $SF_6$. A minor use of this gas is also reported in its use as a blanketing (i.e. oxygen inhibiting inert gas) agent during magnesium production. Hence $SF_6$ will have many, and more diffuse, sources relative to the other perfluorinated species. Its atmospheric trend was predicted to rise at a rate faster than

linear, as older electrical switchgear is switched to higher efficiency units; this is corroborated by the constantly increasing atmospheric growth rate since measurements began.

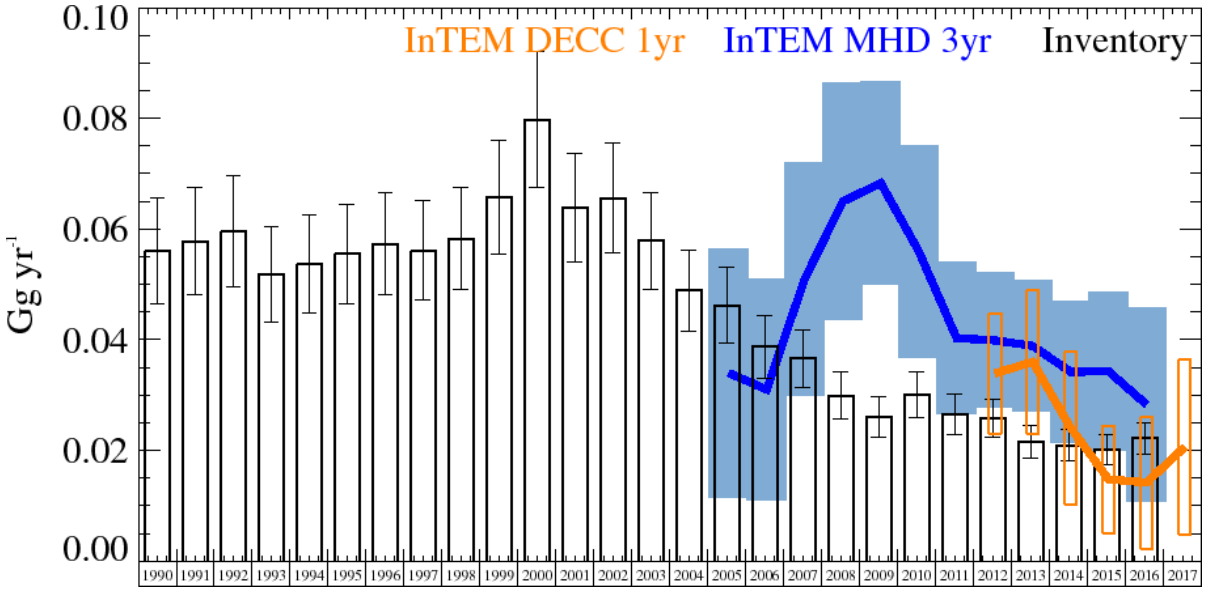


**Figure 86: $SF_6$ UK Emission estimates (Gg $yr^{-1}$) from the UNFCCC Inventory (black) and InTEM with global meteorology: 3-year MHD (blue) and 12-month DECC+GAUGE network (orange). Uncertainty bars = 1 std.**

| Years | Inventory 1yr | MHD 3yr | DECC 1yr |
|---|---|---|---|
| 1990 | 0.0561 (0.0466-0.0656) | | |
| 1991 | 0.0578 (0.0481-0.0676) | | |
| 1992 | 0.0596 (0.0496-0.0695) | | |
| 1993 | 0.0519 (0.0433-0.0605) | | |
| 1994 | 0.0537 (0.0449-0.0625) | | |
| 1995 | 0.0555 (0.0465-0.0645) | | |
| 1996 | 0.0573 (0.0481-0.0665) | | |
| 1997 | 0.0561 (0.0472-0.0651) | | |
| 1998 | 0.0583 (0.0491-0.0675) | | |
| 1999 | 0.0657 (0.0554-0.0759) | | |
| 2000 | 0.0797 (0.0674-0.0920) | | |
| 2001 | 0.0638 (0.0540-0.0735) | | |
| 2002 | 0.0656 (0.0556-0.0755) | | |
| 2003 | 0.0579 (0.0492-0.0666) | | |
| 2004 | 0.0489 (0.0417-0.0562) | | |
| 2005 | 0.0462 (0.0394-0.0530) | 0.034 (0.011-0.056) | |
| 2006 | 0.0387 (0.0331-0.0443) | 0.031 (0.011-0.051) | |
| 2007 | 0.0366 (0.0314-0.0419) | 0.051 (0.030-0.072) | |
| 2008 | 0.0299 (0.0257-0.0342) | 0.065 (0.043-0.086) | |
| 2009 | 0.0260 (0.0223-0.0296) | 0.0683 (0.0500-0.0866) | |
| 2010 | 0.0301 (0.0259-0.0343) | 0.0560 (0.0368-0.0752) | |
| 2011 | 0.0266 (0.0230-0.0303) | 0.0403 (0.0265-0.0541) | |
| 2012 | 0.0258 (0.0223-0.0293) | 0.0399 (0.0277-0.0521) | 0.0339 (0.0231-0.0447) |
| 2013 | 0.0216 (0.0187-0.0246) | 0.0389 (0.0271-0.0507) | 0.0360 (0.0230-0.0490) |
| 2014 | 0.0209 (0.0181-0.0237) | 0.0342 (0.0214-0.0470) | 0.0241 (0.0103-0.0379) |
| 2015 | 0.0201 (0.0174-0.0227) | 0.0343 (0.0200-0.0486) | 0.0148 (0.0051-0.0245) |
| 2016 | 0.0222 (0.0193-0.0251) | 0.0283 (0.0107-0.0459) | 0.0142 (0.0023-0.0261) |
| 2017 | | | 0.0206 (0.0048-0.0364) |

**Table 21: $SF_6$ emission (Gg $yr^{-1}$) estimates for the UK with uncertainty (1std).**

After 2006, the UK InTEM estimates using MHD-only are consistently elevated compared to the inventory; the InTEM uncertainty ranges are above the inventory estimates. The rise in InTEM MHD-only emission estimates for the UK from 2006 to 2009 are at odds with a decline in the inventory. In the 2007-2010 InTEM emission map, there is a significant emission source

estimated in SE England. The 5-site (DECC) 1-year InTEM estimates are lower than the MHD-only estimates and are more consistent with the inventory.

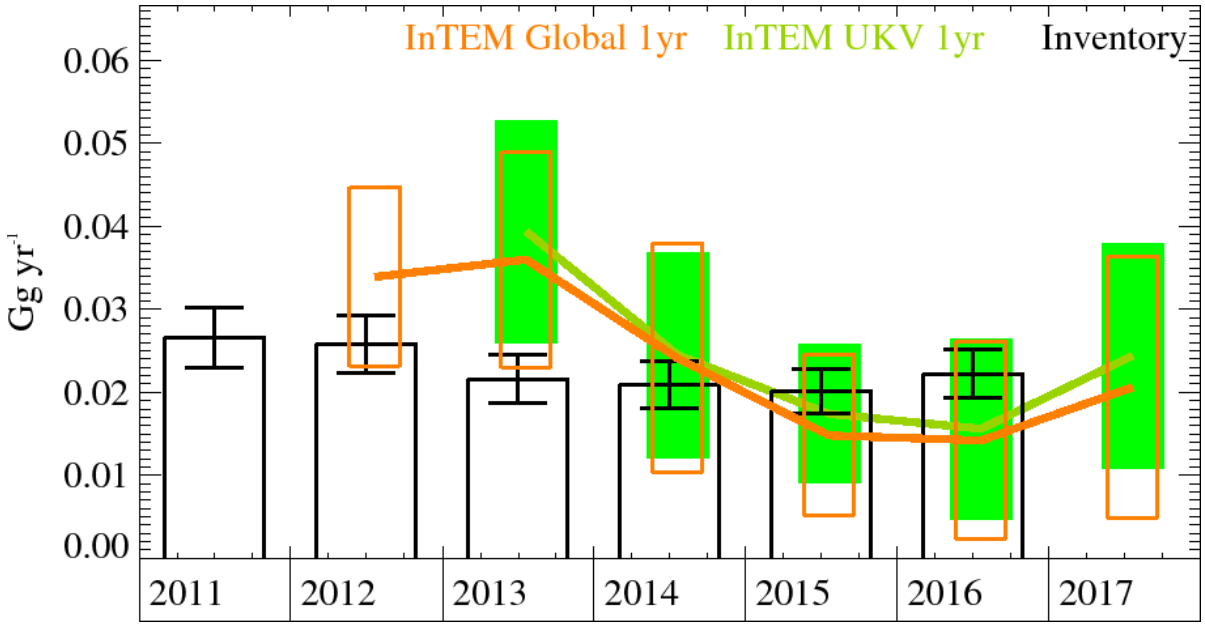


**Figure 87: $SF_6$ emission estimates for the UK (Gg $yr^{-1}$) from the UNFCCC Inventory (black) and InTEM using the DECC+GAUGE observations, 1-year inversions with different meteorology: (orange) global meteorology and (green) 1.5 km high resolution meteorology. The uncertainty bars represent 1 std.**

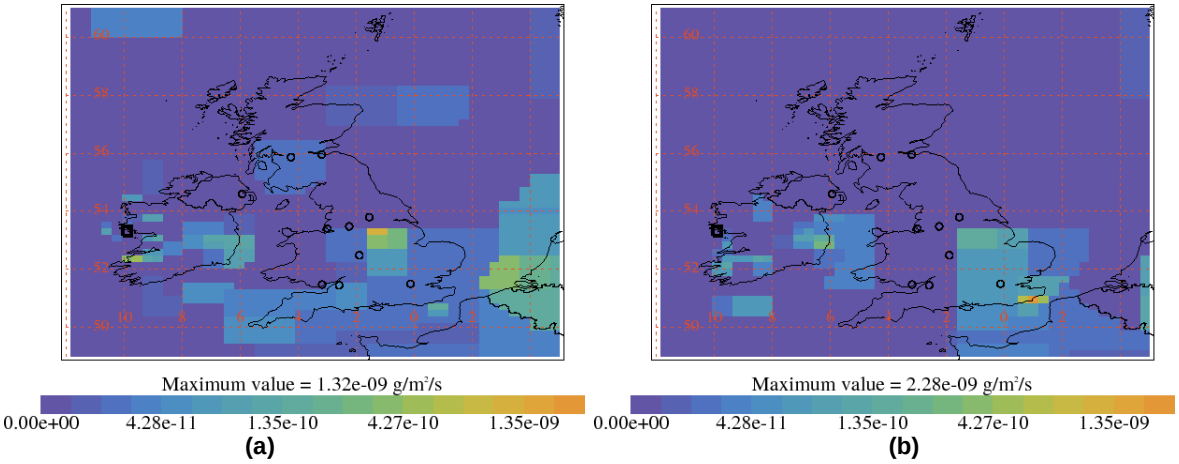


**Figure 88: InTEM estimates of spatial distribution of $SF_6$ emissions using global meteorology and MHD observations with minimal prior information. Black squares are measurement stations and circles are major cities in UK. (a) Average 2004-2007 (b) Average 2014-2017.**

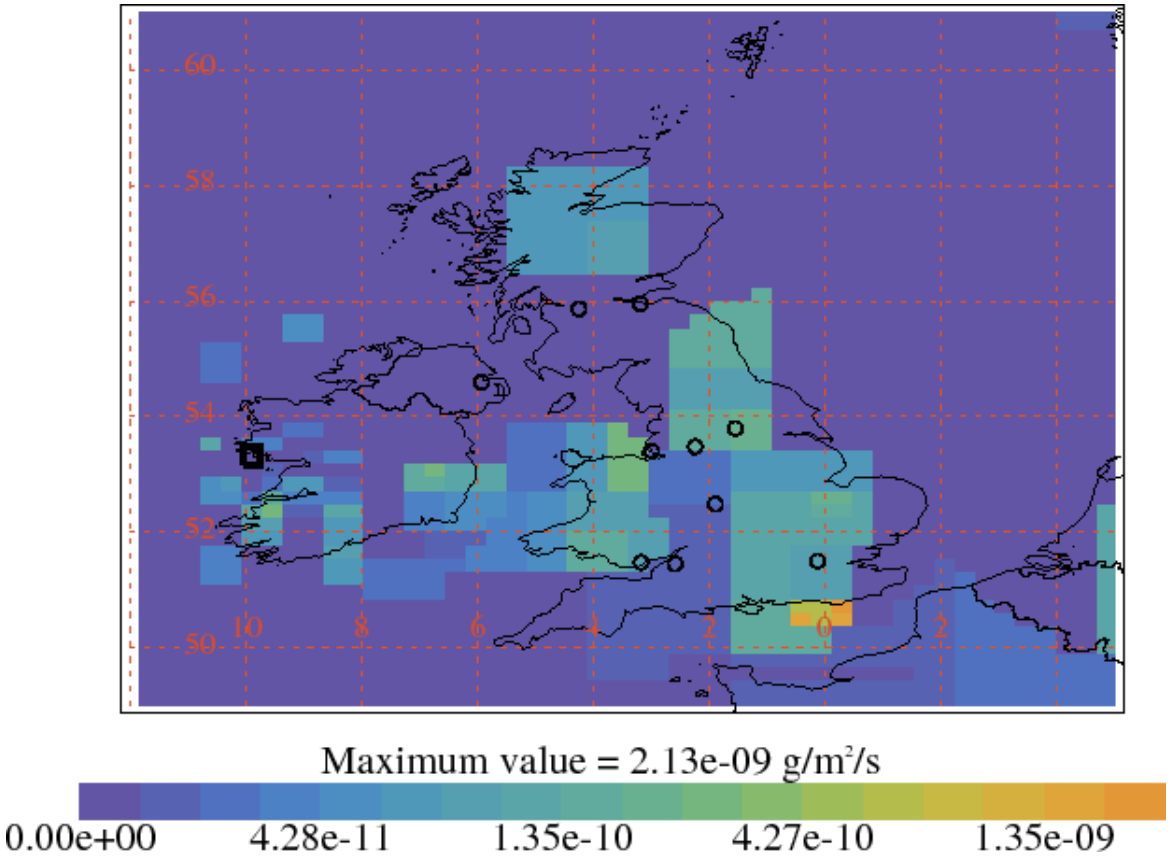


**Figure 89: InTEM estimate 2007-2010 of spatial distribution of $SF_6$ emissions using global meteorology and MHD observations with minimal prior information. Black squares are measurement stations and circles are major cities in UK.**

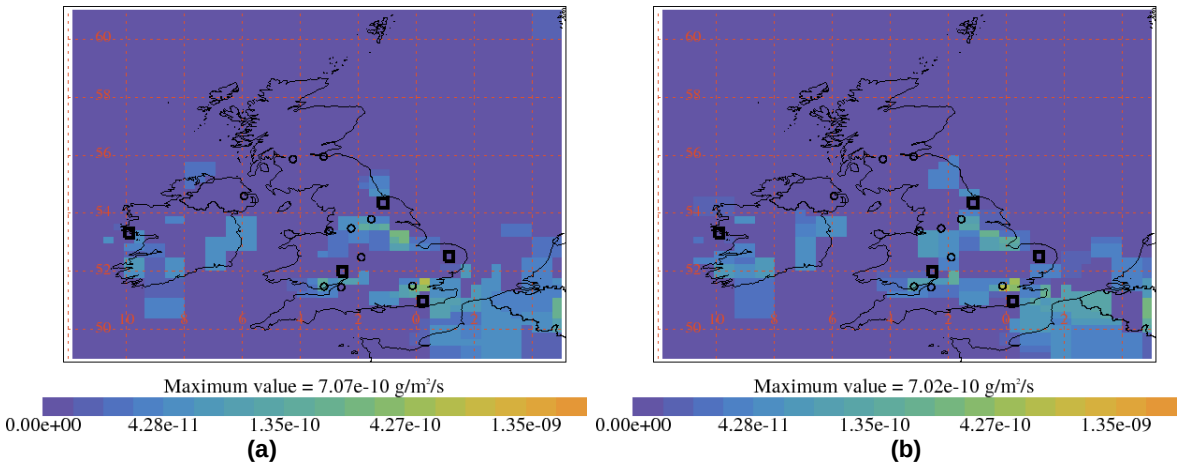


**Figure 90: Average InTEM estimates 2014-2017 of spatial distribution of $SF_6$ emissions using DECC+GAUGE observations with minimal prior information. Black squares are measurement stations and circles are major cities in UK. (a) Global meteorology and (b) UKV meteorology.**

## 4.22 $NF_3$

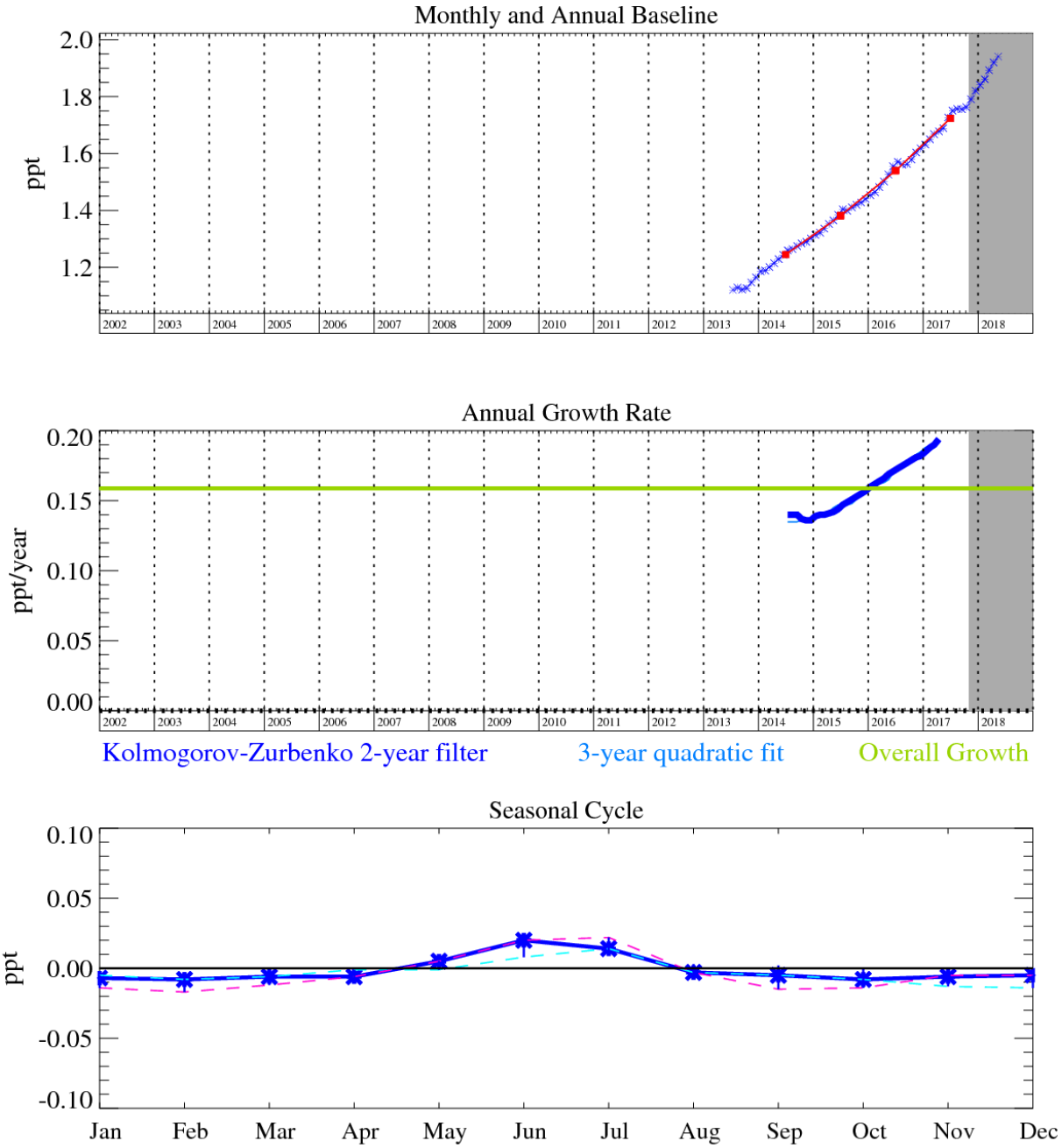


**Figure 91: $NF_3$: Monthly (blue) baseline mole fractions. Grey area covers un-ratified and therefore provisional data.**

Production of nitrogen trifluoride ($NF_3$) has been increasing rapidly to meet demand in end use applications (the manufacture of semiconductor devices, flat panel displays and photovoltaic cells). The new ambient air measurements from the Advanced Global Atmospheric Gases Experiment have shown the rapidly rising global atmospheric abundance of this gas due to this market expansion. Although the current contribution of $NF_3$ to radiative forcing is small, its potential to impact the climate is significant (its $GWP_{100}$ is 16,100).

The UK emissions of this gas, both estimated in the inventory and using InTEM, are very small. The pollution events seen at Mace Head are almost all lost within the baseline noise. The only exception to this was an episode when the air travelled quickly and directly from the NE USA (please refer to the 2015 report for more details).

# 5 Global emission estimates

## *5.1 Introduction*

Global emissions and mean lower tropospheric mole fraction estimates were made using baseline AGAGE observations from five “background” AGAGE stations (Mace Head, Ireland; Trinidad Head, California; Ragged Point, Barbados; Cape Matatula, American Samoa; and Cape Grim, Tasmania) using the method outlined in Rigby et al. (2014). A two-dimensional model of global atmospheric chemistry and transport was used to simulate baseline mole fractions in four latitudinal bands, separated at the equator and ±30 degrees (Rigby et al., 2013). The modelled mole fractions were brought into consistency with the AGAGE observations using a Bayesian method in which an initial estimate of the emissions growth rate was adjusted in the inversion. Uncertainties in the derived global emissions estimates are determined by the observational uncertainty, model uncertainty and uncertainties in the atmospheric lifetimes of each gas. Global mole fractions and emissions of each of the measured gases that are reported to the UNFCCC are shown in Table 22 - Table 25 and Table 26 - Table 29 respectively.

## *5.2 Recent trends in non-$CO_2$ Kyoto gases*

### 5.2.1 $CH_4$

Methane concentrations grew at 8 ppt $yr^{-1}$ between 2016 and 2017. This positive growth trend has continued since 2007, before which, growth was close to zero between 2000 and 2006. The previous Reports have noted that there are several competing explanations for these changes in growth rate. The uncertainty surrounding the potential changes in methane sources and its atmospheric sink (primarily the OH radical in the troposphere) persists. Studies published since the previous Report have suggested that changes in livestock and/or fossil fuel emissions may have contributed to recent mole fraction growth (Wolf et al., 2017; Worden et al., 2017). However, the reasons for the pause in methane growth and its renewed rise remain highly uncertain.

### 5.2.2 $N_2O$

Nitrous oxide is the third most important greenhouse gas after $CO_2$ and $CH_4$ and it plays a major role in ozone depletion. Its growth rate has remained close to 0.8 ppt $yr^{-1}$ for at least the last decade. During this time, global emissions remained close to 28 Tg $yr^{-1}$. There has been little work re-examining the global budget of nitrous oxide since the previous Report. The relative contribution of anthropogenic and natural emissions remains relatively uncertain at the global scale.

### 5.2.3 HFCs

Emissions and global mole fractions of all of the major HFCs grew between 2016 and 2017. There is a well-known gap between total $CO_2$-equivalent HFC emissions reported the UNFCCC and total global emissions derived from atmospheric measurements (e.g. Rigby et al., 2014). Evidence from atmospheric observations has suggested that this gap is largely due to non-reporting (non-Annex-1) countries, although discrepancies were found at the species-specific level between top-down and bottom-up reports for Annex-1 countries (e.g. Lunt et al., 2015). A recent study of European emissions also finds consistency between reported and top-down emissions when HFCs are aggregated but some disagreement for individual gases (Graziosi et al., 2017), whilst a regional study in the USA found aggregated emissions that were lower than the USA’s UNFCCC reports (Hu et al., 2017). A recent study has shown that global emissions of HFC-23 increased rapidly after the Clean Development Mechanism (CDM) measures tackling HFC-23 emissions ended in 2009 (Simmonds et al., 2018). Emissions reached a maximum in 2014 and dropped until 2016. The cause of this decrease may be linked to efforts to reduce emissions by the Chinese government. However, this decline appears to have halted, and emissions grew between 2016 and 2017.

### 5.2.4 PFCs, $SF_6$ and $NF_3$

Emissions of PFC-14 ($CF_4$), the most abundant PFC, increased between 2016 and 2017, reaching levels not seen since the 1990s. The cause of this recent rise is not yet known. Emissions of PFC-116 and PFC-318 have remained relatively constant in recent years. Emissions of $SF_6$ and $NF_3$ have continued to grow strongly between 2016 and 2017. There has been little change in our understanding of the sources of these long-lived greenhouse gases since the previous Report.

| Date | $CH_4$ (ppb) | $N_2O$ (ppb) | HFC-23 (ppt) | HFC-32 (ppt) | HFC-125 (ppt) |
|---|---|---|---|---|---|
| 1978 | ( - ) | 300 (298 - 301) | ( - ) | ( - ) | ( - ) |
| 1979 | ( - ) | 301 (299 - 302) | ( - ) | ( - ) | ( - ) |
| 1980 | ( - ) | 301 (300 - 303) | ( - ) | ( - ) | ( - ) |
| 1981 | ( - ) | 302 (300 - 303) | ( - ) | ( - ) | ( - ) |
| 1982 | ( - ) | 303 (301 - 304) | ( - ) | ( - ) | ( - ) |
| 1983 | ( - ) | 304 (302 - 305) | ( - ) | ( - ) | ( - ) |
| 1984 | ( - ) | 304 (303 - 305) | ( - ) | ( - ) | ( - ) |
| 1985 | 1680 (1670 - 1700) | 304 (303 - 306) | ( - ) | ( - ) | ( - ) |
| 1986 | 1670 (1660 - 1670) | 305 (304 - 307) | ( - ) | ( - ) | ( - ) |
| 1987 | 1680 (1670 - 1690) | 306 (304 - 307) | ( - ) | ( - ) | ( - ) |
| 1988 | 1690 (1680 - 1700) | 307 (305 - 308) | ( - ) | ( - ) | ( - ) |
| 1989 | 1710 (1700 - 1720) | 308 (306 - 309) | ( - ) | ( - ) | ( - ) |
| 1990 | 1710 (1710 - 1720) | 309 (307 - 310) | ( - ) | ( - ) | ( - ) |
| 1991 | 1730 (1720 - 1740) | 310 (308 - 311) | ( - ) | ( - ) | ( - ) |
| 1992 | 1740 (1730 - 1740) | 310 (308 - 311) | ( - ) | ( - ) | ( - ) |
| 1993 | 1740 (1730 - 1750) | 310 (309 - 312) | ( - ) | ( - ) | ( - ) |
| 1994 | 1740 (1740 - 1750) | 311 (309 - 312) | ( - ) | ( - ) | ( - ) |
| 1995 | 1750 (1740 - 1760) | 312 (310 - 313) | ( - ) | ( - ) | ( - ) |
| 1996 | 1750 (1740 - 1760) | 313 (311 - 314) | ( - ) | ( - ) | ( - ) |
| 1997 | 1750 (1740 - 1760) | 314 (312 - 315) | ( - ) | ( - ) | ( - ) |
| 1998 | 1760 (1750 - 1770) | 314 (313 - 316) | ( - ) | 0.124 (0.0726 - 0.179) | 0.99 (0.94 - 1.04) |
| 1999 | 1770 (1760 - 1780) | 315 (314 - 317) | ( - ) | 0.172 (0.121 - 0.229) | 1.22 (1.16 - 1.29) |
| 2000 | 1770 (1760 - 1780) | 316 (315 - 318) | ( - ) | 0.228 (0.184 - 0.271) | 1.53 (1.45 - 1.61) |
| 2001 | 1770 (1760 - 1780) | 317 (315 - 318) | ( - ) | 0.301 (0.249 - 0.356) | 1.93 (1.83 - 2.03) |
| 2002 | 1770 (1760 - 1780) | 318 (316 - 319) | ( - ) | 0.412 (0.362 - 0.464) | 2.35 (2.23 - 2.47) |
| 2003 | 1780 (1770 - 1780) | 318 (317 - 320) | ( - ) | 0.563 (0.523 - 0.603) | 2.88 (2.73 - 3.03) |
| 2004 | 1780 (1770 - 1780) | 319 (317 - 320) | ( - ) | 0.835 (0.805 - 0.865) | 3.44 (3.27 - 3.61) |
| 2005 | 1770 (1770 - 1780) | 320 (318 - 321) | ( - ) | 1.21 (1.17 - 1.25) | 4.07 (3.87 - 4.27) |
| 2006 | 1770 (1760 - 1780) | 320 (319 - 322) | ( - ) | 1.61 (1.56 - 1.66) | 4.78 (4.55 - 5.03) |
| 2007 | 1780 (1770 - 1790) | 321 (320 - 323) | 21.0 (20.6 - 21.4) | 2.13 (2.07 - 2.20) | 5.62 (5.35 - 5.91) |
| 2008 | 1790 (1780 - 1800) | 322 (321 - 324) | 21.9 (21.4 - 22.3) | 2.69 (2.61 - 2.78) | 6.60 (6.28 - 6.93) |
| 2009 | 1790 (1780 - 1800) | 323 (321 - 324) | 22.6 (22.1 - 23.0) | 3.28 (3.18 - 3.38) | 7.68 (7.29 - 8.07) |
| 2010 | 1800 (1790 - 1800) | 324 (322 - 325) | 23.3 (22.8 - 23.7) | 4.09 (3.97 - 4.21) | 8.95 (8.51 - 9.40) |
| 2011 | 1800 (1800 - 1810) | 325 (323 - 326) | 24.1 (23.6 - 24.5) | 5.14 (4.99 - 5.31) | 10.5 (9.93 - 11.0) |
| 2012 | 1810 (1800 - 1820) | 326 (324 - 327) | 25.0 (24.4 - 25.4) | 6.23 (6.05 - 6.43) | 12.1 (11.5 - 12.7) |
| 2013 | 1810 (1810 - 1820) | 327 (325 - 328) | 26.0 (25.4 - 26.5) | 7.51 (7.30 - 7.75) | 14.0 (13.3 - 14.7) |
| 2014 | 1820 (1820 - 1830) | 328 (326 - 329) | 27.0 (26.5 - 27.5) | 8.98 (8.72 - 9.26) | 16.1 (15.3 - 16.9) |
| 2015 | 1830 (1830 - 1840) | 329 (327 - 330) | 28.0 (27.5 - 28.6) | 10.7 (10.4 - 11.1) | 18.5 (17.6 - 19.4) |
| 2016 | 1840 (1830 - 1850) | 329 (328 - 331) | 28.9 (28.3 - 29.5) | 12.5 (12.1 - 12.9) | 20.8 (19.8 - 21.8) |
| 2017 | 1850 (1840 - 1860) | 330 (329 - 332) | 29.9 (29.3 - 30.5) | 14.4 (14.0 - 14.8) | 23.4 (22.2 - 24.5) |

**Table 22: Modelled global mole fractions with uncertainties**

| Date | HFC-134a (ppt) | HFC-143a (ppt) | HFC-152a (ppt) | HFC-227ea (ppt) | HFC-236fa (ppt) |
|---|---|---|---|---|---|
| 1978 | ( - ) | ( - ) | ( - ) | ( - ) | ( - ) |
| 1979 | ( - ) | ( - ) | ( - ) | ( - ) | ( - ) |
| 1980 | ( - ) | 0.0961 (0.0361 - 0.150) | ( - ) | ( - ) | ( - ) |
| 1981 | ( - ) | 0.208 (0.0665 - 0.345) | ( - ) | ( - ) | ( - ) |
| 1982 | ( - ) | 0.191 (0.0907 - 0.302) | ( - ) | ( - ) | ( - ) |
| 1983 | ( - ) | 0.191 (0.141 - 0.237) | ( - ) | ( - ) | ( - ) |
| 1984 | ( - ) | 0.206 (0.106 - 0.304) | ( - ) | ( - ) | ( - ) |
| 1985 | ( - ) | 0.239 (0.179 - 0.289) | ( - ) | ( - ) | ( - ) |
| 1986 | ( - ) | 0.287 (0.242 - 0.331) | ( - ) | ( - ) | ( - ) |
| 1987 | ( - ) | 0.306 (0.221 - 0.390) | ( - ) | ( - ) | ( - ) |
| 1988 | ( - ) | 0.364 (0.313 - 0.416) | ( - ) | ( - ) | ( - ) |
| 1989 | ( - ) | 0.422 (0.376 - 0.472) | ( - ) | ( - ) | ( - ) |
| 1990 | ( - ) | 0.479 (0.426 - 0.540) | ( - ) | ( - ) | ( - ) |
| 1991 | ( - ) | 0.534 (0.489 - 0.583) | ( - ) | ( - ) | ( - ) |
| 1992 | ( - ) | 0.570 (0.517 - 0.625) | ( - ) | ( - ) | ( - ) |
| 1993 | ( - ) | 0.615 (0.559 - 0.674) | ( - ) | ( - ) | ( - ) |
| 1994 | 1.03 (0.924 - 1.12) | 0.688 (0.645 - 0.738) | 0.824 (0.79 - 0.86) | ( - ) | ( - ) |
| 1995 | 1.99 (1.90 - 2.08) | 0.806 (0.765 - 0.855) | 1.06 (1.02 - 1.09) | ( - ) | ( - ) |
| 1996 | 3.43 (3.33 - 3.52) | 0.991 (0.944 - 1.05) | 1.16 (1.12 - 1.20) | ( - ) | ( - ) |
| 1997 | 5.35 (5.22 - 5.46) | 1.24 (1.18 - 1.31) | 1.28 (1.24 - 1.33) | ( - ) | ( - ) |
| 1998 | 7.98 (7.82 - 8.12) | 1.61 (1.54 - 1.68) | 1.54 (1.49 - 1.59) | ( - ) | ( - ) |
| 1999 | 11.1 (10.9 - 11.3) | 2.00 (1.93 - 2.08) | 1.70 (1.64 - 1.75) | ( - ) | ( - ) |
| 2000 | 14.5 (14.2 - 14.7) | 2.45 (2.37 - 2.55) | 1.88 (1.82 - 1.94) | ( - ) | ( - ) |
| 2001 | 18.0 (17.7 - 18.2) | 2.97 (2.87 - 3.08) | 2.11 (2.04 - 2.17) | ( - ) | ( - ) |
| 2002 | 21.8 (21.4 - 22.1) | 3.58 (3.47 - 3.72) | 2.41 (2.33 - 2.49) | ( - ) | ( - ) |
| 2003 | 25.9 (25.5 - 26.3) | 4.20 (4.08 - 4.35) | 2.83 (2.74 - 2.92) | ( - ) | ( - ) |
| 2004 | 30.3 (29.9 - 30.8) | 4.93 (4.79 - 5.10) | 3.26 (3.16 - 3.36) | ( - ) | ( - ) |
| 2005 | 34.7 (34.1 - 35.2) | 5.71 (5.56 - 5.91) | 3.76 (3.65 - 3.88) | ( - ) | ( - ) |
| 2006 | 39.0 (38.4 - 39.6) | 6.63 (6.45 - 6.85) | 4.49 (4.35 - 4.63) | 0.365 (0.334 - 0.395) | 0.0583 (0.046 - 0.070) |
| 2007 | 43.4 (42.7 - 44.0) | 7.59 (7.39 - 7.84) | 5.29 (5.13 - 5.44) | 0.430 (0.394 - 0.465) | 0.0656 (0.052 - 0.079) |
| 2008 | 48.1 (47.3 - 48.7) | 8.63 (8.41 - 8.92) | 5.82 (5.65 - 5.99) | 0.497 (0.457 - 0.538) | 0.0732 (0.058 - 0.088) |
| 2009 | 52.8 (52.0 - 53.5) | 9.74 (9.48 - 10.1) | 5.99 (5.81 - 6.18) | 0.574 (0.527 - 0.620) | 0.0812 (0.065 - 0.098) |
| 2010 | 57.8 (56.9 - 58.7) | 10.9 (10.6 - 11.2) | 6.28 (6.09 - 6.47) | 0.655 (0.602 - 0.708) | 0.0898 (0.0719 - 0.108) |
| 2011 | 62.8 (61.8 - 63.8) | 12.1 (11.8 - 12.5) | 6.62 (6.42 - 6.82) | 0.737 (0.678 - 0.797) | 0.0992 (0.0797 - 0.120) |
| 2012 | 67.7 (66.6 - 68.7) | 13.4 (13.1 - 13.8) | 6.78 (6.57 - 6.99) | 0.822 (0.756 - 0.891) | 0.109 (0.0881 - 0.132) |
| 2013 | 72.7 (71.6 - 73.8) | 14.7 (14.4 - 15.2) | 6.75 (6.54 - 6.95) | 0.922 (0.848 - 0.998) | 0.120 (0.0962 - 0.145) |
| 2014 | 77.9 (76.8 - 79.1) | 16.2 (15.8 - 16.7) | 6.65 (6.46 - 6.85) | 1.02 (0.940 - 1.11) | 0.130 (0.104 - 0.157) |
| 2015 | 83.4 (82.1 - 84.6) | 17.7 (17.2 - 18.3) | 6.62 (6.43 - 6.82) | 1.12 (1.03 - 1.22) | 0.141 (0.113 - 0.170) |
| 2016 | 89.3 (88.0 - 90.7) | 19.3 (18.8 - 19.9) | 6.72 (6.51 - 6.93) | 1.24 (1.14 - 1.34) | 0.151 (0.121 - 0.183) |
| 2017 | 95.5 (94.1 - 97.0) | 21.0 (20.5 - 21.7) | 6.83 (6.62 - 7.04) | 1.37 (1.26 - 1.48) | 0.162 (0.130 - 0.195) |

**Table 23: Modelled global mole fractions with uncertainties**

| Date | HFC-245fa (ppt) | HFC-365mfc (ppt) | PFC-14 (ppt) | PFC-116 (ppt) |
|---|---|---|---|---|
| 1978 | ( - ) | ( - ) | 50.8 (49.4 - 52.3) | 1.04 (1.00 - 1.07) |
| 1979 | ( - ) | ( - ) | 52.2 (50.7 - 53.8) | 1.13 (1.09 - 1.16) |
| 1980 | ( - ) | ( - ) | 53.5 (51.9 - 55.0) | 1.21 (1.17 - 1.26) |
| 1981 | ( - ) | ( - ) | 54.6 (53.0 - 56.2) | 1.30 (1.25 - 1.34) |
| 1982 | ( - ) | ( - ) | 55.6 (54.0 - 57.3) | 1.37 (1.32 - 1.41) |
| 1983 | ( - ) | ( - ) | 56.6 (55.0 - 58.3) | 1.44 (1.39 - 1.48) |
| 1984 | ( - ) | ( - ) | 57.7 (56.1 - 59.4) | 1.53 (1.48 - 1.57) |
| 1985 | ( - ) | ( - ) | 58.7 (57.1 - 60.5) | 1.62 (1.57 - 1.67) |
| 1986 | ( - ) | ( - ) | 59.7 (58.1 - 61.5) | 1.71 (1.65 - 1.76) |
| 1987 | ( - ) | ( - ) | 60.7 (59.0 - 62.5) | 1.80 (1.74 - 1.85) |
| 1988 | ( - ) | ( - ) | 61.7 (60.0 - 63.6) | 1.89 (1.83 - 1.95) |
| 1989 | ( - ) | ( - ) | 62.8 (61.0 - 64.7) | 1.98 (1.92 - 2.04) |
| 1990 | ( - ) | ( - ) | 63.8 (62.0 - 65.7) | 2.07 (2.01 - 2.14) |
| 1991 | ( - ) | ( - ) | 64.8 (63.0 - 66.8) | 2.16 (2.10 - 2.23) |
| 1992 | ( - ) | ( - ) | 65.7 (63.8 - 67.6) | 2.25 (2.18 - 2.32) |
| 1993 | ( - ) | ( - ) | 66.5 (64.6 - 68.5) | 2.34 (2.26 - 2.41) |
| 1994 | ( - ) | ( - ) | 67.2 (65.3 - 69.2) | 2.42 (2.35 - 2.49) |
| 1995 | ( - ) | ( - ) | 67.9 (66.0 - 69.9) | 2.52 (2.44 - 2.59) |
| 1996 | ( - ) | ( - ) | 68.7 (66.7 - 70.7) | 2.62 (2.54 - 2.70) |
| 1997 | ( - ) | ( - ) | 69.4 (67.4 - 71.5) | 2.73 (2.65 - 2.81) |
| 1998 | ( - ) | ( - ) | 70.1 (68.1 - 72.2) | 2.86 (2.77 - 2.94) |
| 1999 | ( - ) | ( - ) | 70.8 (68.8 - 72.9) | 2.99 (2.90 - 3.07) |
| 2000 | ( - ) | ( - ) | 71.5 (69.5 - 73.6) | 3.11 (3.02 - 3.20) |
| 2001 | ( - ) | ( - ) | 72.1 (70.1 - 74.3) | 3.23 (3.13 - 3.33) |
| 2002 | ( - ) | ( - ) | 72.8 (70.7 - 75.0) | 3.35 (3.25 - 3.45) |
| 2003 | ( - ) | 0.0606 (0.0509 - 0.0713) | 73.5 (71.4 - 75.7) | 3.47 (3.36 - 3.57) |
| 2004 | ( - ) | 0.128 (0.109 - 0.147) | 74.3 (72.2 - 76.5) | 3.57 (3.46 - 3.68) |
| 2005 | ( - ) | 0.218 (0.188 - 0.250) | 75.0 (72.8 - 77.2) | 3.66 (3.55 - 3.77) |
| 2006 | 0.603 (0.555 - 0.655) | 0.317 (0.273 - 0.363) | 75.7 (73.5 - 77.9) | 3.76 (3.64 - 3.87) |
| 2007 | 0.833 (0.772 - 0.903) | 0.407 (0.351 - 0.467) | 76.4 (74.2 - 78.7) | 3.85 (3.73 - 3.96) |
| 2008 | 1.03 (0.954 - 1.12) | 0.480 (0.415 - 0.550) | 77.1 (74.9 - 79.4) | 3.94 (3.82 - 4.05) |
| 2009 | 1.19 (1.10 - 1.29) | 0.538 (0.464 - 0.615) | 77.7 (75.5 - 80.0) | 4.01 (3.89 - 4.13) |
| 2010 | 1.34 (1.24 - 1.45) | 0.590 (0.510 - 0.674) | 78.3 (76.1 - 80.6) | 4.09 (3.97 - 4.21) |
| 2011 | 1.51 (1.40 - 1.64) | 0.649 (0.558 - 0.743) | 79.0 (76.8 - 81.4) | 4.17 (4.04 - 4.29) |
| 2012 | 1.70 (1.57 - 1.85) | 0.712 (0.613 - 0.814) | 79.7 (77.5 - 82.1) | 4.25 (4.12 - 4.38) |
| 2013 | 1.88 (1.75 - 2.04) | 0.777 (0.671 - 0.890) | 80.5 (78.2 - 82.8) | 4.33 (4.20 - 4.46) |
| 2014 | 2.05 (1.90 - 2.22) | 0.846 (0.728 - 0.969) | 81.2 (78.9 - 83.6) | 4.41 (4.27 - 4.54) |
| 2015 | 2.23 (2.06 - 2.42) | 0.919 (0.791 - 1.05) | 81.9 (79.6 - 84.3) | 4.49 (4.35 - 4.62) |
| 2016 | 2.42 (2.24 - 2.63) | 0.994 (0.856 - 1.14) | 82.7 (80.4 - 85.2) | 4.57 (4.43 - 4.70) |
| 2017 | 2.62 (2.42 - 2.85) | 1.07 (0.918 - 1.22) | 83.6 (81.2 - 86.0) | 4.65 (4.51 - 4.79) |

**Table 24: Modelled global mole fractions with uncertainties**

| Date | PFC-318 (ppt) | $SF_6$ (ppt) | $NF_3$ (ppt) |
|---|---|---|---|
| 1978 | ( - ) | 0.660 (0.644 - 0.676) | ( - ) |
| 1979 | ( - ) | 0.762 (0.740 - 0.784) | ( - ) |
| 1980 | ( - ) | 0.868 (0.846 - 0.889) | ( - ) |
| 1981 | ( - ) | 0.983 (0.959 - 1.01) | ( - ) |
| 1982 | ( - ) | 1.11 (1.08 - 1.14) | ( - ) |
| 1983 | 0.0715 (0.0661 - 0.0769) | 1.21 (1.19 - 1.24) | ( - ) |
| 1984 | 0.0762 (0.0722 - 0.0802) | 1.33 (1.30 - 1.36) | ( - ) |
| 1985 | 0.0824 (0.0783 - 0.0863) | 1.48 (1.45 - 1.51) | ( - ) |
| 1986 | 0.0892 (0.0851 - 0.0935) | 1.66 (1.62 - 1.69) | ( - ) |
| 1987 | 0.0965 (0.0923 - 0.101) | 1.84 (1.80 - 1.88) | ( - ) |
| 1988 | 0.104 (0.0992 - 0.108) | 2.00 (1.96 - 2.05) | ( - ) |
| 1989 | 0.111 (0.106 - 0.116) | 2.17 (2.12 - 2.21) | ( - ) |
| 1990 | 0.118 (0.113 - 0.123) | 2.36 (2.31 - 2.40) | ( - ) |
| 1991 | 0.126 (0.120 - 0.131) | 2.57 (2.51 - 2.62) | ( - ) |
| 1992 | 0.135 (0.129 - 0.141) | 2.76 (2.71 - 2.82) | ( - ) |
| 1993 | 0.145 (0.138 - 0.151) | 2.97 (2.91 - 3.03) | ( - ) |
| 1994 | 0.157 (0.150 - 0.164) | 3.19 (3.13 - 3.26) | ( - ) |
| 1995 | 0.171 (0.164 - 0.179) | 3.44 (3.37 - 3.51) | ( - ) |
| 1996 | 0.189 (0.181 - 0.197) | 3.70 (3.62 - 3.77) | ( - ) |
| 1997 | 0.209 (0.200 - 0.218) | 3.93 (3.85 - 4.01) | ( - ) |
| 1998 | 0.232 (0.222 - 0.242) | 4.15 (4.06 - 4.23) | ( - ) |
| 1999 | 0.257 (0.247 - 0.268) | 4.34 (4.25 - 4.43) | ( - ) |
| 2000 | 0.284 (0.273 - 0.296) | 4.53 (4.44 - 4.62) | ( - ) |
| 2001 | 0.312 (0.300 - 0.325) | 4.73 (4.63 - 4.82) | ( - ) |
| 2002 | 0.342 (0.328 - 0.355) | 4.94 (4.84 - 5.04) | ( - ) |
| 2003 | 0.371 (0.356 - 0.386) | 5.17 (5.06 - 5.27) | ( - ) |
| 2004 | 0.400 (0.384 - 0.416) | 5.40 (5.28 - 5.51) | ( - ) |
| 2005 | 0.428 (0.411 - 0.445) | 5.62 (5.51 - 5.74) | ( - ) |
| 2006 | 0.454 (0.436 - 0.472) | 5.87 (5.75 - 5.99) | ( - ) |
| 2007 | 0.477 (0.458 - 0.497) | 6.14 (6.01 - 6.26) | ( - ) |
| 2008 | 0.499 (0.479 - 0.519) | 6.42 (6.29 - 6.55) | ( - ) |
| 2009 | 0.519 (0.498 - 0.539) | 6.70 (6.56 - 6.84) | ( - ) |
| 2010 | 0.537 (0.516 - 0.559) | 6.99 (6.84 - 7.13) | ( - ) |
| 2011 | 0.555 (0.533 - 0.577) | 7.28 (7.13 - 7.43) | ( - ) |
| 2012 | 0.571 (0.549 - 0.594) | 7.58 (7.43 - 7.74) | ( - ) |
| 2013 | 0.588 (0.564 - 0.611) | 7.90 (7.74 - 8.06) | 1.04 (1.01 - 1.08) |
| 2014 | 0.603 (0.579 - 0.628) | 8.23 (8.06 - 8.40) | 1.16 (1.13 - 1.20) |
| 2015 | 0.619 (0.594 - 0.644) | 8.56 (8.38 - 8.73) | 1.30 (1.26 - 1.34) |
| 2016 | 0.635 (0.609 - 0.660) | 8.89 (8.70 - 9.07) | 1.45 (1.41 - 1.49) |
| 2017 | 0.650 (0.624 - 0.677) | 9.24 (9.05 - 9.43) | 1.61 (1.57 - 1.66) |

**Table 25: Modelled global mole fractions with uncertainties**

| Date | $CH_4$ (Tg $yr^{-1}$) | $N_2O$ (Tg $yr^{-1}$) | HFC-23 (Gg $yr^{-1}$) | HFC-32 (Gg $yr^{-1}$) | HFC-125 (Gg $yr^{-1}$) |
|---|---|---|---|---|---|
| 1978 | ( - ) | 24.4 (22.2 - 26.4) | ( - ) | ( - ) | ( - ) |
| 1979 | ( - ) | 22.9 (20.8 - 25.0) | ( - ) | ( - ) | ( - ) |
| 1980 | ( - ) | 23.0 (20.9 - 25.0) | ( - ) | ( - ) | ( - ) |
| 1981 | ( - ) | 25.3 (23.2 - 27.4) | ( - ) | ( - ) | ( - ) |
| 1982 | ( - ) | 26.7 (24.7 - 28.8) | ( - ) | ( - ) | ( - ) |
| 1983 | ( - ) | 22.4 (20.2 - 24.5) | ( - ) | ( - ) | ( - ) |
| 1984 | ( - ) | 22.5 (20.4 - 24.6) | ( - ) | ( - ) | ( - ) |
| 1985 | ( - ) | 23.3 (21.2 - 25.4) | ( - ) | ( - ) | ( - ) |
| 1986 | 479 (405 - 549) | 24.7 (22.6 - 26.8) | ( - ) | ( - ) | ( - ) |
| 1987 | 502 (431 - 575) | 24.8 (22.6 - 26.9) | ( - ) | ( - ) | ( - ) |
| 1988 | 536 (463 - 612) | 25.4 (23.1 - 27.5) | ( - ) | ( - ) | ( - ) |
| 1989 | 493 (419 - 566) | 26.4 (24.2 - 28.6) | ( - ) | ( - ) | ( - ) |
| 1990 | 549 (475 - 624) | 27.3 (25.2 - 29.4) | ( - ) | ( - ) | ( - ) |
| 1991 | 543 (469 - 616) | 24.3 (22.2 - 26.2) | ( - ) | ( - ) | ( - ) |
| 1992 | 491 (413 - 564) | 22.4 (20.3 - 24.5) | ( - ) | ( - ) | ( - ) |
| 1993 | 527 (452 - 602) | 22.4 (20.4 - 24.5) | ( - ) | ( - ) | ( - ) |
| 1994 | 518 (444 - 594) | 25.1 (22.9 - 27.1) | ( - ) | ( - ) | ( - ) |
| 1995 | 515 (439 - 590) | 25.4 (23.2 - 27.4) | ( - ) | ( - ) | ( - ) |
| 1996 | 517 (440 - 592) | 26.7 (24.7 - 28.7) | ( - ) | ( - ) | ( - ) |
| 1997 | 516 (440 - 591) | 25.7 (23.5 - 27.7) | ( - ) | ( - ) | ( - ) |
| 1998 | 552 (475 - 627) | 25.9 (23.8 - 28.0) | ( - ) | 0.832 (-0.169 - 1.88) | 7.39 (6.83 - 7.97) |
| 1999 | 522 (447 - 597) | 26.3 (24.2 - 28.2) | ( - ) | 0.648 (-0.398 - 1.61) | 6.26 (5.74 - 6.73) |
| 2000 | 514 (437 - 587) | 27.2 (25.1 - 29.3) | ( - ) | 0.675 (-0.223 - 1.61) | 8.54 (7.85 - 9.22) |
| 2001 | 517 (440 - 592) | 24.8 (22.7 - 26.9) | ( - ) | 1.34 (0.479 - 2.16) | 9.07 (8.29 - 9.84) |
| 2002 | 520 (443 - 595) | 24.5 (22.3 - 26.5) | ( - ) | 1.69 (0.725 - 2.78) | 11.1 (10.3 - 12.0) |
| 2003 | 527 (450 - 602) | 25.9 (23.7 - 27.9) | ( - ) | 3.08 (2.20 - 3.90) | 13.6 (12.5 - 14.7) |
| 2004 | 510 (431 - 586) | 24.7 (22.7 - 26.7) | ( - ) | 4.17 (3.78 - 4.54) | 14.3 (13.2 - 15.5) |
| 2005 | 520 (445 - 598) | 25.0 (22.7 - 27.0) | ( - ) | 5.41 (4.91 - 5.88) | 16.6 (15.3 - 17.8) |
| 2006 | 512 (435 - 587) | 25.2 (23.1 - 27.1) | ( - ) | 6.82 (6.21 - 7.43) | 19.2 (17.8 - 20.6) |
| 2007 | 545 (470 - 620) | 27.5 (25.3 - 29.6) | 11.7 (11.0 - 12.4) | 8.33 (7.56 - 9.17) | 21.7 (20.1 - 23.3) |
| 2008 | 533 (455 - 608) | 26.9 (24.8 - 29.0) | 11.2 (10.6 - 11.8) | 9.74 (8.78 - 10.7) | 26.1 (24.2 - 28.1) |
| 2009 | 525 (447 - 601) | 26.1 (24.1 - 28.2) | 9.58 (9.05 - 10.1) | 11.2 (9.96 - 12.3) | 28.0 (25.9 - 30.0) |
| 2010 | 549 (471 - 626) | 26.7 (24.4 - 28.7) | 10.4 (9.91 - 11.0) | 15.4 (14.0 - 16.9) | 35.1 (32.6 - 37.9) |
| 2011 | 539 (458 - 619) | 27.5 (25.3 - 29.5) | 11.6 (11.0 - 12.3) | 18.0 (16.3 - 19.7) | 39.3 (36.3 - 42.3) |
| 2012 | 540 (462 - 616) | 27.1 (25.0 - 29.2) | 12.9 (12.3 - 13.5) | 20.9 (18.9 - 23.2) | 44.4 (41.3 - 47.6) |
| 2013 | 546 (468 - 623) | 27.8 (25.7 - 30.0) | 14.0 (13.3 - 14.6) | 24.5 (22.1 - 27.0) | 49.4 (45.7 - 52.8) |
| 2014 | 557 (477 - 634) | 28.3 (26.1 - 30.4) | 14.5 (13.8 - 15.1) | 30.0 (27.0 - 32.9) | 58.7 (54.5 - 63.1) |
| 2015 | 559 (478 - 636) | 26.7 (24.5 - 28.8) | 13.1 (12.5 - 13.7) | 33.5 (30.0 - 37.3) | 59.8 (55.4 - 64.5) |
| 2016 | 559 (480 - 639) | 26.9 (24.7 - 29.1) | 12.7 (12.0 - 13.3) | 37.7 (33.6 - 41.9) | 64.9 (60.0 - 69.5) |
| 2017 | 557 (474 - 642) | 27.6 (24.9 - 30.2) | 13.8 (12.9 - 14.8) | 39.7 (34.7 - 44.9) | 70.8 (64.2 - 76.5) |

**Table 26: Modelled global emissions with uncertainties**

| Date | HFC-134a (Gg $yr^{-1}$) | HFC-143a (Gg $yr^{-1}$) | HFC-152a (Gg $yr^{-1}$) | HFC-227ea (Gg $yr^{-1}$) | HFC-236fa (Gg $yr^{-1}$) |
|---|---|---|---|---|---|
| 1978 | ( - ) | ( - ) | ( - ) | ( - ) | ( - ) |
| 1979 | ( - ) | ( - ) | ( - ) | ( - ) | ( - ) |
| 1980 | ( - ) | 2.28 (0.200 - 4.47) | ( - ) | ( - ) | ( - ) |
| 1981 | ( - ) | 0.942 (-1.522 - 3.36) | ( - ) | ( - ) | ( - ) |
| 1982 | ( - ) | -0.487 (-2.626 - 1.75) | ( - ) | ( - ) | ( - ) |
| 1983 | ( - ) | 0.171 (-1.544 - 1.81) | ( - ) | ( - ) | ( - ) |
| 1984 | ( - ) | 0.0481 (-1.632 - 1.53) | ( - ) | ( - ) | ( - ) |
| 1985 | ( - ) | 0.609 (-1.122 - 2.35) | ( - ) | ( - ) | ( - ) |
| 1986 | ( - ) | 0.816 (-0.524 - 2.16) | ( - ) | ( - ) | ( - ) |
| 1987 | ( - ) | 0.400 (-0.710 - 1.67) | ( - ) | ( - ) | ( - ) |
| 1988 | ( - ) | 1.39 (0.133 - 2.74) | ( - ) | ( - ) | ( - ) |
| 1989 | ( - ) | 0.778 (-0.230 - 1.92) | ( - ) | ( - ) | ( - ) |
| 1990 | ( - ) | 0.917 (-0.295 - 2.02) | ( - ) | ( - ) | ( - ) |
| 1991 | ( - ) | 1.10 (-0.178 - 2.55) | ( - ) | ( - ) | ( - ) |
| 1992 | ( - ) | 0.582 (-0.720 - 1.90) | ( - ) | ( - ) | ( - ) |
| 1993 | ( - ) | 1.33 (-0.140 - 2.82) | ( - ) | ( - ) | ( - ) |
| 1994 | 15.0 (12.6 - 17.7) | 1.11 (-0.059 - 2.25) | 10.9 (9.60 - 12.2) | ( - ) | ( - ) |
| 1995 | 21.3 (20.2 - 22.4) | 2.46 (1.36 - 3.57) | 10.9 (9.59 - 12.2) | ( - ) | ( - ) |
| 1996 | 33.1 (31.8 - 34.5) | 3.44 (2.33 - 4.36) | 11.7 (10.3 - 13.2) | ( - ) | ( - ) |
| 1997 | 43.3 (41.2 - 45.2) | 4.55 (3.49 - 5.64) | 13.5 (11.8 - 15.1) | ( - ) | ( - ) |
| 1998 | 60.2 (57.4 - 63.0) | 5.63 (4.35 - 6.91) | 14.8 (12.9 - 16.7) | ( - ) | ( - ) |
| 1999 | 71.7 (68.2 - 75.2) | 6.29 (4.78 - 7.87) | 16.2 (14.1 - 18.3) | ( - ) | ( - ) |
| 2000 | 80.1 (75.7 - 84.3) | 7.35 (5.78 - 8.75) | 18.2 (15.9 - 20.5) | ( - ) | ( - ) |
| 2001 | 86.5 (81.4 - 91.4) | 9.03 (7.46 - 10.7) | 19.7 (17.1 - 22.2) | ( - ) | ( - ) |
| 2002 | 100. (93.4 - 106) | 9.74 (7.99 - 11.6) | 23.5 (20.4 - 26.6) | ( - ) | ( - ) |
| 2003 | 109 (102 - 116) | 11.4 (9.74 - 13.0) | 27.1 (23.5 - 30.5) | ( - ) | ( - ) |
| 2004 | 117 (109 - 125) | 11.9 (11.0 - 12.7) | 30.0 (26.1 - 34.0) | ( - ) | ( - ) |
| 2005 | 125 (115 - 134) | 13.8 (13.0 - 14.7) | 36.1 (31.4 - 40.7) | ( - ) | ( - ) |
| 2006 | 129 (118 - 138) | 15.5 (14.6 - 16.5) | 43.0 (37.6 - 48.5) | 2.20 (1.73 - 2.70) | 0.195 (0.149 - 0.239) |
| 2007 | 138 (126 - 149) | 16.1 (15.0 - 17.0) | 48.0 (41.7 - 54.4) | 2.21 (1.92 - 2.51) | 0.205 (0.157 - 0.253) |
| 2008 | 149 (136 - 162) | 18.5 (17.4 - 19.6) | 48.8 (41.8 - 55.8) | 2.53 (2.23 - 2.86) | 0.216 (0.168 - 0.266) |
| 2009 | 156 (142 - 169) | 18.7 (17.4 - 19.8) | 47.7 (40.5 - 54.8) | 2.76 (2.42 - 3.11) | 0.225 (0.175 - 0.277) |
| 2010 | 170 (155 - 184) | 20.5 (19.3 - 21.8) | 52.5 (45.0 - 59.9) | 2.98 (2.60 - 3.38) | 0.246 (0.191 - 0.304) |
| 2011 | 172 (155 - 188) | 21.5 (20.1 - 22.9) | 53.9 (46.0 - 61.9) | 3.06 (2.66 - 3.47) | 0.272 (0.212 - 0.335) |
| 2012 | 179 (161 - 196) | 23.1 (21.6 - 24.6) | 52.4 (44.2 - 59.9) | 3.36 (2.94 - 3.82) | 0.286 (0.223 - 0.350) |
| 2013 | 188 (169 - 206) | 24.3 (22.8 - 25.9) | 50.9 (43.1 - 59.2) | 3.73 (3.25 - 4.21) | 0.291 (0.228 - 0.355) |
| 2014 | 202 (181 - 222) | 25.9 (24.3 - 27.5) | 50.5 (42.3 - 58.4) | 3.81 (3.31 - 4.33) | 0.291 (0.228 - 0.359) |
| 2015 | 212 (190 - 232) | 27.6 (25.8 - 29.3) | 50.8 (43.1 - 58.9) | 3.97 (3.45 - 4.47) | 0.291 (0.225 - 0.358) |
| 2016 | 227 (203 - 249) | 29.3 (27.4 - 31.3) | 52.3 (44.3 - 60.1) | 4.56 (4.00 - 5.15) | 0.296 (0.227 - 0.366) |
| 2017 | 239 (210 - 266) | 31.9 (28.6 - 35.3) | 54.2 (45.8 - 62.3) | 5.18 (4.27 - 6.21) | 0.304 (0.231 - 0.375) |

**Table 27: Modelled global emissions with uncertainties**

| Date | HFC-245fa (Gg $yr^{-1}$) | HFC-365mfc (Gg $yr^{-1}$) | PFC-14 (Gg $yr^{-1}$) | PFC-116 (Gg $yr^{-1}$) |
|---|---|---|---|---|
| 1978 | ( - ) | ( - ) | 21.2 (19.9 - 22.5) | 2.20 (1.90 - 2.49) |
| 1979 | ( - ) | ( - ) | 20.5 (19.4 - 21.5) | 2.23 (1.99 - 2.47) |
| 1980 | ( - ) | ( - ) | 19.4 (18.2 - 20.6) | 2.14 (1.93 - 2.34) |
| 1981 | ( - ) | ( - ) | 17.1 (16.0 - 18.1) | 1.89 (1.69 - 2.07) |
| 1982 | ( - ) | ( - ) | 15.7 (14.5 - 16.6) | 1.74 (1.54 - 1.95) |
| 1983 | ( - ) | ( - ) | 16.4 (15.2 - 17.5) | 1.91 (1.71 - 2.12) |
| 1984 | ( - ) | ( - ) | 16.5 (15.3 - 17.8) | 2.17 (1.96 - 2.39) |
| 1985 | ( - ) | ( - ) | 15.7 (14.6 - 16.7) | 2.18 (1.96 - 2.37) |
| 1986 | ( - ) | ( - ) | 15.6 (14.4 - 16.6) | 2.16 (1.96 - 2.36) |
| 1987 | ( - ) | ( - ) | 15.7 (14.6 - 16.8) | 2.19 (1.97 - 2.39) |
| 1988 | ( - ) | ( - ) | 16.1 (15.0 - 17.2) | 2.25 (2.06 - 2.43) |
| 1989 | ( - ) | ( - ) | 16.1 (15.1 - 17.2) | 2.26 (2.03 - 2.46) |
| 1990 | ( - ) | ( - ) | 16.0 (14.9 - 17.0) | 2.24 (2.02 - 2.46) |
| 1991 | ( - ) | ( - ) | 14.8 (13.7 - 15.8) | 2.16 (1.94 - 2.37) |
| 1992 | ( - ) | ( - ) | 13.0 (12.0 - 13.9) | 2.09 (1.90 - 2.28) |
| 1993 | ( - ) | ( - ) | 12.3 (11.3 - 13.1) | 2.12 (1.90 - 2.31) |
| 1994 | ( - ) | ( - ) | 11.7 (10.8 - 12.7) | 2.16 (1.92 - 2.36) |
| 1995 | ( - ) | ( - ) | 11.9 (10.9 - 12.8) | 2.35 (2.14 - 2.55) |
| 1996 | ( - ) | ( - ) | 11.5 (10.6 - 12.5) | 2.60 (2.39 - 2.80) |
| 1997 | ( - ) | ( - ) | 11.3 (10.4 - 12.3) | 2.86 (2.67 - 3.07) |
| 1998 | ( - ) | ( - ) | 11.1 (10.1 - 12.0) | 3.02 (2.81 - 3.22) |
| 1999 | ( - ) | ( - ) | 10.8 (9.85 - 11.7) | 3.11 (2.89 - 3.30) |
| 2000 | ( - ) | ( - ) | 10.5 (9.52 - 11.4) | 3.03 (2.80 - 3.23) |
| 2001 | ( - ) | ( - ) | 10.2 (9.25 - 11.1) | 2.91 (2.69 - 3.10) |
| 2002 | ( - ) | ( - ) | 10.7 (9.79 - 11.6) | 2.86 (2.67 - 3.08) |
| 2003 | ( - ) | 1.24 (0.990 - 1.47) | 11.6 (10.7 - 12.5) | 2.72 (2.54 - 2.90) |
| 2004 | ( - ) | 2.33 (1.95 - 2.69) | 11.4 (10.6 - 12.1) | 2.45 (2.28 - 2.65) |
| 2005 | ( - ) | 2.97 (2.45 - 3.43) | 10.7 (10.0 - 11.4) | 2.31 (2.14 - 2.48) |
| 2006 | 7.38 (6.61 - 8.33) | 3.35 (2.81 - 3.88) | 11.3 (10.7 - 11.9) | 2.29 (2.13 - 2.46) |
| 2007 | 7.43 (6.61 - 8.38) | 3.28 (2.72 - 3.85) | 10.8 (10.2 - 11.4) | 2.26 (2.10 - 2.40) |
| 2008 | 7.36 (6.50 - 8.41) | 3.13 (2.53 - 3.65) | 10.6 (9.97 - 11.2) | 2.08 (1.93 - 2.23) |
| 2009 | 7.17 (6.20 - 8.32) | 2.95 (2.36 - 3.48) | 9.05 (8.45 - 9.60) | 1.89 (1.73 - 2.03) |
| 2010 | 7.88 (6.76 - 9.13) | 3.13 (2.51 - 3.70) | 10.1 (9.51 - 10.7) | 1.93 (1.79 - 2.08) |
| 2011 | 8.77 (7.58 - 10.1) | 3.41 (2.75 - 4.09) | 11.3 (10.7 - 11.9) | 1.93 (1.78 - 2.07) |
| 2012 | 9.46 (8.18 - 11.0) | 3.65 (2.92 - 4.35) | 11.3 (10.7 - 12.0) | 1.91 (1.76 - 2.05) |
| 2013 | 9.73 (8.36 - 11.4) | 3.88 (3.11 - 4.61) | 11.0 (10.3 - 11.6) | 1.93 (1.79 - 2.08) |
| 2014 | 10.2 (8.72 - 12.0) | 4.20 (3.38 - 5.00) | 11.1 (10.5 - 11.7) | 1.95 (1.79 - 2.10) |
| 2015 | 11.0 (9.35 - 12.9) | 4.48 (3.59 - 5.30) | 11.8 (11.1 - 12.5) | 1.96 (1.81 - 2.11) |
| 2016 | 11.8 (10.1 - 13.9) | 4.69 (3.72 - 5.58) | 12.6 (11.9 - 13.3) | 2.01 (1.85 - 2.18) |
| 2017 | 12.5 (10.5 - 14.8) | 4.89 (3.80 - 5.85) | 13.2 (12.2 - 14.3) | 2.03 (1.79 - 2.26) |

**Table 28: Modelled global emissions with uncertainties**

| Date | PFC-318 (Gg $yr^{-1}$) | $SF_6$ (Gg $yr^{-1}$) | $NF_3$ (Gg $yr^{-1}$) |
|---|---|---|---|
| 1978 | ( - ) | 2.67 (2.12 - 3.18) | ( - ) |
| 1979 | ( - ) | 2.65 (2.28 - 3.00) | ( - ) |
| 1980 | ( - ) | 2.76 (2.34 - 3.19) | ( - ) |
| 1981 | ( - ) | 3.07 (2.69 - 3.51) | ( - ) |
| 1982 | ( - ) | 3.04 (2.66 - 3.40) | ( - ) |
| 1983 | 0.263 (0.201 - 0.324) | 2.86 (2.44 - 3.29) | ( - ) |
| 1984 | 0.256 (0.202 - 0.311) | 3.38 (2.99 - 3.76) | ( - ) |
| 1985 | 0.250 (0.201 - 0.296) | 4.08 (3.68 - 4.46) | ( - ) |
| 1986 | 0.254 (0.212 - 0.297) | 4.74 (4.30 - 5.13) | ( - ) |
| 1987 | 0.249 (0.209 - 0.286) | 4.37 (3.99 - 4.75) | ( - ) |
| 1988 | 0.244 (0.205 - 0.282) | 4.26 (3.85 - 4.68) | ( - ) |
| 1989 | 0.242 (0.206 - 0.276) | 4.35 (3.96 - 4.80) | ( - ) |
| 1990 | 0.248 (0.211 - 0.287) | 4.94 (4.52 - 5.30) | ( - ) |
| 1991 | 0.266 (0.231 - 0.300) | 5.21 (4.82 - 5.60) | ( - ) |
| 1992 | 0.297 (0.261 - 0.332) | 5.07 (4.64 - 5.47) | ( - ) |
| 1993 | 0.348 (0.313 - 0.387) | 5.47 (5.09 - 5.84) | ( - ) |
| 1994 | 0.418 (0.380 - 0.459) | 6.05 (5.62 - 6.48) | ( - ) |
| 1995 | 0.505 (0.460 - 0.548) | 6.44 (5.99 - 6.83) | ( - ) |
| 1996 | 0.598 (0.551 - 0.644) | 6.31 (5.90 - 6.71) | ( - ) |
| 1997 | 0.690 (0.638 - 0.737) | 5.85 (5.43 - 6.26) | ( - ) |
| 1998 | 0.772 (0.718 - 0.827) | 5.50 (5.10 - 5.91) | ( - ) |
| 1999 | 0.842 (0.783 - 0.898) | 5.03 (4.63 - 5.43) | ( - ) |
| 2000 | 0.899 (0.837 - 0.958) | 4.97 (4.56 - 5.37) | ( - ) |
| 2001 | 0.940 (0.880 - 1.00) | 5.25 (4.81 - 5.66) | ( - ) |
| 2002 | 0.964 (0.905 - 1.03) | 5.68 (5.26 - 6.06) | ( - ) |
| 2003 | 0.970 (0.909 - 1.03) | 5.89 (5.50 - 6.27) | ( - ) |
| 2004 | 0.951 (0.891 - 1.01) | 5.80 (5.46 - 6.12) | ( - ) |
| 2005 | 0.906 (0.845 - 0.966) | 6.08 (5.76 - 6.42) | ( - ) |
| 2006 | 0.841 (0.785 - 0.897) | 6.42 (6.11 - 6.74) | ( - ) |
| 2007 | 0.771 (0.718 - 0.823) | 7.02 (6.69 - 7.34) | ( - ) |
| 2008 | 0.707 (0.658 - 0.757) | 7.35 (7.02 - 7.66) | ( - ) |
| 2009 | 0.655 (0.608 - 0.704) | 7.10 (6.76 - 7.42) | ( - ) |
| 2010 | 0.615 (0.572 - 0.660) | 7.35 (7.00 - 7.68) | ( - ) |
| 2011 | 0.580 (0.535 - 0.624) | 7.66 (7.32 - 8.02) | ( - ) |
| 2012 | 0.553 (0.509 - 0.598) | 7.98 (7.60 - 8.30) | ( - ) |
| 2013 | 0.536 (0.493 - 0.580) | 8.22 (7.88 - 8.57) | 1.40 (1.32 - 1.48) |
| 2014 | 0.527 (0.483 - 0.570) | 8.43 (8.06 - 8.78) | 1.55 (1.47 - 1.65) |
| 2015 | 0.524 (0.475 - 0.572) | 8.34 (7.97 - 8.71) | 1.74 (1.66 - 1.83) |
| 2016 | 0.522 (0.468 - 0.571) | 8.71 (8.31 - 9.09) | 1.92 (1.84 - 2.03) |
| 2017 | 0.522 (0.462 - 0.585) | 9.10 (8.52 - 9.67) | 2.03 (1.92 - 2.16) |

**Table 29: Modelled global emissions with uncertainties**

# 6 Estimating biogenic and anthropogenic $CO_2$

There remains no single, robust methodology to isolate $ffCO_2$ from atmospheric measurements of $CO_2$ alone.

There has been concerted modelling efforts to understand the performance of the current $^{14}CO_2$ network over Europe to quantify fossil fuel $CO_2$ ($ffCO_2$) (Wang et al, 2017, Wang et al, 2018), and the added benefit of increasing the spatial and temporal coverage of these measurements. Results from $^{14}CO_2$ data collected within the NERC-funded GAUGE project over the UK are still in preparation, but early results suggest care must be taken to remove the signal from the nuclear processing industry.

There have also been a number of recently-reported studies that have instrumented cities, taking advantage of geographical disaggregation of sources. These studies range from a high-density network of low-cost urban sensors over Berkeley, California (Shusterman et al., 2018) using an inverse model to infer city-wide $CO_2$ fluxes using 1-2 ground-based sensors across a city (Nickless et al., 2018), to installing a small network of atmospheric ground-based remote sensing sensors around a city (Vogel et al., 2018). The high-density of low-cost sensors has been attempted before but using sparser networks, arguing against redundant constraints on local fluxes provided by high density networks. Shusterman et al. (2018) present a method to separate local and regional influences on their network, and argue they can deliver policy-relevant trends from individual sectors (e.g. highway traffic) without the need for atmospheric transport models. Nickless et al. (2018) used a Lagrangian dispersion model and showed that the data collected at two sites across Cape Town, South Africa, after considering uncertainties, were not sufficient to estimate independent biospheric and fossil fuel $CO_2$ fluxes, although they were able to improve estimates of the net $CO_2$ flux. They are argued that separating $ffCO_2$ from the biospheric fluxes would require the use of carbon isotopes in the inversion. Vogel et al., 2018 reported column $CO_2$ variations upwind and downwind of Paris. They found a large gradient across the city but the magnitude and timing of diurnal variations were similar. From this, they concluded that despite Paris being home to 12 million people the natural biosphere imprinted a strong diurnal signature on the columns, and that the gradient between upwind and downwind sensors was mostly due to $ffCO_2$. This is an encouraging result for ground-based remote sensing for two reasons. First, the column measurements appear to be less sensitive to very local fluxes so that a few, well-positioned sites can be used to infer city-scale $CO_2$ fluxes. Second, Vogel et al., (2018) suggest that we can use the amplitude of the column $CO_2$ diurnal cycle and the offset between stations upwind and downwind of a city to isolate $ffCO_2$, but this remains to be shown using an inverse model. Also, how this result relates to satellite observations of $CO_2$ column that observe city-scale gradients but only once per day at a fixed time of day remains to be shown.

Data collected by commercial aircraft that fly in the upper troposphere have in the past been used exclusively to evaluate models after they have fitted to the data in the lower troposphere. These experiments are beginning to collect data during take-off and landing, providing vertical profiles of trace gases over major cities. Recent synthetic work used a multi-species inversion using data collected by the In-service Aircraft for a Global Observing System (IAGOS; Boschetti et al., 2018). They explored how to use correlations between $CO$-$CH_4$-$CO_2$ to show they can effectively separate $ffCO_2$ and the net biospheric flux of $CO_2$. This potentially opens up important new data constraints across Europe, North America, and eastern Asia (e.g., Umezawa et al., 2018).

# 7 Use of satellite data in inversion modelling

## 7.1 Introduction

Each section in this chapter builds on the work presented in the previous annual report. It is widely agreed that space-borne observations have a role to play in verifying nationwide GHG emission. They represent global, and high geographical coverage of the atmosphere subject to the constraints imposed by clouds and sub-optimal viewing geometries (e.g. high solar zenith angle associated with sampling polar regions during winter months).

There is growing interest in using existing and future satellite instruments to underpin the Paris Agreement. Since the 16/17 report three relevant satellites sensors have been launched: Feng Yun-3D GAS (https://www.wmo-sat.info/oscar/satellites/view/116) and GaoFen-5 GMI (https://www.wmo-sat.info/oscar/satellites/view/609) launched by China, the Tropomi (https://www.wmo-sat.info/oscar/instruments/view/586) instrument aboard the ESA Sentinel-5P. Current and future satellite sensors that measure $CH_4$ and $CO_2$ are now extensive, for example as shown in https://www.wmo-sat.info/oscar/gapanalyses?variable=23 and https://www.wmo-sat.info/oscar/gapanalyses?variable=39.

Two major reports have been published or in preparation since the 16/17 BEIS report. One was published in late 2017 by the $CO_2$ Task Force (Pinty et al., 2017) established by the European Commission (EC) to help design the $CO_2$ Copernicus service and one is in the final stages of writing (Crisp et al., 2018) commissioned by the Committee on Earth Observation Satellites (CEOS). These reports address how satellite data can help inform the quinquennial global stock takes that are a linchpin of the Paris Agreement, and define the key characteristics of a global architecture for monitoring atmospheric $CO_2$ and $CH_4$ concentrations and their natural and anthropogenic fluxes.

The EC $CO_2$ Task Force was established in Autumn 2016, in tandem with an ESA-led $CO_2$ Task Force, and concluded in Winter 2017. The EC Task Force was re-established in Spring 2018 and continues to refine the science requirements for the $CO_2$ service, and the ESA $CO_2$ Task Force has reconvened as a Mission Advisory Group, a first step towards designing the instrument requirements. The service will likely take the form of a small constellation of sun-synchronous satellites, complemented by an enhanced pan-European ground $CO_2$ network, which will launch ~2023. It is anticipated that a prototype service using existing satellites will be able to inform the 2023 global stock-take, and the purpose-built system will inform the subsequent global stock-take in 2028.

## 7.2 Preparation of existing satellite data

Both GOSAT and OCO-2 instrument performance is good with no major outages (e.g., Crisp et al., 2017; Eldering et al., 2017). Data processing continues with modifications associated with improved bias corrections. A series of papers were published recently that showcased OCO-2 with an emphasis on analysis of the 15/16 El Nino (Heymann et al., 2017; Chatterjee et al., 2017; Liu et al., 2017; Sun et al., 2017; Patra et al., 2017) but also on quantifying emission from power plants (Nassar et al, 2017) and over the greater Los Angeles area (Hedelius et al., 2017). A number of papers are currently in preparation characterizing OCO-2 $CO_2$ retrievals, validation of data, and multi-model comparison of regional $CO_2$ flux estimates.

The Chinese TanSAT, operated by China Meteorological Administration, was launched in December 2016. TanSat began collecting science observations in January 2017 and delivering radiometrically-calibrated data products in October 2017. Preliminary $CO_2$ column data have been shown at conferences and a brief paper (Yang et al., 2018), but at the time of writing have not been distributed.

Feng Yun 3D (FY-3D) was launched in November 2017 and is the fourth satellite in the FY-3 series of Chinese polar-orbiting meteorological satellites. FY-3D carries 10 atmospheric and space physics instruments including the Greenhouse gases Absorption Spectrometer (GAS), a high-resolution, double pendulum Fourier transform Interferometer, similar in concept to the GOSAT Fourier transform spectrometer. GAS measures spectral bands relevant to $CO_2$, $CH_4$, CO, and $N_2O$, but there are few details about the performance of this instrument in the published literature.

GaoFen-5 is the fifth member of the China High-Resolution Earth Observation System fleet of civilian remote sensing satellites flown by China National Space Administration. GaoFen-5 was launched in May 2018. GaoFen-5 carries a suite of six instruments, including the Greenhouse-gases Monitoring Instrument (GMI). GMI is a 4-channel spatial heterodyne spectrometer that measures spectral bands relevant to $CO_2$ and $CH_4$. At the time of writing, little additional information is available in the open literature.

GHGSat-D, a ~15 kg microsatellite was launched by a commercial company GHGSat on June 21, 2016 into a 520 km sun-synchronous orbit with a 9:30 local equator crossing time. Instrument complications have resulted in column $CH_4$ measurement uncertainties of order 10%, and column $CO_2$ measurement uncertainties of ~30%. With this performance, GHGSat-D would only be able to detect strong, isolated sources (e.g. Varon et al., 2018). GHGSat will launch two new microsatellites in 2019 and 2020 that address the lessons learned with GHGSat-D.

TROPOMI was launched on Sentinel-5P in October 2017. It uses a wide-field telescope from the Ozone Monitoring Instrument (OMI), which yields observations with a near-nadir resolution of 7 km by 7 km over a 2600-km wide swath, providing high spatial resolution, 2-dimensional images of CO and $CH_4$ columns with daily global coverage. TROPOMI is a precursor to the Sentinel 5 operational mission. Data products are becoming available, with $CH_4$ columns due to become publicly available in late 2018. Based on a statistical argument, the spatial resolution and daily coverage associated with these data will result in more cloud-free data and therefore a great potential for verifying emission inventories for smaller, cloudier geographical regions such as the UK.

## *7.3 Future mission concepts*

A range of concepts are in various stages of development. In the immediate future, GOSAT-2 and OCO-3 are due for launch in 2018 and 2019 respectively.

GOSAT-2 carries similar instruments to GOSAT but notably include an additional spectral band that is sensitive to CO and $CH_4$. The sensor technology and optical payload have been improved to deliver higher precision requirements.

OCO-3 incorporates the flight spare optical bench of OCO-2 and therefore it shares many of the physical characteristics of its predecessor. OCO-3 will be installed on the International Space Station that has a low inclination precessing orbit that will spend more time over the tropics. To reproduce the pointing capabilities of OCO-2, the ISS-mounted OCO-3 has been fitted with a bespoke pointing mechanism. This, together with modifications to the telescope, result in a footprint size similar to OCO-2 but with signal to noise values that are higher than OCO-2. Of relevance, the new pointing system allows a new opportunity to map large point sources such as cities, power plants, and coastlines.

Preparation for the $CO_2$ Copernicus system is ongoing, with the latest information described by Pinty et al., 2017 and Crisp et al., 2018.

There are also a number of smaller satellite concepts being developed. For example, the MeznSat is a 3U CubeSat being developed by the United Arab Emirates (Jallad et al., 2018) to

monitor $CO_2$, $CH_4$ and algal blooms. A CubeSat is comprised of 10x10x10 $cm^3$ units, each unit having a mass of < 1.33 kg.

## *7.4 Emission estimates using satellite observations of $CO_2$ and $CH_4$*

Aside from a few papers that have highlighted the ability of current sensors to observe $CO_2$ and $CH_4$ hotspots (Nassar et al., 2017, Sheng et al., 2018), there has been little progress in the open literature about using satellite observations to verify inventories of $CO_2$ and $CH_4$. However, there are many papers focused on the capabilities of future satellites to observe hotspots and trends (e.g. Cusworth et al., 2018, Turner et al., 2018).

The Horizon 2020 projects, CHE and VERIFY, focussed on quantifying European anthropogenic $CO_2$ emissions are ongoing:

- $CO_2$ Human Emissions (CHE) in response to call EO-3-2017 “Preparation for a European capacity to monitor $CO_2$ anthropogenic emissions”.

- An observation-based system for monitoring and verification of greenhouse gases (VERIFY) in response to call SC5-04-2017 “Towards a robust and comprehensive greenhouse gas verification system”.

# 8 Results and analysis of additional gases

## 8.1 Introduction

This section discusses the atmospheric trends and regional emissions of the other gases that are measured at Mace Head. The table below describes, if applicable, the principle uses of each of the gases, their radiative efficiency, atmospheric lifetime, global warming potential in a 100-year framework ($GWP_{100}$) and ozone depleting potential (ODP). In the following sections each of these gases are presented.

| Gas | Primary use | Radiative Efficiency (W $m^{-2}$ $ppb^{-1}$) | Atmospheric Lifetime (years) | $GWP_{100}$ | ODP |
|---|---|---|---|---|---|
| CFC-11 | Widespread | 0.26 | 45 | 4,660 | 1 |
| CFC-12 | Refrigerant | 0.32 | 100 | 10,200 | 0.82 |
| CFC-113 | Coolant, electronics | 0.30 | 85 | 5,820 | 0.85 |
| CFC-115 | Refrigerant | 0.20 | 1,020 | 7,670 | 0.57 |
| HCFC-124 | Refrigerant, fire suppression | 0.20 | 5.9 | 527 | 0.02 |
| HCFC-141b | Foam blowing | 0.16 | 9.2 | 782 | 0.12 |
| HCFC-142b | Chem. synthesis/foam blowing | 0.19 | 17.2 | 1,980 | 0.06 |
| HCFC-22 | Propellant, air conditioning | 0.21 | 11.9 | 1,760 | 0.04 |
| HFC-236fa | Fire extinguisher | 0.24 | 242 | 8060 | |
| HFC-245fa | Foam blowing | 0.24 | 7.7 | 858 | |
| $SO_2F_2$ | Fumigant | 0.2 | 36 | 4090 | |
| $CH_3Cl$ | Natural, refrigerant | 0.01 | 1 | 12 | 0.02 |
| $CH_2Cl_2$ | Foam plastic, solvent, natural | | 144 days | | |
| $CHCl_3$ | Bi-product, natural | | 149 days | | |
| $CCl_4$ | Fire suppression, precursor | 0.17 | 26 | 1,730 | 0.82 |
| $CH_3CCl_3$ | Solvent | 0.07 | 5.0 | 160 | 0.16 |
| $CHClCCl_2$ | Degreasing solvent | | 5 days | 5 | |
| $CCl_2CCl_2$ | Solvent, dry cleaning | | 90 days | 15 | |
| $CH_3Br$ | Natural (seaweed), fumigant | | 0.8 | | |
| $CH_2Br_2$ | Natural (seaweed) | | 123 days | | |
| $CHBr_3$ | Fumigant, natural (seaweed) | | 24 days | | 0.66 |
| $CBrClF_2$ | Fire suppression (military) | 0.29 | 16 | 1,750 | 7.9 |
| $CBrF_3$ | Fire suppression | 0.30 | 65 | 6,290 | 15.9 |
| $C_2Br_2F_4$ | Fire suppression | 0.31 | 20 | 1,470 | 13.0 |
| $CH_3I$ | Natural (seaweed) | | 7 days | | |
| $C_2H_6$ | Combustion, gas leakage | | | | |
| CO | Combustion | | 30-90 days | | |
| $O_3$ | Reactions in atmosphere | | | | |
| $H_2$ | Combustion, photolysis | | | | |

**Table 30: The principle uses of the gases observed at Mace Head, their radiative efficiency, atmospheric lifetime, global warming potential in a 100-year framework ($GWP_{100}$) and ozone depleting potential (ODP). The gases listed in red are specifically covered by the Montreal Protocol. All of the gases with a GWP are GHGs but not all GHGs are covered by the Kyoto Protocol.**

## 8.2 CFC-11

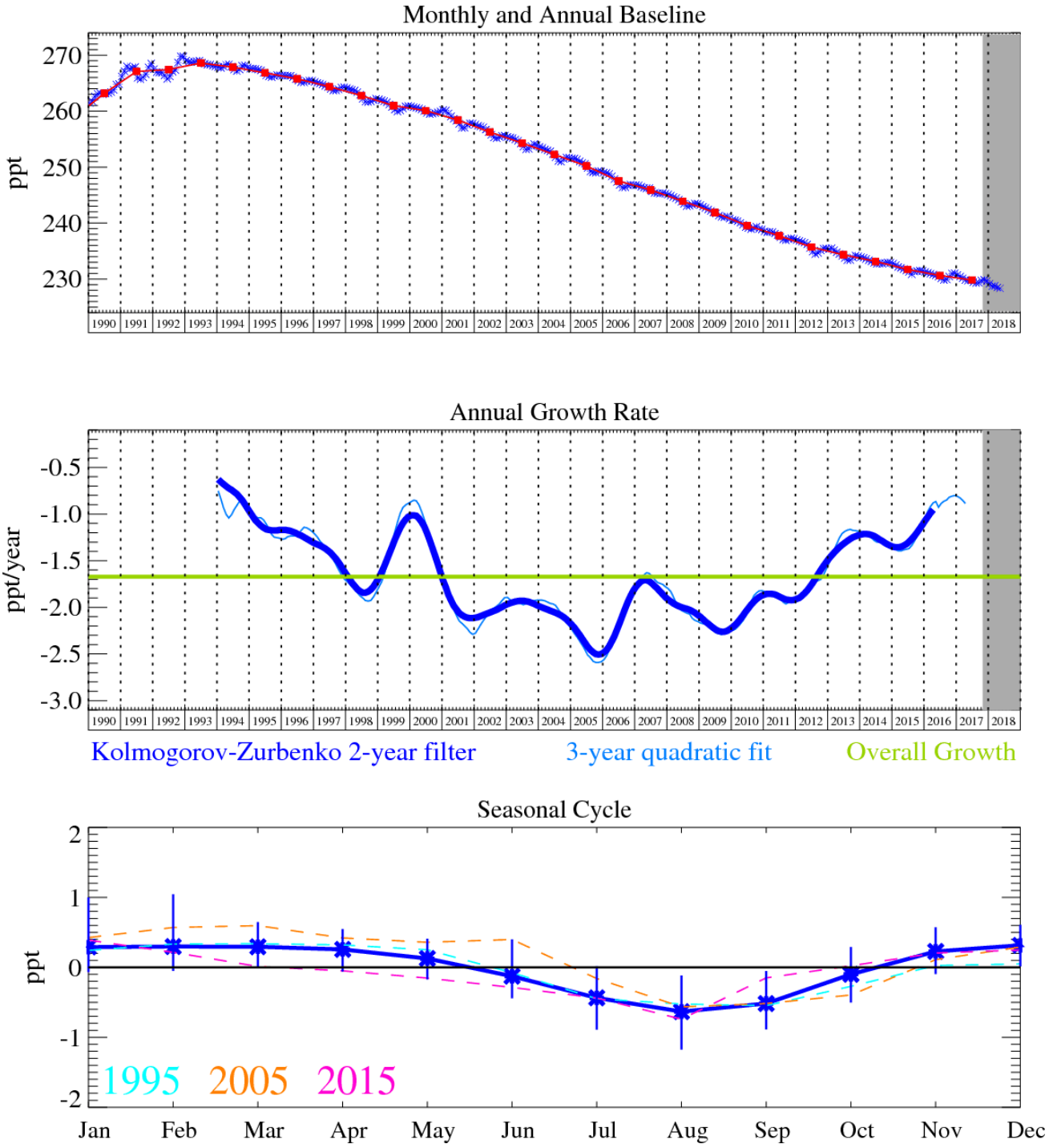


**Figure 92: CFC-11 ($CCl_3F$): Monthly (blue) and annual (red) baseline (top plot). Annual (blue) and overall average growth rate (green) (middle plot). Seasonal cycle (de-trended) with year-to-year variability (lower plot). The grey area covers un-ratified and therefore provisional data.**

The NH baseline mole fraction of CFC-11 has fallen since the introduction of the Montreal Protocol in the early 1990s. However, in recent years the rate of decline of CFC-11 in the atmosphere has slowed considerably. A recent paper by Montzka et al. (2018) has linked this slow down to renewed emissions from East Asia.

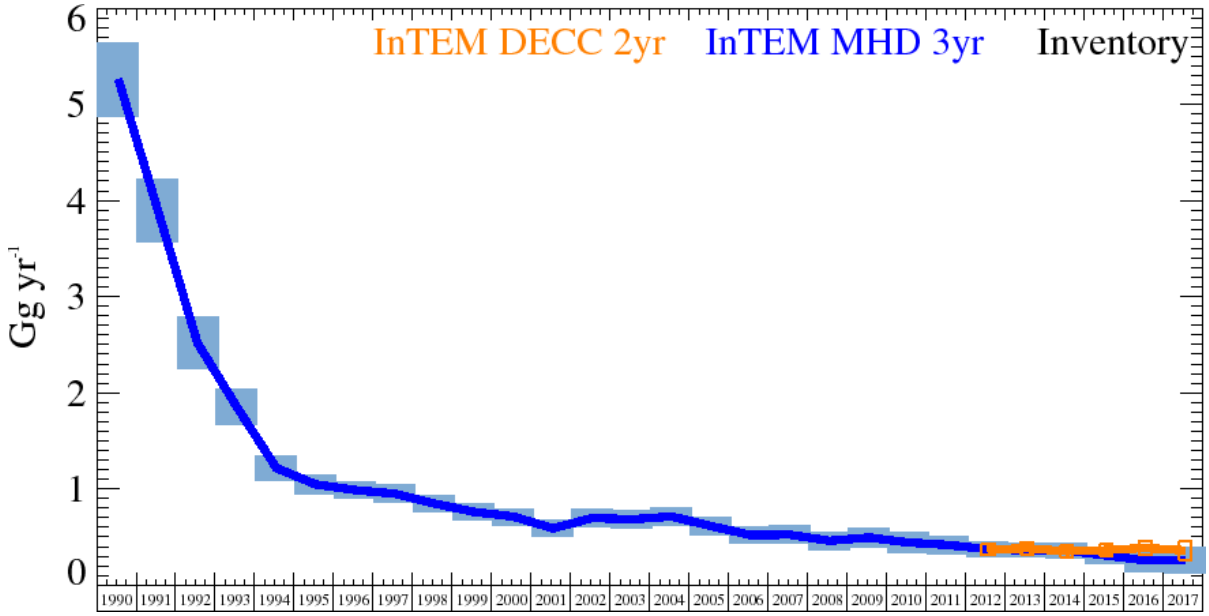


**Figure 93: CFC-11 UK Emission estimates (Gg yr$^{-1}$) from InTEM with global meteorology: 3-year MHD (blue) and 2-year DECC network (orange). Uncertainty bars = 1 std.**

The UK emissions of CFC-11 fell sharply between 1990 and 1994 from more than 5 Gg yr$^{-1}$ to 1 Gg yr$^{-1}$. Since then the decline has been much slower as the banked emissions are slowly depleted and are currently estimated to be ~0.4 Gg yr$^{-1}$. The current emissions across NW Europe are from populated areas re-enforcing the current understanding that the emissions are from old appliances (Figure 96).

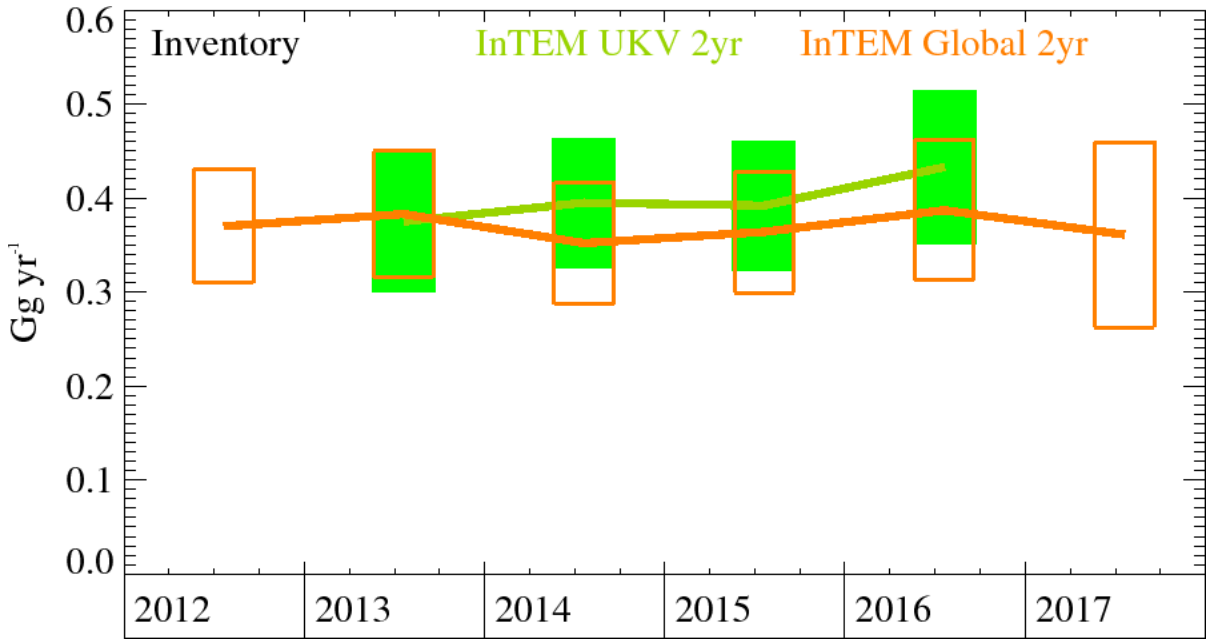


**Figure 94: CFC-11 emission estimates for the UK (Gg yr$^{-1}$) from InTEM using the DECC observations, 2-year inversions with different meteorology: (orange) global meteorology and (green) 1.5 km high resolution meteorology. The uncertainty bars represent 1 std.**

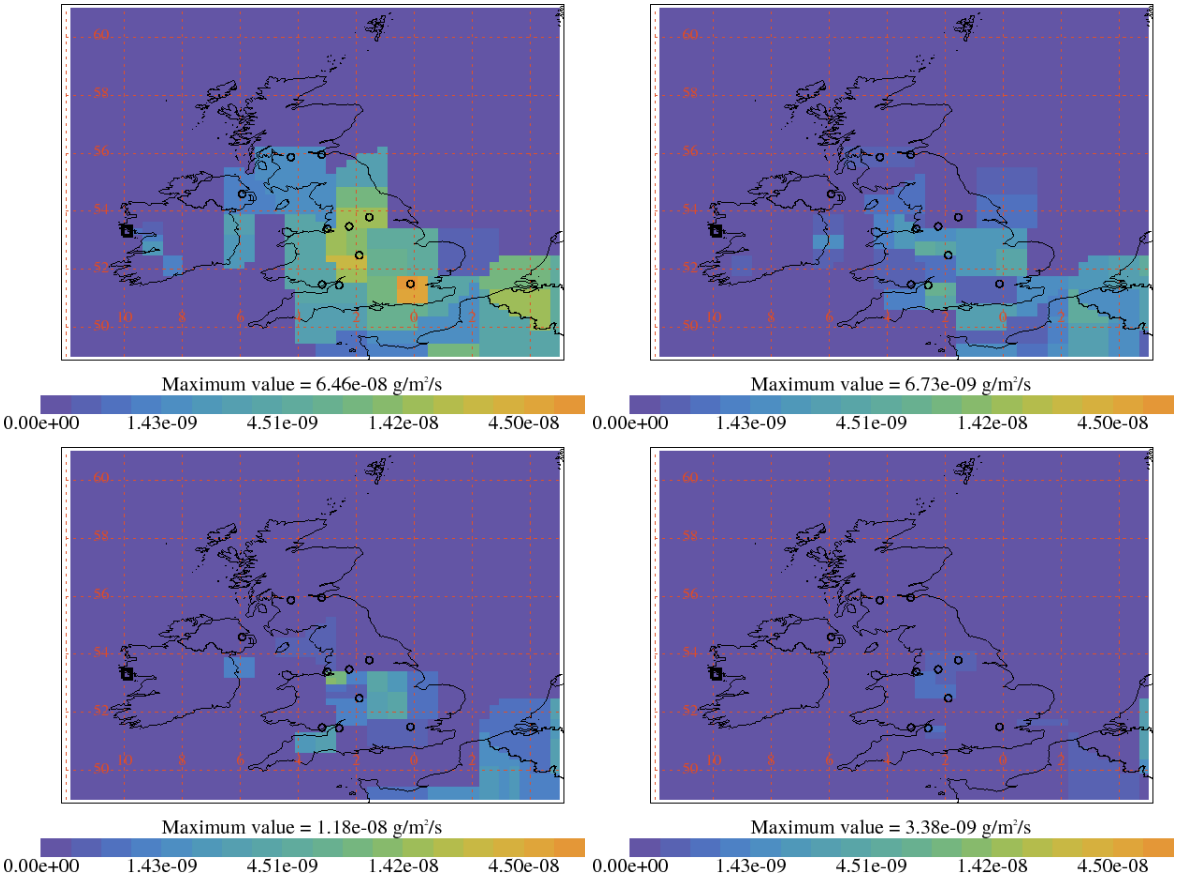


**Figure 95: InTEM estimates for 1989-1992 (top LHS), 1994-1997 (top RHS), 2004-2007(lower LHS), 2014-2017 (lower RHS) of spatial distributions of CFC-11 emissions using global meteorology and MHD observations with minimal prior information. Black squares are measurement stations and circles are major cities in UK.**

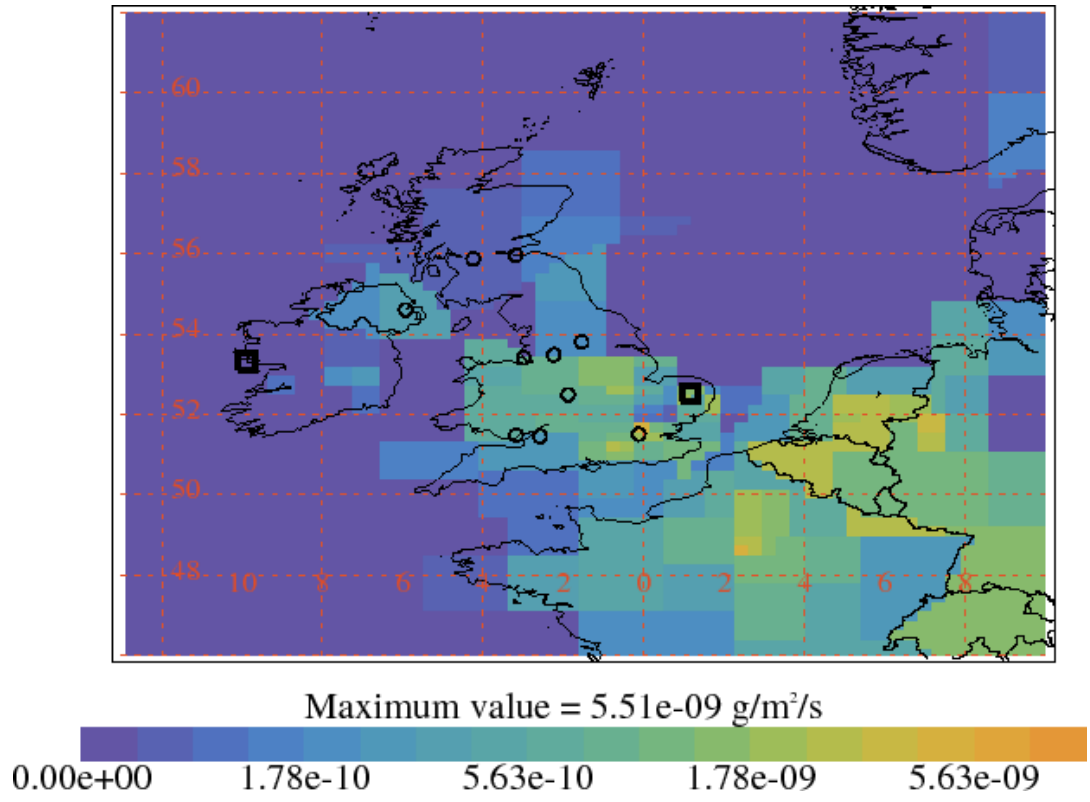


**Figure 96: Average InTEM estimate 2014-2017 using UKV high resolution meteorology of spatial distribution of CFC-11 emissions using DECC observations with minimal prior information. Black squares are measurement stations and circles are major cities in UK. Note, the scale in this figure is an order of magnitude smaller than in Figure 95 and the geographical extent is larger.**

## 8.3 CFC-12

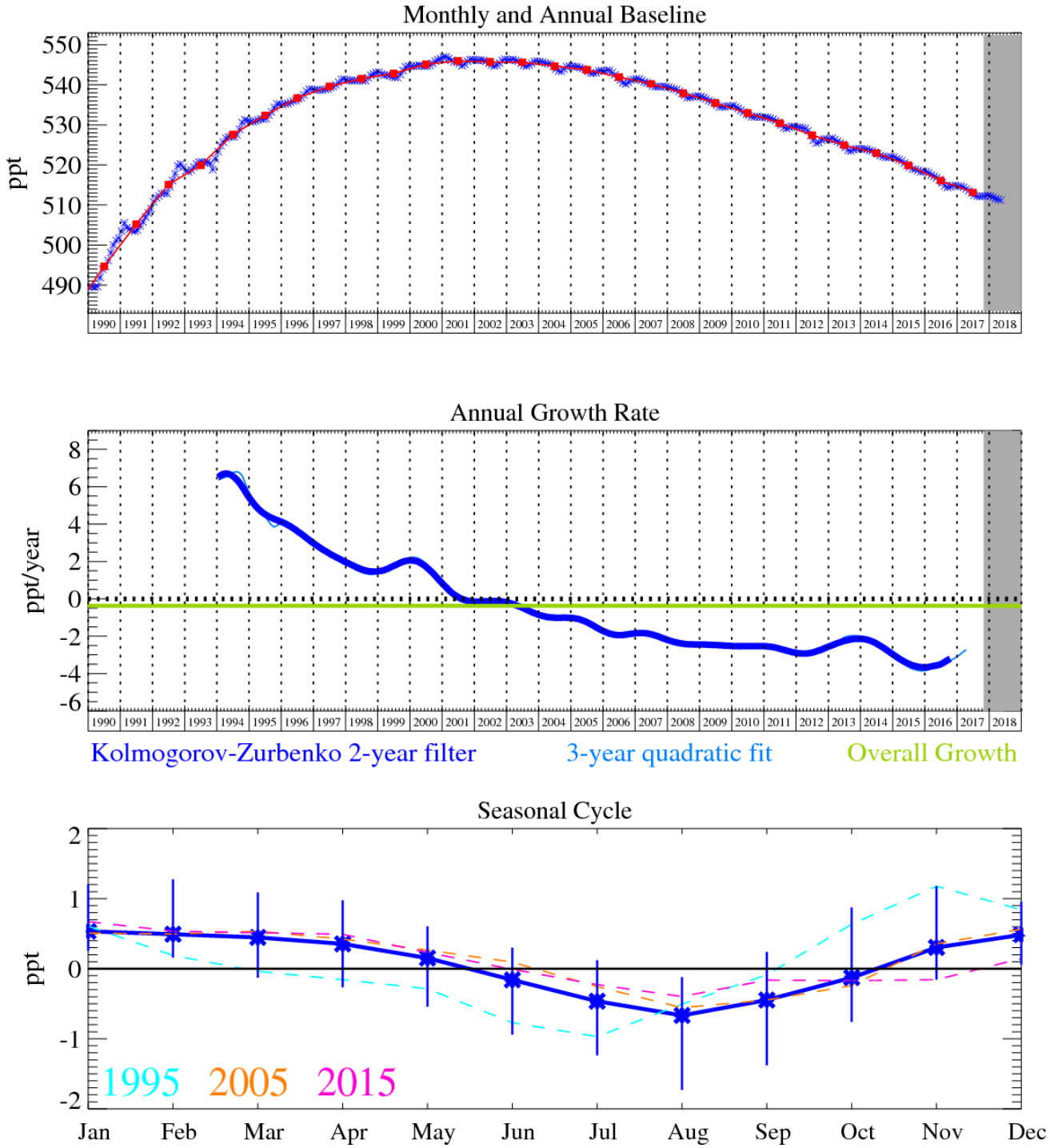


**Figure 97: CFC-12 ($CCl_2F_2$): Monthly (blue) and annual (red) baseline (top plot). Annual (blue) and overall average growth rate (green) (middle plot). Seasonal cycle (de-trended) with year-to-year variability (lower plot). The grey area covers un-ratified and therefore provisional data.**

## 8.4 CFC-113

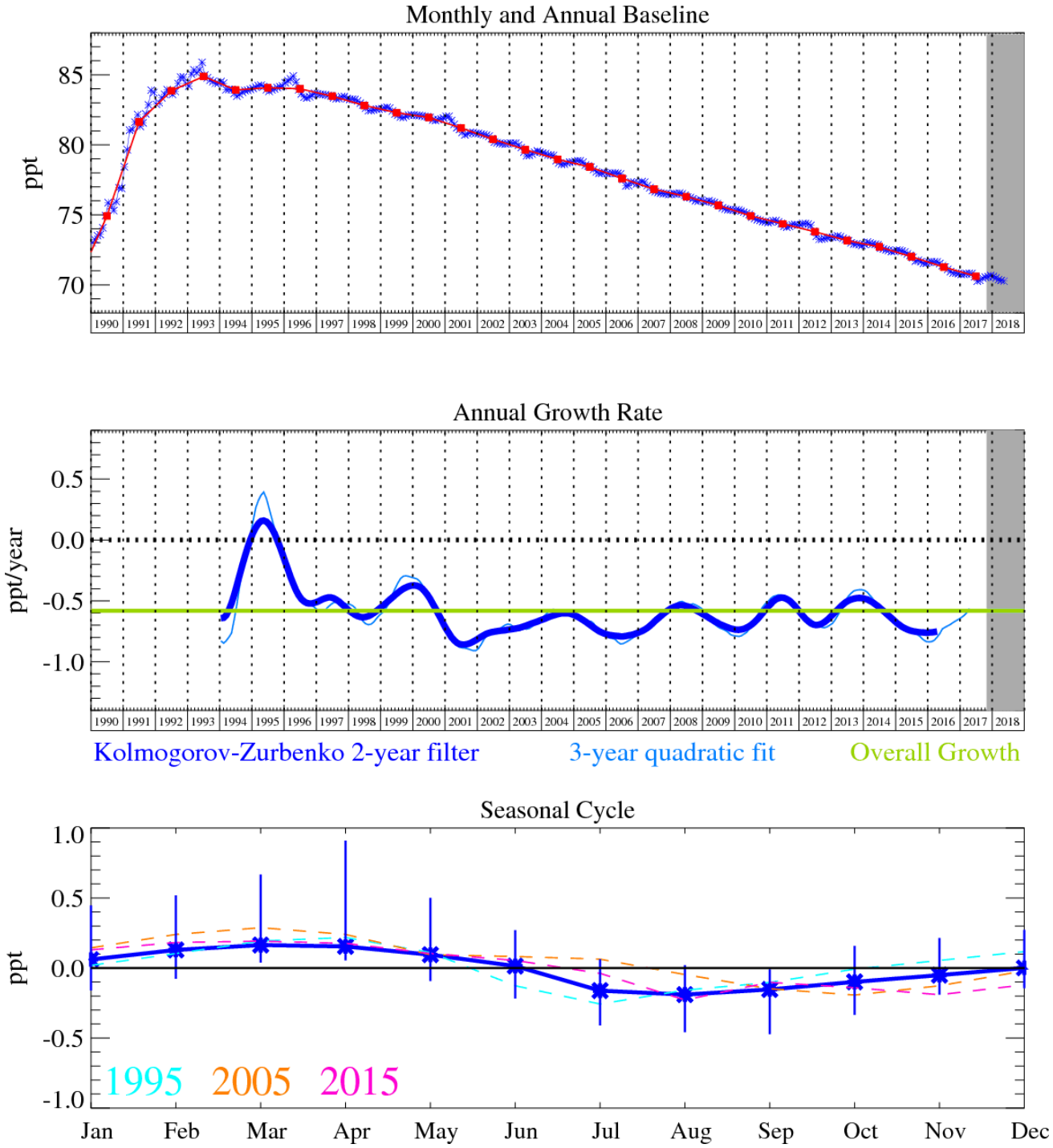


**Figure 98: CFC-113 ($C_2Cl_3F_3$): Monthly (blue) and annual (red) baseline (top plot). Annual (blue) and overall average growth rate (green) (middle plot). Seasonal cycle (de-trended) with year-to-year variability (lower plot). The grey area covers un-ratified and therefore provisional data.**

## 8.5 HCFC-124

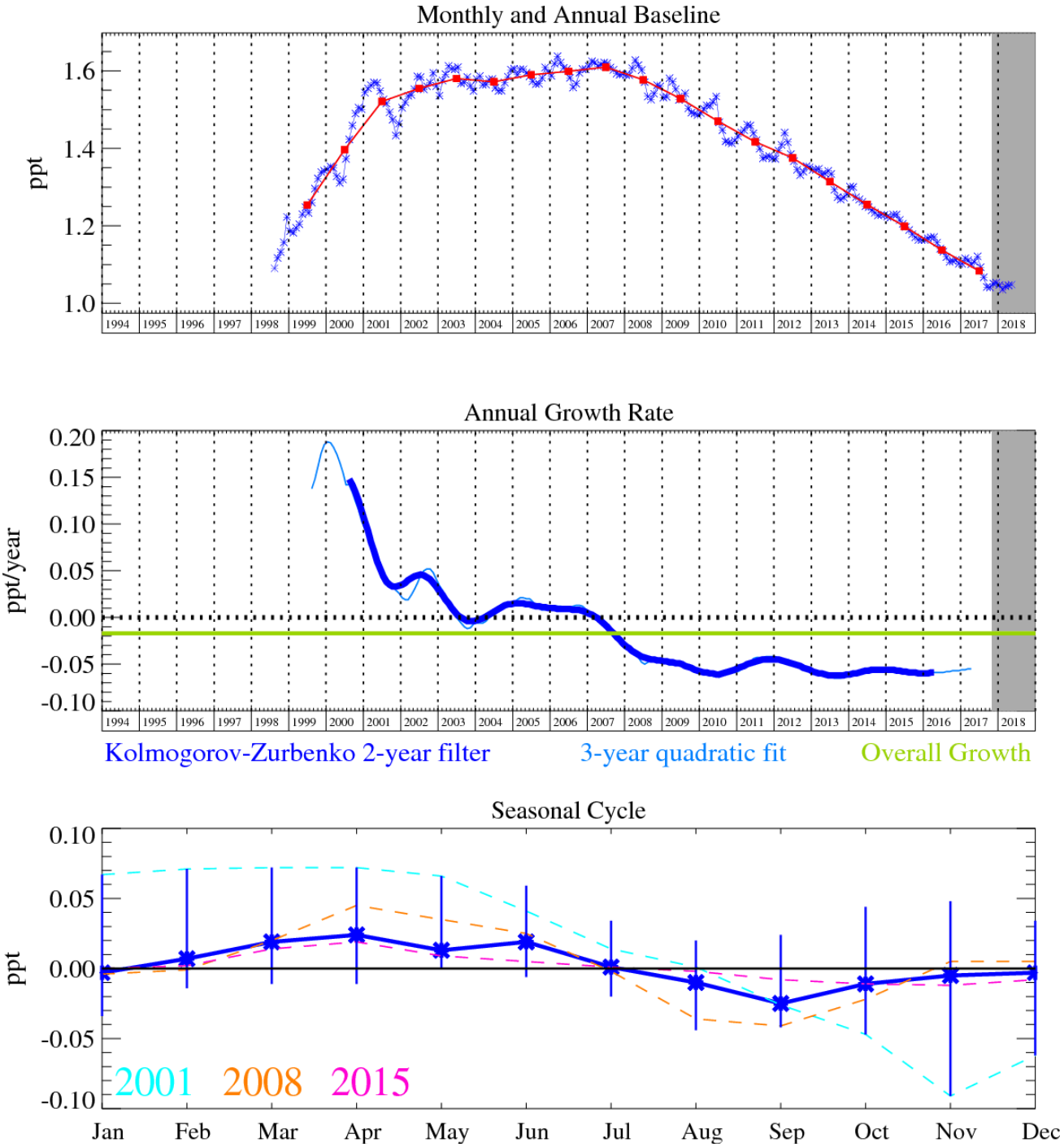


**Figure 99: HCFC-124 ($C_2HClF_4$): Monthly (blue) and annual (red) baseline (top plot). Annual (blue) and overall average growth rate (green) (middle plot). Seasonal cycle (de-trended) with year-to-year variability (lower plot). The grey area covers un-ratified and therefore provisional data.**

## 8.6 HCFC-141b

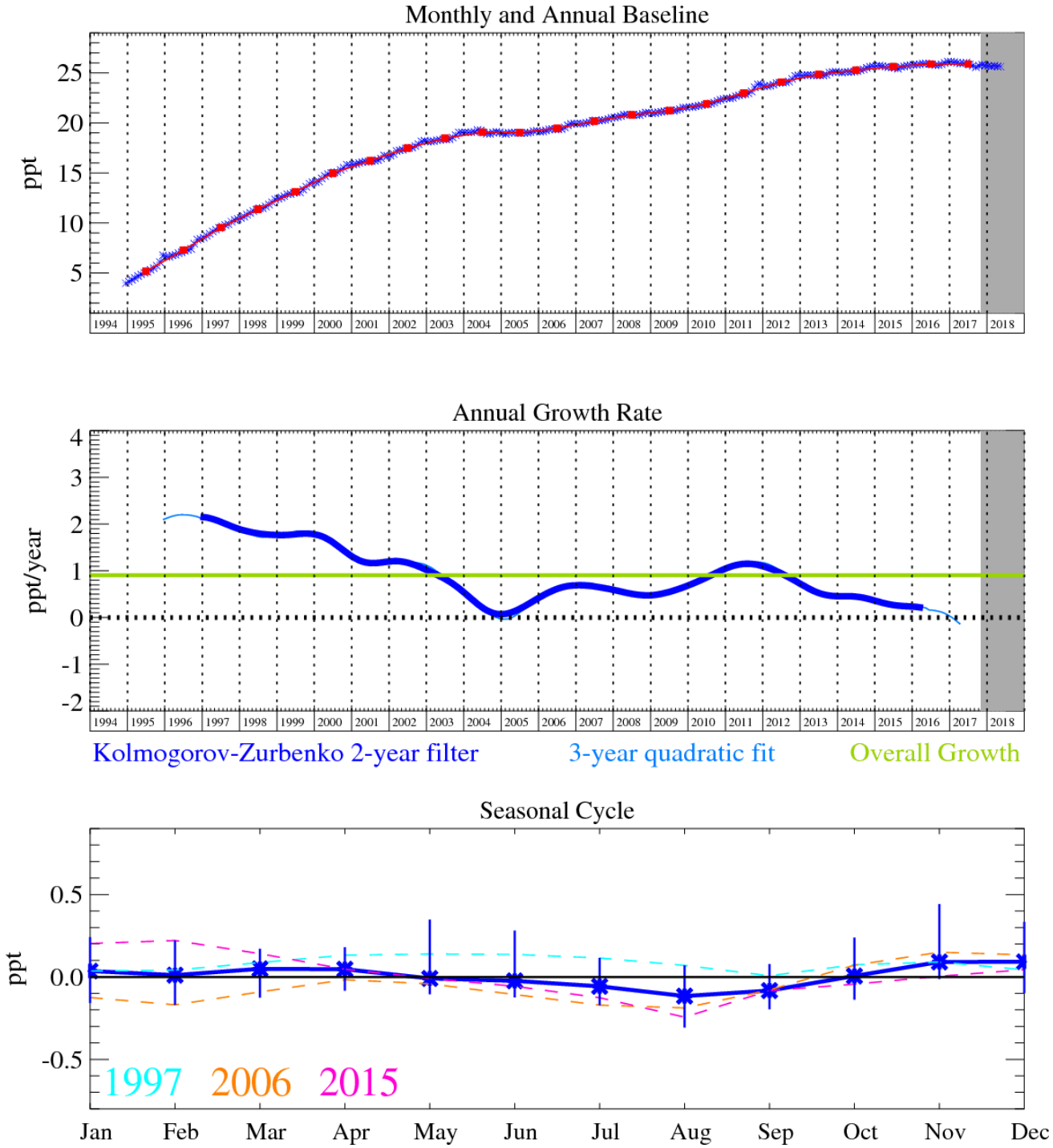


**Figure 100: HCFC-141b ($C_2H_3Cl_2F$): Monthly (blue) and annual (red) baseline (top). Annual (blue) and overall average growth rate (green) (middle plot). Seasonal cycle (de-trended) with year-to-year variability (lower plot). The grey area covers un-ratified and therefore provisional data.**

## 8.7 HCFC-142b

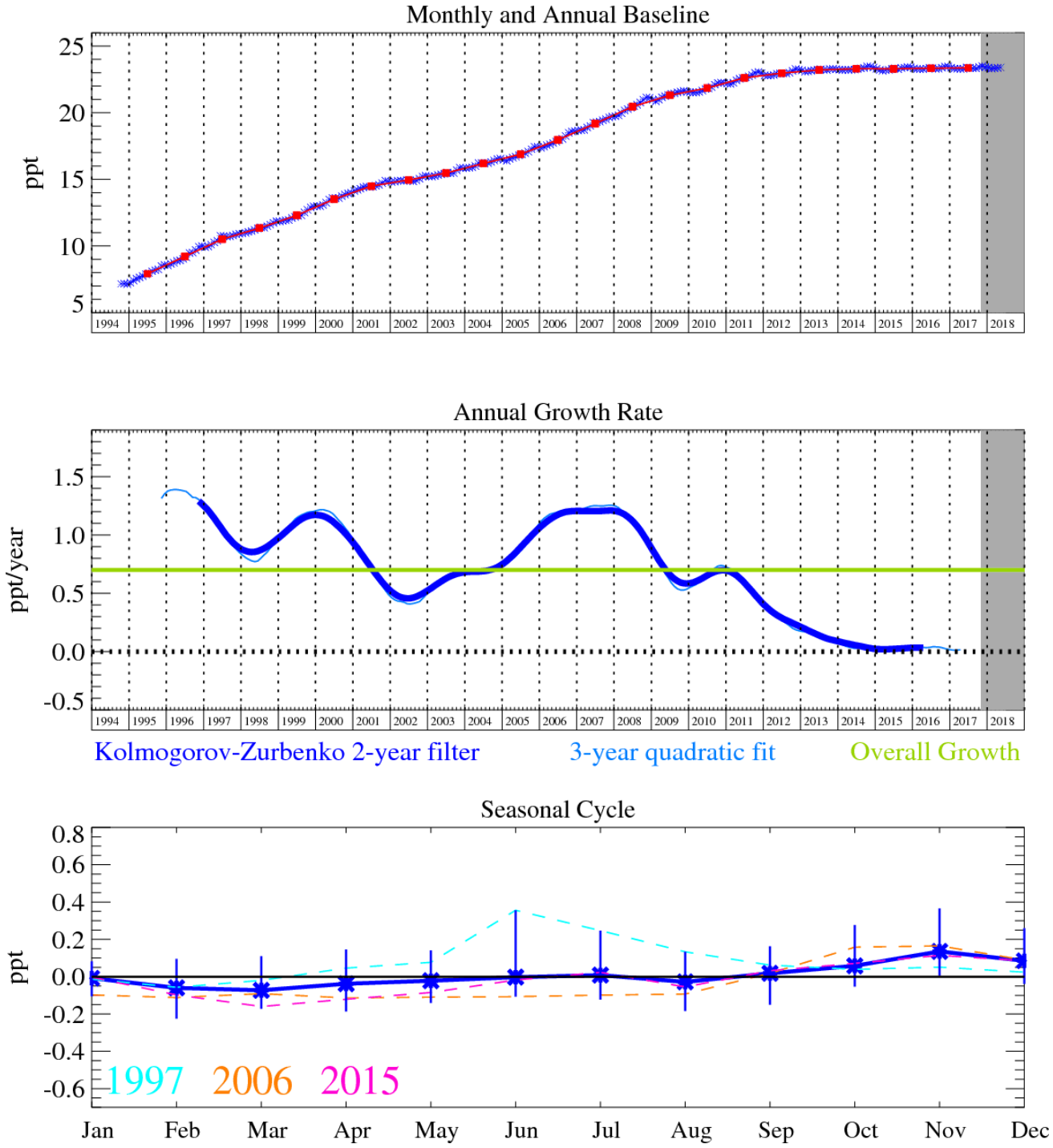


**Figure 101: HCFC-142b ($C_2H_3ClF_2$): Monthly (blue) and annual (red) baseline (top). Annual (blue) and overall average growth rate (green) (middle plot). Seasonal cycle (de-trended) with year-to-year variability (lower plot). The grey area covers un-ratified and therefore provisional data.**

## 8.8 HCFC-22

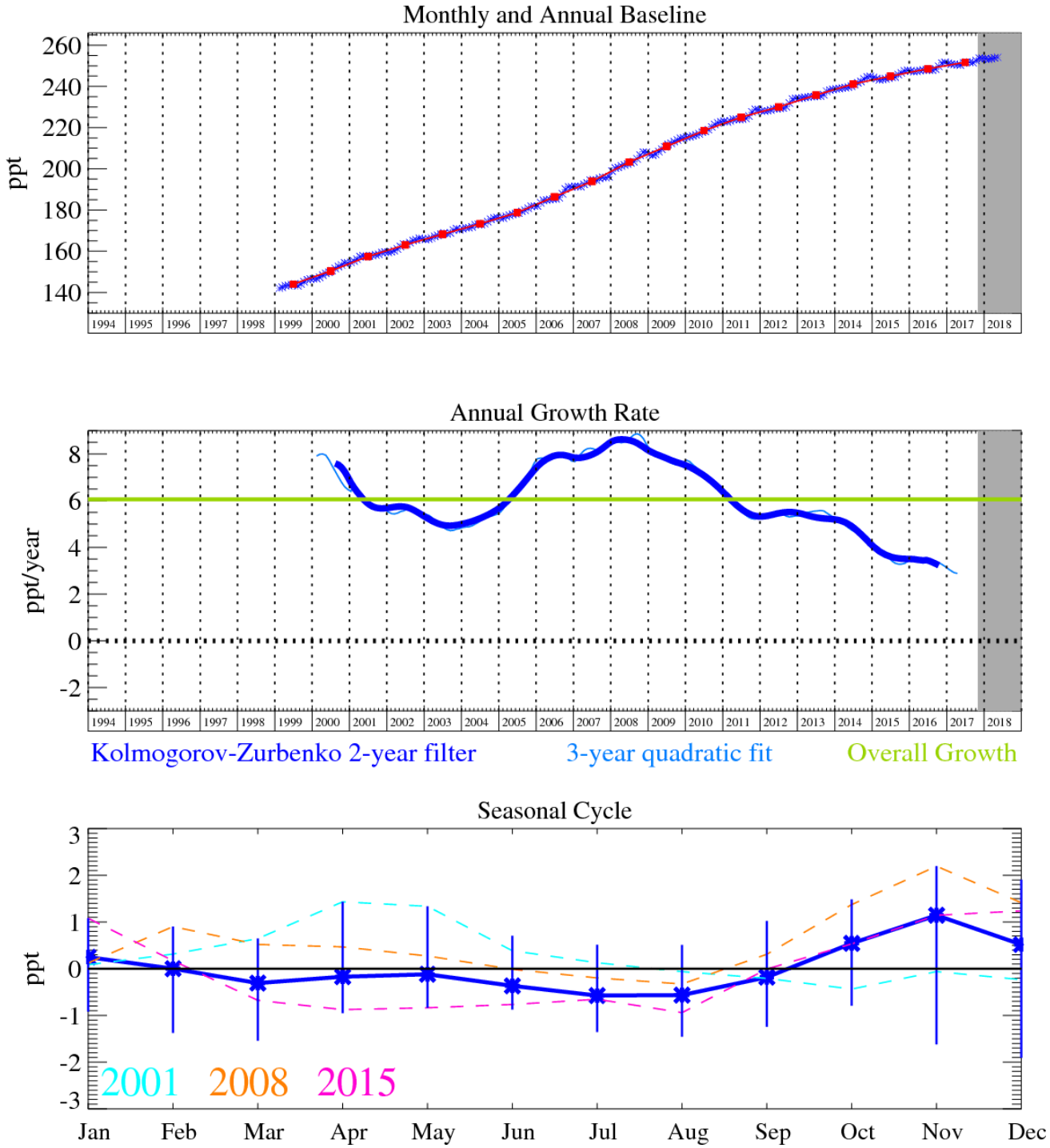


**Figure 102: HCFC-22 ($CHClF_2$): Monthly (blue) and annual (red) baseline (top plot). Annual (blue) and overall average growth rate (green) (middle plot). Seasonal cycle (de-trended) with year-to-year variability (lower plot). Grey area covers un-ratified and therefore provisional data.**

## 8.9 HFC-236fa

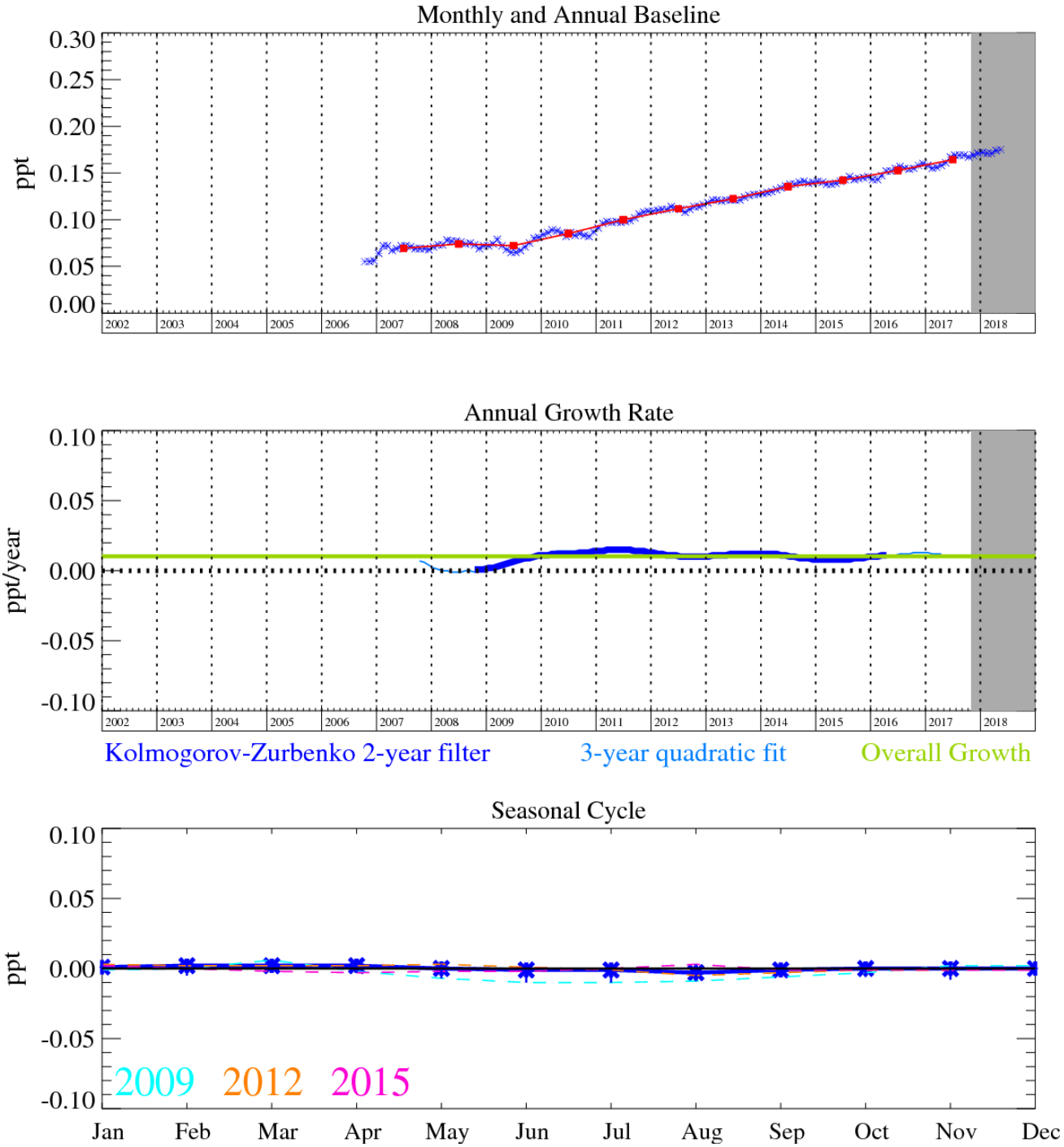


**Figure 103: HFC-236fa ($C_3H_2F_6$): Monthly (blue) and annual (red) baseline (top plot). Annual (blue) and overall average growth rate (green) (middle plot). Seasonal cycle (de-trended) with year-to-year variability (lower plot). Grey area covers un-ratified and therefore provisional data.**

## 8.10 $SO_2F_2$

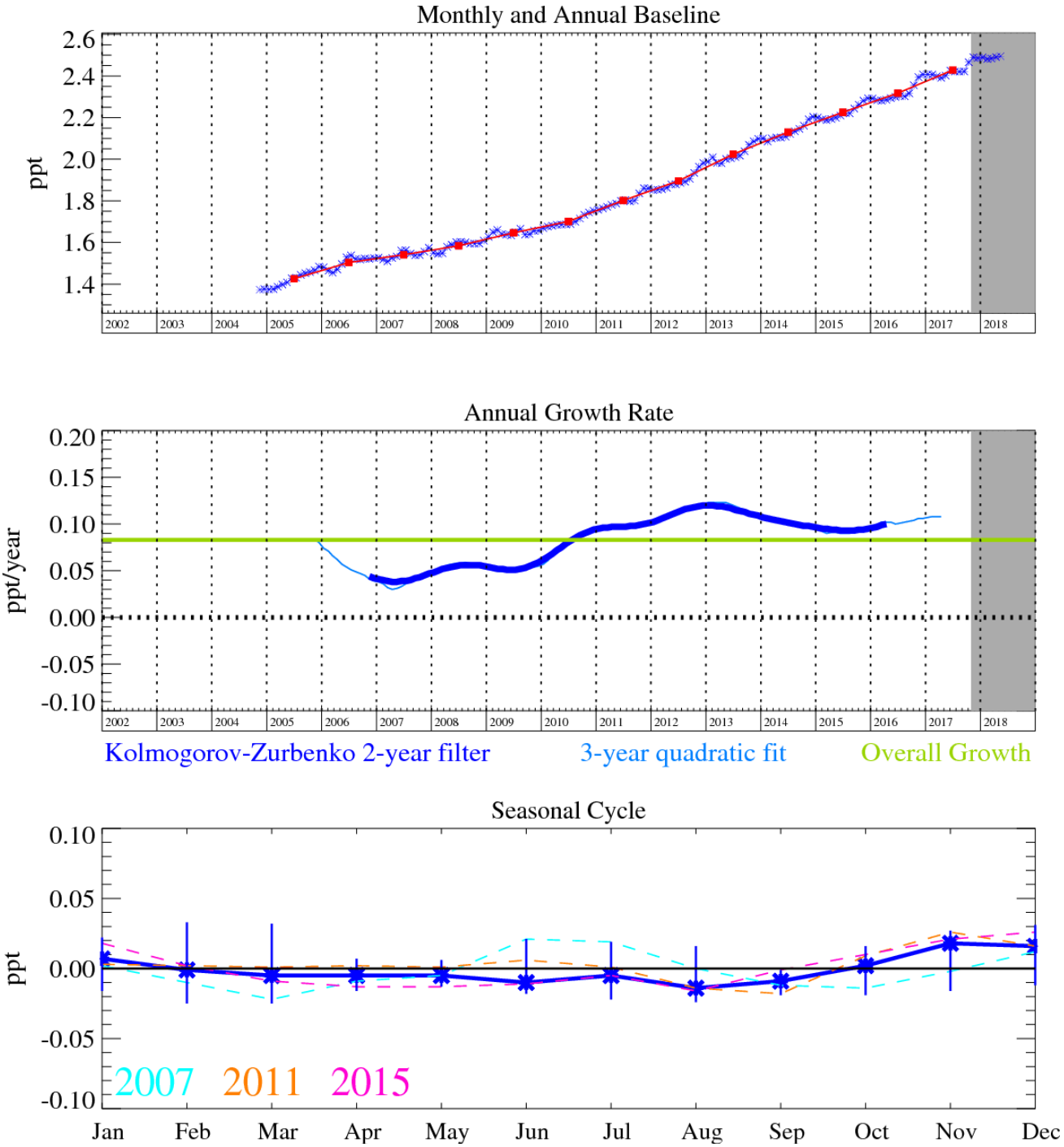


**Figure 104: $SO_2F_2$: Monthly (blue) and annual (red) Northern Hemisphere baseline mole fractions (top plot). Annual (blue) and overall average growth rate (green) (middle plot). Seasonal cycle (de-trended) with year-to-year variability (lower plot). Grey area covers un-ratified and therefore provisional data.**

## 8.11 $CH_3Cl$

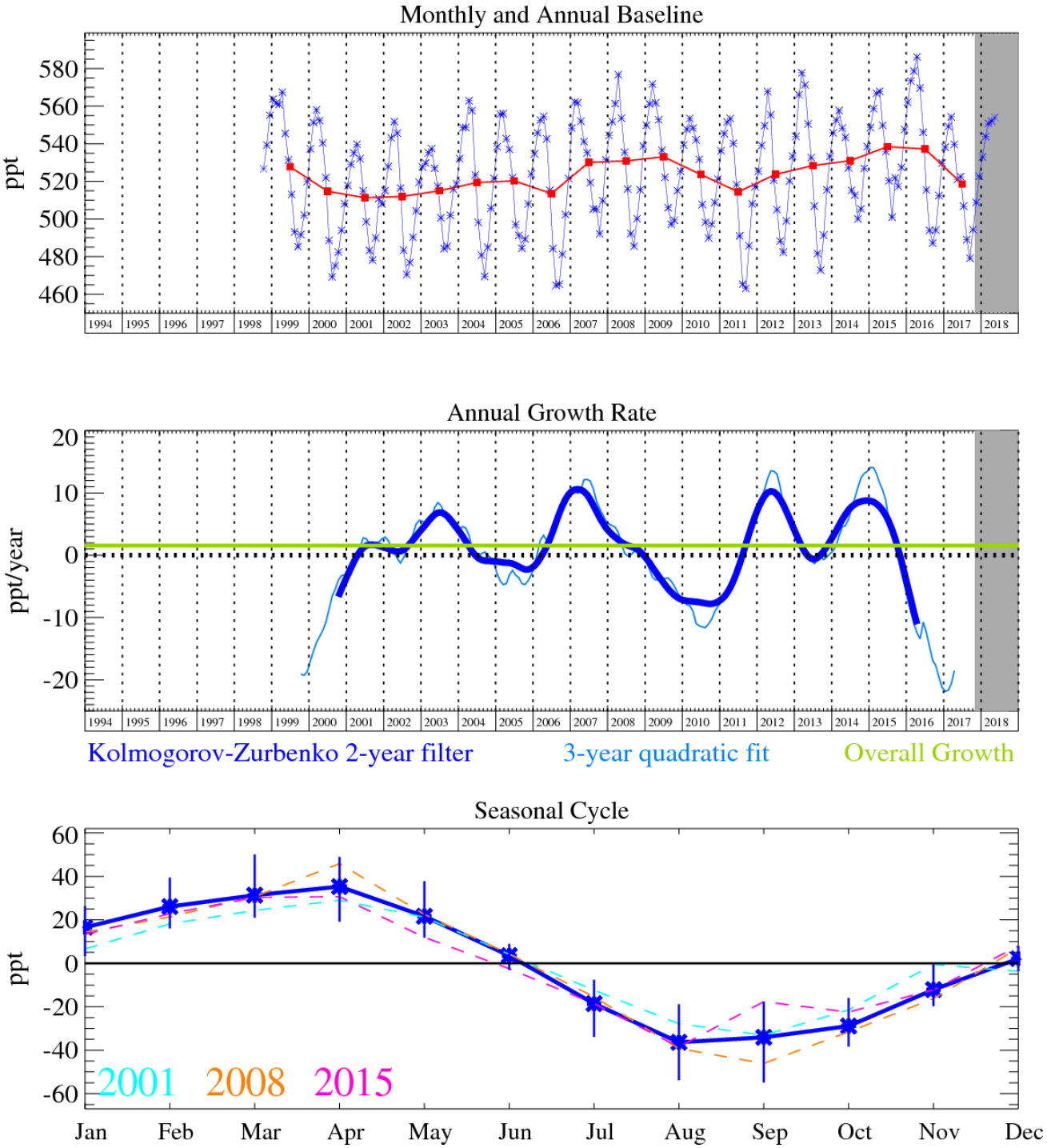


**Figure 105: $CH_3Cl$: Monthly (blue) and annual (red) Northern Hemisphere baseline mole fractions (top plot). Annual (blue) and overall growth rate (green) (middle). Seasonal cycle (de-trended) with year-to-year variability (lower plot). Grey area covers un-ratified and therefore provisional data.**

## 8.12 $CH_2Cl_2$

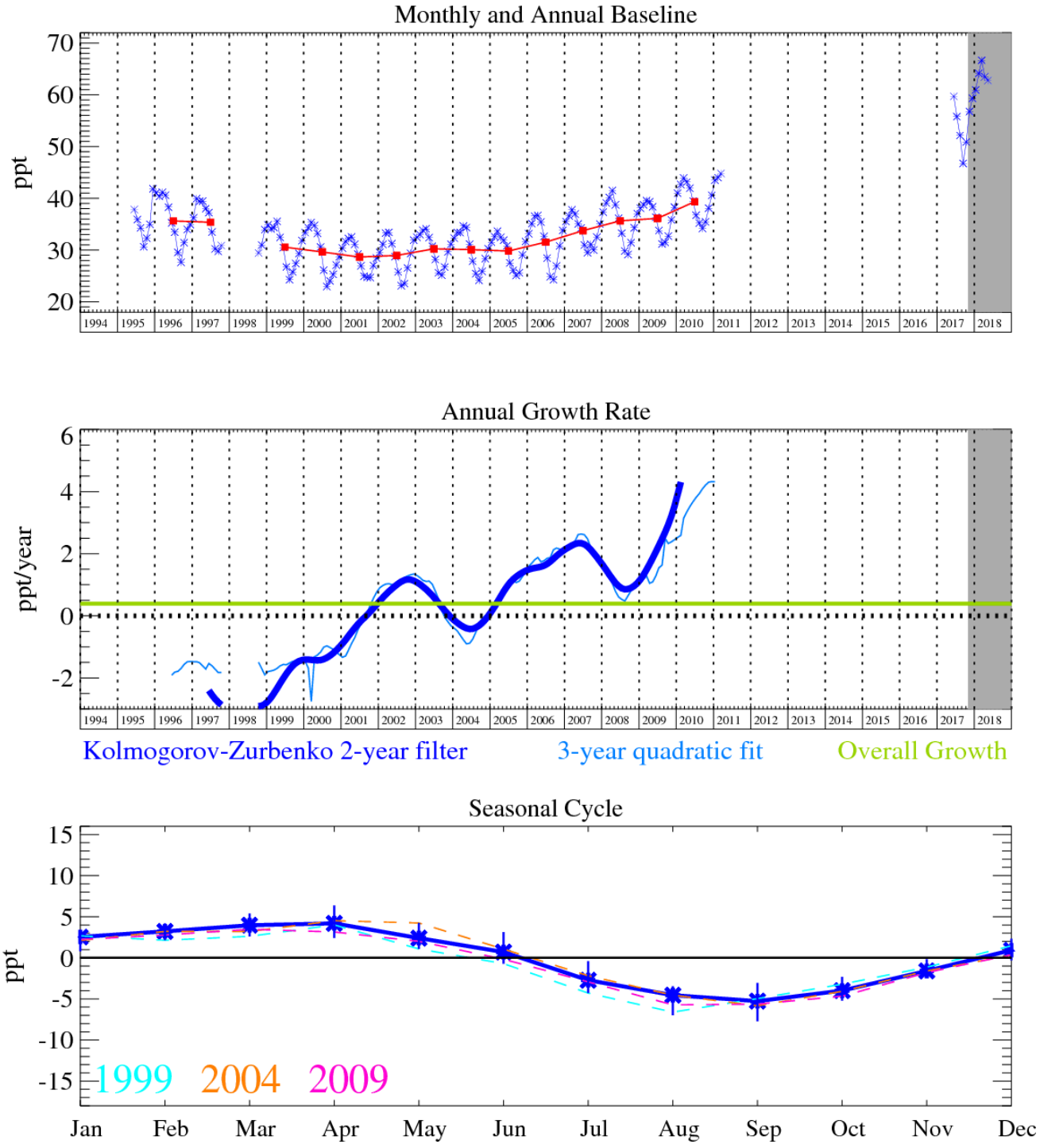


**Figure 106: $CH_2Cl_2$: Monthly (blue) and annual (red) Northern Hemisphere baseline mole fractions (top plot). Annual (blue) and overall average growth rate (green) (middle plot). Seasonal cycle (de-trended) with year-to-year variability (lower plot). Grey area covers un-ratified and therefore provisional data.**

There are significant gaps in the Mace Head observation record, principally 2011-2017. This gas can co-elute with CFC-11 due to GC column aging and was analysed using identical mass-to-charge ratios for fragmentation ions. This made isolation of the peaks in the chromatography very difficult; where co-elution happens the data have had to be removed. Other, less abundant, ions are now routinely analysed to ensure interference by CFC-11 co-elution will not happen in the future.

## 8.13 $CHCl_3$ (chloroform)

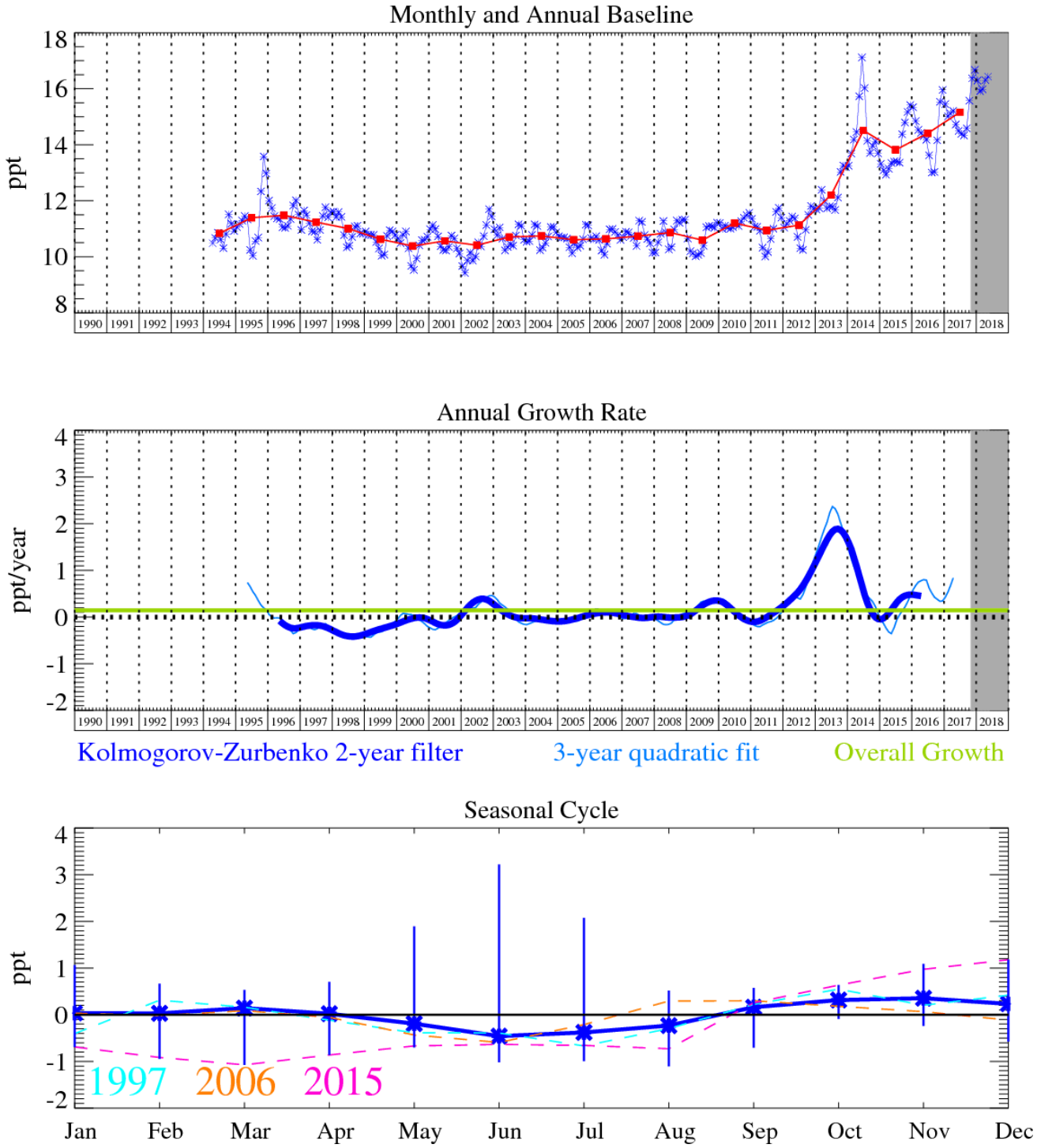


**Figure 107: $CHCl_3$: Monthly (blue) and annual (red) Northern Hemisphere baseline mole fractions (top plot). Annual (blue) and overall average growth rate (green) (middle plot). Seasonal cycle (de-trended) with year-to-year variability (lower plot). Grey area covers un-ratified and therefore provisional data.**

## 8.14 $CCl_4$ (carbon tetrachloride)

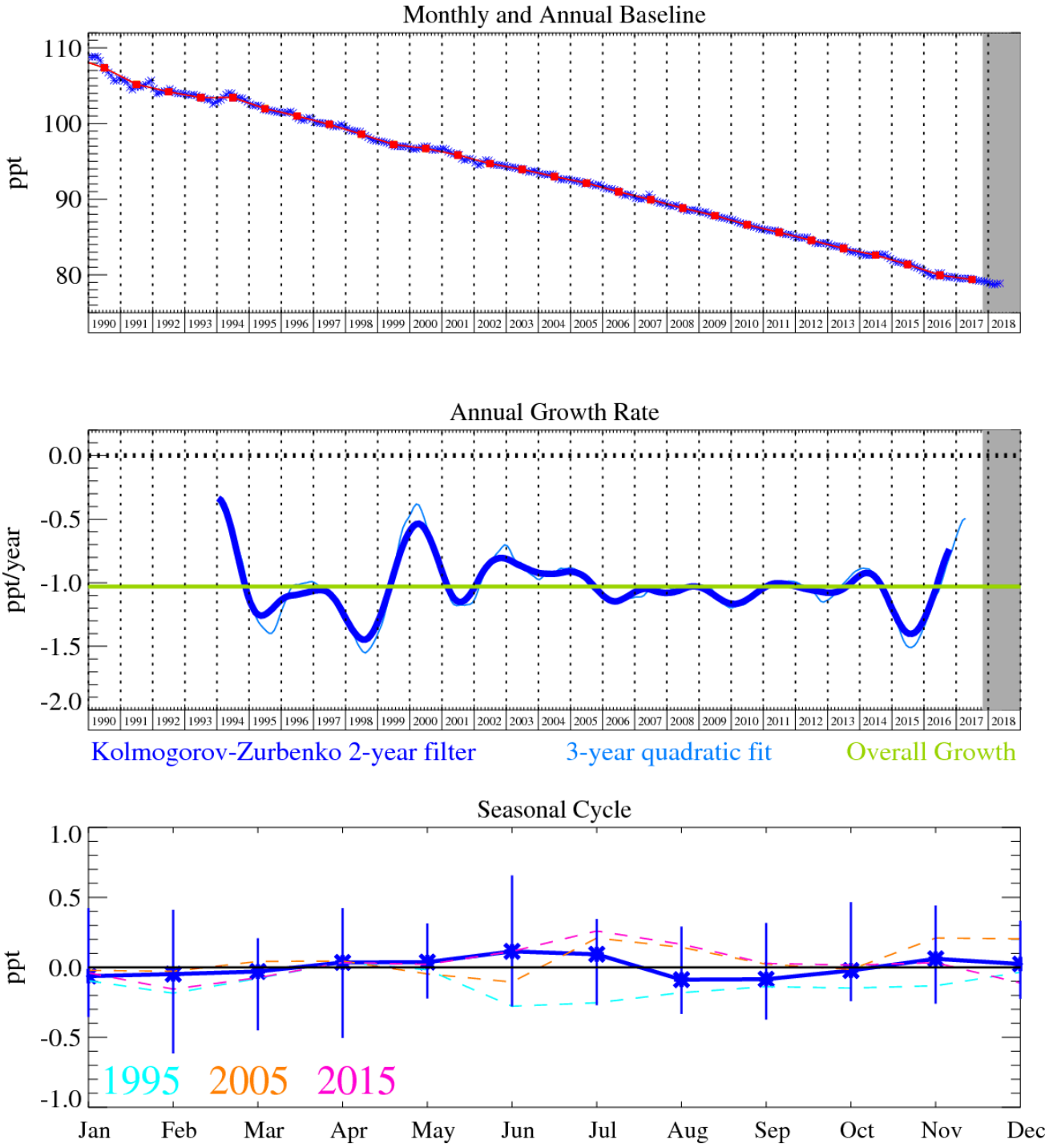


**Figure 108: $CCl_4$: Monthly (blue) and annual (red) Northern Hemisphere baseline mole fractions (top plot). Annual (blue) and overall average growth rate (green) (middle plot). Seasonal cycle (de-trended) with year-to-year variability (lower plot). Grey area covers un-ratified and therefore provisional data.**

## 8.15 $CH_3CCl_3$ (methyl chloroform)

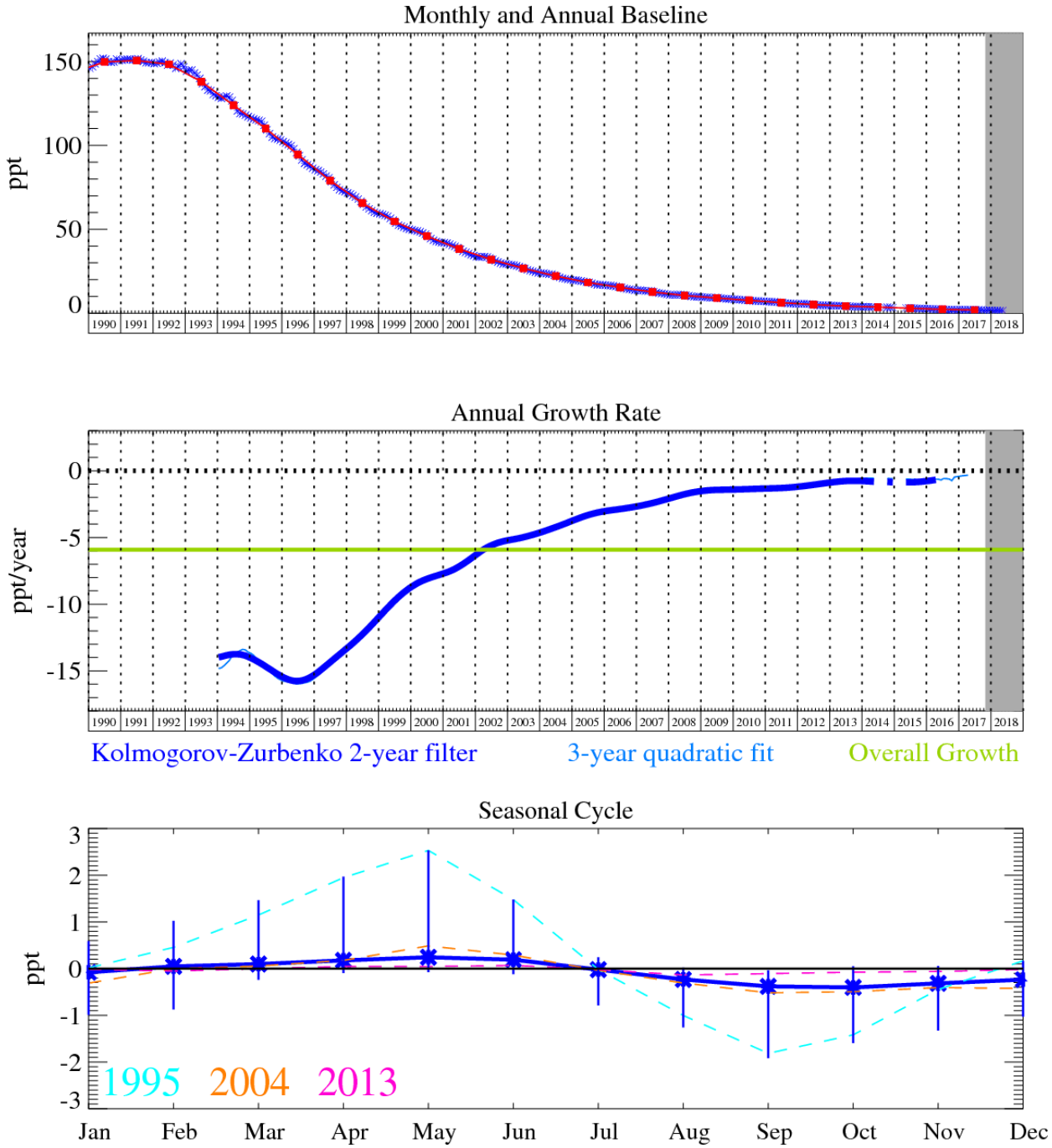


**Figure 109: $CH_3CCl_3$: Monthly (blue) and annual (red) Northern Hemisphere baseline mole fractions (top plot). Annual (blue) and overall average growth rate (green) (middle plot). Seasonal cycle (de-trended) with year-to-year variability (lower plot). Grey area covers un-ratified and therefore provisional data.**

## 8.16 $CCl_2CCl_2$

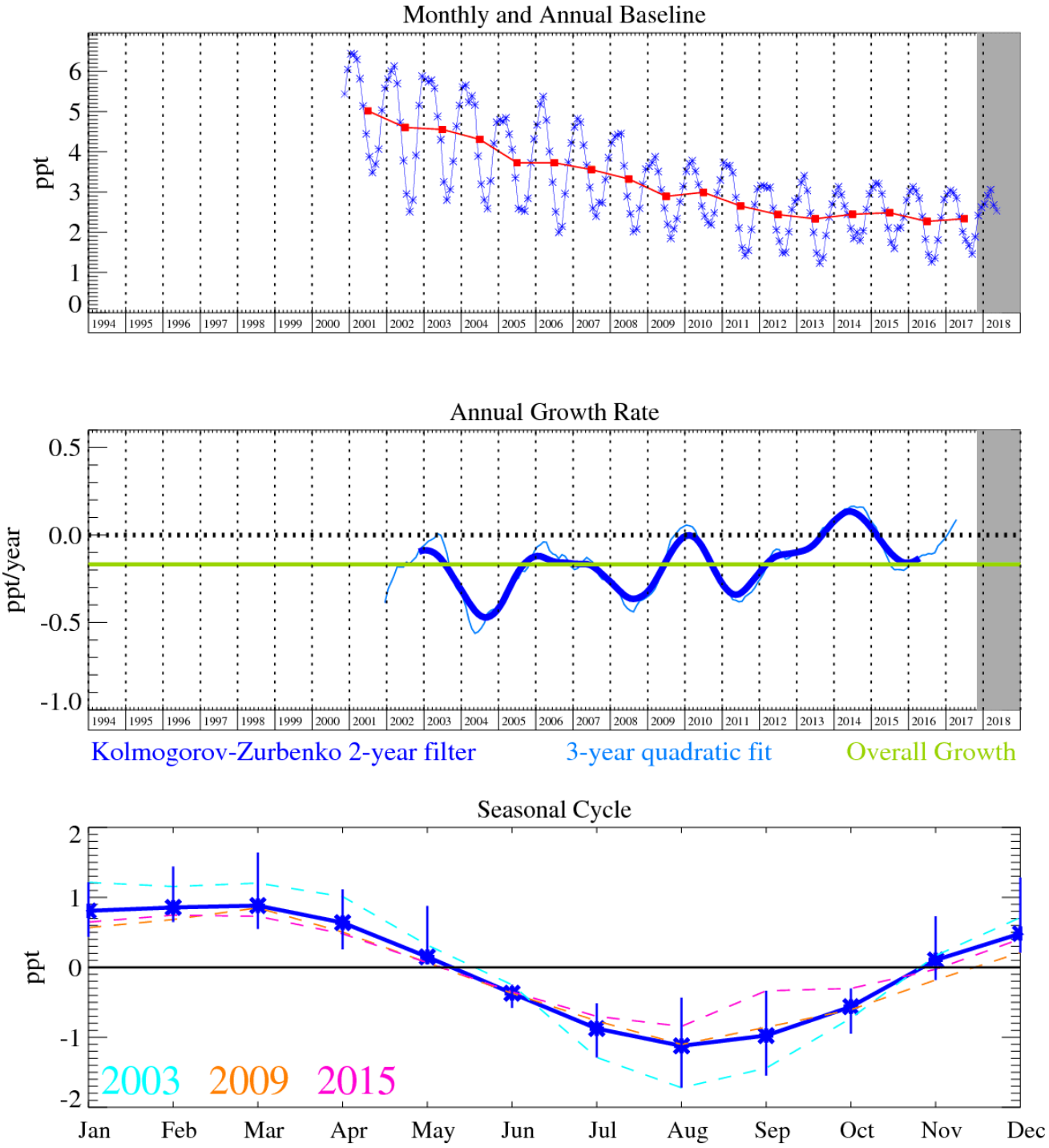


**Figure 110: $CCl_2CCl_2$: Monthly (blue) and annual (red) Northern Hemisphere baseline mole fractions (top plot). Annual (blue) and overall average growth rate (green) (middle plot). Seasonal cycle (de-trended) with year-to-year variability (lower plot). Grey area covers un-ratified and therefore provisional data.**

## 8.17 *Methyl bromide ($CH_3Br$)*

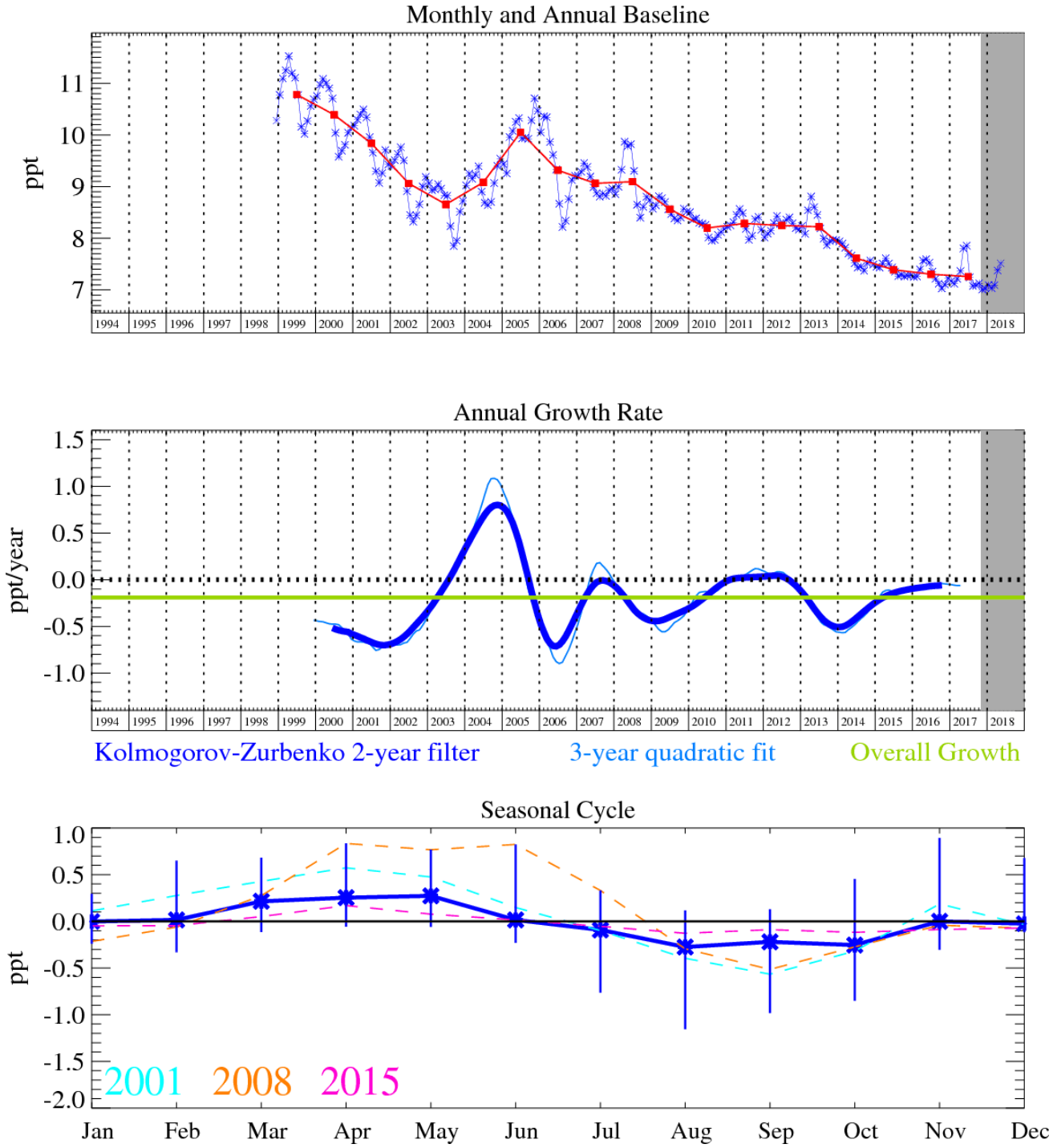


**Figure 111: Methyl bromide: Monthly (blue) and annual (red) baseline (top plot). Annual (blue) and overall average growth rate (green) (middle plot). Seasonal cycle (de-trended) with year-to-year variability (lower plot). Grey area covers un-ratified and therefore provisional data.**

The instrument change in 2005 to the Medusa system produced a discontinuity in the methyl bromide record, this jump should be discounted as it is an artefact of the measurement system.

## 8.18 Halon-1211

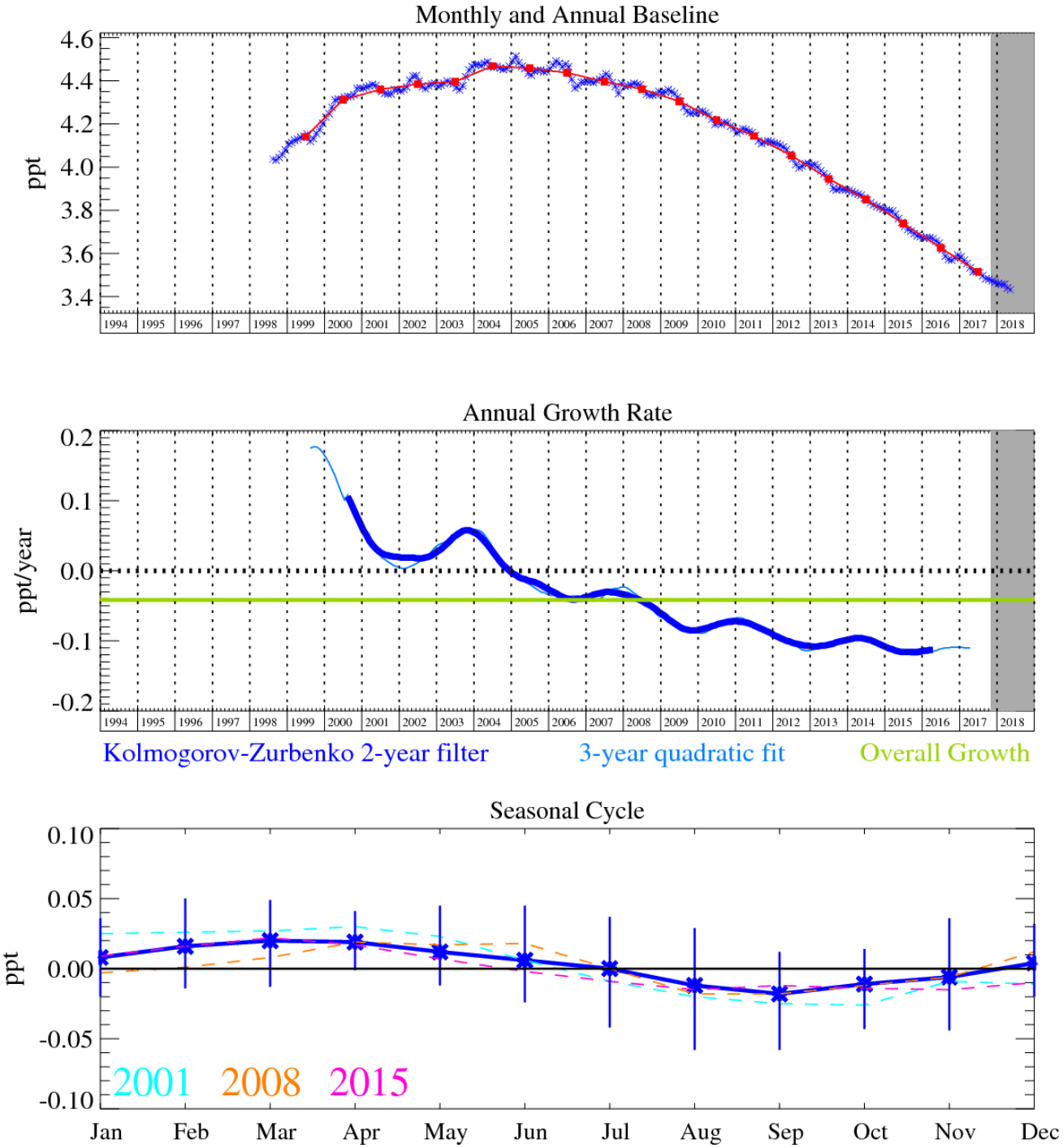


**Figure 112: Halon-1211 ($CBrClF_2$): Monthly (blue) and annual (red) baseline (top plot). Annual (blue) and overall average growth rate (green) (middle plot). Seasonal cycle (de-trended) with year-to-year variability (lower plot). Grey area covers un-ratified and therefore provisional data.**

## 8.19 Halon-1301

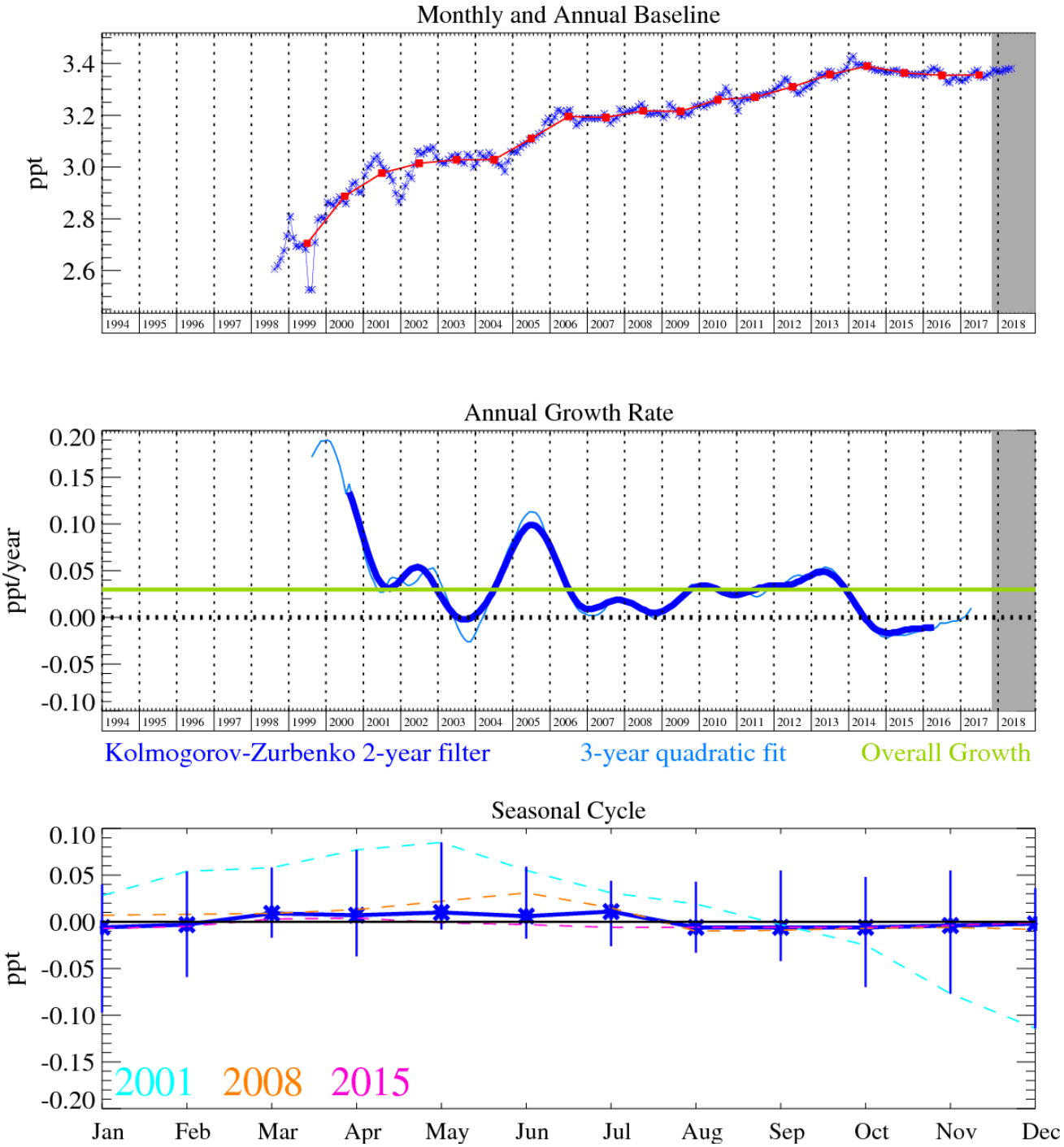


**Figure 113: Halon-1301 ($CBrF_3$): Monthly (blue) and annual (red) baseline (top plot). Annual (blue) and overall average growth rate (green) (middle plot). Seasonal cycle (de-trended) with year-to-year variability (lower plot). Grey area covers un-ratified and therefore provisional data.**

## 8.20 Halon-2402

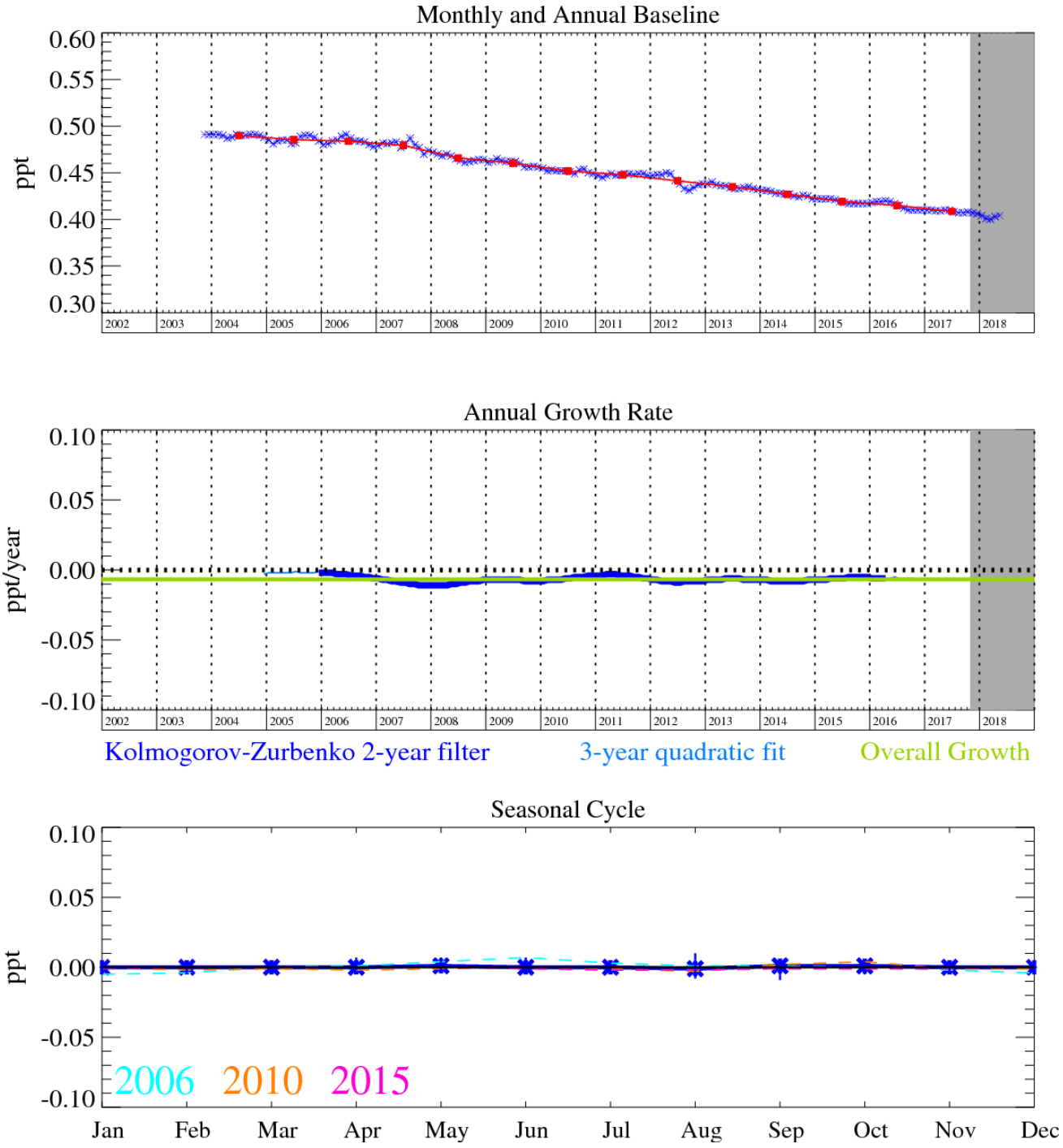


**Figure 114: Halon-2402 ($C_2Br_2F_4$): Monthly (blue) and annual (red) baseline (top plot). Annual (blue) and overall average growth rate (green) (middle plot). Seasonal cycle (de-trended) with year-to-year variability (lower plot). Grey area covers un-ratified and therefore provisional data.**

## 8.21 Carbon monoxide (CO)

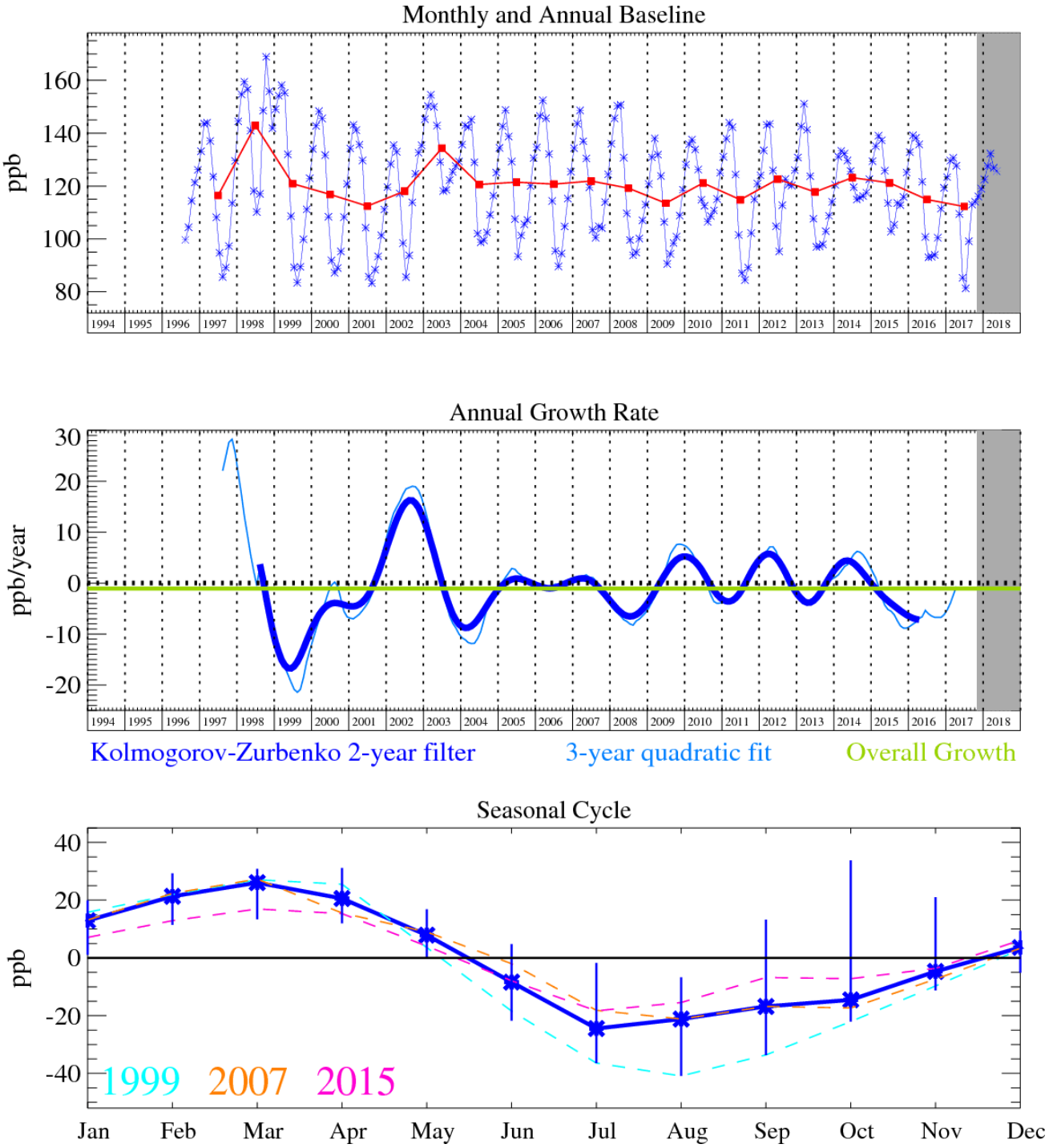


**Figure 115: CO: Monthly (blue) and annual (red) Northern Hemisphere baseline mole fractions (top plot). Annual (blue) and overall average growth rate (green) (middle plot). Seasonal cycle (de-trended) with year-to-year variability (lower plot). Grey area covers un-ratified and therefore provisional data.**

## 8.22 Ozone ($O_3$)

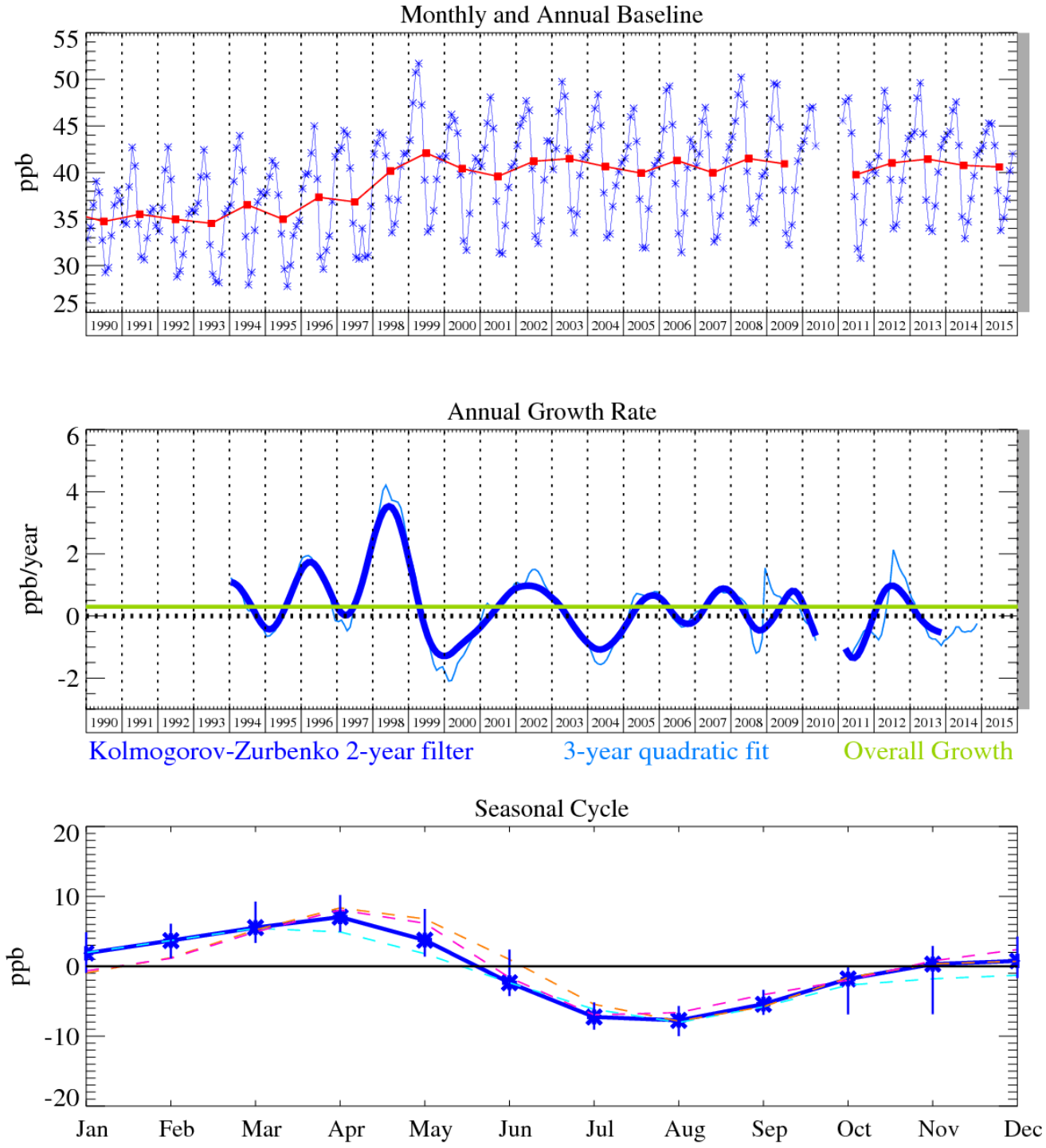


**Figure 116: Ozone ($O_3$): Monthly (blue) and annual (red) Northern Hemisphere baseline mole fractions (top plot). Annual (blue) and overall average growth rate (green) (middle plot). Seasonal cycle (de-trended) with year-to-year variability (lower plot). Grey area covers un-ratified and therefore provisional data.**

## 8.23 Hydrogen

Hydrogen is an oxidation product of $CH_4$ and isoprene, whose main sink is ground surface uptake, mainly in the northern hemisphere. Annual mean baseline levels have remained roughly constant (within measurement uncertainty) for much of the Mace Head record. There is evidence of anomalous growth in 2010-2011 through the influence of the forest fires in the Russian Federation.

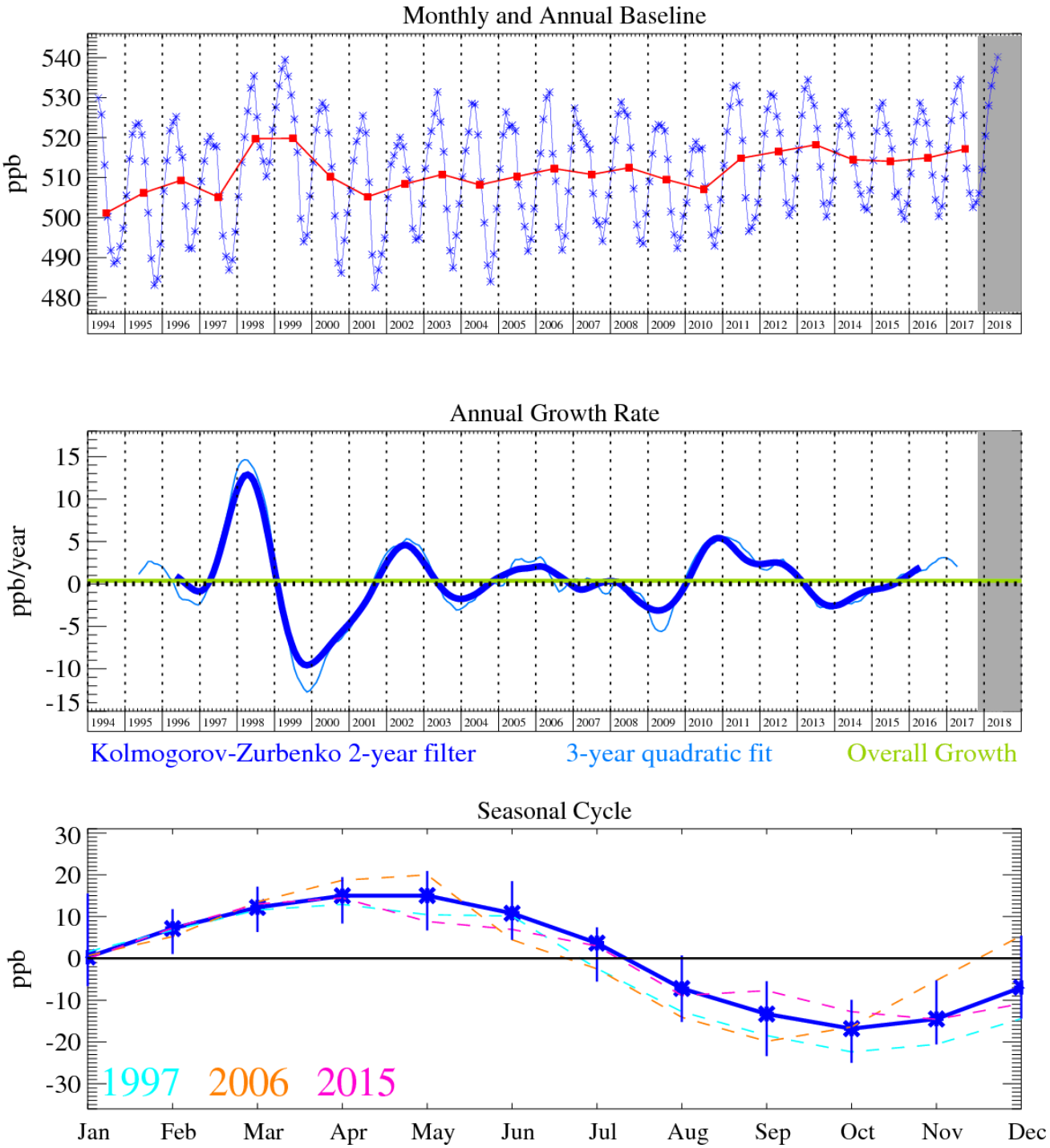


**Figure 117: Hydrogen ($H_2$): Monthly (blue) and annual (red) baseline (top plot). Annual (blue) and overall average growth rate (green) (middle plot). Seasonal cycle (de-trended) with year-to-year variability (lower plot). Grey area covers un-ratified and therefore provisional data.**

# 9 References


Boschetti, F., Thouret, V., Maenhout, G. J., Totsche, K. U., Marshall, J., and Gerbig, C.: Multi-species inversion and IAGOS airborne data for a better constraint of continental-scale fluxes, Atmos. Chem. Phys., 18, 9225-9241, https://doi.org/10.5194/acp-18-9225-2018, 2018.

Chatterjee, A., M. Gierach, A. Sutton, D. Crisp, A. Eldering, R. A. Feely, M. Gunson, C. W. O'Dell, B. B. Stephens, D. Schimel: Influence of El Niño on atmospheric CO2 over the tropical Pacific Ocean: Findings from NASA's OCO-2 mission. Science 358, eaam5776, doi:10.1126/science.aam5776, 2017.

Crisp, D., Pollock, H. R., Rosenberg, R., Chapsky, L., Lee, R. A. M., Oyafuso, F. A., Frankenberg, C., O'Dell, C. W., Bruegge, C. J., Doran, G. B., Eldering, A., Fisher, B. M., Fu, D., Gunson, M. R., Mandrake, L., Osterman, G. B., Schwandner, F. M., Sun, K., Taylor, T. E., Wennberg, P. O., and Wunch, D.: The on-orbit performance of the Orbiting Carbon Observatory-2 (OCO-2) instrument and its radiometrically calibrated products, Atmos. Meas. Tech., 10, 59-81, https://doi.org/10.5194/amt-10-59-2017, 2017.

Crisp et al. A constellation architecture for monitoring carbon dioxide and methane from space, prepared by the CEOS Atmospheric Composition Virtual Constellation Greenhouse Gas Team, 2018.

Cusworth, D. H., Jacob, D. J., Sheng, J.-X., Benmergui, J., Turner, A. J., Brandman, J., White, L., and Randles, C. A.: Detecting high-emitting methane sources in oil/gas fields using satellite observations, Atmos. Chem. Phys. Discuss., https://doi.org/10.5194/acp-2018-741, in review, 2018.

Eldering, A., O'Dell, C. W., Wennberg, P. O., Crisp, D., Gunson, M. R., Viatte, C., Avis, C., Braverman, A., Castano, R., Chang, A., Chapsky, L., Cheng, C., Connor, B., Dang, L., Doran, G., Fisher, B., Frankenberg, C., Fu, D., Granat, R., Hobbs, J., Lee, R. A. M., Mandrake, L., McDuffie, J., Miller, C. E., Myers, V., Natraj, V., O'Brien, D., Osterman, G. B., Oyafuso, F., Payne, V. H., Pollock, H. R., Polonsky, I., Roehl, C. M., Rosenberg, R., Schwandner, F., Smyth, M., Tang, V., Taylor, T. E., To, C., Wunch, D., and Yoshimizu, J: The Orbiting Carbon Observatory-2: first 18 months of science data products, Atmos. Meas. Tech., 10, 549– 563, doi:10.5194/amt-10-549-2017, 2017.

Graziosi, F., Arduini, J., Furlani, F., Giostra, U., Cristofanelli, P., Fang, X., Hermanssen, O., Lunder, C., Maenhout, G., O'Doherty, S., Reimann, S., Schmidbauer, N., Vollmer, M. K., Young, D. and Maione, M.: European emissions of the powerful greenhouse gases hydrofluorocarbons inferred from atmospheric measurements and their comparison with annual national reports to UNFCCC, Atmospheric Environment, 158, 85–97, doi:10.1016/j.atmosenv.2017.03.029, 2017.

Hedelius, J. K., et al., Emissions and topographic effects on column CO2 (XCO2) variations, with a focus on the Southern California Megacity, J. Geophys. Res. Atmos., 122, 7200–7215, doi:10.1002/2017JD026455, 2017.

Hu, L., Montzka, S. A., Lehman, S. J., Godwin, D. S., Miller, B. R., Andrews, A. E., Thoning, K., Miller, J. B., Sweeney, C., Siso, C., Elkins, J. W., Hall, B. D., Mondeel, D. J., Nance, D., Nehrkorn, T., Mountain, M., Fischer, M. L., Biraud, S. C., Chen, H. and Tans, P. P.: Considerable contribution of the Montreal Protocol to declining greenhouse gas emissions from the United States: U.S. CFCs, HCFCs, and HFCs Emissions, Geophysical Research Letters, doi:10.1002/2017GL074388, 2017.

Jallad, A-H., et al, MeznSat: a cubesat for greenhouse gas monitoring and algal bloom prediction, paper #SSC18-WKIX-03, 32nd Annual AIAA/USU Conference on Small Satellites, 2018. Keller, C. A., Matthias Hill, Martin K. Vollmer, Stephan Henne, Dominik Brunner, Stefan Reimann, Simon O'Doherty, Jgor Arduini, Michela Maione, Zita Ferenczi, Laszlo Haszpra, Alistair J. Manning, and Thomas Peter, "European Emissions of Halogenated Greenhouse Gases Inferred from Atmospheric Measurements" (2011)

Liu, J., K. Bowman, D. Schimel, N. Parazoo, Z. Jiang, M. Lee, A. Bloom, D. Wunch, K. Gurney, D. Menemenlis, M. Girerach, D. Crisp, and A. Eldering: Contrasting carbon cycle responses of the tropical continents to the 2015–2016 El Niño. Science 358, eaam5690, doi:10.1126/science.aam5690, 2017.

Nassar, R., Hill, T. G., McLinden, C. A., Wunch, D., Jones, D. B. A., & Crisp, D., Quantifying CO2 emissions from individual power plants from space, Geophysical Research Letters, doi:10.1002/2017GL074702, 2017.

Nickless, A., Rayner, P. J., Scholes, R. J., Engelbrecht, F., and Erni, B.: An atmospheric inversion over the city of Cape Town: sensitivity analyses, Atmos. Chem. Phys. Discuss., https://doi.org/10.5194/acp-2018-535, in review, 2018.

Lunt, M. F., Rigby, M., Ganesan, A. L., Manning, A. J., Prinn, R. G., O'Doherty, S., Mühle, J., Harth, C. M., Salameh, P. K., Arnold, T., Weiss, R. F., Saito, T., Yokouchi, Y., Krummel, P. B., Steele, L. P., Fraser, P. J., Li, S., Park, S., Reimann, S., Vollmer, M. K., Lunder, C., Hermansen, O., Schmidbauer, N., Maione, M., Arduini, J., Young, D. and Simmonds, P. G.: Reconciling reported and unreported HFC emissions with atmospheric observations, Proceedings of the National Academy of Sciences, 112(19), 5927–5931, doi:10.1073/pnas.1420247112, 2015.

Patra, P., Crisp, D., Kaiser, J., Wunch, D., Saeki, T., Ichii, K., Sekiya, T., Wennberg, P., Feist, D.,. Pollard, D, Griffith, D., Velazco, V., De Maziere, M., Sha, M. K., Roehl C., Chatterjee A.: Orbiting Carbon Observatory-2 (OCO-2) tracks 2-3 peta-grams increase of carbon release to the atmosphere during the 2014-2016 El Niño. Nature Scientific Reports, 7: 13567, doi:10.1038/s41598-017-13459-0, 2017.

Pinty B., G. Janssens-Maenhout, M. Dowell, H. Zunker, T. Brunhes, P. Ciais, D. Dee, H. Denier van der Gon, H. Dolman, M. Drinkwater, R. Engelen, M. Heiman, K. Holmlund, R. Husband, A. Kentarchos, Y. Meijer, P. Palmer and M. Scholze (2017): An Operational Anthropogenic CO2 Emissions Monitoring & Verification Support capacity - Baseline Requirements, Model Components and Functional Architecture, doi: 10.2760/08644, European Commission Joint Research Centre, EUR 28736 EN

Rigby, M., Prinn, R. G., O'Doherty, S., Montzka, S. a., McCulloch, A., Harth, C. M., Mühle, J., Salameh, P. K., Weiss, R. F., Young, D., Simmonds, P. G., Hall, B. D., Dutton, G. S., Nance, D., Mondeel, D. J., Elkins, J. W., Krummel, P. B., Steele, L. P. and Fraser, P. J.: Re-evaluation of the lifetimes of the major CFCs and CH3CCl3 using atmospheric trends, Atmospheric Chemistry and Physics, 13(5), 2691–2702, doi:10.5194/acp-13-2691-2013, 2013.

Rigby, M., Prinn, R. G., O'Doherty, S., Miller, B. R., Ivy, D., Mühle, J., Harth, C. M., Salameh, P. K., Arnold, T., Weiss, R. F., Krummel, P. B., Steele, L. P., Fraser, P. J., Young, D. and Simmonds, P. G.: Recent and future trends in synthetic greenhouse gas radiative forcing, Geophysical Research Letters, 41(7), 2623–2630, doi:10.1002/2013GL059099, 2014.

Sheng, J.-X., Jacob, D. J., Turner, A. J., Maasakkers, J. D., Benmergui, J., Bloom, A. A., Arndt, C., Gautam, R., Zavala-Araiza, D., Boesch, H., and Parker, R. J.: 2010–2016 methane trends over Canada, the United States, and Mexico observed by the GOSAT satellite: contributions from different source sectors, Atmos. Chem. Phys., 18, 12257-12267, https://doi.org/10.5194/acp-18-12257-2018, 2018.

Shusterman, A. A., Kim, J., Lieschke, K. J., Newman, C., Wooldridge, P. J., and Cohen, R. C.: Observing local CO2 sources using low-cost, near-surface urban monitors, Atmos. Chem. Phys. Discuss., https://doi.org/10.5194/acp-2018-344, in review, 2018.

Simmonds, P. G., Rigby, M., McCulloch, A., Vollmer, M. K., Henne, S., Mühle, J., O'Doherty, S., Manning, A. J., Krummel, P. B., Fraser, P. J., Young, D., Weiss, R. F., Salameh, P. K., Harth, C. M., Reimann, S., Trudinger, C. M., Steele, L. P., Wang, R. H. J., Ivy, D. J., Prinn, R. G., Mitrevski, B. and Etheridge, D. M.: Recent increases in the atmospheric growth rate and emissions of HFC-23 (CHF3) and the link to HCFC-22 (CHClF2) production, Atmospheric Chemistry and Physics, 18(6), 4153–4169, doi:10.5194/acp-18-4153-2018, 2018.

Sun, Y., Frankenberg, C., Wood ,J. D., Schimel, D. S., Jung, M., Guanter, L., Drewry, D. T., Verma, M., Porcar-Castell, A., Griffis, T. J., Gu, L., Magney, T. S., Köhler, P., Evans, B., and Yuen, K. OCO-2 advances photosynthesis observation from space via solar induced chlorophyll fluorescence. Science 358, eaam5747, doi:10.1126/science.aam5747, 2017.

Turner, A. J., Jacob, D. J., Benmergui, J., Brandman, J., White, L., and Randles, C. A.: Assessing the capability of different satellite observing configurations to resolve the distribution of methane emissions at kilometer scales, Atmos. Chem. Phys., 18, 8265-8278, https://doi.org/10.5194/acp-18-8265-2018, 2018.

Umezawa, T., Matsueda, H., Sawa, Y., Niwa, Y., Machida, T., and Zhou, L.: Seasonal evaluation of tropospheric CO2 over the Asia-Pacific region observed by the CONTRAIL commercial airliner measurements, Atmos. Chem. Phys. Discuss., https://doi.org/10.5194/acp-2018-519, in review, 2018.

Varon, D. J., Jacob, D. J., McKeever, J., Jervis, D., Durak, B. O. A., Xia, Y., and Huang, Y.: Quantifying methane point sources from fine-scale (GHGSat) satellite observations of atmospheric methane plumes, Atmos. Meas. Tech. Discuss., https://doi.org/10.5194/amt-2018-171, in review, 2018.

Velders, G. J. M., Fahey, D. W., Daniel, J. S., Mcfarland, M. and Andersen, S. O.: The large contribution of projected HFC emissions to future climate forcing, Proceedings of the National Academy of Sciences of the United States of America, 106(27), 10949–10954, 2009.

Vogel, F. R., Frey, M., Staufer, J., Hase, F., Broquet, G., Xueref-Remy, I., Chevallier, F., Ciais, P., Sha, M. K., Chelin, P., Jeseck, P., Janssen, C., Te, Y.-V., Groß, J., Blumenstock, T., Tu, Q., and Orphal, J.: XCO2 in an emission hot-spot region: the COCCON Paris campaign 2015, Atmos. Chem. Phys. Discuss., https://doi.org/10.5194/acp-2018-595, in review, 2018.

Wang, Y., G. Broquet, P. Ciais, F. Chevallier, F. Vogel, N. Kadygrov, L. Wu, Y. Yin, R. Wang, and S. Tao, Estimation of observation errors for large-scale atmospheric inversion of CO2 emissions from fossil fuel combustion, Tellus B: Chemical and Physical Meteorology, 69:1, DOI: 10.1080/16000889.2017.1325723, 2017.

Wang, Y., Broquet, G., Ciais, P., Chevallier, F., Vogel, F., Wu, L., Yin, Y., Wang, R., and Tao, S.: Potential of European 14CO2 observation network to estimate the fossil fuel CO2 emissions via atmospheric inversions, Atmos. Chem. Phys., 18, 4229-4250, https://doi.org/10.5194/acp-18-4229-2018, 2018.

Wolf, J., Asrar, G. R. and West, T. O.: Revised methane emissions factors and spatially distributed annual carbon fluxes for global livestock, Carbon Balance and Management, 12(1), doi:10.1186/s13021-017-0084-y, 2017.

Worden, J. R., Bloom, A. A., Pandey, S., Jiang, Z., Worden, H. M., Walker, T. W., Houweling, S. and Röckmann, T.: Reduced biomass burning emissions reconcile conflicting estimates of the post-2006 atmospheric methane budget, Nature Communications, 8(1), doi:10.1038/s41467-017-02246-0, 2017.

Yang, D. X., Y. Liu, Z. N. Cai, X. Chen, L. Yao, and D. R. Lu: First global carbon dioxide maps produced from TanSat measurements. Adv. Atmos. Sci.,, doi:10.1007/s00376-018-7312-6, 2018.